University of Antwerp

Faculty of Science
Department of Bioscience Engineering

# Singlet oxygen-based photoelectrochemical detection of nucleic acids

PhD thesis submitted for the degree of
**Doctor in Bioscience Engineering**
at the University of Antwerp to be defended by
**Saranya Thiruvottriyur Shanmugam**

Promoter: **Prof. Dr. Karolien De Wael**
Co-Promoter: **Dr. Stanislav Trashin**

Antwerp, 2022

# Table of Contents

# Acknowledgements

This work is a result of more than four years of my research at A-Sense Lab in the University of Antwerp. Unlike most of them in our group, I started my Ph.D. after 5 years of being a lecturer in India and it has been an interesting learning process ever since. This thesis has become a reality with the kind support and help of many people, whom I would like to acknowledge here.

Firstly, I would like to acknowledge my supervisor Prof. Karolien De Wael. Thank you for believing in me and providing the opportunity to pursue a Ph.D. Especially, you always encouraged me when I came up with wild ideas, even though I was not 100% sure if they will work. Thanks for that! I am always grateful for the support and guidance you offered during difficult times like COVID-19 or for being understanding enough when I put family/my kid first. I also appreciate your time, effort and knowledge to help me in completing this dissertation.

My sincere thanks to my co-promoter and mentor Dr. Stanislav Trashin. Stas, every moment spent with you at work was a learning time for me. Your insights and experience in this field have been very important for tackling the challenges faced throughout this work. Thanks for always being there, for the useful discussions regarding the research, for patiently listening when I share my frustrations, our never-ending conversations about Komida food and most importantly tolerantly fixing the Arduino setup whenever I break the contacts!

I would like to also thank Dr. Ricardo Ribeiro from Centro Hospitalar do Porto, Portugal, for providing patient samples and useful discussions. Also, Dennis Laurijssen from FTI-CoSys Lab, University of Antwerp, for patiently listening to what I wanted and designing LeDlisa96x accordingly.

Thanks to all the current and former members of the A-Sense Lab for making the past few years pleasant and interesting. Rui, though it was during the last year of my Ph.D., I enjoyed doing experiments with you and your go-easy attitude and most importantly your “Its Friday” playlist. Thanks for all the useful insights and for introducing me to reverse pipetting! Elise and Amelia, thanks a lot for reading and correcting a few chapters of this thesis. Oli, thanks for being the go-to person if I need any help with instruments, Dutch or finding good restaurants. I will be always grateful!

Lis, Mats, Nick, Jonas, Hanan, Nick, Sara, Simone, Rocio, Gert, Andrea, Dmitrii, Ermanno, Marc, Sensu, Florine and all the previous members of the group, thanks for all the nice time spent during these past years.

A few of my colleagues turned into very good friends, making this experience enjoyable and memorable. Anca and Vanoushe, thank you so much for your encouragement, advice and for being there as my pillars of support professionally and outside work. I missed you both during the last part of my stay in Antwerp. Ehab, I will be always grateful for your brotherly care and support throughout this journey. Camilla, Victoria, Noelia, thanks for all the nice trips and good times spent together. Shahid, I was excited when I heard a fellow Indian was joining the team, and I am happy to have known you. Thanks for all the support and for making the last six months of my stay in Belgium without my family less gloomy.

Thanks to all my Indian friends, Archana, Jyothi, Arjun, Vasi, Saranya and Aruna who were like my second family in Antwerp.

This acknowledgement would be incomplete if I don't thank my family. To my parents always stood by my side and encouraged me to do my best. Special thanks to my mom, who would travel every summer from India to happily babysit my daughter so that I can go to work. To my brother Ganesh, for helping with the cover page design. I owe you one!

Of course, to my husband Vijayaraghavan, who first of all, supported my crazy idea of leaving a tenure position to follow my interest in research and has been there every step of the way. Raghava, you always lift my spirits up, help me to keep things in perspective whenever I believed that it was not possible to continue. Thanks for that! Lastly and importantly, to my daughters Sadhana and Arya. Sadhana, you made me strong and more capable than I could have ever imagined. I love you both to the moon and back!

## Dedication

I dedicate this thesis to the loving memory of my late grandfather Dr. Rammurthi, who always inspired me to follow my heart.

# Abstract

MicroRNAs (miRNAs) are small oligonucleotides (18-25 bases) that play a key role in epigenetic regulation. Since the discovery of miRNAs in 1993, their role in biological processes has been extensively investigated. By now, it has been evidenced that monitoring and detection of miRNAs can improve (early) disease diagnosis. The existing diagnostic approaches have limitations such as the need for complex multistep protocols for sample preparation, analysis, data interpretation, high cost of equipment, the need for highly qualified personnel, and high laboratory standards. As opposed to this, point-of-care biosensors and chips aim to facilitate the procedure and avoid sending samples into centralized laboratories, which saves time, reduces the chance of sample degradation, and enables analysis of patient samples in remote areas, directly at home or primary and secondary care facilities (i.e. general practitioners and specialists). The latter is essential for therapy assessment and follow-up monitoring of patients with chronic diseases and cancer. Nevertheless, the development of such sensors is lagging compared to the projections of 10 – 20 years ago, mainly due to insufficient sensitivity, poor reproducibility, and the complexity of sensors' design reported in the research literature. This motivates the development of new detection strategies and technologies such as photoelectrochemical sensors that combine the best features of different sensing approaches.

The primary concern when developing detection technologies for miRNA is the need for a highly sensitive and selective platform. This thesis explores a novel photoelectrochemical (PEC) method that is distinctive owing to its sensitive nature and simple and robust design. Firstly, we focused on the usage of recently emerging commercial gold-sputtered electrode systems for the detection of short nucleic acid with enzymatic amplification. Importantly, cleaning such electrodes is a challenge since the standard procedures known for regular disk electrodes such as polishing cannot be employed here, since it will damage the protective layer on the electrode. However, the electrodes can be washed and pretreated chemically and/or electrochemically. Thus, a procedure to effectively clean and modify the gold-sputtered electrode has been developed, resulting in high-performance gold-sputtered nucleic acid sensors.

Next, the usage of molecular photosensitizers as an alternative to enzymatic amplification has been evaluated. We took advantage of the $^1O_2$ production by photosensitizers upon photoexcitation, leading to a photocurrent response due to the $^1O_2$-induced (electro)chemical conversions. Following the demonstration of the detection strategy, the

analytical performance of the sensing system was evaluated using magnetic beads-based nucleic acid assay on disposable electrode platforms, with a focus to enhance the sensitivity and robustness of the technique in detecting complementary nucleic acid targets.

Following the fundamental evaluation of the singlet oxygen-based PEC detection of nucleic acids, we further optimized the assay and measurement parameters and employed the sensing strategy for a polymerase chain reaction-free (PCR-free) quantification of miRNAs related to prostate cancer. By successfully detecting and quantifying low-picomolar range concentrations (< 10 pM) in plasma samples from prostate cancer patients, we successfully showed the applicability of the novel sensing strategy. We have also compared and positioned the performance of our developed PEC strategy with an existing state-of-art technique, i.e. electrochemiluminescence (ECL). Our PEC strategy performed on par with ECL, both yielding low-picomolar detection limits in serum matrices, however quicker and cheaper than ECL.

Owing to the versatility of this PEC technique, the final study explored its multiplexing capability. As a starting point in this branch of the research, we have investigated two possible ways for multiplexing. To perform multiple measurements at the same time, constructing calibration plots and quantifying unknown miRNA concentrations in patient samples at the same time, we have developed a high-throughput detection with 96X multi-channel electrode systems and in-house designed and constructed 96XLED illumination sources. Secondly, to detect more than one target miRNA in a single measurement, intra-vial multiplexing where the samples were analyzed for different targets in one vial was also explored.

Altogether, this thesis presents the fundamentals, development and application of a novel PEC strategy for detecting short (< 25 bases) nucleic acid sequences, in particular, miRNA. With an aim to serve as a distinctive technique to function as a clinical testing platform without any need for PCR, this work adds value to the development of nucleic acid-based sensors for miRNAs and other short-stranded nucleic acid biomarkers, and benefits in the early detection of diseases like cancer.

# Samenvatting

MicroRNA's (miRNA's), ontdekt in 1993, zijn kleine oligonucleotiden (18-25 basen) die biologisch relevant zijn voor de epigenetische regulatie van belangrijke biologische processen. Onderzoeksinspanningen zijn veelal gericht op de detectie van miRNA's om de diagnose (in een vroeg stadium) te verbeteren. De bestaande diagnostische benaderingen, zoals PCR gebaseerde technieken en microarray-technologieën, hebben hun beperkingen zoals de behoefte aan complexe meerstapsprotocollen voor staalvoorbereiding, analyse, gegevensinterpretatie, hoge kosten van apparatuur, de behoefte aan hooggekwalificeerde personeel en strenge laboratoriumnormen. In tegenstelling hiermee zijn er *point-of-care* biosensoren en chips, bedoeld om de procedure te vergemakkelijken en te voorkomen dat stalen naar gecentraliseerde laboratoria worden gestuurd, wat tijd bespaart, de kans op staaldegradatie vermindert en de analyse van patiëntstalen in afgelegen gebieden, direct thuis of in ziekenhuizen mogelijk maakt. Dit laatste is essentieel voor therapiebeoordeling en opvolging van patiënten met chronische ziekten of kanker. Desalniettemin blijft de ontwikkeling van dergelijke sensoren achter in vergelijking met de prognoses van 10 tot 20 jaar geleden, voornamelijk als gevolg van onvoldoende gevoeligheid, beperkte reproduceerbaarheid en de complexiteit van het ontwerp van sensoren. Dit stimuleert tot de ontwikkeling van nieuwe detectiestrategieën en -technologieën zoals foto-elektrochemische sensoren die de beste eigenschappen van verschillende detectiebenaderingen combineren.

Bij het ontwikkelen van detectietechnologieën voor miRNA staat de behoefte aan een gevoelig en selectief platform centraal. Dit proefschrift onderzoekt een nieuwe foto-elektrochemische (PEC) methode, die zich onderscheidt door zijn hoge gevoeligheid, eenvoudig en robuust ontwerp. Ten eerste hebben we ons gericht op de voorbereiding en karakterisering van goud-gesputterde elektroden voor de detectie van korte nucleïnezuren. Aangezien de inzichten over het reinigen van polykristallijne gouden schijfelektroden (met een referentie-elektrodeoppervlak voor nucleïnezuur- gebaseerde sensoren) niet kunnen overgedragen worden om geminiaturiseerde, goud-gesputterde micro-elektroden te reinigen, werd een effectieve procedure opgesteld om het goud-gesputterde elektrodeoppervlak te reinigen en zo de voorbereiding te vergemakkelijken. Manieren om gethioleerde capture-probes met maximale dekking te immobiliseren, werden methodologisch geëvalueerd, waardoor een degelijk inzicht in de reiniging, modificatie en prestaties van goud-gesputterde micro-elektroden werd verworven.

Vervolgens werden lichtgevoelige nucleïnezuur-gebaseerde detectieprobes met moleculaire fotosensitizers, die singlet-zuurstof ($^1O_2$) genereren, geëvalueerd. We hebben gebruik gemaakt van hun vermogen om $^1O_2$ te produceren bij foto-excitatie en de daaropvolgende fotostroomrespons. Na de demonstratie van de detectiestrategie werden de analytische prestaties van het detectiesysteem geëvalueerd op wegwerpelektroden met behulp van een op magnetische *beads* gebaseerd DNA-assay. Hierbij lag de nadruk op het verbeteren van de gevoeligheid en robuustheid van de techniek voor het detecteren van complementaire nucleïnezuur sequenties.

Na de fundamentele evaluatie van de op $^1O_2$ gebaseerde PEC-detectie van nucleïnezuren, werden de test- en meetparameters verder geoptimaliseerd en de detectiestrategie gebruikt voor een PCR-vrije kwantificering van miRNA's gerelateerd aan prostaatkanker. De toepasbaarheid van de nieuwe detectiestrategie werd aangetoond door miRNA's met lage-picomolair concentraties (< 10 pM) in plasmamonsters van prostaatkankerpatiënten te detecteren en te kwantificeren. Bovendien hebben we de prestaties van onze ontwikkelde PEC-technologie vergeleken met en gepositioneerd ten opzichte van een bestaande *state-of-the-art* techniek, meer bepaald elektrochemiluminescentie (ECL). Onze PEC-strategie presteerde gelijkaardig aan ECL aangezien beiden detectielimieten in het lage-picomolair bereik opleverden in serum matrices, maar PEC bleek sneller en goedkoper dan ECL.

Vanwege de veelzijdigheid van de PEC-technologie, onderzocht de laatste studie het multiplexvermogen. Als uitgangspunt hebben we twee mogelijke manieren voor multiplexen onderzocht. Om meerdere metingen gelijktijdig uit te voeren, kalibratieplots te construeren en tegelijkertijd onbekende miRNA-concentraties in patiëntmonsters te kwantificeren, hebben we een *high-throughput* detectiesysteem ontwikkeld dat bestaat uit 96X meerkanaals elektrodesystemen en zelfontworpen, gebouwde 96XLED-verlichtingsbronnen. Vervolgens werd met succes de analytische capaciteit van dit systeem gedemonstreerd. Ten tweede werd een intra-*vial* multiplex manier onderzocht om meer dan één miRNA in een enkele meting te detecteren. Hierbij werden de stalen onderzocht op de aanwezigheid van verschillende miRNA's in één *vial*.

Samengevat beschrijft dit proefschrift de fundamenten, ontwikkeling en toepassing van een nieuwe foto-elektrochemische strategie voor het detecteren van korte (< 25 basen) nucleïnezuren, in het bijzonder miRNA. Deze technologie heeft als doel om te functioneren als een klinisch testplatform zonder dat PCR nodig is. Daarom draagt dit werk bij aan de ontwikkeling van op nucleïnezuur-gebaseerde sensoren voor miRNA's en andere korte nucleïnezuurbiomerkers die belangrijk zijn in de vroege opsporing van ziekten.

# Chapter 1
# Introduction to nucleic acid diagnostics

## 1.1 Abstract

This chapter introduces the concept of biomarkers and their contribution to disease diagnosis and prognosis with a particular focus on microRNA (miRNA) detection and liquid biopsy as a rapidly growing, minimally invasive testing method. This is followed by a comprehensive overview of the standard molecular diagnostic tools and electrochemical platforms for miRNA detection. Emphasis is made on the problems and limitations of existing state-of-the-art diagnostic approaches, namely the need for complex multistep protocols for sample preparation, analysis, data interpretation, high cost of equipment, the need for highly qualified personnel, and advanced laboratory standards. The (photo)electrochemical sensing strategies and current challenges in miRNA detection will be predominantly discussed in the context of the overall aim of this Ph.D. thesis to explore a novel PEC platform. Also, the need to increase the sensitivity and reliability of miRNA detection in patient samples without sample preparation and PCR amplification will be challenged. The final part of chapter 1 gives an overview of the thesis structure.

## 1.2 Biomarkers

Biomarkers or "biological markers" are objective medical signs used in medical research and clinical practice to understand the disease and formulate treatment plans. The Biomarkers, EndpointS and other Tools (BEST) glossary defines a biomarker as a "*defined characteristic that is measured as an indicator of normal biological processes, pathogenic processes or responses to an exposure or intervention, including therapeutic interventions.*"[5]

Classical biomarkers such as heart rate and blood pressure aim to measure rather obvious conditions, whereas newly emerging biomarkers often aim at less obvious conditions such as predisposition to develop a cancerous tumour or the ability to get pregnant and deliver a full-term baby. These biomarkers can have molecular (e.g. blood glucose), histologic (e.g. grading neoplasms), radiographic (e.g. tumour size), or physiologic (e.g. blood pressure) characteristics.[5] An overview is given in Table 1.1. There is also growing interest in a biomarker-driven approach in clinical trials by replacing the traditional approach of using surrogate markers which are known as the true endpoints, thus saving time and cost. For example, it is easier to measure the blood pressure of a patient than to measure the left ventricular function using an echocardiogram and more appropriate than to measure the chance of mortality from hypertension in the long term. MicroRNA (miRNA), a molecular biomarker, will be used in this Ph.D. research, therefore being the focus of discussion hereafter.

### 1.2.1 Molecular biomarkers for medical diagnosis

Molecular biomarkers are compounds measured in a patient's sample that reveal characteristics specific to the origin and disease. Molecular biomarkers can range from small molecules (e.g. blood glucose or lactate) to more complex systems of biological origin (e.g. cells) (Figure 1.1). To summarize, small molecules, metabolites, nucleic acids, proteins and cells indicative of certain disease traits at various stages of the disease can be termed molecular biomarkers.[6] These molecular biomarkers can be obtained from tissues, body fluids including plasma, serum, cerebrospinal fluid, or other body secretions such as urine and saliva and can be categorized according to their clinical purpose as:[7]

(i) Biomarkers of risk, to foresee the individual's predisposition to develop diseases,
(ii) Diagnostic biomarkers reflecting the presence of disease,
(iii) Acuity biomarkers reflecting the severity of the disease/disorder,

*Table 1.1 Overview of biomarkers according to their category.*

| Category of biomarkers | | Source | Examples | Measurement place | Price per analysis | Techniques |
|---|---|---|---|---|---|---|
| Physical | Physiologic | Physical measure of body processes | Blood pressure, heart rate, fetal size | Home/ clinic | €-€€ | Blood pressure: digital or aneroid sphygmomanometer |
| | | | | | | Heart rate: portable wireless electrocardiogram (ECG) monitor, hospital monitor/ defibrillator units or a fitness tracker |
| | | | | | | Fetal assessment: Ultrasound |
| | Imaging | Biological or anatomical features detected through imaging studies | Radiographic: quantitative measures of size/volume, multiparametric MRI scores, | Lab | €€- €€€€ | Radiology: X-Ray, computerized tomography (CT) scan, magnetic resonance imaging (MRI), positron emission tomography (PET) scan |
| | | | Histology: characterizing features such as calcium, fat and iron deposition, cellularity, perfusion, hypoxia, diffusion, necrosis, metabolism, lung airspace density, fibrosis | | | Histology: optical microscope, Fluorescence microscopy and confocal microscopy, transmission electron microscope (TEM) analysis for ultra-thin sections of specimens |
| Chemical | Molecular | Biospecimen derived measure of levels molecules/ metabolites | Glucose, hemoglobin, cholesterol, low-density lipoproteins (LDL), and high-density lipoproteins (HDL), thyroid-stimulating hormone, nucleic acids, cell counts | Home/ clinic/ lab | €- €€€ | Glucometers, hemoglobin monitors, cell counters, calorimetric/fluorimetric assays, immunoassays, ELISA, DNA microarrays, mass spectrometry (MS), chromatographic techniques |

(iv) Stage biomarkers to reflect the present disease stage of the patient,
(v) Response biomarkers reveal the efficiency of individuals' response to a given treatment,
(vi) Prognostic biomarkers predicting the course and outcome of the disease,
(vii) Safety biomarkers to measure the toxicity of therapeutics and environmental exposures.

The use of validated molecular biomarkers (which will be addressed as biomarkers from now on) allows for a better understanding of the disease processes and early diagnosis of the disease, in turn providing better prevention or combat of the disease.

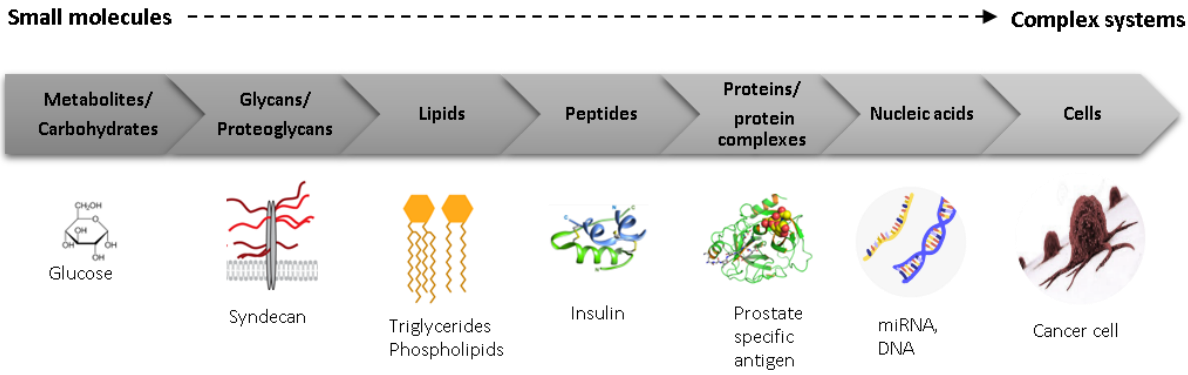


*Figure 1.1 Range of molecular biomarkers from small molecules to complex systems with examples.*

### 1.2.2 Role of biomarkers for liquid biopsy

In patients with cancer, biopsies aid in defining the disease, its progression and response to therapies by offering a way to sample the biomarkers. While biomarkers are found inside the cells/tissues excised from the cancerous tissue, there are limitations to the bias of analyzing tissue biopsies such as tumour heterogeneity. This means the characteristics of the primary tumour and its metastases are different, and a single biopsy taken from one part of the tissue would make therapeutic decision-making difficult. Though taking multiple tissue biopsies seem to be the obvious next step, it is not practical due to discomfort, surgical complications suffered by the patients, possible seeding of cancer cells to other sites[8] and delay in follow-up treatment because of sample analysis time. Moreover, in a multi-focal disease like multiple myeloma, a single biopsy test is never an option for a conclusive diagnosis or prognosis, leading to patients suffering from painful multiple biopsies. To overcome these limitations, different non-invasive/minimally invasive techniques for sampling the biomarkers like imaging, and liquid biopsies have evolved.

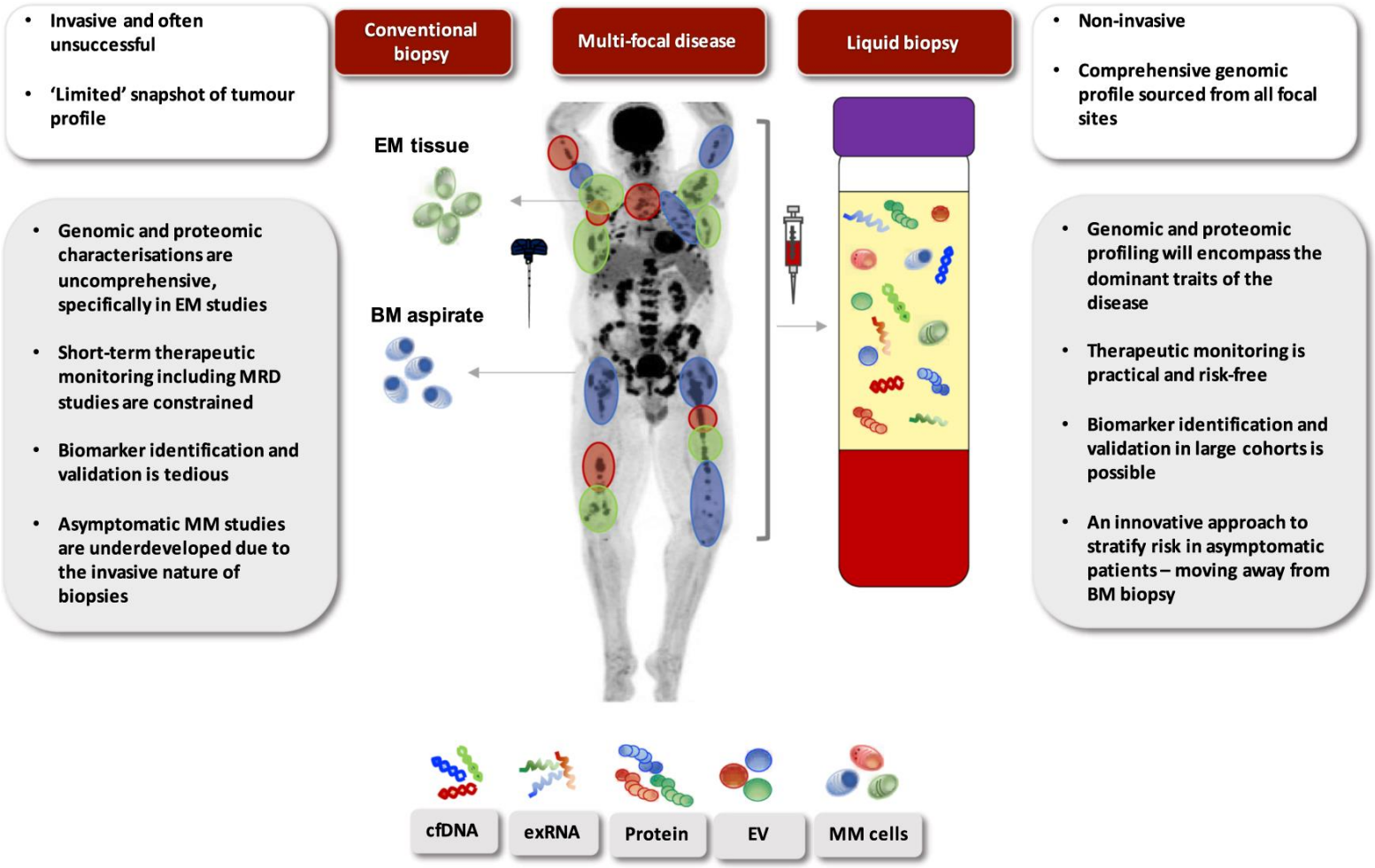


*Figure 1.2 Comparison on information derived from conventional biopsy or liquid biopsy in a multi-focal disease like multiple myeloma (MM). BM - bone marrow, EM - extra medullary, cfDNA - cell-free DNA, exRNA - extracellular RNA (including miRNA), EV - extracellular vesicles. Different tumour clones are indicated by the different colours—blue, green and red.*[2]

All body fluids are in principle sources of biomarkers, with blood and urine being commonly used sources and other sources like saliva, cerebrospinal fluid, seminal fluids, etc., may also be considered.[9] Sampling of biomarkers in these sources is called a liquid biopsy. While the tissue biopsy contains only biomarkers of spatial and temporal genetic composition from that site, in liquid biopsy, the plasma or serum from the peripheral blood will contain biomarkers comprehensive of all the sites in multifocal diseases. Useful for vast diagnostic applications, the possibility of repeated blood sampling for these biomarkers, enables us to monitor the disease progression and response to treatments. Analysis of biomarkers like cell-free nucleic acids, extracellular vesicles, proteins and metabolites via liquid biopsy has gained considerable momentum in recent years. A comparison between the information obtained from tissue biopsy and liquid biopsy is demonstrated in Figure 1.2 with a focus on a multi-focal disease like multiple myeloma (MM).[2] Analysis of cell-free nucleic acids (cfNA) including DNA and RNA fragments derived from primary and/or secondary tumour sites provide the clinicians with rapid and non-invasive genomic characterization. Apart from the cfNAs, proteins, metabolites and extracellular vesicles (EVs) provide comprehensive characteristic information on the disease. This also aids in the early detection of recurrences and/or relapse of cancer and therapeutic monitoring. Further information on cfNA as biomarkers are discussed in the next section.

### 1.2.3 Circulating cell-free nucleic acids

Cell-free nucleic acids (cfNA) circulating in the blood have different biogenesis and functions making them suitable candidates as biomarkers for liquid biopsy. They are a mix of single-stranded or double-stranded nucleic acids that are usually released into the blood by cells due to apoptosis, tissue necrosis and other secretions. They are suitable for prenatal diagnosis, for the screening of genetic disorders in the fetus from mothers' plasma, diagnosis and prognosis of cancer, neurological or cardiovascular diseases, obesity and diabetes.[10-12] Different types of cfNAs are present in the body fluids in free form, attached to proteins such as nucleosomes, or enclosed in extracellular vesicles. Despite the presence of plasma nucleases, stable cfNAs can be isolated from blood, e.g. by making use of magnetic beads/columns with proper stabilization.

*Table 1.2 Types of cell-free circulating nucleic acid sequences found in human blood.*

| Cell-free nucleic acids | Size* | References |
|---|---|---|
| **Circulating DNA** | | |
| Cell-free nuclear DNA (cf-nDNA) and Cell-free mitochondrial (cf-mtDNA) | Short: 57–168 bp<br>Medium: 167–241 bp<br>Long: > 241 bp | [13, 14] |

| | | |
|---|---|---|
| Circulating tumour DNA (ctDNA) | ~20–50 bp shorter than cfDNA | [15] |
| Ultrashort circulating tumour DNA (usctDNA) | 40–60 bp | [16] |
| Fetal DNA (cf-fDNA) | < 313 bp, shorter than maternal cfDNA | [17] |
| **Circulating RNA** | | |
| **Protein coding RNA** | | |
| Messenger RNA (mRNA) | < 1000 bp | [18] |
| **Small non-coding RNA** | | |
| Micro RNA (miRNA) | 18–25 nt | [19, 20] |
| Small interfering RNA (siRNA) | 21–22 nt | [21] |
| Transfer RNA halves (tRNA) | 29–50 nt | [22] |
| Transfer RNA-derived fragments (tRFs) | 14–30 nt | |
| YRNA | 83–112 nt | [23] |
| YRNA-derived fragments (YsRNAs) | 22–36 nt | [21] |
| Piwi-interacting RNA (piRNA) | 24–31 nt | [24] |
| Small nucleolar RNA (snoRNA) | 60–300 nt | [25] |
| **Long non-coding RNA** | | |
| Long non-coding RNA (lncRNA)<br>- Psuedogenes<br>- Telomerase RNA | 200– ~100,000 nt | [26] |
| Circular RNA (circRNA) | 100–1000 nt | [27] |

**sizes are presented as bp (base pairs) and nt (nucleotides) for double-stranded and single-stranded nucleic acid sequences respectively*

The most widely known cfNAs including several types of DNA and RNA molecules are listed in Table 1.2. These cfNAs are involved in different epigenetic modifications demonstrating disease-related variations in plasma/serum levels, making them clinically relevant for the diagnosis and prognosis of a disease. While several other non-coding nucleic acids have been found in body fluids, their exact functions as biomarkers and biogenesis are yet to be explored. The cell-free DNAs (cf-DNA) such as cell-free nuclear DNA (cf-nDNA) and cell-free mitochondrial DNA (cf-mtDNA) originate from apoptosis of lymphoid and myeloid cells in healthy individuals, whereas in cancer patients, they are released into the bloodstream via apoptosis or necrosis of tumour cells and termed as circulating tumour DNA (ct-DNA). Apart from this major classification of cf-DNAs mentioned in Table 1.2, cell-free DNA fragments (sequence not bound to any other molecules), extracellular vesicle bound DNA, DNA-macromolecule complexes (example: DNA-histone protein complex), cell-free viral or microbial DNA infecting the host can also be found in the circulation.

Cell-free RNA (cfRNA) molecules are also found in the circulation, originating from necrotic or apoptotic cells, or secretion from live cells through membrane-bound vesicles or vesicle-free RNA-binding protein-related pathways. Falling under the umbrella of either coding RNA(cRNA) or non-coding RNA (ncRNA), these cfRNA molecules are generally more fragile than larger cell-free DNAs, because of the high RNAse level in the blood, ncRNA are surprisingly stable in the plasma due to their association with proteins or integration into vesicles protecting them from RNAses and offer advantages over DNA biomarkers by providing more information about the change in cellular states and regulations. For example, upregulation or downregulation of ncRNA specific to a certain group of cells is possible only in specific conditions or disorders. These ncRNA are further divided into small ncRNA with size < 200nt and long ncRNA with size >= 200nt.[28] One of the most researched ncRNA is the microRNA (miRNA), a small ncRNA (18–23 nt) involved in post-transcriptional gene regulation and also the biomarker of interest in this thesis. Comprehensive information on miRNA is given separately in the 1.3 section of this chapter. Long non-coding RNAs (lncRNAs) are transcripts longer than 200 nt having broad molecular functions, with low/no protein-coding potential and are generally originated from the transcription of introns of protein genes, intergenic regions, sense or antisense regions of genes.[26]

Currently, the use of cfDNA and cfRNA markers is being investigated for diagnostics and prognostic applications. Despite their great promise in this area of diagnostics, only a few liquid biopsy tests based on cfNAs have been approved for clinical use.[29, 30] This is likely due to (i) inadequate information of the behaviour of these cfNA components once released into the circulation, (ii) concentrations of these relevant cfNA biomarkers in the circulation are very low, masked by thousand-fold excess of non-informative cfNA from other cells and (iii) lack of large-scale studies to prove the connection between the NA concentrations and their relevance in the diagnosis of certain diseases. Thus, addressing these issues will make these promising biomarker candidates as recommended diagnostic biomarkers in future.

### 1.2.4 Importance in cancer diagnosis and management

Cancer remains second leading cause of death globally and 28.4 million new cancer cases are projected to occur in 2040, which is a 47% rise compared to 19.3 million cases in 2020.[31] This cancer burden can be reduced by detecting it at an early stage, effectively treating the patient and monitoring the response to the therapy. While early diagnosis leads to a greater chance of survival and less expensive treatment, screening individuals will help in identifying if the patient is at risk of developing cancer even before they develop symptoms. Simple and cost-effective diagnostics are warranted for early diagnosis and screening which will reduce a high percentage of morbidity in developing countries. This is where

biomarkers play a major role by indicating the patients' disposition to develop cancer, helping in characterizing the tumour and the severity of cancer.

Prostate cancer (PCa) exhibits a good example of the importance of molecular biomarkers in cancer diagnosis and their relevance to being detected in liquid biopsies. PCa is a heterogeneous disease that can slowly develop from a benign form into more aggressive metastatic and fatal forms, despite treatment. In Belgium, PCa is the most common cancer in men particularly aged 60 years and above.[32] Prostate specific antigen (PSA) levels in blood and prostate checks at clinics are used as screening markers with biopsy for confirming the diagnosis. An average of ~172000 PSA immunoassay tests per year, measuring the serum concentrations of PSA are conducted in Belgium.[33] The chances of developing PCa increase as the levels of PSA increase, with no definite cut-off value. However, based on serum PSA measurements of 860 healthy men, the upper limit for PSA was 4 ng/mL, but recently, a reduction of the upper limit is recommended to 2.5–3 ng/mL for patients between 60 and 65 years of age and younger.[34]

The current diagnostic recommendations include screening through estimation of PSA concentration and digital rectal examination (DRE), followed by tissue biopsy to confirm the diagnosis.[35]The disadvantage of these screening recommendations is that, while DRE is not sensitive, the levels of PSA in circulation are not specific to the presence of the tumour and can be elevated due to non-cancerous conditions such as infection, trauma, inflammation, and benign prostatic hyperplasia (BPH).[36, 37] In other words, PSA is prostate-specific but not PCa-specific (i.e. all PCa patients have an increased PSA level, but not all patients with increased PSA have PCa). This unspecific nature of the elevated PSA levels leads to inaccurate prediction of the disease.[38] Moreover, its use is associated with disadvantages such as diagnosis of clinically irrelevant tumours and possible overtreatment.

Confirmation of the disease requires a biopsy of the prostate gland. In Belgium, patients with elevated PSA (3 ng/ml or more) are advised to confirm the diagnosis by prostate biopsy[33] which is painful and problematic for frequent sample collection during treatment follow-up. Moreover, negative results of the biopsy procedure cannot guarantee the absence of PCa, because the probes could be accidentally taken from a healthy part of the prostate gland, while the cancerous tissue remained undetected. In other words, the biopsy procedure is highly specific but insensitive. Thus, highly specific, and highly sensitive markers are needed to improve PCa diagnostics and prevent unnecessary prostate biopsies.

PCa antigen 3 (PCA3) is a non-coding untranslated region of mRNA, which is prostate-specific and overexpressed in more than 95% of primary and metastatic PCa tumours. Although PCA3 was discovered in the year 1999[39], its use in prostate cancer diagnosis is recently available in some countries including Belgium. The analysis involves dual time-resolved fluorescence (TRF)–based reverse transcription-PCR of both PCA3 and PSA mRNAs in the first-catch urine following a digital rectal examination or after prostatic massage and results in a PCA3 score (PCA3-mRNA/PSA-mRNA) in urine specimens.[40, 41] If the PCA3 score is < 35, there is a low risk for PCa, and hence prostate biopsy may not be recommended. In a study to validate the usefulness of PCA3 urine test, PCA3 test showed a negative predictive value of 90% in a population of men, admitted for prostate biopsies based on a serum PSA value >3 ng/mL.[42] Thus, this presents greater diagnostic accuracy than free PSA and great potential in reducing the number of unnecessary biopsies. However, the test is still poorly available to people due to the complexity of using RT-PCR for two mRNAs and the high price (€250 per test compared to €40 per biopsy test and ∼€3 per PSA test).[33] Therefore, there is a need for developing and/or validating clinically relevant biomarkers that will help in PCa disease management. This is where another subclass of cfNAs, miRNA is currently emerging as a possible candidate to improve diagnostic and screening procedures.

## 1.3 miRNA biomarkers

MiRNAs are small non-coding RNAs, implicated in every aspect of gene expression and are synthesized through multiple enzymatic cleavage reactions by RNase enzymes, such as Drosha and Dicer.[1] miRNAs are the most researched RNAs as disease biomarkers with well-described biogenesis.[43] A schematic diagram showing miRNA biogenesis, modes of their secretion into body fluids, RNA extraction and quantitative approaches are presented in Figure 1.3. The reason for the high stability of these circulating miRNAs is the protection offered against denaturation via inclusion into extracellular vesicles like exosomes or complexation with RNA-binding proteins.[44] This makes miRNAs not just extracellular secretions into the bloodstream, but stable candidates as potential biomarkers for liquid biopsies. In the future, clinical decisions may be made based on the expression levels of miRNAs.

Apart from being prospective cancer biomarkers, an additional benefit of circulating miRNAs as cancer biomarkers is their potential for multiplexed detection of a panel of miRNAs. This panel can be monitored for early diagnosis of cancer, guided treatments and post-treatment follow-up since the levels of miRNAs can vary according to the progression of the disease, and differentiation between cancer stages. A good example to prove this is

the study by Xiong et al., where they identified a multimarker panel of nine miRNAs for accurate breast cancer diagnosis with high specificity and sensitivity.[45] This study also proves that the detection of a panel of miRNAs together improves the specificity due to multiple parameters used for clustered analysis. Apart from their application in cancer diagnosis, miRNAs also serve as biomarkers for: cardiovascular diseases, indicative of myocardial infarction (myomiRs) and sepsis, which can substitute time-consuming microbial analysis and nervous system disorders, e.g. Parkinson's disease.

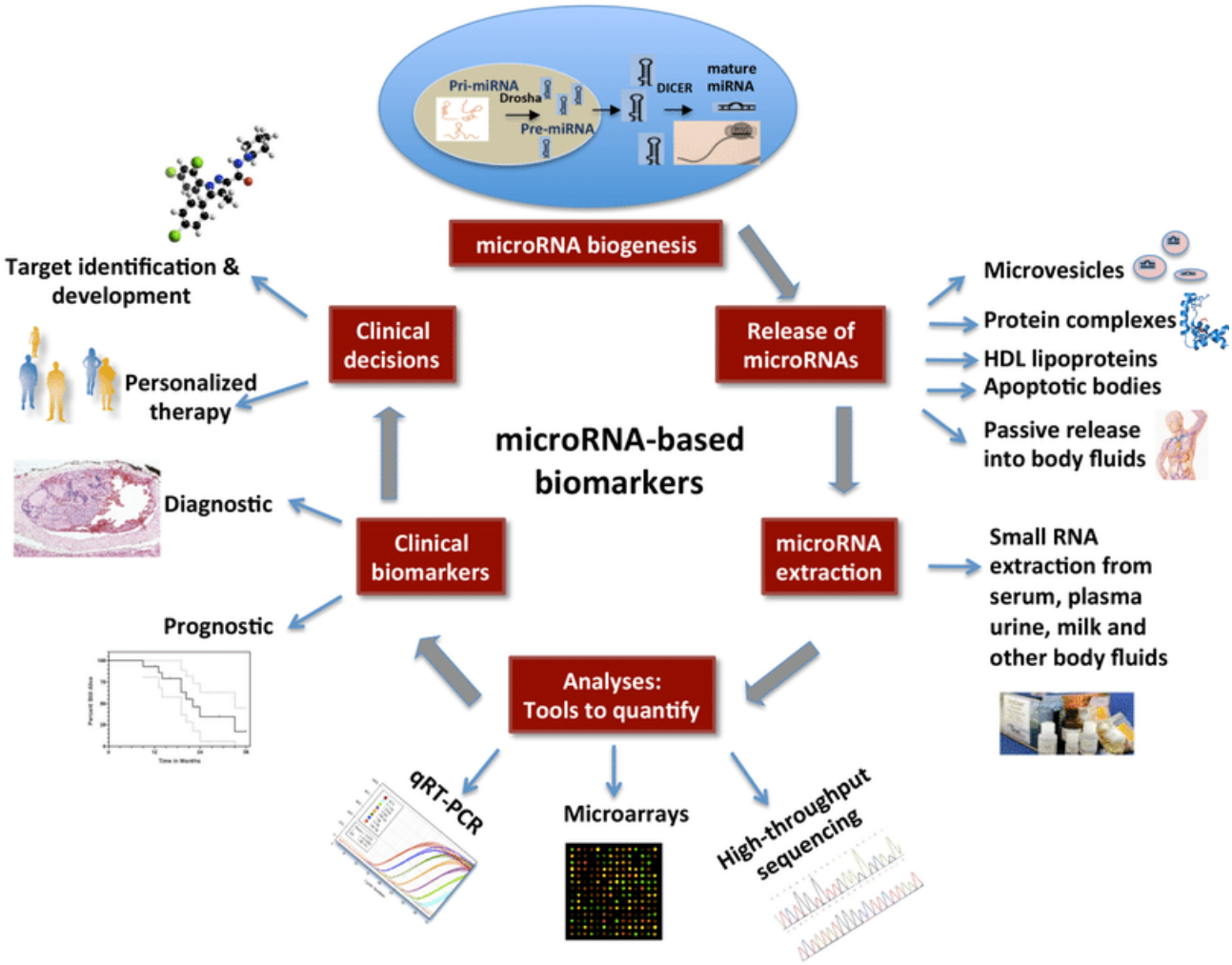


*Figure 1.3 Circulating miRNAs as biomarkers: A schematic diagram showing miRNA biogenesis, modes of their secretion into body fluids, RNA extraction and quantitative approaches.*[1]

Despite the promising nature of miRNAs as biomarkers for several important diseases, challenges do exist as a developing field of research with undefined levels of OncomiRs and tumour suppressor miRNAs. This inflection in the up-/down-regulated levels of miRNAs is due to different parameters such as gender, ethnicity, age, stage of cancer and lifestyle. Therefore, reproducible data on clinically relevant levels in body fluids and the specificity of that miRNA for the disease needs to be defined. Recently, a thorough analysis of the

literature aimed at the applicability of miRNAs in the medical field was made by Condrat et al., where they elaborate on the role of miRNAs in the diagnosis and prognosis of different diseases.[46]

The main challenge is in developing accurate, easy-to-use, cost-effective and high-throughput methods for analyzing a large number of samples to define the levels and confirm the observations from a preliminary study. For example, a miRNA can be dysregulated depending on the severity of the disease and data from detection in a large sample size would give clarity on the levels at each stage of the disease. The following section gives a brief description of current standard techniques used to detect, profile and quantify miRNAs with their advantages and disadvantages.

## 1.4 Molecular diagnostic tools for circulating miRNA

The use of circulating miRNA for the diagnosis and prognosis of diseases depends on the reliable quantification of miRNA efficiently and cost-effectively. There are three steps involved in miRNA analysis: (i) sample collection and handling, (ii) miRNA extraction and (iii) detection and profiling of miRNAs. However, the short length of miRNA is a key challenge for creating a reliable assay to profile and quantify them. The selectivity of miRNA detection is further hindered by high sequence homology amongst miRNAs belonging to the same class (including the ones with only a single base variation).[47]

The three most frequently used methods for detection of miRNAs are reverse transcription-quantitative PCR (RT qPCR, for quantification), high-throughput sequencings such as next-generation sequencing (NGS, for profiling) and microarray technologies (for profiling and quantification). Each of these methods has its pros and cons and the choice of method depends on the aims of the study.[48] Apart from the most conventionally used methods, amplification-based assays based on enzyme-assisted replication, digestion, or enzyme-free strand displacement processes, for example, rolling circle amplification (RCA), hybridization chain reaction (HCR), loop-mediated isothermal amplification (LAMP), exponential amplification reaction (EXPAR) are also currently on the market.[49]

### 1.4.1 Reverse transcription qPCR (RT-qPCR)

Quantitative polymerase chain reaction (qPCR) is the gold standard technique for quantification of miRNAs with standard commercial assays. While the short length of mature miRNAs and the similarities between the miRNAs of the same family pose several challenges for PCR, many methods have taken advantage of the reverse transcription (RT)

step to facilitate amplification and quantification and RT-qPCR is utilized independently and for validating results acquired from microarrays and NGS. The principle of RT-qPCR involves two steps: (i) synthesis of complementary DNA (cDNA) via RT using RT primers and (ii) amplification and detection of the products using Taqman or fluorescent intercalating probes.[50] The RT primers designed can be universal or specific for transcribing miRNAs and additional sequences (used for amplification due to the short length of the target miRNA).[51] Designing primers for short miRNAs is challenging since a typical miRNA has only ~22 bases that are approximately the same length as a typical PCR primer. Several strategies have been developed to overcome this issue and aim for enhanced specificity.

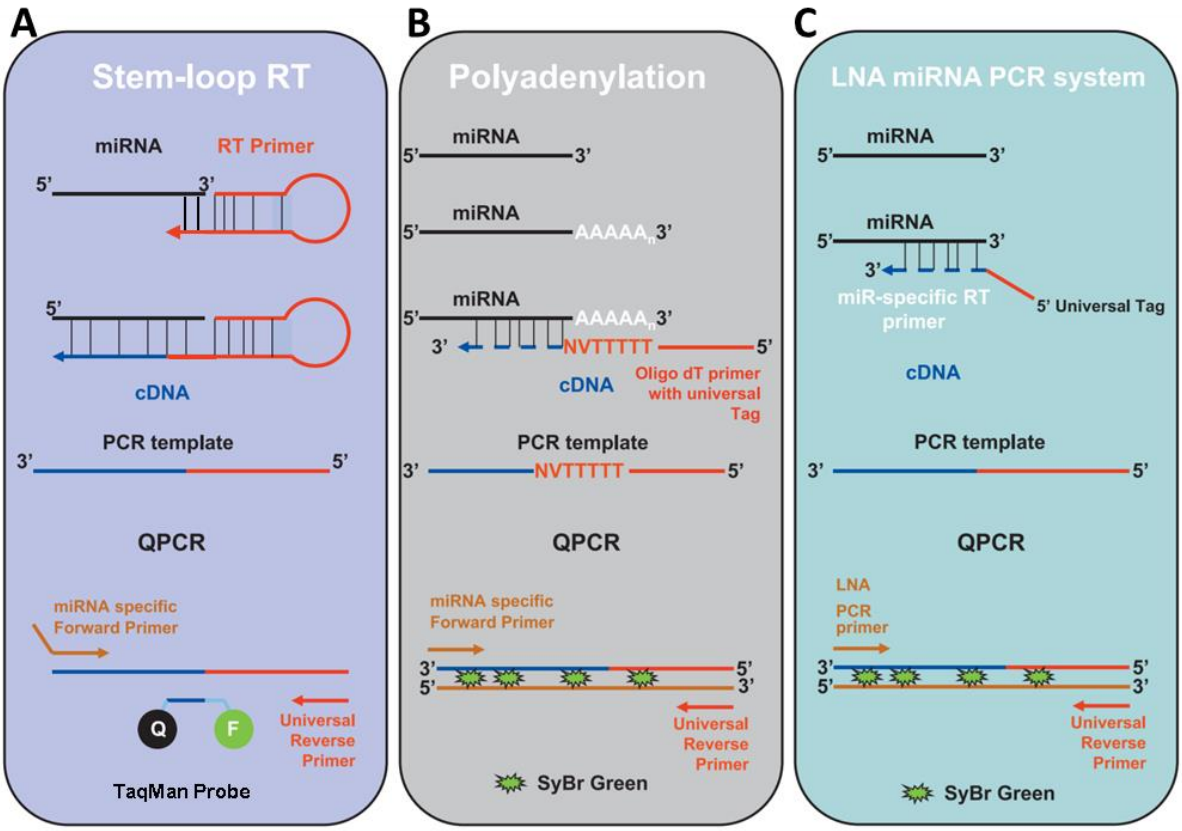


*Figure 1.4 Schematics of commonly used RT-qPCR techniques. (A) Stem-loop RT-qPCR; (B) Poly(A) tailing RT-qPCR; (C) RT-qPCR with locked nucleic acids.[3]*

The stem-loop RT technique (Figure 1.4 A) involves an RT primer with a stable stem-loop structure (which is later disrupted by a universal reverse primer). This is followed by amplification with a specific forward primer, a TaqMan probe (for detection) and the universal reverse primer.[52, 53] Unfortunately, there is reduced control on the specificity when using stem-loop RT-qPCR. The TaqMan probe binds to a part of the cDNA sequence (PCR template) that originates from the RT primer. If the RT primer binds to another

sequence than the miRNA of interest, it will make an unspecific PCR template and the PCR amplicon, which will generate the fluorescent signal due to the TaqMan probe.[54]

Another way to reverse transcribe is to add a poly (A or U) tail to the 3'-end of miRNAs and then reverse transcribe with a tagged poly(T) primer (Figure 1.4 B). This is followed by amplification with a miRNA-specific forward primer, a universal reverse primer, intercalating with fluorescent dyes. Since only one specific primer is used here, specificity still could be an issue.

Locked nucleic acids (LNA, nucleotide analogs that are constrained in the ideal conformation for Watson-Crick binding) offer a more rapid and stable pairing with the complementary nucleotides thus increasing the melting temperature (*T*m) and specificity (Figure 1.4 C). However, the amplification efficiency is compromised in this case.[55]

Though RT-qPCR is a powerful diagnostic tool for quantifying miRNAs, there are several limitations. Firstly, quantitation depends on external reference or standard material, and for effective quantitation by qRT-PCR, precise determination of the reference/standard is needed. Secondly, it is time-consuming and requires careful designing of primers, bulky and expensive thermocyclers and charge-coupled devices for detection and is not suitable for point-of-care (POC) testing. Third, very low concentrations of miRNA in body fluids might affect the yield in samples after the NA extraction step. This might affect the sensitivity of quantification and result in false negatives. Despite these challenges, RT-qPCR remains the standard for miRNA quantification, and over the past decade, there has been steady progress in developing more sensitive RT-qPCR techniques. New subtypes of RT-qPCR such as digital droplet PCR or digital RT-qPCR, and microfluidic chip-based digital PCR, are being developed to improve sensitivity and lower the detection limit of the conventional RT-qPCR.

Digital droplet PCR (ddPCR) or digital PCR (dPCR) techniques can target quantities in samples well below the limit of conventional qPCR methods.[56] Here, measurements are made by partitioning the sample into fractions or droplets with at least zero or one or more miRNA in each fraction. Each fraction is amplified with RT-qPCR for the presence (positive) or absence (negative) of targets and detected via fluorescence signal. The exact number of miRNAs present in the sample is calculated using Poisson's distribution, thus eliminating the need for standard curves.[57] Overall, ddPCR is a better choice for absolute quantification of miRNA, and more miRNAs should be tested robustly with controls to better define their clinical application.

### 1.4.2 Next-generation sequencing

Next-generation sequencing for miRNA profiling defines the nucleotide sequence and the concept involves the ligation of sequencing adapters (short nucleic acid strands) to the size-selected miRNA molecules, followed by RT to cDNA. Then, the corresponding cDNA fragments are filtered out (electrophoresis) for successive sequencing.[58] The output of a miRNA-NGS will generally consist of millions of short reads that are analyzed to eliminate low-quality adapters and sequences. Then, numerous data preprocessing steps and mapping reads onto the genome reference sequence using specific software are needed to isolate the relevant information.[59] NGS advantages include large processing capacity and millions of sequences read in parallel in a few days, yielding accurate, thorough and complete analyses of all miRNAs. The downside is that NGS is expensive for routine laboratory work and demands computational infrastructure, thus, incompatible with the POC detection of miRNA.

### 1.4.3 Microarray platforms

Nucleic acid-based microarrays are useful for high-throughput detection and profiling tools for miRNAs skipping the tedious amplification steps, thus saving overall run-time. While variable microarray approaches are being developed for miRNA profiling and quantification, the principal concept remains the same; hybridization between the target miRNAs with their complementary probes (a detailed flowchart of the miRNA profiling process using microarrays is given in Figure 1.5).[60] With many advantages such as low sample input, benchtop setup, minimal run-to-run inconsistency and laborious pipetting, microarray platforms do have limitations such as comparatively high cost and low sensitivity due to low abundance of miRNa in each spot. They are generally used for comparison between two or more miRNA groups and cannot be used for absolute quantification. Because of its limited specificity, data obtained are typically validated by a qRT-PCR. Also, it can only identify known miRNAs unlike NGS.[61]

When it comes to the need for POC diagnostics, RT-qPCR and microarrays are more sensible choices. However, the requirement of a thermocycler and a scanner increases the price and requires specialized settings and highly skilled personnel. In general, PCR-based methods require sample preparation and, after the analysis, data normalization, which complicates interpretation and may generate inconsistency in data sets. Most of them use fluorescence as the detection platform. Other principally different detection techniques on the market are based on colourimetry,[62] chemiluminescence,[63] surface-enhanced Raman scattering (SERS),[64] and electrochemistry.

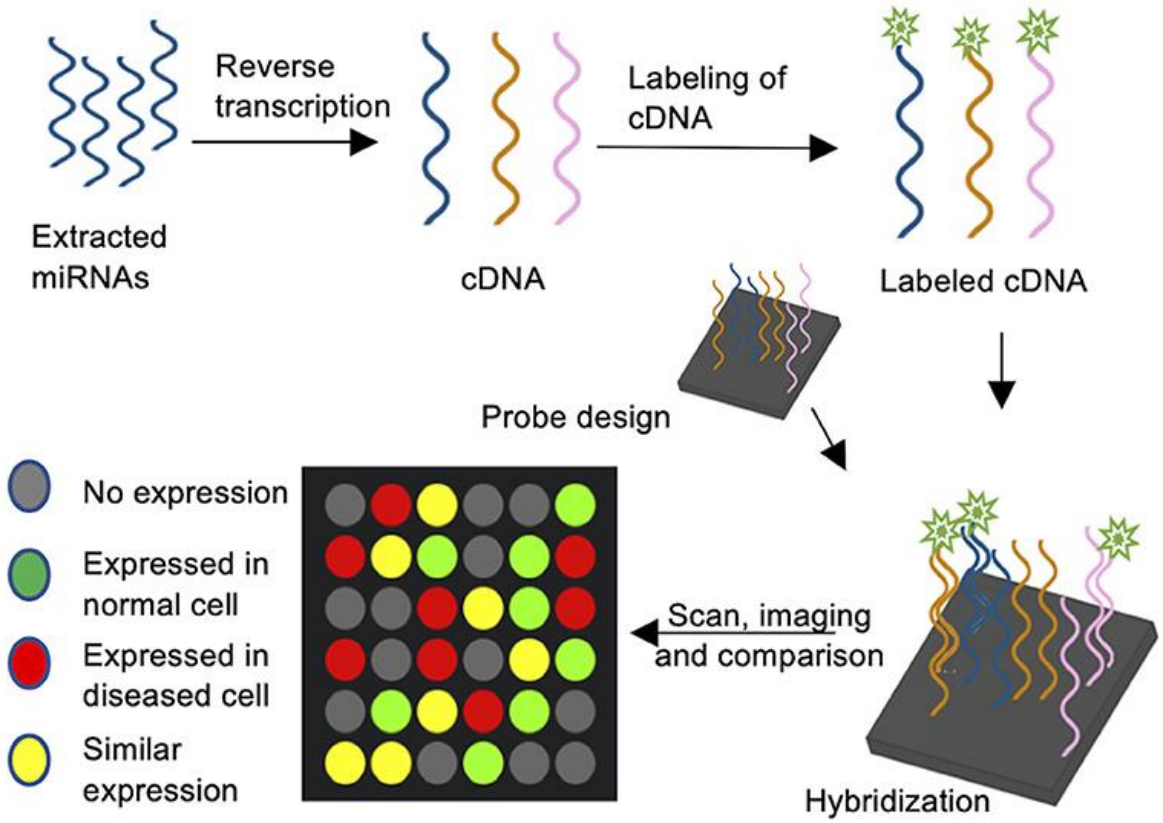


*Figure 1.5 MiRNA Microarrays. cDNA is synthesized by reverse transcription of extracted miRNAs and the cDNAs are subsequently labelled with e.g., a fluorophore tag. Oligonucleotide probes complementary to target miRNAs are spotted on a carrier plate and the fluorescently labelled cDNA is hybridized. The signal intensity corresponds to miRNA abundance.*

However, there is a dire need for the development of low-cost detection strategies with high efficiency useful for rapid tests or clinical checks. New techniques for miRNA detection and quantification are constantly developing and evolving to address the challenges in miRNA detection research, such as cost-effectiveness, sensitivity, specificity, and standardization. Electrochemical detection is a promising alternative to today's well-established methods due to its high sensitivity, fast response, and adoption of simple instrumentation that can be efficiently transferred to smaller and portable handheld devices due to micro-electronics technology. The following sections will describe the position of electrochemical and PEC platforms in miRNA detection and the gap(s) in this research field toward a robust detection platform.

## 1.5 Electrochemical and PEC miRNA detection

Despite steady progress in the field of DNA-based testing platforms, POC miRNA detection/quantification is still in the preliminary stages and calls for further advancement.

Looking back, research in the field of miRNA detection, in general, has been constantly expanding in the past decade (Figure 1.6), of which 10% of the research publications concerning "miRNA detection" involve electrochemistry. This can be attributed to challenges in realizing high-throughput detection and, because of miRNA's small size, low natural abundance, and a high degree of sequence similarity among family members. When compared to optical-based methods, electrochemical sensors offer many advantages in terms of sensitivity and scalability, thus miRNA can be directly detected in clinical samples without any amplification.[65] Moreover, PEC sensing approaches have emerged in recent years and have attracted increasing interest from the scientific community, approaching regular electrochemical techniques in the number of publications (Figure 1.6).

With continuous technological evolution and miniaturization (for example, from solid-state disk electrodes to disposable sputtered microelectrodes,[66] thanks to the microfabrication technology), electrochemical sensors have shown increasing potential in the detection of miRNA.

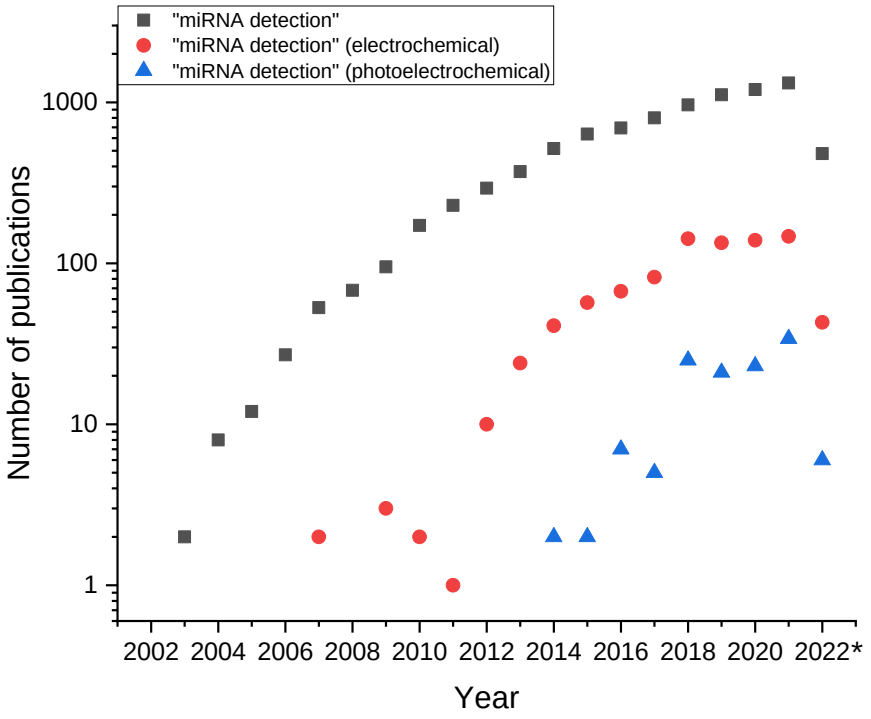


*Figure 1.6 Web of Science™ search report showing number of articles published on overall "microRNA detection OR miRNA detection" and refined within "electrochemical" and "photoelectrochemical" search terms in the past 19 years (*data obtained in July 2022).*

### 1.5.1 Electrochemical platforms for miRNA detection

Typically, an electrochemical nucleic acid sensor comprises two key components: (1) an electrode with short, single-stranded DNA/RNA probes, which can specifically hybridize with the target nucleic acid sequences, and (2) an electroactive hybridization indicator that translates the hybridization signal into the measurable current (amperometry, voltammetry) or charge accumulation (potentiometry).[67] Existing electrochemical methodologies can be grouped according to the redox (reduction/oxidation) principle, how the signal is obtained and the amplification of the signal (Table 1.4). Out of the different architectures, the redox indicators as labels, intercalators, or free indicators have been used for miRNA detection. In addition, multiplexed detection of more than one miRNA in a sample is more beneficial and achievable with the labelled probe sequence methodology, compared to the other mentioned approaches.

*Table 1.3 Electrochemical methodologies for the detection of miRNA.*

| Electrochemical methodology | Properties |
|---|---|
| **Electroactive labels** | • Direct redox current response related to the signal variation (signal ON/OFF) after the miRNA hybridization.[4, 68]<br>• Redox molecule labelled to the probe through a linker such as nanomaterials, polymers, streptavidin, microparticles leading to signal amplification (signal ON).[69-71] |
| **Electroactive intercalators** | • A redox molecule or a complex of redox molecules intercalate into the nucleic acid with different affinities depending on the presence/absence of the target miRNA.[72, 73] |
| **Catalysts** | • Enzymes,[74-76] chemical catalysts,[77, 78] and DNA[78-80] lead to obtaining electroactive species detected electrochemically. |
| **Label-free sensors** | • An electrochemical response is based on electrostatic repulsion or interaction depending on the redox-free labels.[81-83] |

The labelled DNA probes may well be utilized in different constructions providing a decrease (ON-OFF signal) in the current response after a change in its confirmation or removal of the labelled probe sequence following hybridization with the target, thus preventing the electron transfer step (Figure 1.7, A & B). It is also possible for an increase in current response (OFF-ON signal) with the use of a secondary probe labelled with a redox molecule or two-probe labelled sequence (Figure 1.7, B & C). Electrochemical sensors

based on these labelled probes have straightforward assay steps and are easy to scale up since the label-coupled probes and intercalators are commercially available. When combining these labelled probes architecture with amplification techniques, the sensitivity of the sensing strategies can be greatly increased while keeping the platform cost-effective and minimal.

There are sufficient review articles in the literature offering a comprehensive overview of the current developments in electrochemical biosensors for miRNA and listing different approaches to the detection of miRNA.[65, 84-87] Especially, Sfragano et al., have summarized the recent advancements in the field and have given an account of the various approaches to overcome obstacles in miRNA detection mentioned earlier.[85] Gillespie, P et al. surveyed the latest development of electrochemical sensors combined with amplification. [65] Low et al., have summarized the recent advances in nanomaterial-based electrochemical biosensors for the detection of different types of miRNAs.[87]

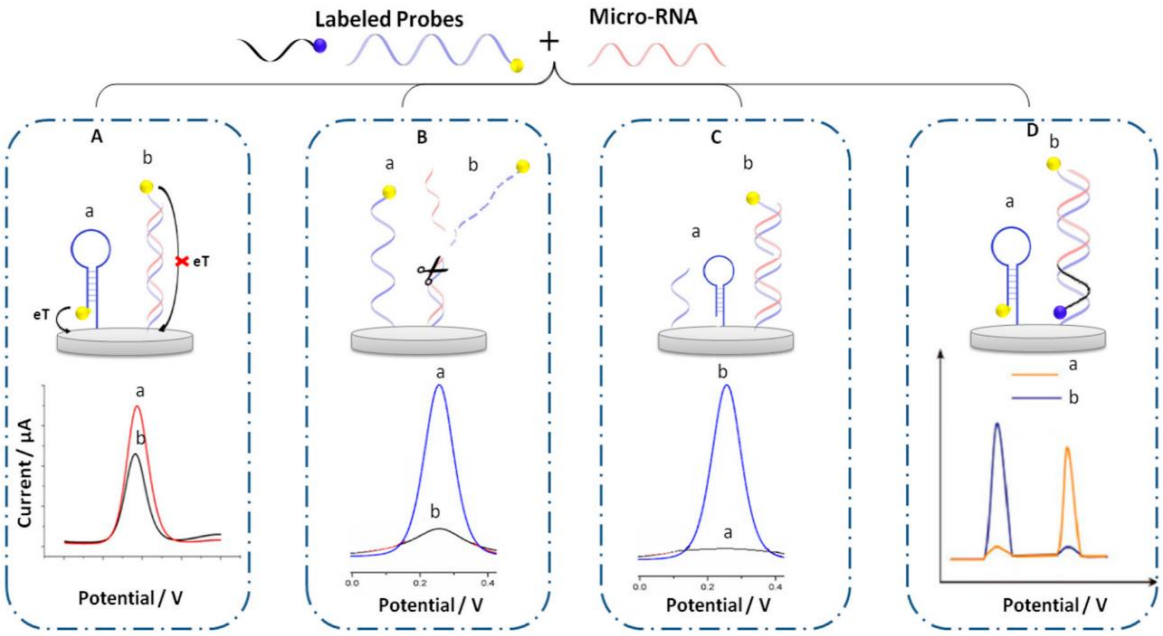


*Figure 1.7 Different architectures of labelled probes before and after hybridization with target miRNA. (A) Hybridization of target DNA increases the electrode-label distance leading to decrease in the response. (B) Decrease in response based on the elimination of the labelled probe in the presence of target. (C) Sandwich approach with a capture probe (immobilized on the electrode surface) binding to a part of the target and detection probe (with label) to bind to the other part of the target. (D) Approach with two probes labelled with different labels, one placed near the electrode surface electrode (yellow) and the second far from the surface (blue). On binding to the target, the signal from the blue label increases because it becomes closer to the surface and the one from the yellow label decreases. Voltammograms 'a' and 'b' indicate the responses before and after hybridization respectively.*[4]

In general, electrochemistry offers a valuable diagnostic tool owing to its low cost, miniaturization capability and mass production potential compared to other detection

techniques. There are however some challenges to meet before a robust, portable, and user-friendly POC electrochemical biosensor for clinical miRNA detection becomes a reality. Moreover, the targeted LOD for miRNA quantification in human samples (≤ nM) was only achieved with enzymes as labels, which possess serious drawbacks such as instability, irreproducibility of their reactivity and the need to add reagents (e.g. $H_2O_2$), next to multi-step bioassays (restricting use by non-specialists), impeding the technology's market entry. Additionally, because of these challenges, to the best of our knowledge, there is no electrochemical miRNA sensor on the market to date. Thus, further research should be dedicated to simplification of the assay steps, time, validation, and commercialization of the technology.

### 1.5.2 PEC platforms for miRNA detection

PEC biosensors are promising platforms for detecting biomolecules owing to their low background noise due to the separation of the excitation source (light) and detection signal (current), thus offering excellent sensitivity.[88] The inherent low cost of electrochemical instrumentation makes the PEC method easy-to-use, rapid and cost-effective compared to its optical counterparts such as fluorimeters which need bulky and expensive excitation sources and detectors,[89] thus directing our research trajectory towards the validation of electrochemical technology discussed in the previous section.

At the start of this Ph.D. research (2016), fewer than ten research articles on PEC detection of miRNA were published (Figure 1.6). Lately, due to the growth of new detection schemes and novel photoactive molecules (molecules that are either electroactive when photoexcited or those that indirectly initiate a PEC response), this field has received rising interest in protein biosensing and as well as nucleic acid recognition through different hybridization assays. However, only 125 articles were published on "microRNA detection" or "miRNA detection", refined with the "photoelectrochemical" search term since 2014 in Web of Science™ as of July 2022 (Figure 1.6). Table 1.5 summarizes the common trend in research publications on PEC miRNA detection in a recent couple of years. Most of those works involve complicated fabrication steps with nanomaterials and sophisticated amplification techniques. Though there are many photoelectroactive materials and semiconductor nanomaterials, where particularly inorganic semiconductor nanomaterials prominently have been reported (likely due to the boom in the semiconductor industry). N-type semiconductors such as $TiO_2$, CdS, CdSe and p-type semiconductors such as NiO, BiOI, $Cu_2O$ are widely used, as such or in different structural forms in PEC platforms.[90]

Adding to photoactive components, signal amplification also dictates the performance of PEC sensing, especially when detecting very low concentrations of miRNA present in biological samples. Numerous signal amplification strategies have been developed to facilitate improved sensitivity of PEC systems. The enhancement or amplification of the signal from low concentrations of miRNA target can be brought about using enzymes, nanomaterials, oligonucleotides and a combination of these.[91] For instance, Sui et al. enhanced the PEC response by using carbon quantum dots modified with phenylboronic acid and 2-D nanomaterial tungsten disulfide.[92] Isothermal amplification of nucleic acids strategies based on catalytic hairpin assembly (CHA), strand-displacement amplification (SDA), target-triggered rolling circle amplification (RCA), hybridization chain reaction (HCR) and loop-mediated isothermal amplification (LAMP) are also used to construct sensitive PEC biosensors.

*Table 1.4 Recent examples of PEC platforms for miRNA detection.*

| Target | Platform | Amplification and detection strategy | LOD | Analysis matrix | Ref |
|---|---|---|---|---|---|
| miRNA-21 | Target-triggered self-assembly of energy band position-matched cadmium selenide nanoparticles (NPs) and carbon nitride nanosheets on glassy carbon electrode (GCE) with hairpin oligonucleotide probes | Target triggered catalytic hairpin assembly (CHA) reaction | 92 aM | Serum | [93] |
| miRNA-122 | Z-Scheme Heterojunctions of Zinc defective cadmium sulfide (CdS)/zinc sulfide (ZnS) NPs on GCE | Exonuclease III (Exo-III)-assisted signal amplification | 3.3 aM | Serum | [94] |
| miRNA-21 | CdS NPs-modified carbon cloth (CC) on polyimide (PI) film flexible electrode. Probe attached via carboxylic-amino group amidation reaction | CHA, hybridization chain reaction (HCR), and alkaline phosphatase (ALP) for catalyzing the generation of ascorbic acid (AA) which undergoes redox cycling at the electrode | 0.41 fM | Serum | [95] |
| miRNA-141 | Au NPs@g-C3N4 coated on GCE; Probe attached via Au-S bond | T7 exonuclease involved target cycle amplification process | 0.3 fM | Serum | [96] |

| | | | | | |
|---|---|---|---|---|---|
| let-7a miRNA | BiOI-Bi/CNTs photocathode | Target recycling strand displacement amplification (TRSDA) and detection using $K_3[Fe(CN)_6]$ | 0.1 pM | HeLa cells | [97] |
| miRNA-21 | Au deposited, NaKCN-MB/GCE; Probe attached via Au-S bond | Dual catalytic hairpin assembly (dual CHA) and enzyme cascade catalysis amplification | 0.03 fM | - | [98] |
| miRNA-21 | BiVO4 modified ITO electrode | Rolling circle amplification and methylene blue embedded in dsDNA | 0.3 fM | MCF and HeLa cells | [99] |
| miRNA-141 | Polarity-switchable system using CdS quantum dots (QDs) and 5,10,15,20-tetrakis (4-aminophenyl)-21H,23H-porphine (Tph-2H)-coated GCE | Enzyme-assisted recycle amplification reaction | 0.33 fM | Serum | [100] |
| miRNA-244 | ITO/CdS/MB-DNA/MCH electrode | "Y"-shaped junction structure via hybridization between DNA sequence quenches the signal thus making it a signal OFF sensor | 0.02 fM | Serum | [101] |
| miRNA-133a | A near-infrared light (NIR)-initiated PEC biosensor based on Core–Shell–Shell structured NaYF4:Yb,Tm@NaYF4@TiO2 @CdS | Hybridization chain reaction and a redox circle signal amplification strategy along with magnetic beads | 36.1 aM | Serum | [102] |

| | | | | | |
|---|---|---|---|---|---|
| miRNA-141 | Paper-based electrode with pyramid-like $Cu_2O$ on Au NPs-functionalized tangled cellulose fibers network with $BiVO_4$–$Bi_2S_3$ heterostructures and DNA dendrimers | Multiple-branched hybridization chain reaction (MHCR) and y catalytic the decomposition of $H_2O_2$ | 0.17 fM | human breast cancer cells, human prostate carcinoma cells and human colon cancer cells | [103] |
| miRNA-143 | ITO/ZnO/CdS photoelectrode | Synergy of G4/hemin catalyzed consumption of $H_2O_2$ and dopamine, λ-Exo facilitated target recycling reaction and the inner filter effect | 65 fM | Serum | [104] |
| miRNA-21 | Dual-functional β-CD@CdS nanorod/WS2 nanosheet heterostructures with avidin-CuO NPs | Cyclic strand displacement reaction mediated $Cu^{2+}$ quenching | 25.1 aM | Serum | [105] |

## 1.6 Singlet oxygen-based PEC sensing

Recently, our research group reported a novel singlet oxygen-based PEC sensing ($^1O_2$-based PEC sensing) approach inspired by the advantages of enzymes and PEC sensing, namely the integration of aerobic photocatalysis and electrochemical analysis. Compared with enzymatic detection methods, the proposed strategy uses air instead of internally added reactive reagents and features intrinsic baseline correction via on/off light switching.[106] A type II photosensitizer (PS) that generates singlet oxygen ($^1O_2$) upon illumination is used as a bioinspired catalyst in this approach, oxidizes analytes, yielding electrochemically-detectable products while resisting the oxidizing species it produces. A general possibility of PEC detection of a specific oligonucleotide linked to pheophorbide a, a type II PS is known to generate $^1O_2$ under red light illumination was also explored in this work.

### 1.6.1 PS as light-responsive labels for $^1O_2$-based PEC sensing

Light-responsive labels are agents which are involved in vivo/ in vitro/ ex vivo visualization, characterization and measurement of biological processes at the molecular and cellular levels.[107] They are commonly used to detect particular components of complex biomolecular assemblies offering high sensitivity and selectivity. Upon illumination with light, these labels, being PS, can absorb light and undergo energy transfer reactions. Figure 1.8 graphically illustrates this process.

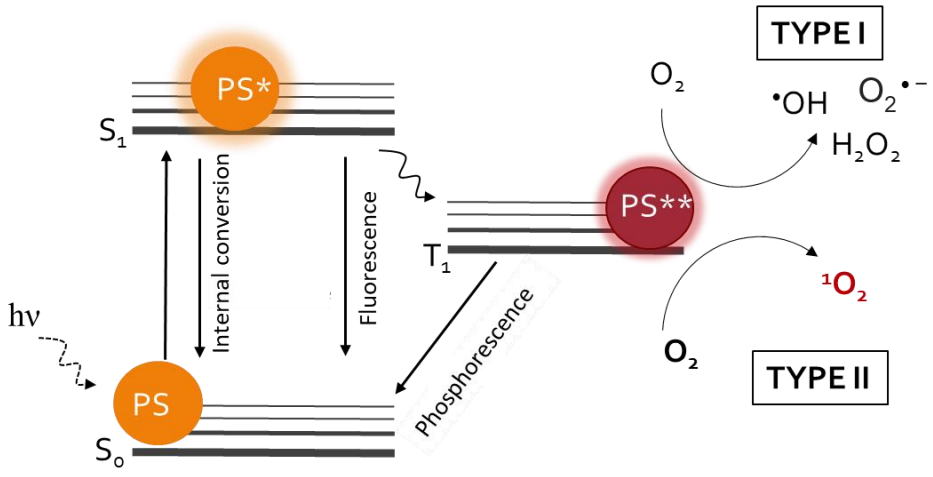


*Figure 1.8 Jablonski diagram illustrating different photophysical and photochemical pathways of light excited PS.*

Following the absorption of light, these PS are electronically excited to the short-lived (nanoseconds) first excited singlet state ($S_1$). From this unstable singlet state, the excited PS can (i) relax back to the ground state by emitting heat (internal conversion) or (ii) light (fluorescence) or it can (iiI) rapidly invert to form the relatively long-lived (microseconds) excited triplet-state ($T_1$) via inter system crosslinking. The excited triplet PS can relax to the ground state ($S_0$) by loss of energy by emitting light (phosphorescence) or undergo two kinds of reactions in the presence of $O_2$, namely, type I and type II photosensitization reactions. The type I reaction mechanism leads to the production of superoxide ($O_2^{\bullet-}$) by electron transfer from the triplet PS to $O_2$. Further, reactive oxygen species (ROS) such as hydroxyl radical ($HO^{\bullet}$), peroxides (ROOR) and hydroperoxides (ROOH) are also produced. Whereas the type II mechanism involves the reaction of the triplet PS with $O_2$, producing $^1O_2$. [108]

In $^1O_2$-based PEC sensing, $^1O_2$ can either undergo subsequent reduction at the surface of the electrode or initiate a redox cycle in the presence of a phenolic substrate (e.g. hydroquinone, HQ).[106] Our focus is to use these type II PS as labels coupled to DNA sequences like fluorescent labels. Though the relationship between the chemical, optical and photosensitizing properties of every PS is not always clear, the photo-electrochemical responses of these PS depend on their ability to produce $^1O_2$ via type II photosensitization mechanism ($^1O_2$ quantum yield, $\Phi_\Delta$) in measuring conditions, irrespective of their fluorescence nature (fluorescent quantum yield, $\Phi_F$).

### 1.6.2 Rationale and positioning $^1O_2$-based PEC sensing with the state-of-the-art nucleic acid biomarker analysis in cancer

This Ph.D. work aims to elaborate an original detection strategy based on the concept of catalytic signal amplification, low-cost mass-produced sensing platforms, and high sensitivity of PEC sensors. Despite the focus on miRNA in this thesis, the suggested detection strategy can be expanded to detect other cf-NAs. Importantly, the analytical performances of the optimized method were assessed in buffer, commercial serum and real clinical samples to prove the principle applicability of the developed sensing platform in real samples for possible cancer diagnosis, therapeutic management and treatment follow-up.

Currently, the available routine cfNA biomarker detection methods in the market are quantitative PCR (qPCR) and digital droplet PCR (ddPCR), and DNA next-generation sequencing (NGS) which are PCR- and sequencing-based, respectively. Moreover, fully automated but closed systems for PCR-based molecular testing, such as Idylla (BioCartis),

recently entered the market. However, these established technologies come with significant challenges: high cost (device and consumables), complexity, requiring specialist knowledge, low miniaturisation potential and limited accessibility (especially for small hospitals). Additionally, for NGS, sample preparation is highly complex with time to result up to 5 days.

Our $^1O_2$-based PEC sensing platform is designed to overcome challenges presented by standard PCR and electrochemical techniques due to combined actions of (i) PS that produce $^1O_2$ upon illumination; (ii) capture and detection NA probes; (iii) redox reporters; and (iv) magnetic beads. The developed platform is highly sensitive, robust, fast, easy to set up and allows for re-use. The essential elements that allow $^1O_2$-based PEC sensing to go beyond the state of the art encompass: (i) the introduction of a light-induced, $^1O_2$ -mediated electrosensing with a high signal-to-noise ratio due to light illumination; (ii) the optimisation of the balance between sensitivity and specificity of PEC detection by NA probe design.

Today, molecular testing on liquid biopsies via PCR technologies is not yet integrated into the standard practice for cancer diagnosis and therapeutic management because of its high cost, low sensitivity, and lack of clinical validation of liquid biopsies. $^1O_2$-based PEC sensing will offer a technology to perform molecular testing on both tissue and liquid biopsies, facilitating the implementation of liquid biopsy analysis for cancer diagnosis. Ultimately, $^1O_2$-based PECsensing will contribute to more affordable, faster, sensitive and accessible molecular testing, allowing for faster and cost-efficient cancer diagnoses and more specific treatment, saving lives in the longer term.

## 1.7 Overview of the thesis

The main objective of the Ph.D. research is to develop an easy-to-use, low-cost and robust platform for the fast detection and quantification of miRNAs using photoelectrochemistry. This was achieved by creating and developing innovative PS-based PEC concepts, using commercially available PSs producing $^1O_2$ as molecular labels for efficient nucleic acid detection. The first part of the thesis introduces the fundamental research concepts on the development of the platform for sensing using short oligonucleotides, while the second part elaborates on the application of the fundamental knowledge in detecting PCa miRNAs. A detailed description of all the chapters in this thesis is given below along with a schematic overview in Figure 1.9.

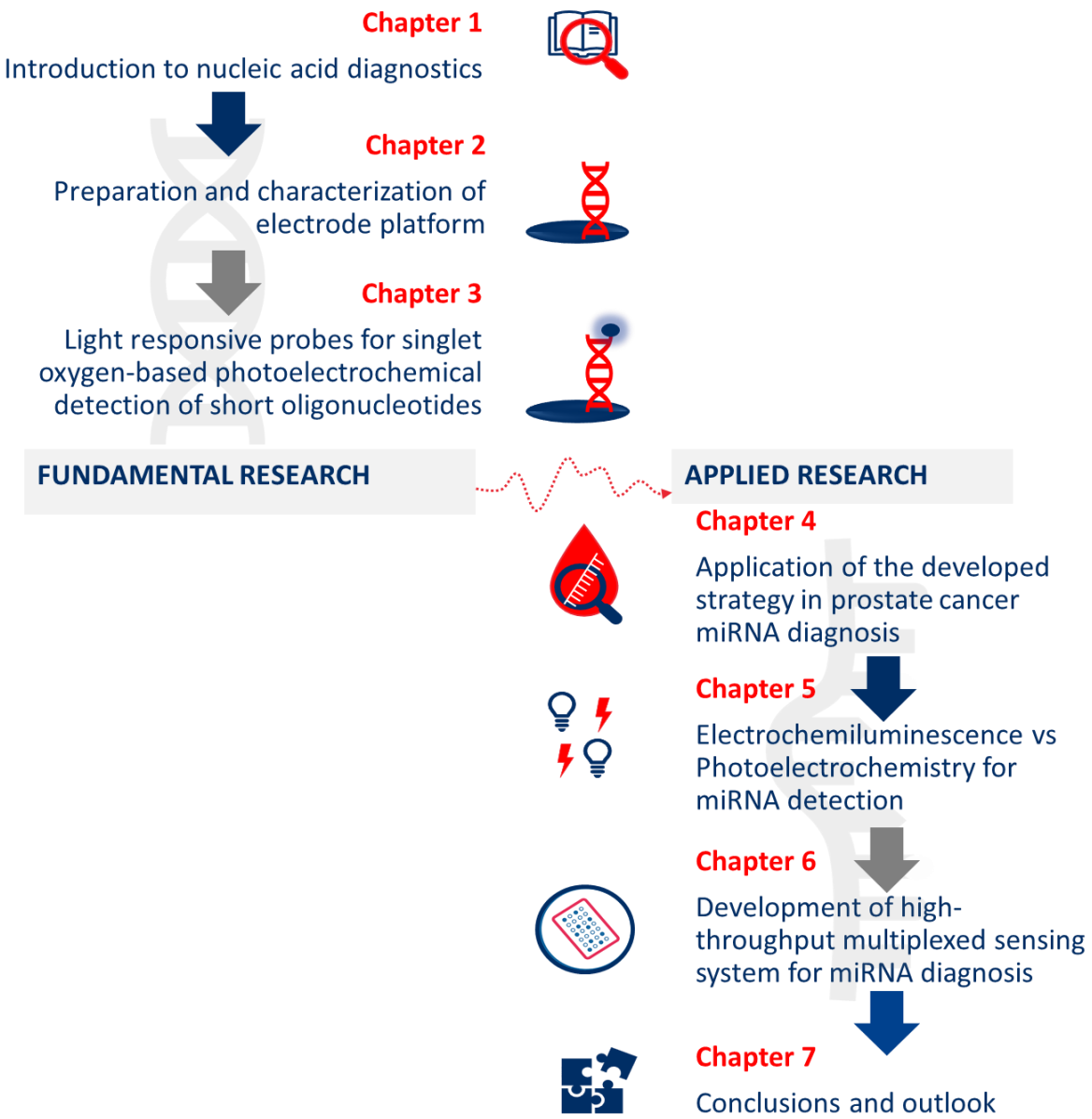


*Figure 1.9 Schematic overview of the Ph.D. research.*

After a short introduction to nucleic acid diagnostics in **chapter 1**, **chapter 2** describes the first essential step of the PEC sensor development; the quest for an easy-to-use and efficient electrode platform avoiding all the complicated fabrication steps that are presented in the previous literature on electrode platforms for miRNA detection. Since DNA is more stable than miRNA, DNA as a model target was used and the practical aspects of developing and preparing a miniaturized sensing platform using gold-sputtered three-electrode planar structures were investigated. We have elaborated on the surface preparation and proper immobilization approaches for tethering DNA probes on thin-film

planar gold electrodes. For this aim, we compared several cleaning protocols and two strategies for the immobilization of a thiolated oligonucleotide (i.e. attachment through conventional chemisorption and the potential pulse-assisted immobilization). Specific attention was paid to a side-by-side comparison of thiol-specific attachment and weak unspecific adsorption of oligonucleotides, as well as the hybridization performance of the probes. This chapter introduces the essential toolbox for cleaning and modification of novel planar three-in-one gold-sputtered electrodes as the cost-efficient transducers for miRNA sensors.

**Chapter 3** deals with the next step in this PEC research, which would be to select PSs for labelling the target oligonucleotides. Fundamental research on a series of generally known light-responsive DNA probes (DNA sequences labelled with chromophores) to assess their ability to generate a photocurrent upon illumination was carried out. More specifically commercially available chromophores were chosen and linked to DNA with absorbance maxima nearly matching the wavelengths of commonly available diode laser pointers. The chromophore's ability to produce $^1O_2$ upon photoexcitation was utilized and subsequent photocurrent response was studied. Type I, fluorescent and type II PSs were studied using diode lasers at 406 nm blue, 532 nm green, and 659 nm red lasers in the presence and absence of a redox reporter, hydroquinone (HQ).

The fact that the type II photosensitizing mechanism is essential for chromophores to generate a photocurrent in the taken conditions, presumably due to the electrochemical reduction of $^1O_2$ at the applied potential of −0.05 V vs SCE was confirmed. Following this, The PEC activity of the chromophores with their extinction coefficients was correlated and the relative $^1O_2$ quantum yields of the used chromophores in our experimental conditions were assessed employing an independent method, i.e. the spectrophotometric monitoring of furfuryl alcohol (FFA) as a $^1O_2$ trap. A strong link between the chromophore's ability to produce $^1O_2$ and the recorded photocurrents was established. The analytical performance of the sensing system was evaluated using a magnetic beads-based DNA assay on disposable electrode platforms, with a focus to enhance the sensitivity and robustness of the technique in detecting complementary DNA targets.

Following the fundamental study of using $^1O_2$-producing chromophores as labels for oligonucleotide detection, the next focus will be to apply this concept to medical diagnostics. **Chapter 4** presents the application of the developed strategy for a PCR-free, portable, and sensitive $^1O_2$-based PEC quantification of miR-145 and miR-141, two miRNAs related to PCa, in collaboration with Centro Hospitalar do Porto, Portugal. The influence of various working parameters on assay performance and analytical performances in buffer

and the ability of the system to detect miRNAs in relevant sample matrices such as plasma and serum were studied. Successful quantification of pM levels of miRNA-141 and miRNA-145 in plasma samples from PCa patients (obtained from Centro Hospitalar do Porto, Portugal) was achieved confirming the applicability of this technology in clinical diagnostics aiding cancer prognosis and treatment follow-ups.

In **chapter 5**, two different oligonucleotide-based assays for the selective and sensitive detection of a circulating miRNA were developed and compared to position the performance of our developed PEC strategy with an existing state-of-art technique, electrochemiluminescence (ECL). In both assays, the excitation and the readout of the signal are performed separately: an electrochemical stimulation and optical readout for ECL and the inverted situation for the developed PEC. For both assays, a sandwich approach was used consisting of a biotinylated capture probe immobilized on streptavidin functionalized surfaces and a detection probe labelled with digoxigenin or chlorin E6 for ECL and PEC, respectively. Also, both assays allow the detection of miR-141 in the pM range in human serum, in the presence of other miRNAs.

As the final experimental chapter of the thesis, **chapter 6** explores the multiplexing capability of the developed sensing strategy using two PEC approaches. The first approach is the development of high-throughput detection with 96X multi-channel electrode systems with in-house made LED illumination sources in collaboration with FTI-CoSys Lab, University of Antwerp and Flanders Make Strategic Research Centre, Lommel, Belgium. For the high throughput analysis, miRNAs relevant to PCa were detected in a 96X well-electrode plate using 96X LEDs for illumination. Screen-printed arrays of 96-well carbon electrode plates were used due to their fast, high-throughput and disposable features to fulfil the need of clinical demands. These 96-well illuminations can be controlled by a LED control subsystem. The application of patient plasma samples for detecting miR-141, miR-145 and miR-375 demonstrated the possible future of the electrochemical ELISA-like immunoassay in clinical practices. The second approach involves intra-vial multiplexing where the samples were analyzed for different targets in one vial. For the intra-vial multiplexing, the different detection probes were coupled to different PSs that have distinct excitation wavelengths.

Finally, **chapter 7** features all the conclusions drawn from the findings detailed throughout the thesis along with discussions on future perspectives.

# Chapter 2

# Preparation and characterization of electrode platforms for nucleic acid detection

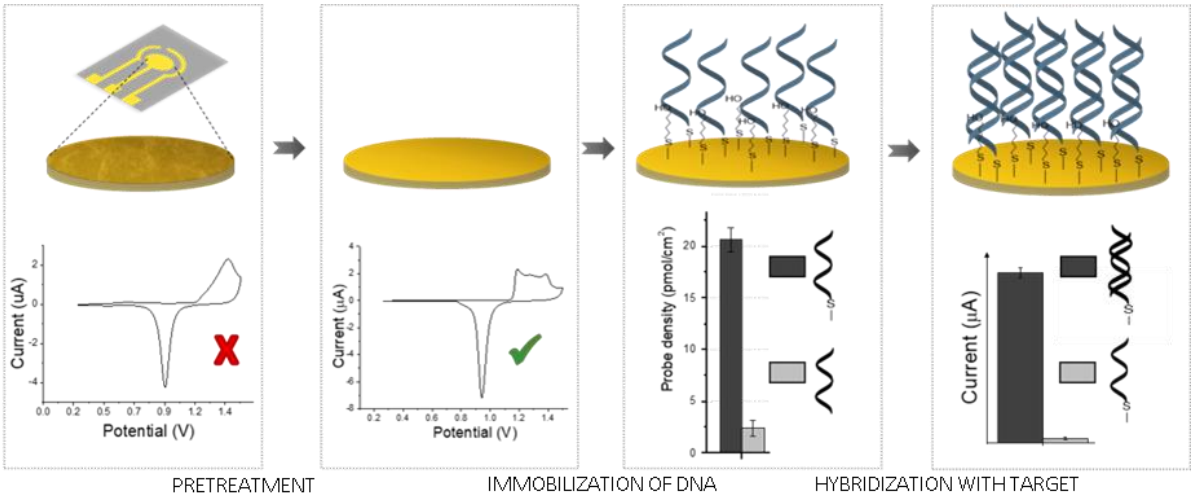


*Critical steps in constructing electrochemical nucleic acid sensors based on gold-sputtered microelectrodes.*

**Adapted from the following article:**

*Thiruvottriyur Shanmugam S., Trashin S., De Wael K. Gold-sputtered microelectrodes with built-in gold reference and counter electrodes for electrochemical DNA detection. Analyst. 2020 Nov 23;145(23):7646-7653. doi: 10.1039/d0an01387k. PMID: 32966365.*

***Contribution:*** *I performed all the experiments and wrote the first draft of the manuscript.*

## 2.1 Abstract

Gold-sputtered microelectrodes with built-in gold reference and counter electrodes represent a promising platform for the development of disposable DNA sensors. Pretreating gold electrode surfaces, preceding the immobilization of DNA thereon, is essential for the preparation of DNA sensors and biosensors in general. However, no practical guidelines and only scarce literature information are available on the pretreatment of such types of gold-sputtered microelectrodes. This motivates the development and optimization of the cleaning pretreatment and DNA immobilization steps, which was the focus of this chapter. The standard pretreatment procedure for cleaning polycrystalline gold disk electrodes includes polishing and cannot be transferred as such to gold-sputtered microelectrodes. Therefore, five different cleaning protocols were compared to find the optimal one for gold-sputtered microelectrodes. Additionally, two immobilization strategies of thiolated single-stranded DNA (ssDNA) were compared, i.e. electrochemically assisted potential perturbation and chemisorption. In our experiments, clean gold-sputtered electrodes performed better after the regular (passive) chemisorption of the thiolated probe incubated on the surface of the electrodes overnight. The overall procedure with a backfilling step resulted in a DNA coverage of 15 – 24 pmol $cm^{-2}$ (in comparison to 3 – 6 pmol $cm^{-2}$ for the potential perturbation method) and only a little higher level of thiol-unspecific adsorption of DNA 2.4 – 3.8 pmol $cm^{-2}$ (in comparison to 0.9 – 1.4 pmol $cm^{-2}$ for the potential perturbation method). Using alkaline phosphatase (ALP) as a label, the sensor demonstrated successful capturing of the complementary target DNA with a detection limit of 0.14 nM and sensitivity of 9.4 A $M^{-1}$ $cm^{-2}$. In general, gold-sputtered all-in-one microelectrodes showed good practical potential for DNA sensing applications.

## 2.2 Introduction

The need for miniaturization in the field of electrochemical biosensors demands reproducible, cost-efficient and easy-to-use transducers with well-controlled properties. Generally, conventional polycrystalline gold disk electrodes are often used to demonstrate new detection principles when developing biosensors. These electrodes are not intended to be single-use and must be pretreated carefully before each use, which is time-consuming. Disposable gold screen-printed electrodes are already available on the market as an alternative to conventional electrodes. More recently, gold-sputtered microelectrodes have become commercially available as an attractive platform for the development of miniaturized biosensors through the covalent attachment of biomolecules to the gold surface via thiols.[109-113] Notably, microelectrodes are by definition small electrodes of a diameter of ca. 1 mm and have no features of ultramicroelectrodes (0.01-0.1 mm in diameter) such as radial diffusion of redox species in voltametric measurements.[114] These microelectrodes are made up of gold, sputtered with a thickness of 10–500 nm on a glass substrate directly or through an intermediate layer of chromium for better adhesion.[109] A single unit includes working, reference and counter electrodes, all made of sputtered gold, to operate in a small drop of liquid. In contrast to gold screen-printed electrodes made with conducting inks of complex composition, gold-sputtered microelectrodes are made of pure gold and, thus, resemble conventional polycrystalline gold electrodes. The latter are polished and pretreated chemically and/or electrochemically before use,[115] whereas, gold-sputtered microelectrodes cannot be subjected to polishing but can be washed and pretreated chemically and/or electrochemically.

In general, chemical pretreatment of gold surfaces in piranha solution leads to severely oxidized gold, while aqua regia etches the gold contaminates the surface with chloride and does not result in significantly cleaner surfaces.[116] Electrochemical methods, especially, reductive potential sweep in alkaline solutions and oxidative potentials in acidic solutions, have proven to be effective for removing surface contaminants.[117] After chemical and/ or electrochemical pretreatment, gold surfaces can be modified by a bio-recognition element such as an ssDNA-probe or an oligonucleotide functionalized by a thiol at one of its ends.

Two principally different immobilization strategies exist for tethering DNA probes through Au-S bonds. First, the electrode surface can be incubated in a solution of thiolated oligonucleotides in a high-ionic-strength buffer (usually for 16 – 24 h) followed by back-filling with mercaptohexanol (MH) or another functionalized short-chain thiol, which may also be added in the solution of the oligonucleotide for better control of oligonucleotide

surface density.[109, 118-122] Second, taking advantage of the negatively charged backbone of DNA, the immobilization can be promoted by applying a sufficiently positive constant potential[111] or by quick switching of the potential to create microscale "stirring" or perturbation of the solution near the electrode surface due to migration of ions induced by charging/discharging of the double-layer capacitance.[123-128] Nevertheless, little information was reported on the optimization of electrochemical pretreatment of gold-sputtered electrodes, their voltammetric characterization in sulphuric acid (to assess the cleanliness and roughness),[117, 129] comparisons of immobilization strategies via thiols including control measurements with non-thiolated sequences. As per our knowledge, none of the literature reported these for gold-sputtered microelectrodes with in-situ gold reference and counter electrodes. This motivated us to study the preparation of such microelectrodes for biosensing applications given their asset of being able to offer high sensitivity, easy operation and portability.

In this chapter, five cleaning protocols for gold-sputtered microelectrodes are compared as it was evident that the insights on cleaning polycrystalline gold disk electrodes with a benchmark electrode surface for DNA sensors, cannot be transferred to clean these miniature gold-sputtered microelectrodes. Secondly, two strategies for immobilization of thiolated oligonucleotides (*i.e.* attachment through conventional chemisorption and immobilization through potential perturbation) are tested. Special attention has been paid to a side-by-side comparison of thiol-specific attachment and weak unspecific adsorption of oligonucleotides. Finally, the hybridization performance of this miniaturized DNA sensor has been checked using biotin-labelled complementary DNA strands. The detection is based on the alkaline phosphatase (ALP) assay for enzymatic signal amplification, a well-known optical or electrochemical enzymatic assay used in the detection of DNA in other gold platforms.[110, 130, 131]

## 2.3 Experimental

### 2.3.1 Equipment

Electrochemical pretreatment and characterization of electrodes were carried out using µAutolab III (Metrohm-Autolab BV). PalmSens3 (PalmSens BV) was used to detect hybridization. Gold-sputtered microelectrodes were purchased from Micrux Technologies (Oviedo, Spain). The diameter of the gold working electrode was 1 mm (Figure 2.1). The sample volume applicable to the sensor is in the range of 1 and 15 µL. volume of 5-10 µL was used for modification and in the detection stages. The measurements were carried out with the electrode connector assembly (AIO Drop Cell-Base) from the same company. The

external electrochemical setup, a polycrystalline gold disk electrode (1.6 mm in diameter) was purchased from BASi, USA. Saturated calomel electrode (SCE, radiometer, Denmark) was used as an external reference electrode. The SCE was separated by a frit to avoid any contamination of the working solution with $Cl^-$. Scanning electron microscopy (SEM) images were taken by the FEI Quanta 250 (Thermo Fisher Scientific) at 30 kV.

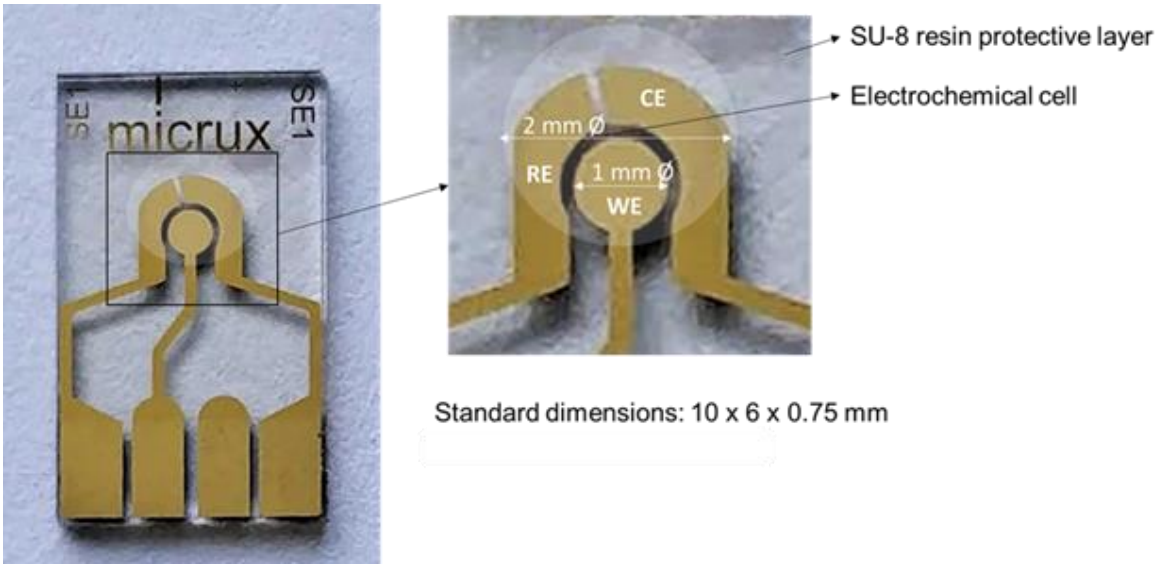


*Figure 2.1 Photograph and dimensions of the commercially available gold sputtered microelectrode used in this study.*

### 2.3.2 Procedure for polishing and electrochemical pretreatment of gold disk electrodes

Gold disk electrodes (BASi®, 1.6 mm in diameter) were polished for 2 min with 1 µm alumina (Buehler) slurry in water followed by 1 µm and 0.25 µm diamond slurry in alcohol lubricant (DP-Spray P, Struers) and, finally, 0.05 µm alumina (Buehler) slurry in water. After each polishing step, the electrodes were sonicated in 70% ethanol (after diamond slurry) and ultrapure water (after alumina slurry) to remove the residues of the polishing materials from the electrodes. Afterwards, the electrodes were subjected to a cyclic potential sweep for 50 cycles at 2 V/s between −0.35 and −1.4 V vs. SCE (saturated calomel electrode, from Radiometer Analytical SAS). This was followed by a cyclic potential sweep in 0.5 M $H_2SO_4$ from 0.25 V to 1.5 V vs. SCE at 0.1 V/s until a characteristic voltammogram [132, 133] was obtained.

### 2.3.3 Pretreatment of gold-sputtered microelectrodes

Gold-sputtered microelectrodes were pretreated using five different protocols (Table 2.1) that were adapted from the literature and inspired by the traditional methods for pretreating polycrystalline gold disk electrodes.[111, 115, 129, 134, 135] For comparison, polycrystalline gold disk electrodes were polished using alumina and diamond slurries and electrochemically pretreated in NaOH and $H_2SO_4$ identically to protocol 2 for the gold-sputtered electrodes. To electrochemically characterize the working electrode surface after pretreatment procedures, cyclic voltammetry was carried out in 0.5 M $H_2SO_4$ using a separate three-electrode cell by connecting only the working electrode of the gold-sputtered microelectrodes and using an external saturated calomel electrode as the reference and platinum rod as a counter electrode. The electrochemically available surface area was estimated from the cyclic voltammograms (CV) in 0.5 M $H_2SO_4$ [136] by taking the charge accumulated during the reduction of gold oxide to the reference value (400 $\mu C/cm^2$). Then, the surface roughness ($R_f$) was calculated as the ratio of electrochemically available and geometric surface area.

*Table 2.1 Pretreatment protocols for gold-sputtered microelectrodes.*

| Protocol | Sonication | | Electrochemical pretreatment |
|---|---|---|---|
| | 70% EtOH | MilliQ Water | Potential (V) -2.0 -1.0 0.0 1.0 2.0 |
| 1 | ✓ | ✓ | |
| 2* | ✓ | ✓ | 2 V/s, 20 cycles 0.5 M NaOH; 0.1 V/s, 20 cycles 0.5 M $H_2SO_4$ |
| 3* | ✓ | ✓ | 2 V/s, 20 cycles 0.5 M $H_2SO_4$; 0.1 V/s, 20 cycles 0.5 M $H_2SO_4$ |
| 4** | ✓ | ✓ | 0.1 V/s, 12 cycles 0.05 M $H_2SO_4$ |
| 5** | ✓ | ✓ | 0.1 V/s, 12 +12 cycles 0.5 M $H_2SO_4$ |
| | | | -2.0 -1.0 0.0 1.0 2.0 Potential (V) |

**performed in a three-electrode cell using an SCE as the reference electrode; **in a drop using pseudo-reference Au electrode. The arrow shapes depict cyclic voltammetry between the indicated potential window. Protocol 5 involves an initial 12 cycles of potential sweep after which the drop was refreshed and additional 12 cycles conducted. Protocol 2 is also used to electrochemically pretreat polycrystalline gold disk electrode after polishing.*

### 2.3.4 Modification reagents

Oligonucleotides were obtained from Eurogentec (Belgium). Their structures and purity were confirmed by mass spectrometry. The oligonucleotide sequence was chosen to be complementary to miRNA21 (miR-21), a marker for several types of cancer and cardiovascular diseases. [137] Thiolated probe (complementary): HS-$(CH_2)_6$-5'TAG-CTT-ATC-AGA-CTG-ATG-TTG-A 3'; non-thiolated probe (complementary): 5' TAG-CTT-ATC-AGA-CTG-ATG-TTG-A 3'; Thiolated probe (non-complementary): HS-$(CH_2)_6$- 5' TAG-CTT-ATG-TGT-ACC-CTG-TCA-G 3'; Target: Biotin-5'-TEG-TCA-ACA-TCA-GTC-TGA-TAA-GCT-A 3'. Immobilization (Tris) buffer contained 500 mM KCl, 50 mM $MgCl_2$, and 10 mM tris pH 7.5. The washing (Tris-$T_{20}$) buffer had the same composition but additionally contained 0.05% w/v tween 20.

### 2.3.5 Immobilization of ssDNA through chemisorption

Initially, a 20 µL solution containing 1 µM probe DNA with 0.1 mM tris (2-carboxyethyl) phosphine (TCEP) and 0.2 µM of either mercaptohexanol (MH) or mercaptobutanol (MB) or mercaptoundecanol (MU, in 30% ethanol) in immobilization buffer (Tris buffer) was dropped on the electrode surface and left for overnight incubation (~16 hours) at room temperature in a closed Petri dish with a wet paper inside to avoid evaporation of the droplet (Figure 2.2). The electrodes were then transferred into vials containing Tris buffer and washed gently by replacing Tris buffer five times. This was followed by incubation for 2 hours in a 1 mM back-filling thiol in Tris buffer. Then electrodes were rinsed and stored in Tris buffer avoiding complete drying of the surface between these steps to ensure good reproducibility of the procedure.

*Figure 2.2 Microelectrodes kept in humid conditions with wet tissue papers in the vicinity and sealed for overnight immobilization of ssDNA through chemisorption.*

### 2.3.6 Immobilization through potential perturbation

Experimental parameters for this method were adopted from the literature.[124, 125] Potential pulses were applied between +0.3 V and −0.2 V vs Au pseudo-reference electrode. The upper and lower potentials were determined from the available potential window limited by the reductive desorption thiols in the cathodic region and Au-S oxidation and gold oxide formation in the anodic region as measured with cyclic voltammetry in 10 mM PB, 450 mM $K_2SO_4$ (Figure 2.3). For the immobilization, 15 µL of 1 µM of probe DNA in 10 mM PB, 450 mM $K_2SO_4$ was placed on the microelectrode's working area and perturbed for 2 minutes between +0.3 V and −0.2 V with 10 ms interval time. Then, the electrode was washed gently with a solution containing 10 mM PB and 450 mM $K_2SO_4$. Afterward, 15 µL of 1 mM thiol (MH/ MB/MU) solution in 10 mM PB, 20 mM $K_2SO_4$ was placed on the electrode and perturbed for 1 min between +0.3 V and −0.2 V with 10 ms interval time. Finally, the electrodes were washed with buffer containing 10 mM PB, 20 mM $K_2SO_4$.

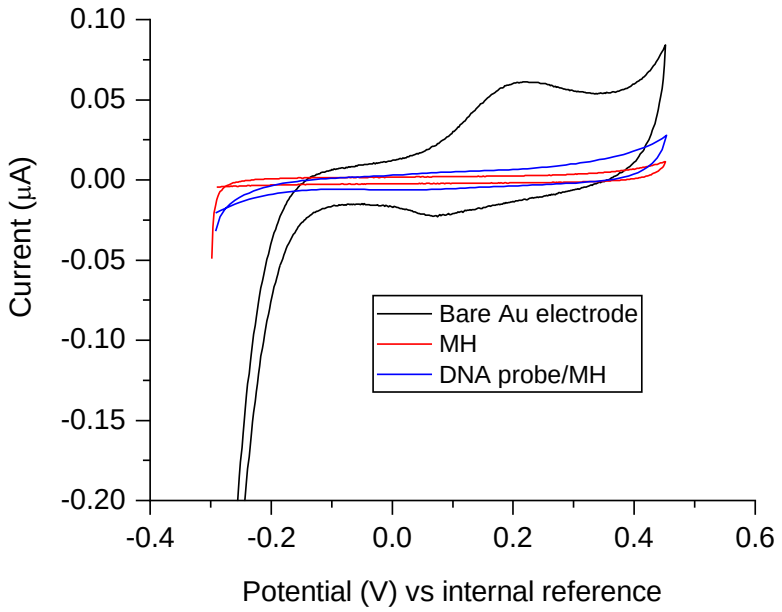


*Figure 2.3 Evaluation of the potential window of the electrodes in the immobilization buffer used for the potential pulse assisted immobilization: a bare gold-sputtered electrode (black), an electrode coated with 1 mM mercaptohexanol (red); an electrode coated with 2 µM of ssDNA probe and mercaptohexanol according to the immobilization procedure (blue). Scan rate, 0.1 V/s ; 450 mM $K_2SO_4$ containing 10 mM $KH_2PO_4$ pH 7.*

### 2.3.7 Estimation of probe density on the surface

The probe density was measured by chronocoulometry through adsorption of ruthenium (III) hexamine chloride (RuHex) in 10 mM Tris buffer (pH = 7.4) as described before.[122] Briefly, the potential step from +150 mV to −450 mV vs SCE was applied and the charge as

a function of time was measured for 1000 ms. For each electrode, the measurements were first conducted in the pure buffer and then in the presence of 3.5 µM RuHex.

### 2.3.8 Hybridization with target DNA and detection

Modified electrodes were incubated for 1 hour in a solution of the biotinylated target DNA in Tris buffer at room temperature. Since hybridization was carried out for detecting sequences with a fully complementary target sequence and not for single point mutations or deletions, room temperature incubation for an hour was sufficient enough to hybridize the complementary target and prevent hybridization with the non-complementary sequence with scrambled bases. Then, the electrodes were washed in Tris-$T_{20}$ buffer and incubated in Tris-$T_{20}$ buffer containing 0.75 µg/mL streptavidin linked alkaline phosphatase for 20 minutes. The electrodes were then rinsed with Tris-$T_{20}$ and stored in Tris buffer before the electrodes were characterized.

Hybridized oligonucleotides were detected in a measuring buffer (50 mM Tris. HCl, 10 mM $MgCl_2$, pH 9.6) containing 3 mM para aminophenyl phosphate (pAPP). To ensure the adequate choice of the potential for amperometric detection of the ALP activity in the drop, cyclic voltammetry was firstly recorded in a conventional three-electrode cell containing 3 mM pAPP in the measuring buffer pH 9.6. The Au built-in reference electrode of the prepared sensors showed adequate stability in the measuring buffer for at least the first 10 min with an average potential of −0.056 ± 0.005 vs SCE. Therefore, amperometric responses at +0.45 V for chemisorption and +0.50 V for potential perturbation were used to construct the calibration plot and the readings for the calibration plot were made at 120 s. The limit of detection (LOD) was calculated from the ratio of 3 times the standard deviation of the blank over the gradient of the calibration curve. While sensitivity was calculated from the ratio of the gradient of the calibration curve over the surface area.

## 2.4 Results and discussion

### 2.4.1 Pretreatment of gold-sputtered microelectrodes

The use of a well-controlled pretreatment protocol is critically important for the reproducible and efficient immobilization of biomolecules and self-assembled monolayers (SAM) layers on gold surface. [135] Gold-sputtered microelectrodes cannot be mechanically polished and, thus, should be carefully cleaned chemically and/or electrochemically. Moreover, harsh chemical cleaning (e.g. by piranha solution) is harmful to the chosen microelectrodes due to a thin layer of insulators around the working area. To test the cleanness of gold-sputtered microelectrodes and thus the quality of the five pretreatment

protocols, cyclic voltammetry in 0.5 M $H_2SO_4$ was performed and compared the profiles with a well-established behaviour of pure polycrystalline gold electrodes. [132]

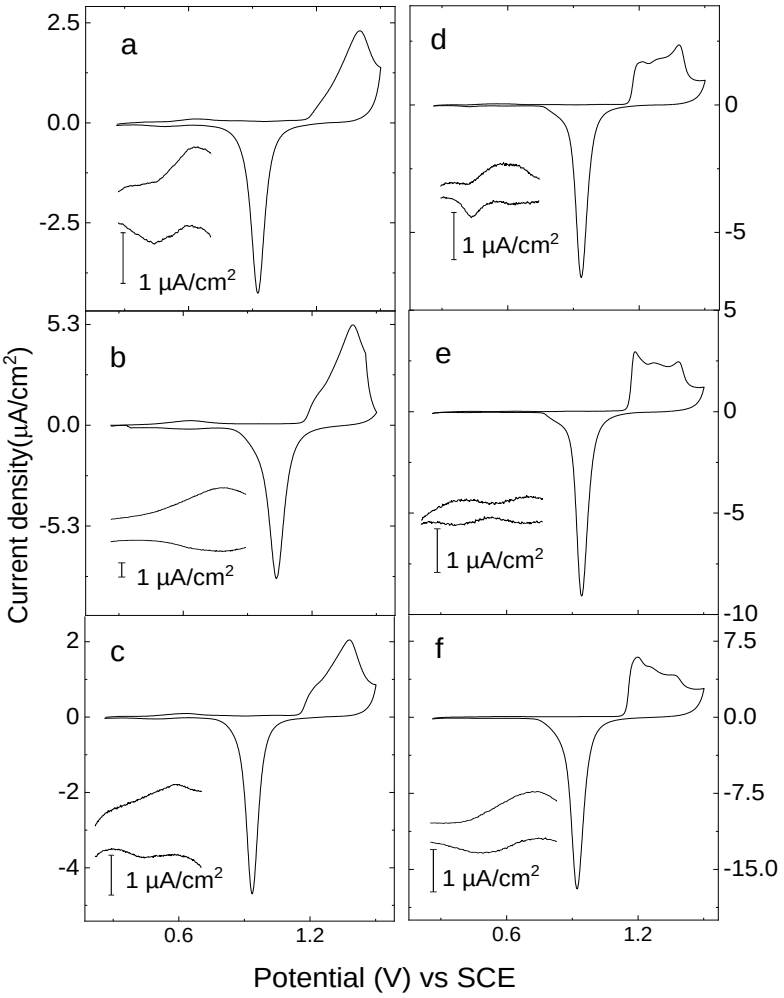


*Figure 2.4 Cyclic voltammograms of gold-sputtered microelectrodes after pretreatment according to protocols 1—5 (a-e) in comparison to a polycrystalline gold disk electrode pretreated following protocol 2 after polishing with alumina and diamond microparticles (f). Measurements were carried out in 0.5 M $H_2SO_4$, with the SCE reference and platinum counter electrode. The insets zoom in on the electrical double layer region of the respective voltammograms.*

The evaluation of the pretreatment quality was based on the shape of cyclic voltammograms (CV) in 0.5 M $H_2SO_4$ obtained in the same conditions for all electrodes using a conventional three-electrode cell with an SCE as the reference electrode. The working electrode surfaces of the pretreated gold-sputtered microelectrodes were compared to mechanically polished and electrochemically pretreated polycrystalline gold disk electrodes (Figure 2.4). The roughness ($R_f$) of the electrodes was calculated as the ratio of electrochemical and geometric surface area as described in the experimental section. $R_f$

value of polished and pretreated polycrystalline gold disk electrodes was found to be 1.73 ± 0.05, whereas the apparent $R_f$ values of planar gold electrodes varied with the pretreatment protocol.

Protocol 1 involves only cleaning with 70% ethanol and ultrapure water in an ultrasonic bath without any followed electrochemical pretreatment step. In comparison to the polycrystalline gold disk electrode (Figure 2.4 f), the CV after protocol 1 (Figure 2.4 a) showed near-complete suppression of the first peak at +1.16 V in the region of gold oxide formation. This suggests surface contamination[138] that remains after washing, partially blocking the gold surface. Thus, the calculated $R_f$ value of 1.15 ± 0.04 is likely underestimated in these conditions, motivating, in general, the addition of an electrochemical step in the pretreatment. Protocol 2 introduces two electrochemical pretreatment steps (cathodic in 0.5 M NaOH and anodic in 0.5 M $H_2SO_4$) and exactly repeats the pretreatment protocol of the polycrystalline gold disk electrodes traditionally mechanically polished first. Surprisingly, the protocol was not efficient for the used gold-sputtered electrodes and resulted in only minor difference in the shape of CV compared to the electrodes only washed in 70% ethanol (protocol 1). Nevertheless, $R_f$ value slightly increased to 1.34 ± 0.04, which indicates better surface decontamination and motivates to further optimize the electrochemical pretreatment step.

The producer of the used gold-sputtered electrodes generally recommends cathodic and anodic electrochemical pretreatment both in $H_2SO_4$ in a wide potential window. Additionally, the use of only $H_2SO_4$ for both anodic and cathodic regions makes the protocol to be simpler and faster. Thus, protocols 3 – 5 were designed for further evaluation. Protocol 3 mimics protocol 2 but the cathodic electrochemical pretreatment was performed in 0.5 M $H_2SO_4$ instead of 0.5 M NaOH. This does not yield any considerable change in the shape of CV and $R_f$ value (1.29 ± 0.12). In contrast, protocols 4 and 5 – based on the pretreatment in $H_2SO_4$ but in a wider potential window – were more successful. Protocol 4 was applied in a drop of 0.05 M $H_2SO_4$. Though this caused some drift in the potential of the built-in pseudo-reference gold electrode, a stable CV was observed by the end of the pretreatment step. However, the exposure to extreme anodic current density during such pretreatment resulted in damage and near-complete dissolution of the counter gold electrode. Nevertheless, the working electrode stayed undamaged, and a CV could be obtained in the three-electrode cell for comparison among the other protocols. The found $R_f$ value of 1.36 ± 0.02 was rather the same as in protocols 2 and 3 but CV, in contrast, revealed the distinct gold oxide formation profile starting from +1.16 V (Figure 2.4 d) and a lower background current in the electrical double layer region indicating improved

decontamination of the surface. The conditions were further modified to preserve the cleaning efficiency but avoid physical damage to the counter electrode.

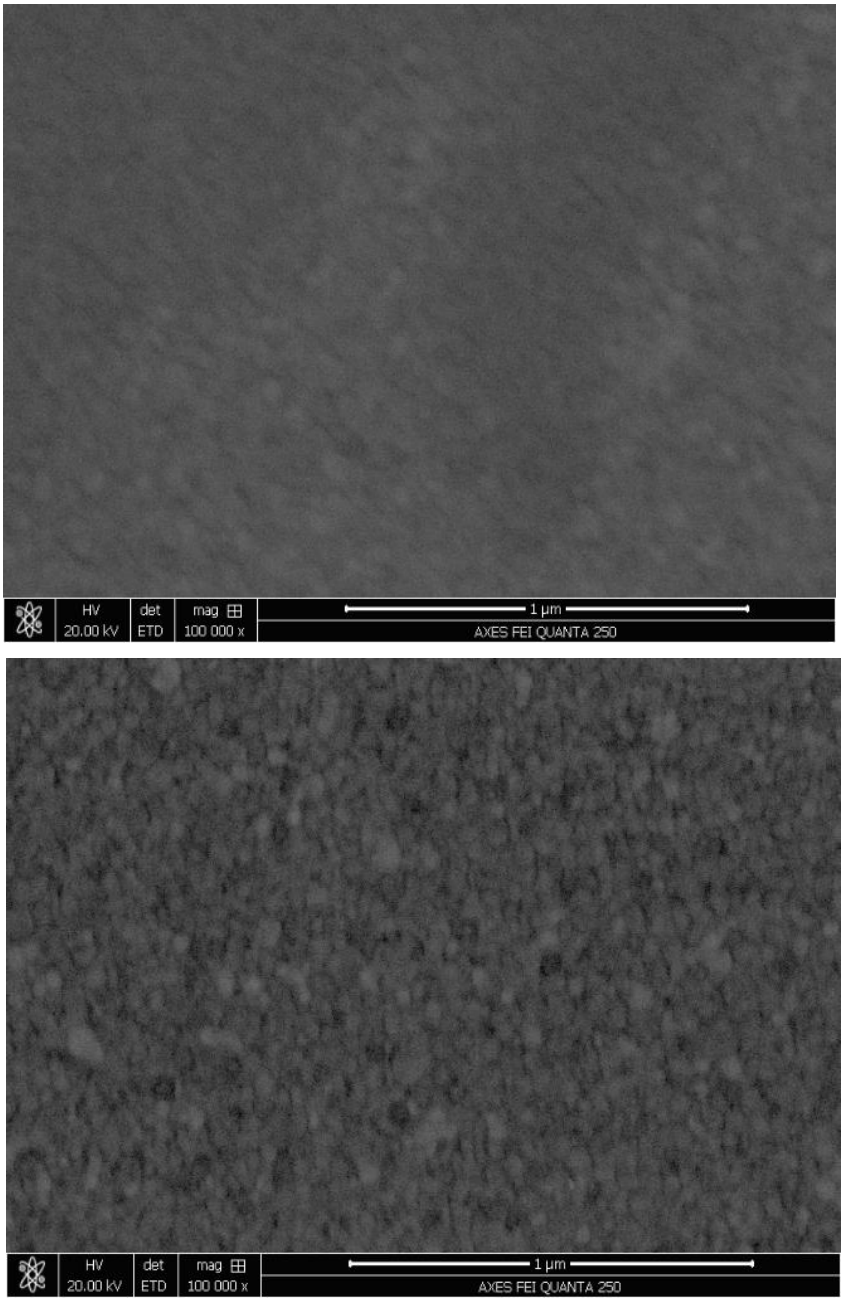


*Figure 2.5 Scanning electron microscopy (SEM) images of the gold-sputtered electrodes after cleaning in an ultrasonic bath with 70% ethanol and water (Protocol 2, A) and after additional electrochemical pretreatment (Protocol 5, B).*

In protocol 5, the electrode was pretreated in a drop of 0.5 M $H_2SO_4$ but within a narrower potential window (between −1.0 V and +1.3 V instead of −1.5 and +1.5 V used in protocol 4). CV shows the characteristic profile of gold oxide formation similar to the profile at the

polycrystalline gold disk electrodes with three distinct peaks with the intense first peak at +1.16 V. Moreover, the lowest currents in the double-layer region were observed suggesting efficient cleaning of the gold surface. In contrast, the $R_f$ value of 1.76 ± 0.04 was calculated from CV after pretreatment by protocol 5 suggesting that the pretreated electrodes are rougher after protocol 5 than after protocols 1–4. Nevertheless, scanning electron microscopy (SEM) showed no noticeable topological difference between working electrodes pretreated according to protocol 1 (only sonication in 70% ethanol) and protocol 5 (Figure 2.5). This confirms that protocol 5 alters only a superficial layer of gold without its deep damage or partial dissolution, while, within protocols 1–4, contamination may remain and cover a fraction of gold atoms on the surface resulting in an low roughness coefficient $R_f$. Thus, protocol 5 appeared to be the most promising for electrode pretreatment and was chosen for the following work.

Protocol 5 can also be used to recover electrodes after their chemical modification. Overnight incubation of the electrodes with the thiolated probe and MH solution resulted in the suppression of the first peak of gold oxide formation (at +1.16 V) and an increase of current in the electrical double layer region on CV in the same manner as it was observed for the electrodes pretreated according to protocols 1–3 (Figure 2.4 a-c, Figure 2.6). However, after pretreatment according to protocol 5, the shape was completely recovered to that before modification.

One can notice suppression of the first peak of the gold oxide formation at around +1.16 V and a decrease of the peak area at the back reduction of the gold oxide layer after introducing the organic molecules to the gold surface. The distinct profile of the gold oxide formation and the peak area for the gold oxide reduction is fully recovered after the pretreatment according to Protocol 5. The electrodes were not reusable after three cycles of modification and detection due to drift in the reference potential and color change in the counter electrode possibly due to wear and tear of the microelectrode.

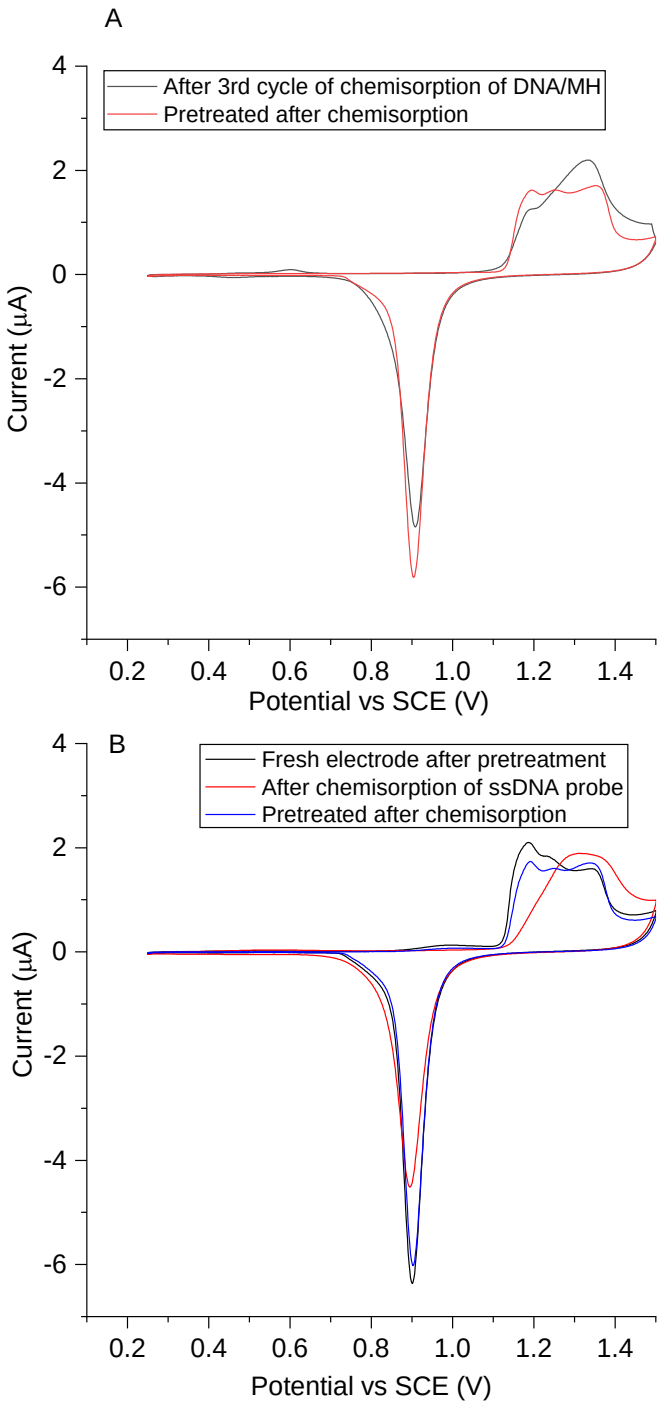


*Figure 2.6 (A) Voltammetric behaviour of gold-sputtered electrodes in 0.5 M $H_2SO_4$ (Test-CV) for an electrode after three cycles of MH/ssDNA immobilization and detection; renewed by repeating the pretreatment according to protocol 5. (B) Voltammetric behaviour of gold-sputtered electrodes in 0.5 M $H_2SO_4$ (Test-CV) for (black) a new freshly cleaned and pretreated electrode according to Protocol 5, an electrode modified by overnight chemisorption of MH/ssDNA according to the immobilization procedure (red) and renewed by repeating the pretreatment according to Protocol 5 (blue). Scan rate, 100 mV/s; the second scan is shown.*

### 2.4.2 Thiol-tethered immobilization of DNA probes

Conventional overnight chemisorption and immobilization through potential perturbation of DNA probes on the pretreated planar gold-sputtered electrodes were compared. The surface density (coverage) of the ssDNA probe on the electrodes was measured by chronocoloumetry using RuHex, a multivalent redox cation interacting with the DNA backbone. A non-thiolated ssDNA probe of the same sequence was used as a control for the assessment of non-specific adsorption of the oligonucleotide on the surface via weak interactions. Such adsorption is unwanted in general because it may reduce the hybridization efficacy due to the steric factor and poor probe spatial orientation.[139] Blank measurements without any DNA sequences (but only with back-filling thiols) served as blank controls. The amount of surface-confined RuHex was converted to apparent ssDNA surface coverages.

*Table 2.2 Surface adsorption of RuHex on modified electrodes.*

| Immobilization method for ssDNA | Back-filling thiol[b] | $Ru(NH_3)_6^{3+}$ (pmol/cm$^2$)[a] | | |
|---|---|---|---|---|
| | | SH-Oligo | Oligo | Blank control |
| Chemisorption | MB | 87.4 ± 6.9 | 25.2 ± 1.4 | 13.2 ± 3.0 |
| | MH | 78.6 ± 3.5 | 21.1 ± 2.2 | 13.6 ± 1.0 |
| | MU | 55.3 ± 5.3 | 15.1 ± 2.1 | 7.5 ± 1.5 |
| Potential perturbation | MB | 30.4 ± 0.7 | 15.4 ± 0.6 | 11.3 ± 1.6 |
| | MH | 32.7 ± 1.3 | 24.0 ± 0.6 | 19.5 ± 1.6 |
| | MU | 17.3 ± 2.2 | 9.7 ± 0.8 | 6.9 ± 2.3 |

*[a] Each value is depicted as an average ± standard error for at least three independent electrodes. [b] MB: mercaptobutanol, MH: mercaptohexanol, MU: mercaptoundecanol. SH-Oligo: thiolated probe, Oligo: non-thiolated probe. Error indicates standard deviation, N=3.*

Table 2.2 lists the surface adsorption of RuHex for a series of electrodes prepared by two different strategies and using three back-filling thiols that differ by carbon chain length. After correction of the values to the blank controls (Figure 2.7), the probe surface coverages are in the range of 15–24 pmol/cm$^2$ (20.7 ± 1.2 for MH) for overnight chemisorption and 3–6 pmol/cm$^2$ (4.2 ± 0.6 for MH) for the potential perturbation method depending on the back-filling thiol. The probe coverage values from the potential perturbation method are rather in the low range of the values obtained in other studies[125, 140] and about 2–3 times lower compared to the coverage obtained in the optimized conditions for this method,[125] which suggests that our conditions might be not optimal. Nevertheless, the overall coverage of the thiolated probe was 4–5 times higher for the overnight chemisorption in comparison to the potential perturbation method in our work and about 2 times higher compared to the reported maximal coverage for the potential

perturbation method in optimized conditions.[125] Based on the theoretical calculations with a maximally dense arrangement of ssDNA, the expected surface coverage for a tightly packed ssDNA layer with a probe length of 22 bases should range between 25 and 30 pmol/cm$^2$.[121] Thus, around 80% of the maximal coverage was attained with overnight chemisorption and 20% with immobilization through the potential perturbation method. It is known that adsorption of oligonucleotides can occur on gold surfaces through non-covalent interactions of gold atoms and nitrogenous bases and may exceed 30% of the maximal probe coverage depending on the probe sequence and its length.[120] Nevertheless, here, non-specific adsorption counted up to 14 ± 2% (2.4 – 3.8 pmol/cm$^2$) of the coverage for the thiolated probe in the procedure with chemisorbed ssDNA and 27 ± 6% (0.9 – 1.4 pmol/cm$^2$) for the potential perturbation method.

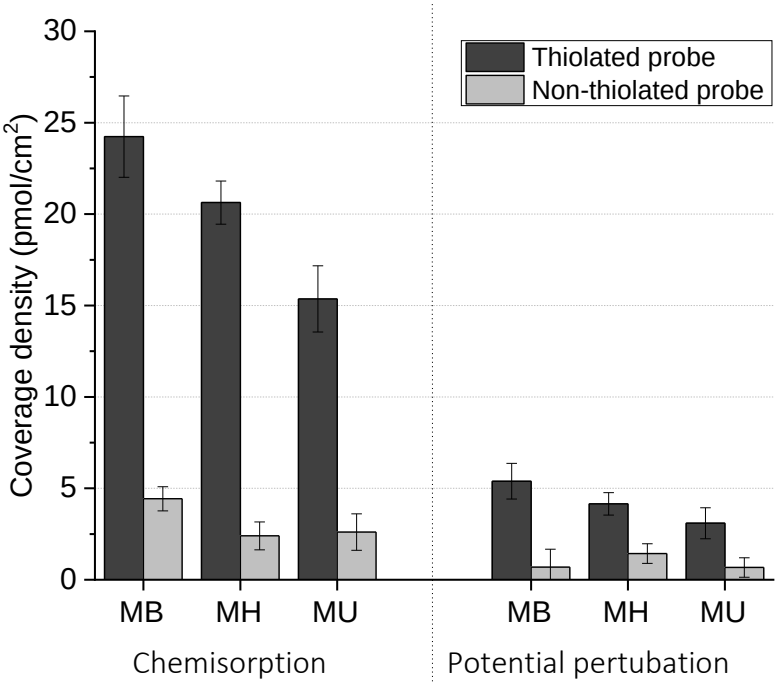


*Figure 2.7 Comparison of coverage density of thiolated and non-thiolated probes between two immobilization methods. Error bars indicate the standard error of measurements with three independent electrodes.*

The chain length of the back-filling agents noticeably influenced the coverage in both procedures (Figure 2.7). The highest coverage was obtained for mercaptobutanol (MB) and the lowest (by 40% compared to MB) coverage was obtained for mercaptoundecanol (MU). MU also resulted in lower blanks and lower coverage for thiol-unspecific adsorption which, however, was not considerably different from those obtained for mercaptohexanol (MH). Moreover, a drop of the MU solution spreads over all the surfaces of the microelectrode due to MU acting as a surfactant, which makes it practically difficult to handle. It was also reported that MH forms more stable layer compared to MB.[141] Thus, MH was selected for the following experiments as the back-filling agent in both procedures.

### 2.4.3 Hybridization efficiency at gold-sputtered microelectrodes

A higher surface coverage for a ssDNA probe does not necessarily guarantee higher responses to complementary DNA because the hybridization efficiency can be lowered by steric crowding effects for densely packed probes.[139] The overnight chemisorption provided approximately five times higher coverage of the probe compared to the immobilization through potential perturbation, but the latter should give more controlled and better-oriented assembly of the ssDNA probe due to the microscale stirring of the solution near the electrode.[124, 140] Here side-by-side the hybridization efficiency for both immobilization methods at gold-sputtered microelectrodes was evaluated. To evaluate the ability to capture a specific sequence, the complementary and non-complementary (with scrambled bases) thiolated probes were used and were attached to the surface by both immobilization methods using MH as the back-filling agent.

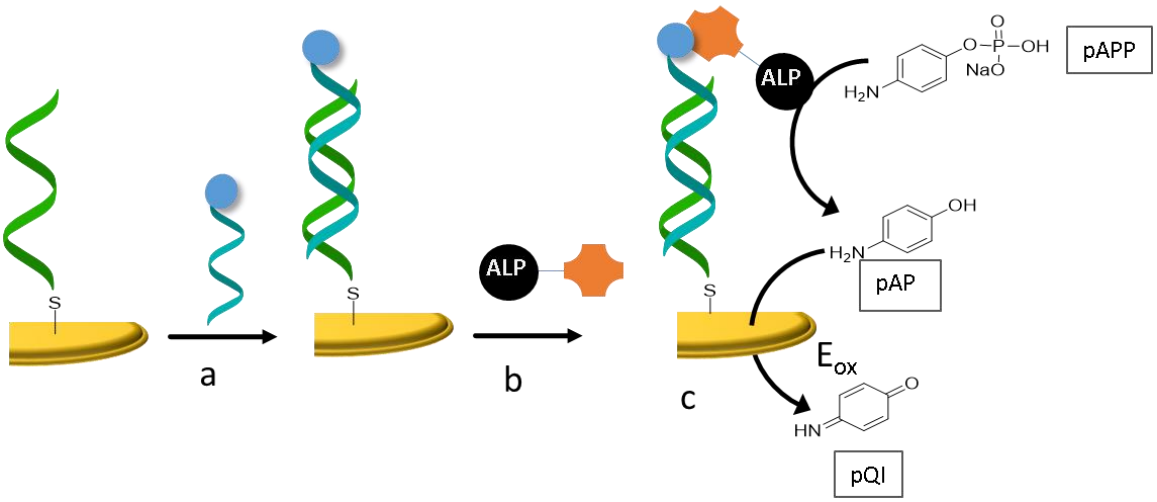


*Figure 2.8 A schematic illustration of DNA hybridization with biotinylated target sequence (a), ALP tagged streptavidin conjugation to biotinylated target (b) and detection strategy based on enzymatic assay (c).*

The amperometric detection principle is based on the ALP enzymatic assay, a schematic diagram of which is shown in Figure 2.8. In this assay, target DNA probes labelled with biotin at 5' end were hybridised with the DNA on electrode (Figure 2.8 a). This is followed by the conjugation of ALP-tagged streptavidin to a biotinylated target (Figure 2.8 b). In the detection step (Figure 2.8 c), ALP molecules convert pAPP in the measuring buffer to p-aminophenol (pAP). This electroactive pAP gets oxidized at a certain potential against the built-in Au reference electrode and the generated signal is indicative of the presence of the target. In order to ensure the adequate choice of this potential for the amperometric detection of the ALP activity in the drop, cyclic voltammetry was firstly recorded in a conventional three-electrode cell containing 3 mM pAPP in the measuring buffer pH 9.6 (Figure 2.9).

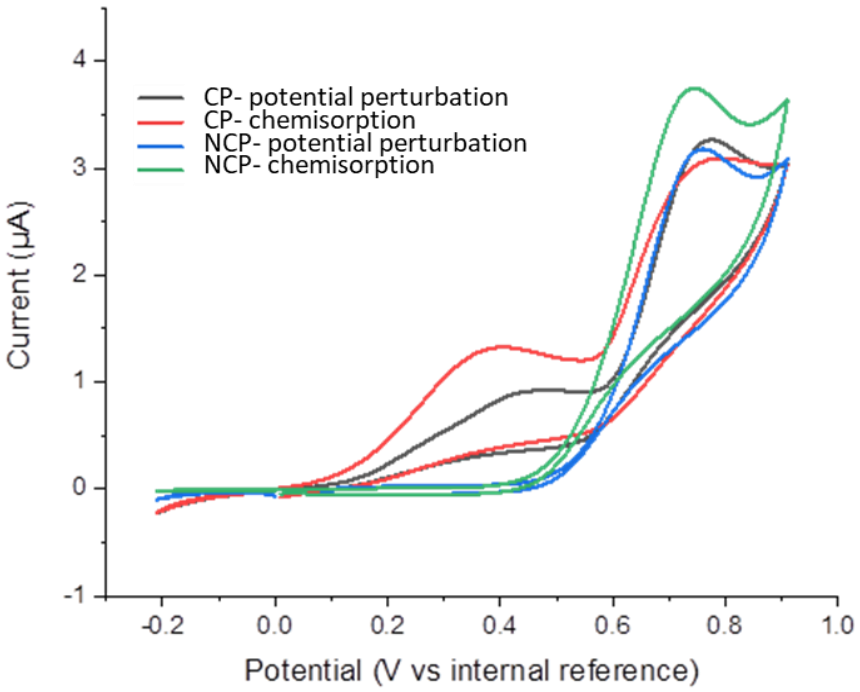


*Figure 2.9 Cyclic voltammograms of the ssDNA modified electrodes after the DNA-detection step recorded in measuring buffer (50 mM Tris. HCl, 10 mM $MgCl_2$, pH 9.6) containing 3 mM pAPP. Scan rate, 0.1 V/s. Current vs in-built reference electrode potentials are presented here with complementary probe (CP) and non-complementary probe (NCP).*

In contrast to the electrode with the non-complementary probe, the electrode with the complementary probe can capture the biotinylated complementary target and, thus, also ALP-streptavidin conjugate via the biotin. In the case of chemisorbed capture probes, an intense current peak at +0.40 V (Figure 2.9) is specific for the electrode with the complementary probe and, thus, the peak was attributed to ALP activity, i.e. the electrochemical oxidation of pAP formed from pAPP. The second peak at +0.74 V was observed for all the electrodes and was attributed to the oxidation of unhydrolyzed pAPP. To avoid an increased background current, the amperometric detection was carried out at a constant potential of +0.45 V, which is sufficient to detect the pAP formation but to avoid the increased background. Noteworthy, the built-in reference electrode was slightly affected by the immobilization procedure leading to a difference of 0.04 V between the built-in Au reference electrodes of the sensors prepared through overnight immobilization and the potential perturbation method. This difference was taken into account for the following amperometric measurements. Because of a small difference in the built-in reference electrodes as mentioned above, the peak was slightly shifted in case of the potential perturbation immobilization method. To compensate for this, a potential of +0.45 V for chemisorbed probes and +0.50 V for potential perturbated probes was applied for the amperometry to ensure an accurate comparison between the immobilization protocols.

The resulting amperometric responses showed that both conventional chemisorption and the potential-perturbation immobilization showed well-detectable responses to the target oligonucleotide (Figure 2.10). The responses from the complementary probes exceeded 45 and 11 times the responses of the controls (scrambled sequences) for the overnight chemisorption and the potential perturbation immobilization, respectively. The electrodes

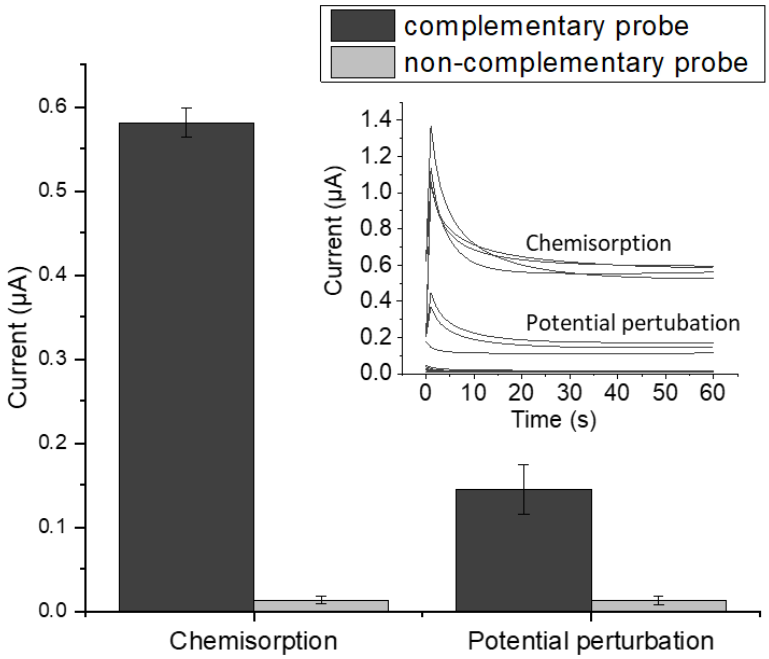


*Figure 2.10 Amperometric responses ssDNA-modified electrodes after incubation in 20 nM target DNA labelled with biotin followed by treatment with the alkaline phosphatase-streptavidin conjugate. Potential applied, +0.45 V for chemisorption and +0.50 V for potential perturbation (to compensate the difference between the potentials of the built-in Au reference electrodes). Error bars indicate the standard deviation from measurements with three independent electrodes. The inset shows the actual amperometric traces.*

with a more densely packed probe obtained via overnight chemisorption resulted in a four times higher average response compared to the electrode modified by the potential pulse-assisted method. This difference is close to the ratio in the amount of immobilized ssDNA (4.9 ± 1.3 times). From this, we conclude that the hybridization efficiency was not altered noticeably by the higher density of the probes. Thus, the response of the sensors prepared through overnight chemisorption was evaluated in the detection of different amounts of target DNA. The calibration curve from this experiment resulted in LOD of 0.14 nM and a sensitivity of 9.38 A $M^{-1}$ $cm^{-2}$ (Figure 2.11).

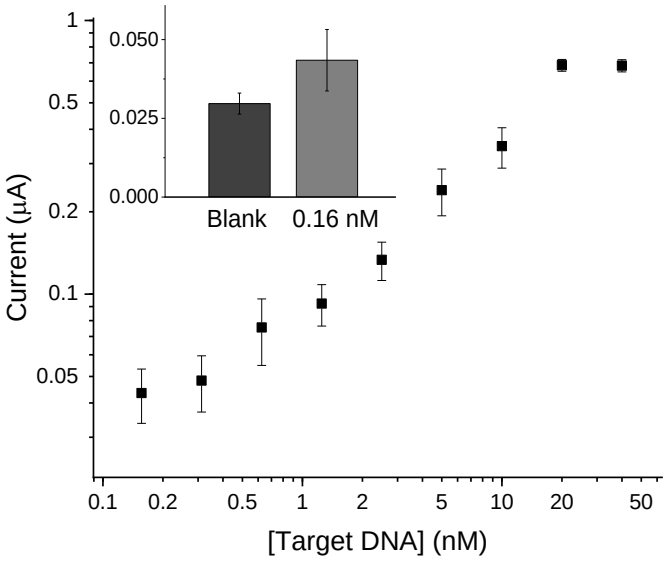


*Figure 2.11 Calibration plot for target-DNA detection from electrodes prepared through conventional chemisorption.*

It is noteworthy that the use of unoptimized cleaning protocols 1 and 2 lowered responses of the sensor to the complementary sequence and increased unspecific responses measured with the scrambled non-complementary probe (Table 2.3). The amplitude of the response was only 21% after protocol 1 and 49% after protocol 2 compared to protocol 5. The non-specific response was also 4 times higher for both protocol 1 and 2 compared to protocol 5. This shows the superiority of protocol 5 and motivates introducing an electrochemical cleaning step in addition to mechanical cleaning in an ultrasonic bath that rather removes large dust particles.

*Table 2.3 Specific and unspecific responses of the sensors prepared after three different cleaning protocols.*

| **Pretreatment protocol** | **Apparent $R_f$** | **Current response, I (µA)** | | **Amplitude (µA)** | **Relative amplitude** |
|---|---|---|---|---|---|
| | | **Complementary ($I_{CP}$)** | **Non-complementary ($I_{NCP}$)** | **$I_{CP}$- $I_{NCP}$** | |
| Protocol 1 | 1.15 | 0.114 ± 0.028 | 0.050 ± 0.012 | 0.064 | 21% |
| Protocol 2 | 1.34 | 0.204 ± 0.009 | 0.055 ± 0.007 | 0.148 | 49% |
| Protocol 5 | 1.76 | 0.314 ± 0.015[a] | 0.013 ± 0.006 | 0.300 | 100% |

*[a]The response in this data set is lower compared to the response given in Figures 2.9 and 2.10 due to the use of a different batch of the detection reagents and considerably lower room temperature (18°C vs 25°C). All data in this table were obtained in the same conditions to compare three cleaning protocols. Error indicate the standard deviation from three independent electrodes.*

Taking into account the need for a potentiostat and one-by-one handling during the potential perturbation method, the overnight chemisorption is advantageous in its simplicity, higher throughput and eventually increased sensitivity in DNA sensing at gold-sputtered microelectrodes. Nevertheless, the potential perturbation method can provide reproducible ssDNA immobilization and thiol back-filling within minutes (about 30 min in total for a set of 6 electrodes), which makes it attractive for systems which require a minimum density of probes but faster immobilization procedure.

## 2.5 Conclusion

Two critical steps in constructing electrochemical DNA sensors based on gold-sputtered microelectrodes with built-in gold reference and counter electrodes were optimized in this chapter: (1) electrochemical pretreatment of the gold working surface and (2) thiol-mediated tethering of ssDNA probes on it, followed by its detection capabilities. Cyclic potential sweeping between −1.0 and +1.3 V in a drop of 0.5 M $H_2SO_4$ was found to be the most effective procedure to clean the gold-sputtered microelectrodes, thus, improving the ease of preparation of electrode surface, compared to the tedious polishing and electrochemical cleaning of the conventional polycrystalline gold disk electrodes. The freshly pretreated gold-sputtered microelectrodes were effectively modified by a thiolated ssDNA probe through overnight chemisorption in a high ionic strength buffer. This resulted in about 70% of the maximal theoretical surface coverage (like conventional polycrystalline gold disk electrodes) and efficient hybridization capability. The modified electrodes could detect a complementary oligo resulting in an intense amperometric response 45 times higher compared to non-complementary blank control. To sum up, this work introduces an essential toolbox for surface preparation and modification and usage of commercial gold-sputtered microelectrodes as the cost-efficient platform for DNA sensors. These optimized protocols can be adapted to other sputtered gold working electrode surfaces (with printed/sputtered reference and counter electrodes made from gold or other elements) that are now emerging in the market as disposable gold electrode platforms.

# Chapter 3
# Singlet oxygen-based photoelectrochemical detection of oligonucleotides

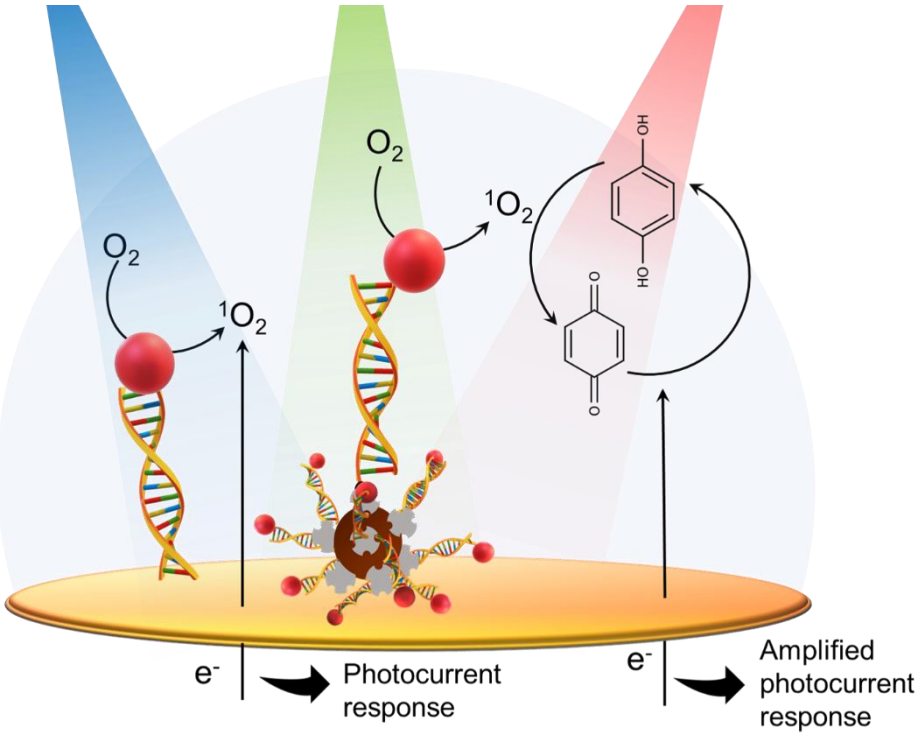


*Light-responsive DNA probes with type II PSs detecting the DNA hybridization event*

**Adapted from the following article:**

*Thiruvottriyur Shanmugam S., Trashin S., De Wael K. Singlet oxygen-based photoelectrochemical detection of DNA, Biosensors and Bioelectronics, Volume 195, 2022. 113652, https://doi.org/10.1016/j.bios.2021.113652.*

***Contribution:*** *I performed all the experiments and wrote the first draft of the manuscript.*

## 3.1 Abstract

This chapter, designed for the PEC detection of DNA, evaluates light-responsive DNA probes carrying molecular PSs generating $^1O_2$ upon photoexcitation and result in a photocurrent response. Type I, fluorescent and type II PSs were studied using diode lasers at 406 nm blue, 532 nm green and 659 nm red lasers in the presence and absence of a redox reporter, hydroquinone (HQ). Only type II PSs (producing $^1O_2$) resulted in a noticeable photocurrent in 1-4 nA range upon illumination, in particular, dissolved DNA probes labelled with chlorin e6 and erythrosine were found to give a well-detectable photocurrent response in the presence of HQ. Whereas type I PSs and fluorescent chromophores generated negligible photocurrents (< 0.15 nA). The analytical performance of the sensing system was evaluated using a magnetic beads-based DNA assay on disposable electrode platforms, with a focus to enhance the sensitivity and robustness of the technique in detecting complementary DNA targets. Amplified photocurrent responses in the range of 70-100 nA were obtained and detection limits of 17 pM and 10 pM were achieved using magnetic beads-captured chlorin e6 and erythrosine labelled DNA probes respectively. The presented novel PEC detection can further be optimized and employed in applications for which enzymatic amplification such as PCR is not applicable owing to their limitations and as an effective alternative to colourimetric detection when rapid detection of specific nucleic acid targets is required.

## 3.2 Introduction

Detection of specific DNA and RNA sequences has a great potential in clinical diagnostics including the detection of pathogens,[142, 143] the diagnosis of genetic diseases,[144] and the detection of markers for different malignancies[145] and other clinical pathologies.[146, 147] Thus, many researchers have attempted to develop analytical strategies to facilitate POC DNA detection and have elaborated multiple platforms with or without PCR amplification.[148] Electrochemical sensors have become one of the most promising platforms due to technological advances in microelectronics, high sensitivity of electrochemical methods and commercial availability of low-cost disposable electrodes used as the sensor transducer. [66, 118, 149, 150]

Since oligonucleotides exhibit poor and irreversible intrinsic electrochemistry due to oxidation at large overpotentials, the use of attached or intercalated redox labels was introduced.[151, 152] However, the electrochemical activity of such electroactive labels and indicators strongly depends on their distance to the electrode surface due to a major potential drop in the electrical double layer (ca. 1 nm). Thus, the orientation of hybridized duplexes, their dynamics on the surface, and backfilling or contamination of the unoccupied surface affect the electrochemical response in a complex manner and may result in poorly reproducible data. For this reason, the use of enzymatic labels generating an electroactive product stays the most prominent analytical strategy.[153, 154]

In contrast to redox and enzymatic labels, fluorescent labels have become a routine tool in bioanalysis and biochemical research. The variety in their excitation spectra covering the visible range made multiplexing possible in the analysis, while high extinction coefficients and fluorescence quantum yields* ensured high sensitivity. However, fluorescent dyes are often prone to photobleaching due to the formation of reactive oxygen species (ROS) due to side reactions.[155] Nevertheless, the labels with a high tendency to form ROS have found applications in electron microscopy[156] and biochemical research for local damaging (ca. 1 nm distance) of biomolecules and cellular components by highly reactive hydroxyl radicals.[157] Such light-responsive fluorescent labels combine the high specificity of biomolecules (DNA or antibody) and photosensitizing properties of the dyes. Despite the

*Quantum yield is the number of times a specific event occurs per photon absorbed by the system.

variety in known fluorescent probes, oligonucleotides labelled by PSs and their applications in (photo)electrochemistry are scarcely represented in the literature.

Previously, PEC detection of a specific oligonucleotide linked to pheophorbide a, a PS known to generate $^1O_2$ under red light illumination was demonstrated.[106] However, large lipophilic labels may show steric hindrance due to aggregation leading to a lower coupling yield, potentially impacting the properties of oligonucleotides. A more systematic study is needed to explore the PEC detectability of the light-responsive DNA probes carrying molecular PSs. Nevertheless, PEC sensors for DNA detection were extensively reported in the literature.[158] All of them were based on photoinduced electron-transfer reactions (mostly in semiconducting or conducting nanoparticles used as labels[159] or changes in photocurrent of underlying photoelectroactive polymers or complex composite coatings [160-162]).

In this chapter, a series of generally known light-responsive DNA probes (DNA sequence labelled with chromophores) has been assessed for their ability to generate a photocurrent upon illumination. More specifically, commercially available chromophores linked to DNA with absorbance maxima nearly matching the wavelengths of commonly available diode laser pointers (405, 532 and 659 nm) have been chosen. Then, the detectability of these DNA probes was assessed in different settings, such as (i) surface captured, via hybridization to the surface-confined complementary capture DNA probe (attached to the electrode surface via the thiol group), (ii) dissolved, in measuring solutions and (iii) captured at the surface of magnetic beads, via hybridization to the complementary capture DNA probe attached to the beads, to correlate the observed photocurrent with their properties to better understand the underlying molecular mechanisms.

## 3.3 Experimental

### 3.3.1 Chemicals

Chlorin e 6 (ChlE6, purity ≥ 98%, Cayman chemical company, USA), methylene blue (MetB, Reag. Ph Eur, Merck KgaA, Germany), malachite green (MalG, purity ≥ 96%, J&K Scientific, Belgium) eosin Y (EosY, purity ~ 99%, Sigma Aldrich), erythrosin B (EryB, purity ≥ 95%, Merck Schuchardt OHG), ATTO 532 (Eurogentec, Belgium), Rose Bengal (RB, purity >95%, Sigma-Aldrich), quinacrine (purity > 90%, Sigma Aldrich), hydroquinone (HQ, Acros Organics, Belgium) were used as received.

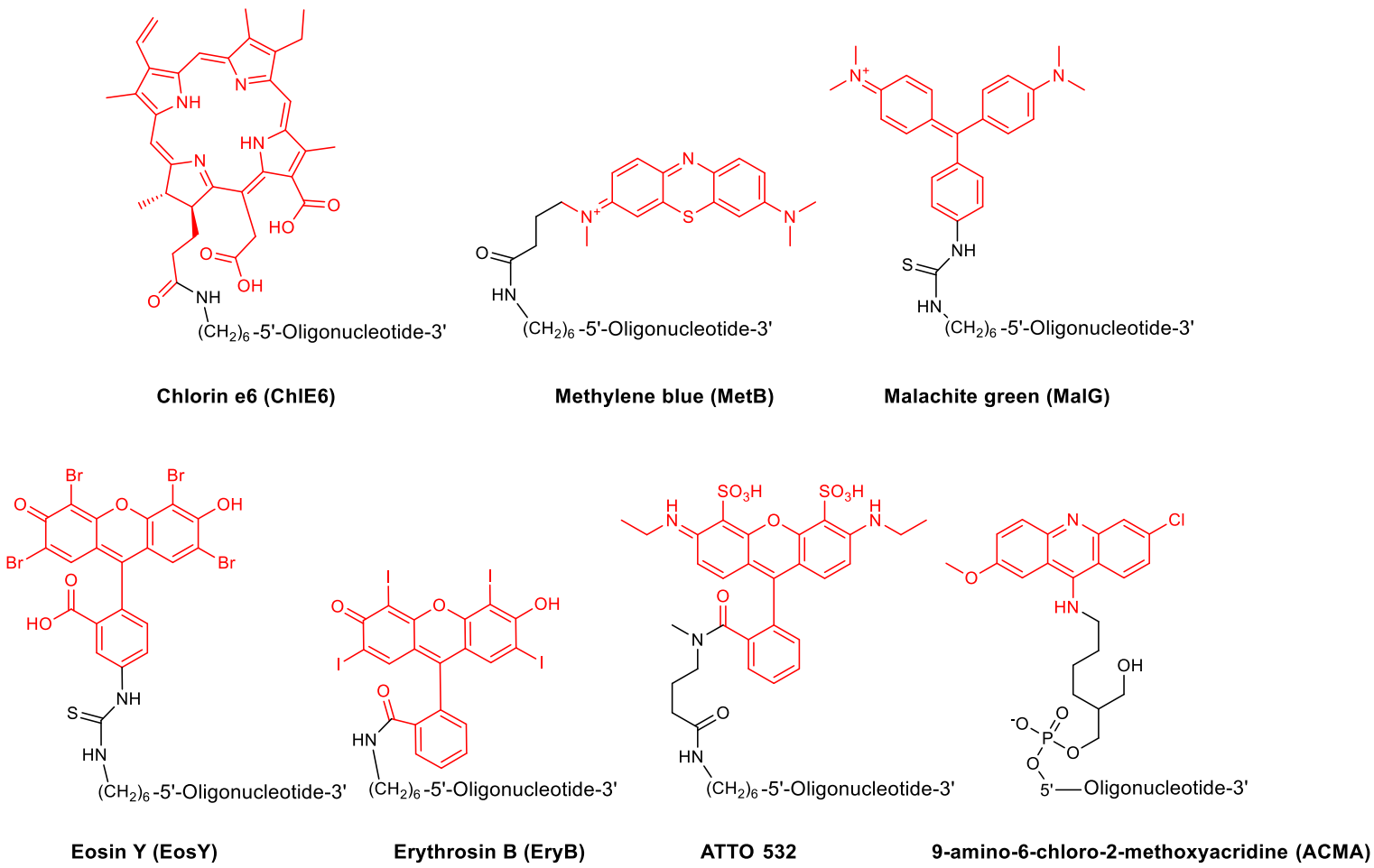


*Figure 3.1 Structures of chromophores attached to DNA used in chapter 3.*

DNA modified at 5'-end by the chromophores (Figure 3.1) were synthesized and purified by Eurogentec (Belgium) except DNA-MetB which was prepared by Metabion (Germany). The structures and purity were confirmed by mass spectrometry by the supplier. The DNA sequence 5'-TCA-ACA-TCA-GTC-TGA-TAA-GCT-A 3' was chosen to be complementary to microRNA-21 (miR-21), an important marker for several types of cancer and cardiovascular diseases. [137] The chromophores were attached to DNA via a 5' amino-C6 linker using either activated carboxylic or isothiocyanate functionality. The acridine derivative was used as phosphoramidite and was attached via direct link extension. Complementary (5' TAG-CTT-ATC-AGA-CTG-ATG-TTG-A-3') and scrambled non-complementary (5' TAG-CTT-ATG-TGT-ACC-CTG-TCA-G-3') DNA were modified at 5'-end by thiol C6 (HS-$(CH_2)_6$-) or Biotin TEG (a 16-atom spacer based on a triethylene glycol) by Eurogentec (Belgium) for immobilization on gold and streptavidin-modified surfaces, respectively.

### 3.3.2 Preparation of gold disk electrodes

The gold disk electrodes (1.6 mm diameter, BASi®, USA) were polished with diamond spray (3, 1, 0.25 μm from Struers) and alumina slurry (0.05 μm from SPI supplies) and cleaned after each step in pure ethanol and MQ water in an ultrasonic bath. Following this, the electrodes were cleaned electrochemically by cyclic voltammetry in 0.5 M NaOH (between −0.35 and −1.4 V vs. SCE) and then in 0.5 M $H_2SO_4$ (between 0.25 V to 1.5 V vs. SCE at 0.1 V/s) until repeatable voltammograms were obtained. Freshly prepared electrodes were incubated in a 1 μM thiolated capture DNA probe containing 0.2 μM mercaptohexanol (MH, purity >98.0%, TCI chemicals) in immobilization buffer overnight (∼16 hours) and then in 1 mM MH for 2 h, for backfilling and removing weakly bound DNA molecules. For the hybridization step, a 40 μL drop of labelled DNA was placed on the electrode for 1 h and washed with a copious amount of wash buffer. Immobilization (Tris) buffer contained 500 mM KCl, 50 mM $MgCl_2$, and 10 mM Tris pH 7.5. The wash buffer (Tris-$T_{20}$) had the same composition but additionally contained 0.05% w/v tween 20.

### 3.3.3 DNA immobilization on magnetic beads

A fraction (10 μl of the stock suspension per one measurement) of streptavidin-modified magnetic beads (Dynabeads® M-280 Streptavidin, 10 mg/mL, Invitrogen) was washed three times with PBS-$T_{20}$ (0.05% Tween 20 in PBS pH 7.4 buffer containing 10 mM $Na_2HPO_4$, 137 mM NaCl, 1.8 mM $KH_2PO_4$ and 2.7 mM KCl). Then they were incubated with 0.5 mL 1 μM biotinylated complementary or non-complementary sequences in PBS-$T_{20}$ on a thermal shaker at 37°C, 250 rpm for 1 hour. Next, they were washed and incubated with the labelled DNA on a thermal shaker at 37°C, 250 rpm for 1 hour. Finally, the beads were washed two times with PBS-$T_{20}$ and another wash with PBS and stored in PBS before measurements.

### 3.3.4 PEC measurements

PEC measurements were carried out with a µAutolab III (Metrohm-Autolab BV) using Nova 1.11 software. Diode lasers operating at 659 nm, 532 nm and 405 nm were purchased from Roithner Lasertechnik (Austria). The light power was adjusted to 30 mW using a light power meter (Thorlabs, Inc.). The diameter of the light beam was adjusted to illuminate the working electrodes. The on/off switch for illumination was preprogrammed and controlled by an Arduino Uno equipped with a relay. The background electrolyte used for all measurements consisted of 0.1 M KCl and 0.01 M $KH_2PO_4$ adjusted to pH 7 (phosphate buffer) providing the same ionic strength for all measurements. HQ solutions used for measurements were prepared in this phosphate buffer and stored in an ice bath until measurements.

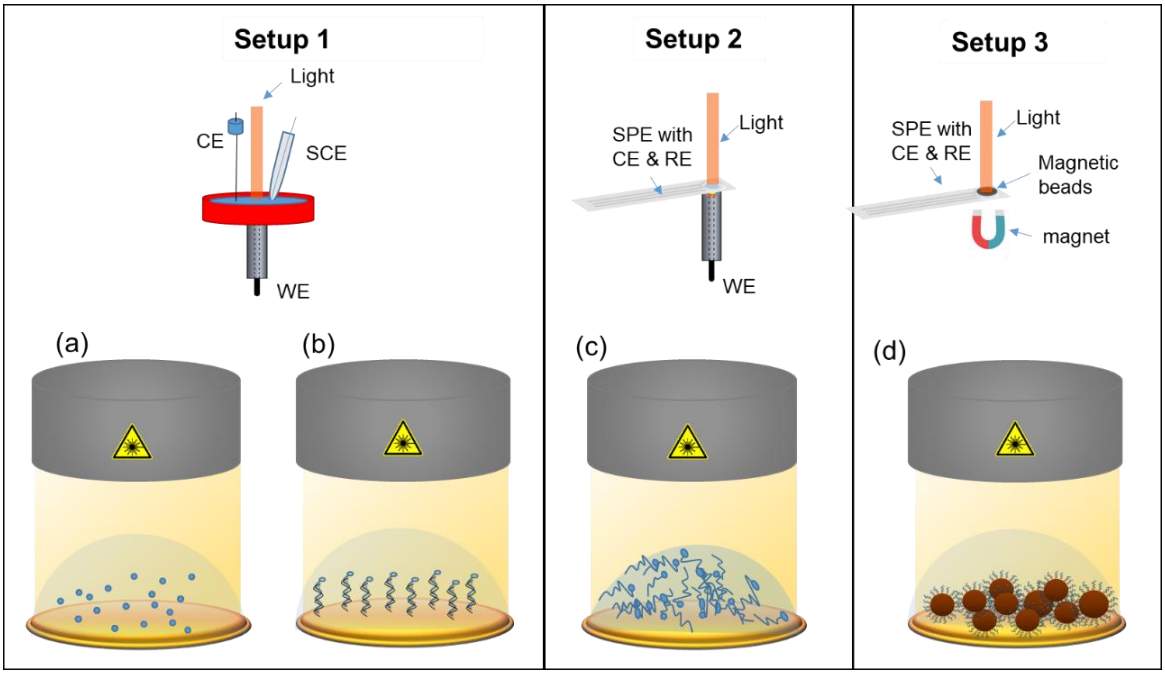


*Figure 3.2 Representation of three photoelectrochemical setups used for four conditions in the study: (a) free chromophore dissolved in solution, (b) labelled DNA captured at the surface of the gold electrode, (c) labelled DNA dissolved in solution and (d) labelled DNA is captured at the surface of magnetic beads. WE: working electrode, RE: reference electrode, CE: counter electrode.*

Three electrochemical setups were used for PEC measurements (Figure 3.2). The pictures of the setups are presented in Figure 3.3. Setup 1 was made of an open vessel containing 10 mL of electrolyte with a working gold disk electrode inserted from the bottom for illumination with light. An SCE reference (SCE, radiometer, Denmark) and platinum wire counter electrodes were placed in solution from the top. Measurements were conducted at a potential of –0.05 V vs. SCE.

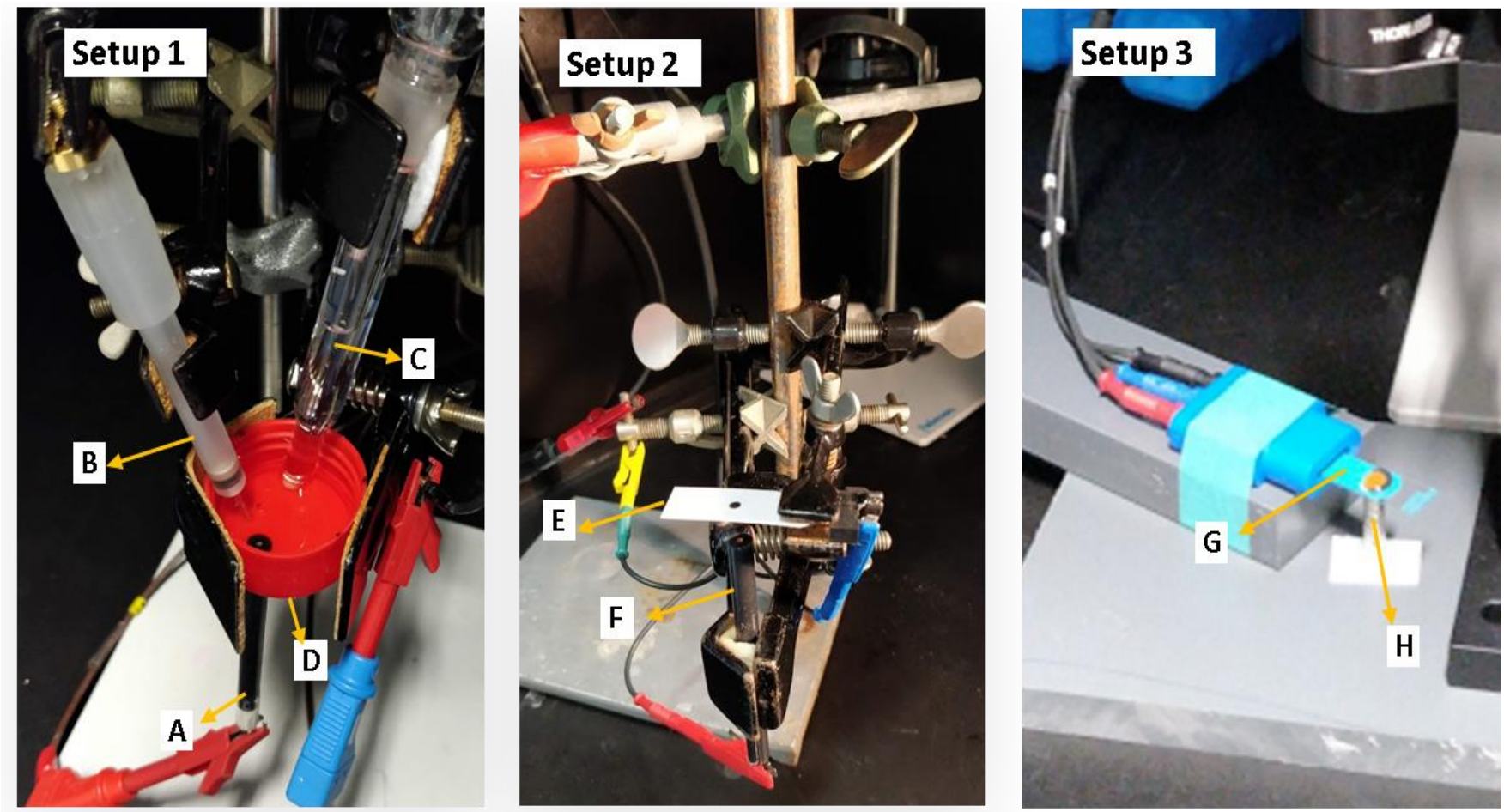


*Figure 3.3 Images of electrochemical setups used for the PEC study in chapter 3: polycrystalline gold disk working electrode (A,F), Platinum counter electrode (B), SCE reference electrode (C), and open vessel cell (D). Italsens graphite screen printed electrode (E) with reference and counter electrode connected to the cell and working electrode punched off to let the laser light fall on the working electrode oriented upwards, gold-sputtered planar electrode (G) and neodymium magnet (H).*

Setup 2 was introduced to minimize the amount of working solution required per experiment. A drop of 80 μL was placed on the gold disk electrode oriented upwards. Then a screen-printed electrode (SPE, IS-C, ItalSens) covered the drop from the top that the SPE reference and counter electrodes of the SPE were immersed in the measuring solution. A hole of 2 mm in diameter was preliminarily punctured in the place of the SPE working electrode (which is not used in the measurements) for illumination with the lasers. The difference of 90 ± 3 mV between the potential of the SCE and the quasi-silver SPE reference electrode was considered (−0.14 V vs the SPE reference electrode was applied) to reproduce conditions in setup 1.

Setup 3 was used for PEC measurements with magnetic beads accumulated on the surface of a gold-sputtered planar electrode (AUTR10, Dropsens) by placing a neodymium magnet underneath. As an alternative, carbon screen printed electrodes (C-SPE, Dropsens) were tested in the same manner. Before the measurements, beads were re-suspended in 10 μL of phosphate buffer and gently transferred into the measuring drop, where all the beads quickly precipitated at the working electrode due to a neodymium magnet below it. Photocurrents in this setup were measured at -0.15 V vs. the SPE quasi-reference electrode (100 ± 5 mV vs. SCE).

All chronoamperometric PEC measurements were conducted in light-chopped conditions (10 s or 30 s ON and 60 s OFF). Polynomial baseline correction was constructed through background current values (in dark) and subtracted from the amperograms to obtain baseline-corrected photocurrent responses. For ease of visual comparison among the electrodes, all the amperograms were plotted after subtraction of the baseline.

### 3.3.5 Spectroscopic measurements

An Implen NanoPhotometer N60 (Implen GmbH, Germany) was used to measure the UV-Vis spectra of labelled DNA. AvaSpec-2048 L from Avantes equipped with an AvaLight-DH-S-BAL light source was used to record the UV-Vis spectra of chromophores. The $^1O_2$ -producing capability of free chromophores was assessed with UV-VIS spectroscopy in the measuring buffer used for PEC studies. Furfuryl alcohol (FFA, 98 %, J&K Scientific) was used as a chemical trap to detect and quantify the capability of the chromophores to generate $^1O_2$.[163-165] The UV-vis spectra (in the range of 210 — 1000 nm) along with the time label were recorded automatically every 20 s under continuous stirring and illumination with a corresponding laser adjusted to 30 mW. The changes in the absorbance region of [FFA-$O_2$] formation at 240 nm were monitored for 16 minutes. The relative ability of the chromophores to produce $^1O_2$ was then calculated after correction with photon flux for the

three light sources. The kinetics were normalized to the absorbance factor ($1\text{-}10^{-absorbance}$) at the laser wavelength for accurate correlation with the $^1O_2$ quantum yields ($\Phi_\Delta$), although the concentrations of the dyes were initially adjusted to provide similar absorbance in solution. The measurements were repeated at least three times.

## 3.4 Results and discussion

### 3.4.1 PEC detection of light-responsive DNA probes

Most of the organic chromophores that are used for DNA labelling (so-called light-responsive probes) can be categorized into three general groups: fluorescent chromophores that do not induce chemical reactions, PSs that produce radicals upon light radiation but do not form $^1O_2$ (so-called type I PSs) and PSs that produce $^1O_2$ (so-called type II PSs). However, some chromophores can exhibit mixed behaviour.[166, 167] Many PSs also show fluorescence whereas many well-known fluorophores can generate small amounts of ROS.[168] A series of chromophores of different types that are commercially available in forms ready for coupling to oligonucleotides were chosen giving us the light-responsive DNA probes. Chromophores acting as type I PS (malachite green (MalG)) and type II PSs (chlorin e6 (ChlE6) and methylene blue (MetB)) were expected to produce noticeable photocurrent[106, 169] and, thus, should be useful as molecular labels in PEC DNA sensors. In contrast, fluorescent dyes (ATTO 532 (structurally similar to rhodamine 6G) and 9-amino-2-methoxy-6-chloroacridine (ACMA)) without photosensitizing properties should not generate a noticeable photocurrent. The near-zero potential of -0.05 V providing a high absolute current and a high signal/blank ratio (Figure 3.4) was chosen as the potential for performing chronoamperometry.

Figure 3.5 A shows the light chopped chronoamperograms of light-responsive DNA probes, labelled with seven different chromophores after being captured by the surface-confined complementary capture DNA probe at the electrode surface (attached to the surface via the thiol group). An identical electrode with non-complementary (scrambled) DNA probes was used as a blank control and showed only diminishing photocurrent responses. Well-known type II PSs chlorin e6 (ChlE6) and methylene blue (MetB) showed strong photocurrent responses for the complementary strands. Whereas a well-known type I PS malachite green (MalG)[170] showed no photocurrent responses. Moreover, familiar fluorescent dye ATTO 532 and 9-amino-2-methoxy-6-chloroacridine (ACMA), gave no photocurrent responses for the complementary strand either. In contrast, eosin Y (EosY) and erythrosine B (EryB), containing the same xanthene core as ATTO 532 but exhibiting well-documented type II photosensitizing behaviour,[168] showed clear photocurrent responses in the same conditions. From this, it was concluded that the type II

photosensitizing mechanism is essential for chromophores to generate a photocurrent in the taken conditions, presumably due to the electrochemical reduction of $^1O_2$ at the applied potential of -0.05 V vs SCE.

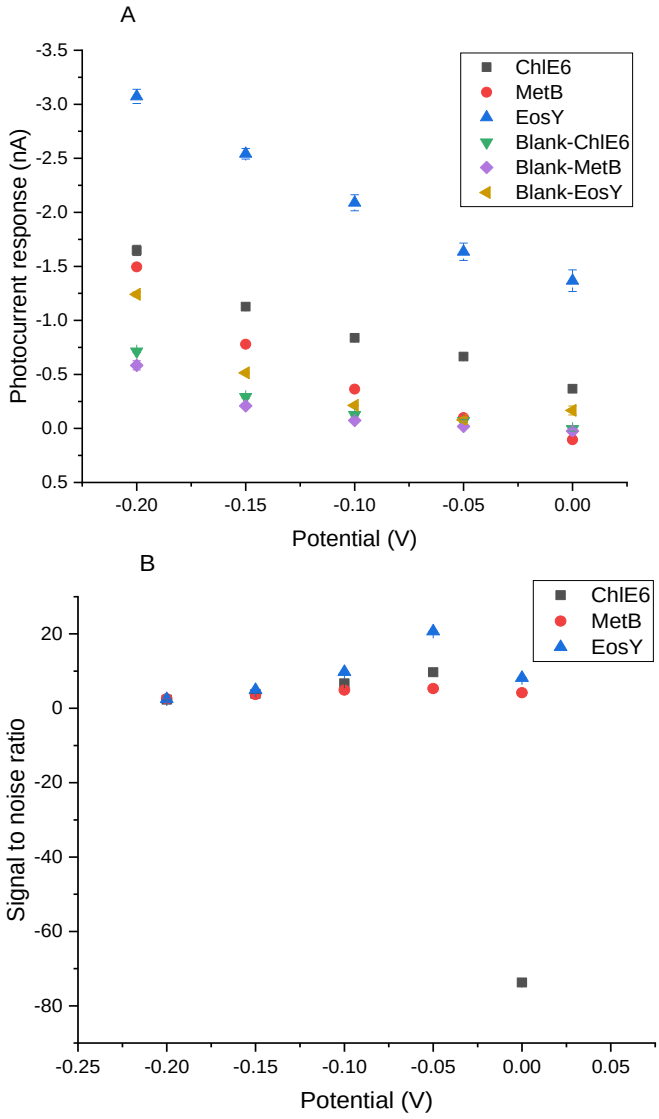


*Figure 3.4 (A) Effect of potential (vs SCE) on the specific photoelectrochemical response from 5 µM photosensitizer and the blank buffer response in PB, pH7 on GDE. (B) Signal to noise ratio of photosensitizer and blank buffer as function of potential. Error bars indicate the standard deviation from three independent electrodes.*

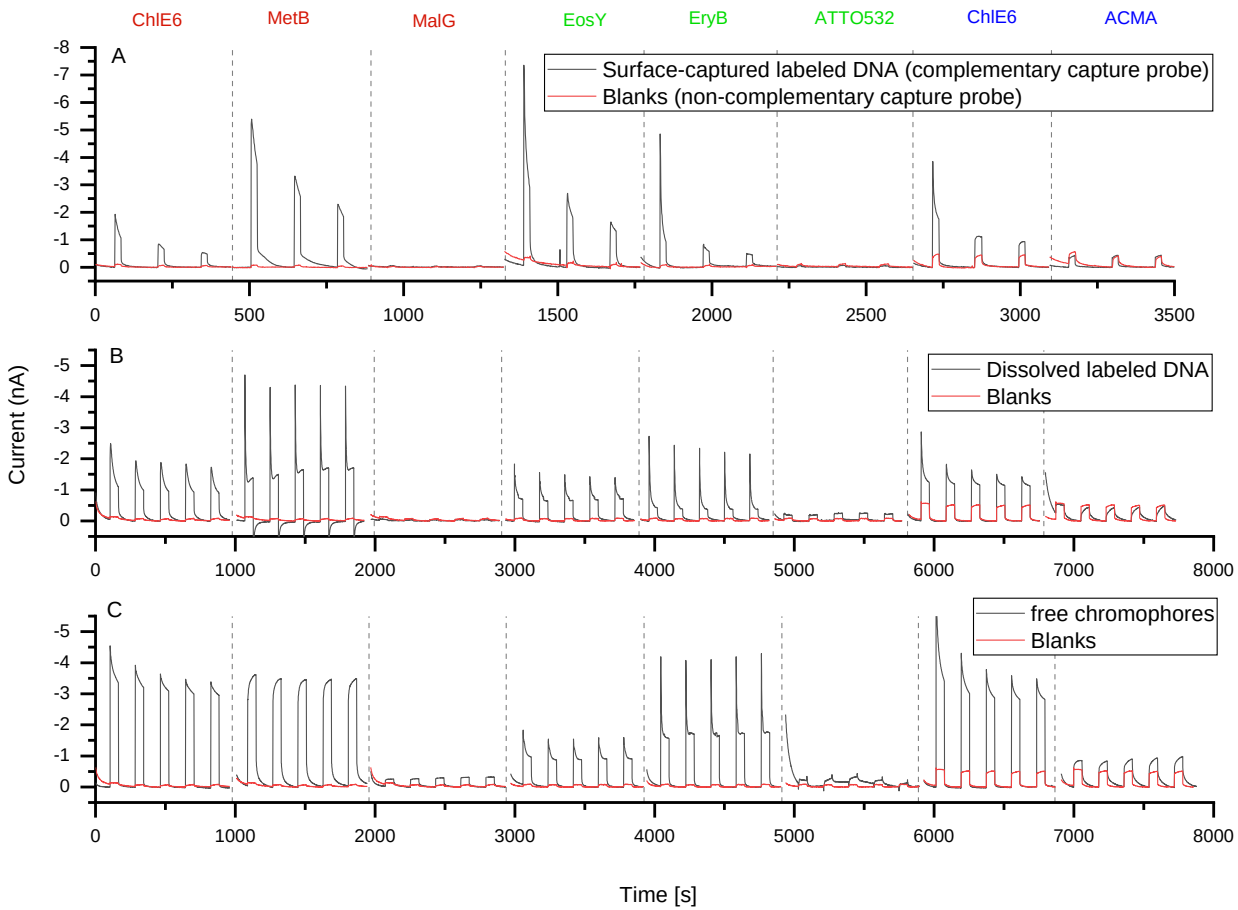


*Figure 3.5 Chronoamperograms under chopped-light conditions for (A) surface-captured labelled DNA hybridized to complementary capture probe immobilized to gold electrode surface via thiol, in comparison to blanks from a non-complementary capture probe, (B) 5 µM dissolved labelled DNA in solution on, (C) 5 µM free chromophores in solution, on gold electrodes. The blanks in (B) and (C) were obtained in pure phosphate buffer. The electrodes were illuminated with the LED lasers (659 nm for ChlE6, MetB, MalG; 532 nm for EosY, EryB, ATTO532; 406 nm for ChlE6, ACMA) with an output power of 30 mW and a spot diameter adjusted to ca. 4 mm.*

Interestingly, the photocurrent response decays rapidly during the illuminations and drops with each new illumination as shown in Figure 3.5 A. For example, in the case of EosY, the photocurrent dropped twice during the first illumination (10 s) and counted only 40% and 20% by the end of the second and the third illuminations, respectively. The same behavior was observed previously for an oligonucleotide labelled by pheophorbide a [106] and this behavior was attributed to DNA cleavages by ROS without more detailed investigation. To discriminate between photobleaching of the chromophore and possible cleavages in the surface-confined duplex with the labelled DNA sequences, the labelled DNA, as well as the chromophores in the free form, were tested as dissolved in the buffer using the same electrodes but without any capture DNA-probe immobilized on the gold surface. In these conditions, only photobleaching can result in photocurrent decay whereas cleavages, even if happened, should not change the concentration and activity of the chromophore. Indeed, in contrast to the surface-captured labelled DNA, the responses for dissolved species were essentially repeatable over a sequence of at least three illuminations (Figure 3.5 B and C). This confirms that the chromophores are stable in the used conditions at least within the experimental time. Thus, the signal decay for the surface-confined chromophores as in Figure 3.5 A indeed results from the DNA cleavages from the gold surface followed by diffusion of the labelled fragments away from the electrode surface.

### 3.4.2 Correlation of photocurrents with optical properties and $^1O_2$ quantum yields of chromophores

Surface-captured DNA, dissolved labelled DNA and free chromophores showed generally similar reactivity profiles for each chromophore (Figure 3.5). Also, some specific features can be identified and attributed to the difference in extinction coefficients[†] (ε) at the corresponding laser wavelengths (Figure 3.6). In particular, EosY gives a higher photocurrent compared to EryB when linked to DNA and opposite in the free form (Figure 3.5 B and C). This behaviour is explained by a shift in positions of the absorbance maxima in linked chromophores compared to the free chromophores (Table 3.1, Figure 3.7), possibly due to changes in the microenvironment or shifts in pKa of dyes linked to DNA [171]. This shift affects the extinction coefficient at 532 nm for EosY and EryB in such a way that the ratio between them reverses in the free form (Table 3.1). This confirms that the PEC activity of the chromophores correlates with their extinction coefficients.

[†]Extinction coefficient is a characteristic that determines how strongly a species absorbs or reflects radiation or light at a particular wavelength.

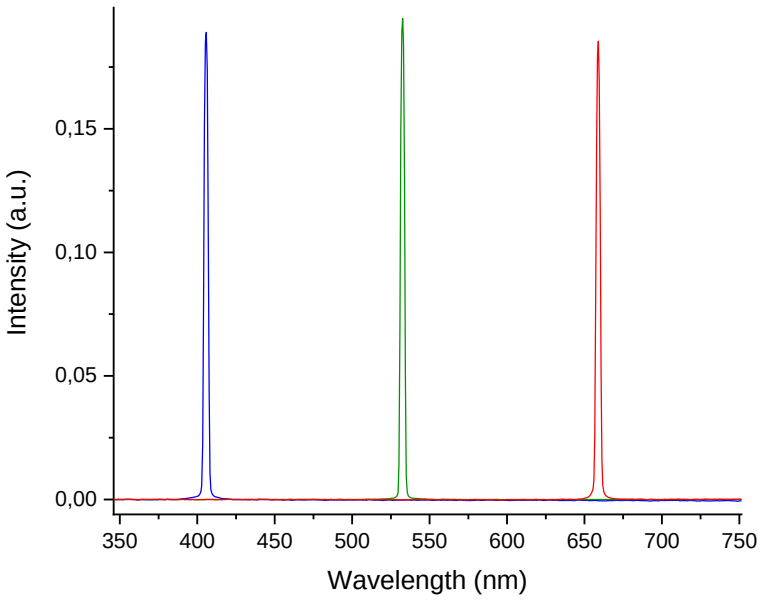


*Figure 3.6 UV-Vis spectra of 3 diode lasers (405 nm- blue, 532 nm- green, 659 nm – red) irradiating the phosphate buffer used in this study.*

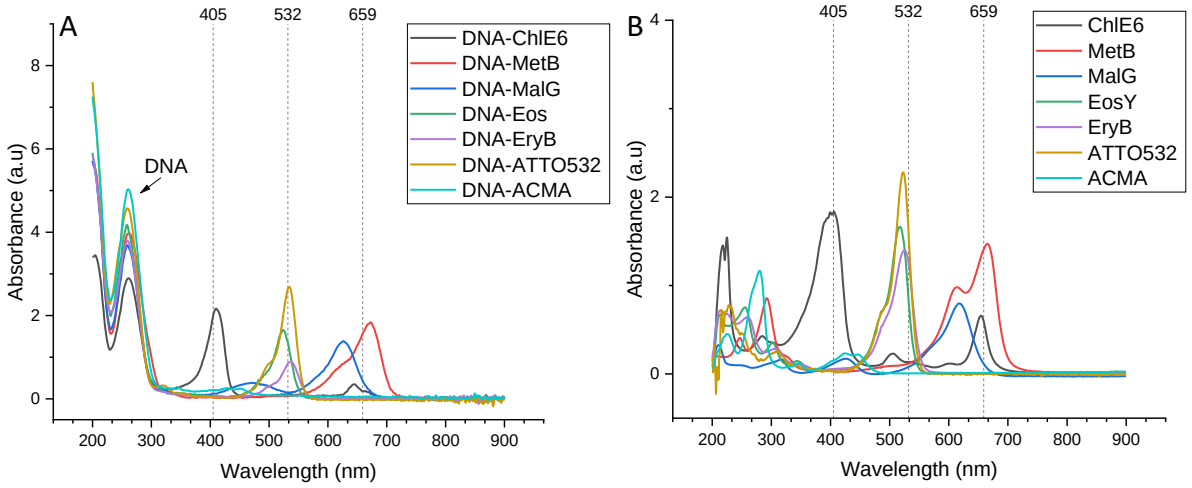


*Figure 3.7 UV-Vis spectra of (A) 20 µM chromophores-DNA in measuring buffer, PB, pH 7. (B) 20 µM chromophores in measuring buffer, PB, pH 7. The vertical reference lines indicate the wavelengths of lasers used in this study.*

In addition, the extinction coefficient for MetB-DNA at 659 nm is 6 times higher compared to that of ChlE6-DNA, which explains a higher photocurrent for MetB-DNA compared to ChlE6-DNA although the $^1O_2$ quantum yield is expected to be higher for ChlE6.[172, 173] The extinction coefficient for MetB in free form is only 2.7 times higher than that of ChlE6. Besides, MetB may dimerize in water,[174, 175] which was evident in our conditions from the

UV-vis spectra that showed an increase of absorbance in the shoulder at 620 nm (Figure 3.7 B). The dimerization is known to suppress $^1O_2$ quantum yields, which, along with the smaller difference in the extinction coefficients, explains the change in the relative activity of MetB in comparison to ChlE6. Surprisingly, the change of the laser wavelength from 659 to 406 nm, where ChlE6 has five times higher extinction coefficient, does not improve the photocurrent. This might be related to a stronger engagement of the chromophore in secondary photoreactions when excited into a more energetic electronic state and noticeable formation of superoxide radical, a known $^1O_2$ quencher.[176]

*Table 3.1 Extinction coefficients $\varepsilon$ ($M^{-1}cm^{-1}$) at given wavelengths $\lambda$ (nm) for the chromophore linked to DNA and in the free form.*

| | **Chromophores linked to DNA** | | | | **Free chromophore** | | | |
|---|---|---|---|---|---|---|---|---|
| | $\lambda_{max}$ | $\varepsilon(\lambda_{max})$ | $\lambda_{laser}$ | $\varepsilon(\lambda_{laser})$ | $\lambda_{max}$ | $\varepsilon(\lambda_{max})$ | $\lambda_{laser}$ | $\varepsilon(\lambda_{laser})$ |
| **ChlE6** | 645 | 2.3E+04 | 659 | 1.2E+04 | 656 | 4.8E+04 | 659 | 4.3E+04 |
| **MetB** | 673 | 8.8E+04 | 659 | 7.6E+04 | 665 | 1.1E+05 | 659 | 1.1E+05 |
| **MalG** | 626 | 7.2E+04 | 659 | 2.2E+04 | 622 | 7.0E+04 | 659 | 1.3E-04 |
| **EosY** | 524 | 8.6E+04 | 532 | 7.0E+04 | 517 | 1.3E+05 | 532 | 5.4E+04 |
| **EryB** | 537 | 4.8E+04 | 532 | 4.6E+04 | 524 | 1.0E+05 | 532 | 8.6E+04 |
| **ATTO532** | 534 | 1.1E+05 | 532 | 1.1E+05 | 534 | 1.4E+05 | 532 | 1.3E+05 |
| **ChlE6** | 410 | 1.4E+05 | 406 | 1.4E+05 | 403 | 2.3E+05 | 406 | 2.2E+05 |
| **ACMA** | 645 | 2.3E+04 | 406 | 1.2E+04 | 425 | 1.3E+04 | 406 | 8.5E+03 |

Because of the clear link between the type II photosensitization mechanism and the registered photocurrent, the relative $^1O_2$ quantum yields of the used chromophores in our experimental conditions were assessed employing an independent method, i.e. the spectrophotometric monitoring of furfuryl alcohol (FFA) as $^1O_2$ trap. The measurements were conducted with the same lasers and the buffer as in the chronoamperometric experiments. The relative activity of the PSs was obtained from the accumulation kinetics for the [FFA-$O_2$] adduct under constant light illumination (Table 3.2). The spectra of the chromophores before and after the illumination, changes in the region of 240 nm and the kinetics of accumulation of FFA-$O_2$ adduct in comparison with blank recorded in the absence of FFA are presented in detail in Figures 3.8- 3.10.

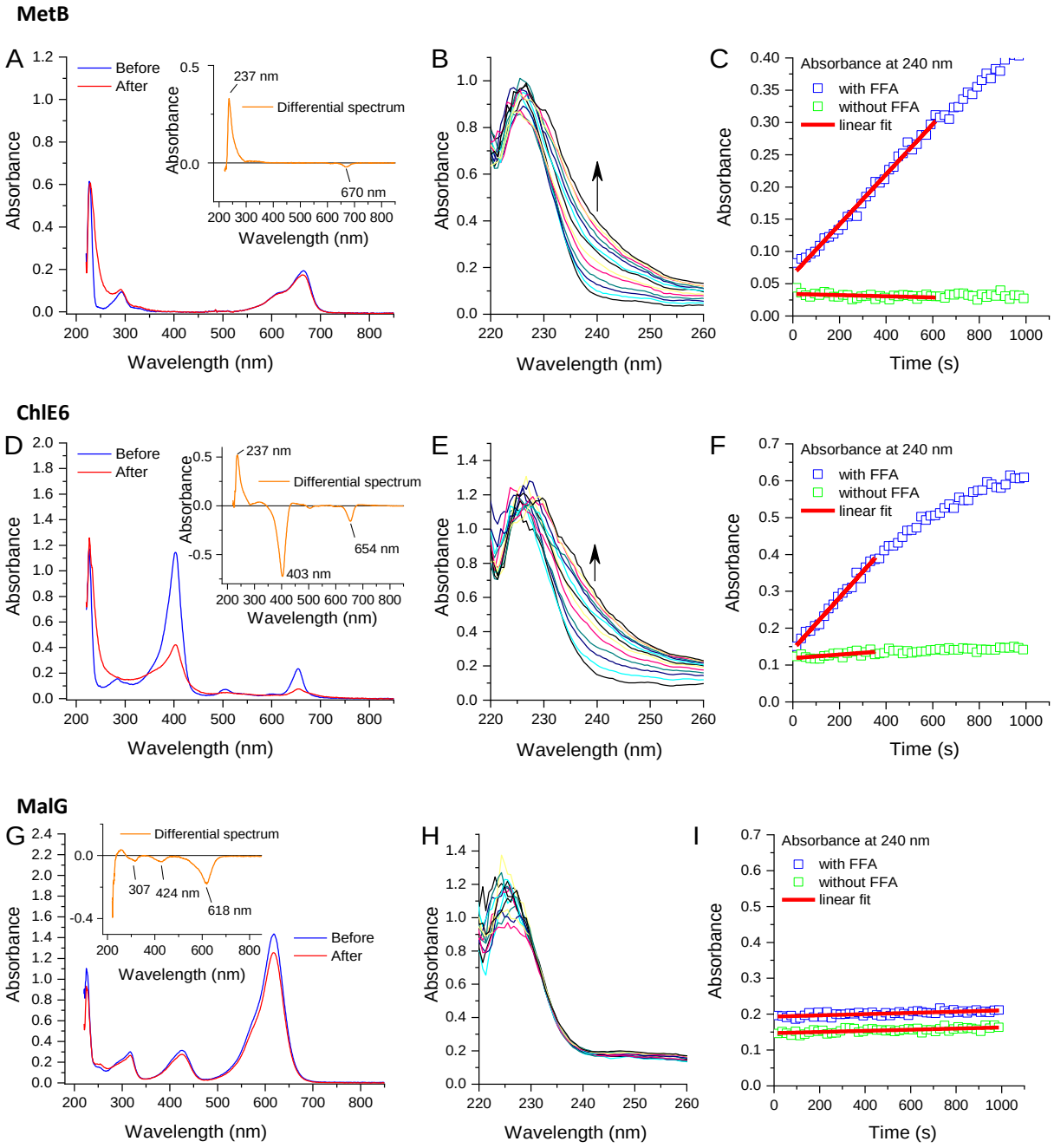


*Figure 3.8 The spectra of chromophores before and after illumination with the red 659 nm laser for 16 min (A, D, G), changes in the region of 240 nm (B, E, H) and the kinetics of accumulation of FFA-$O_2$ adduct in comparison with blank recorded in the absence of FFA (C, F, I).*

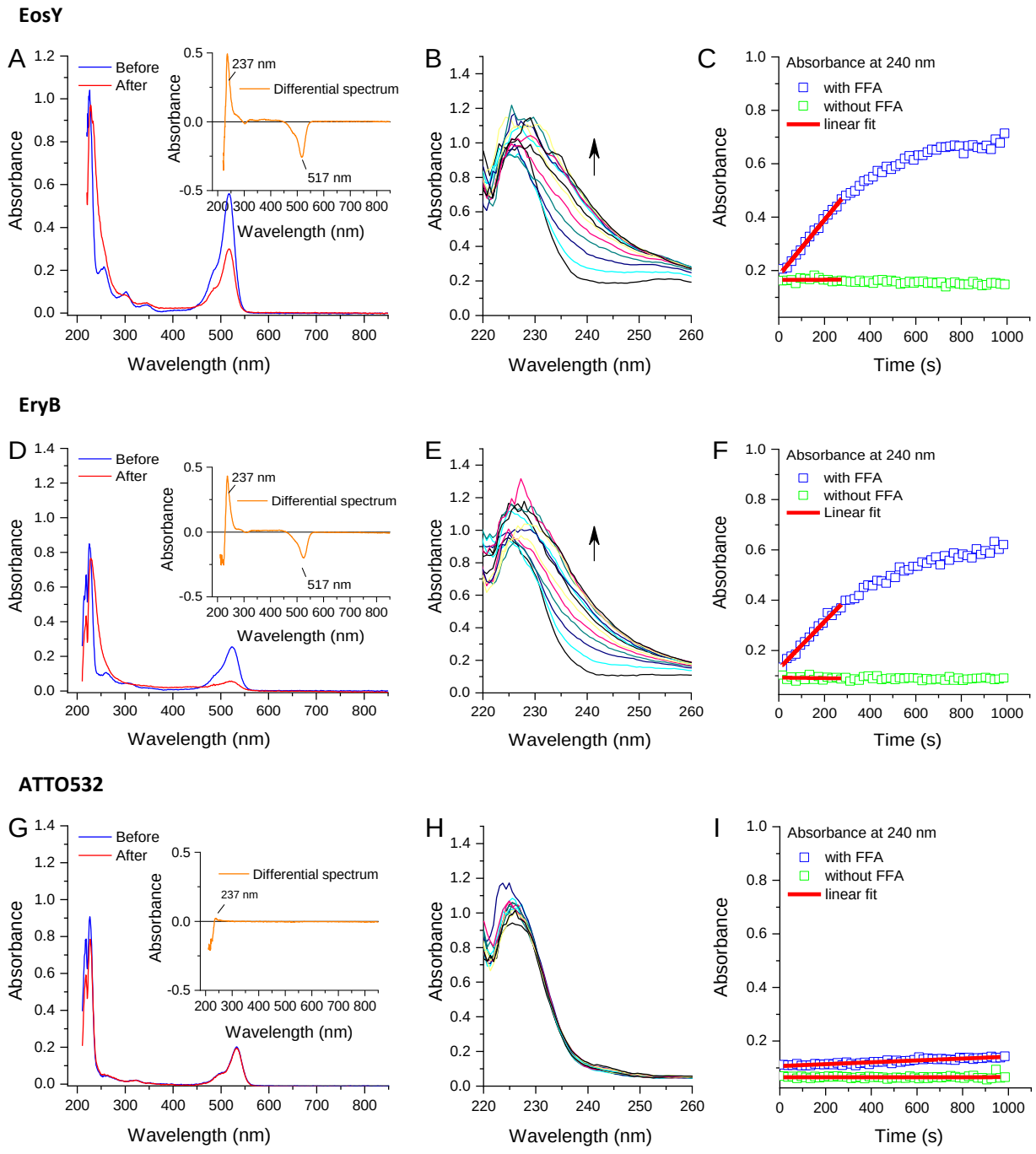


*Figure 3.9 The spectra of chromophores before and after illumination with the green 532 nm laser for 16 min (A, D, G), changes in the region of 240 nm (B, E, H) and the kinetics of accumulation of FFA-$O_2$ adduct in comparison with blank recorded in the absence of FFA (C, F, I).*

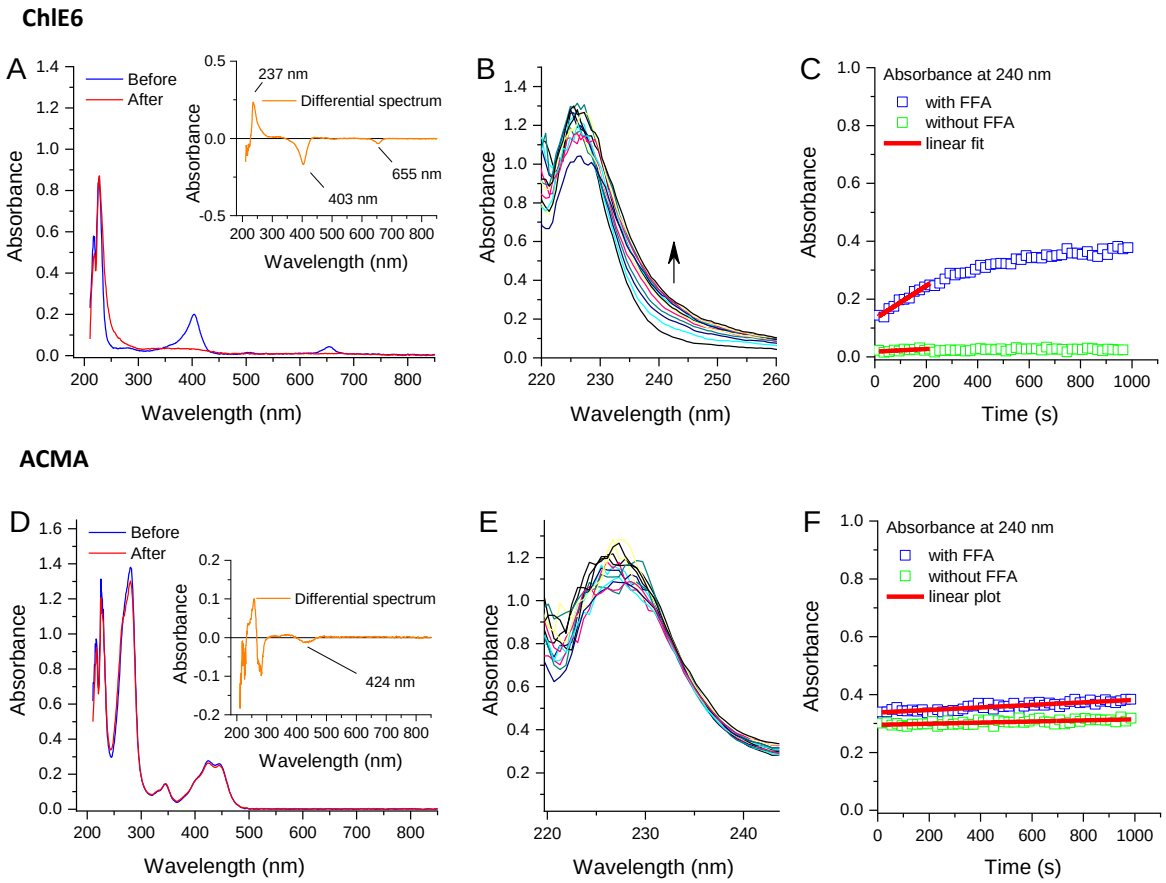


*Figure 3.10 The spectra of chromophores before and after illumination with the green 406 nm laser for 16 min (A, D, G, J), changes in the region of 240 nm (B, E) and the kinetics of accumulation of FFA-$O_2$ adduct in comparison with blank recorded in the absence of FFA (C, F).*

As expected, the type II PSs (MetB, ChlE6, EosY and EryB) resulted in the comparatively fast accumulation of the FFA-$O_2$ adduct, whereas other dyes showed minor or no formation of FFA-$O_2$ (Table 3.2). In particular, this confirms that MalG does not generate any significant amount of $^1O_2$ while ACMA and ATTO532 have very minor $^1O_2$ generation (30 times lower than for ChlE6) which corresponded to the complete absence of the photocurrent for MalG with still very minor photocurrents for ACMA and ATTO532. Additionally, MalG degrades noticeably, faster than other compounds used in this study (Figure 3.8), via type I reaction, undergoing $OH^{\bullet}$, $O_2^{\bullet-}$ and $H^+$ mediated photocatalytic degradation.[177] The highest activity was obtained for EosY, which, in combination with a high extinction coefficient at 532 nm when linked to DNA (70000 $M^{-1}cm^{-1}$) resulted in the highest photocurrent. MetB, in agreement with the evident dimerization, showed a 2 times lower production of $^1O_2$ compared to EosY in the same conditions (Table 3.2). However, DNA-linked MetB does not

suffer from this limitation, which explains its high PEC activity in Figures 3.5 A and B compared to EosY.

*Table 3.2 Relative $^1O_2$ production ability of free chromophores in each wavelength region of light.*

| | Concentration (μM) | Relative kinetics for [FFA-$O_2$] formation[a] | Literature $^1O_2$ quantum yields ($\Phi_\Delta$) |
|---|---|---|---|
| ChlE6 | 5.0 | 1.00 ± 0.02 | 0.71,[178] 0.64,[173] 0.66,[172] |
| MetB | 2.0 | 0.54 ± 0.01 | 0.52,[173] 0.60,[178] 0.49 [179] |
| MalG | 40 | -0.002 ± 0.002 | <0.003 [170] |
| EosY | 5.0 | 1.31 ± 0.09 | 0.52, 0.57,[178] 0.61[179] |
| EryB | 2.5 | 1.22 ± 0.04 | 0.68[178] 0.62[180] |
| ATTO532 | 2.0 | 0.03 ± 0.00 | N/A (fluorescent[181]) |
| ChlE6 | 1.0 | 0.80 ± 0.03 | 0.71,[178] 0.64,[173] 0.66[172] |
| ACMA/ quinacrine | 20 | 0.03 ± 0.01 | 0.013[182, 183] |

*[a]Average values presented with standard deviation from three measurements*

Noteworthy, quinacrine which is identical to ACMA linked to DNA showed only minor $^1O_2$ production (the $^1O_2$ quantum yield $\Phi_\Delta$ ca. 3% is in agreement with previous literature [182, 183]), although, the parent chromophore acridine is known as a good type II PS ($\Phi_\Delta$ = 0.84 in benzene and 0.97 in acetonitrile[184]). Possibly, another acridine derivative can be used as a better type II PS with activity in the blue region of the visible spectrum. Thus, a strong link was established between the chromophore's ability to produce $^1O_2$ and the recorded photocurrents at -0.05 V vs SCE.

### 3.4.3 Enhancement of the photocurrent by the photocatalytic redox cycling

Considering the quick decay of the photocurrent in surface-captured probes and its comparatively overall low absolute values in all three situations (Figure 3.5 A, B & C), an enhancement strategy would be of high interest for the analytical application of the introduced system. Previously it was proved that when reacting with $^1O_2$, HQ provides a

fast, intense and stable photocurrent response without any electrode fouling at pH 7 [106] making it an ideal model for electroactive $^1O_2$ quencher and the redox mediator in the system used. Moreover, HQ has a redox potential of -0.05 V vs SCE at pH 7, [185] whereas the most easily oxidized base guanine oxidizes only at + 0.7 V vs SCE.[186] Though the diffusion distance of $^1O_2$ is relatively short (< 100 nm), it was made sure that the amount of HQ (10 µM) was always kept in excess in comparison to the concentration of PSs in all the measurement conditions used in this study (Figure 3.2). This excess of HQ favourably reacts with $^1O_2$ and, thus, should protect DNA bases from oxidation and cleavages and transforms short-lived and highly reactive $^1O_2$ into a stable compound (BQ), electroactive at a given electrode and potential applied. Moreover, electrochemical reduction of benzoquinone (BQ) back into HQ which reacts again with $^1O_2$ forming the redox cycle.

*Table 3.3 Photocurrents[a] (nA) at 10 s from the start of illuminations.*

| | $\lambda_{laser}$ | **Surface-captured labelled DNA** | | **Dissolved labelled DNA** | |
|---|---|---|---|---|---|
| | | **Pure buffer** | **In the presence 10 µM HQ** | **Pure buffer** | **In the presence 10 µM HQ** |
| ChlE6 | 659 | -1.36 ± 0.21 | -0.55 ± 0.02 | -1.39 ± 0.19 | -6.63 ± 0.51 |
| MetB | 659 | -3.45 ± 0.50 | -0.37 ± 0.06 | -1.99 ± 0.36 | -3.23 ± 0.33 |
| MalG | 659 | -0.02 ± 0.01 | -0.02 ± 0.01 | -0.05 ± 0.04 | -0.04 ± 0.05 |
| EosY | 532 | -1.74 ± 0.81 | -0.2 ± 0.04 | -1.69 ± 0.22 | -7.10 ± 0.52 |
| EryB | 532 | -1.26 ± 0.13 | -0.18 ± 0.04 | -0.99 ± 0.10 | -7.44 ± 0.29 |
| ATTO532 | 532 | -0.08 ± 0.07 | -0.14 ± 0.04 | -0.06 ± 0.04 | -0.11 ± 0.04 |
| ChlE6 | 406 | -1.30 ± 0.30 | -0.36 ± 0.06 | -1.43 ± 0.34 | -5.18 ± 0.26 |
| ACMA | 406 | -0.04 ± 0.07 | -0.06 ± 0.02 | -0.14 ± 0.05 | -0.21 ± 0.08 |

[a] *The values are taken at 10 s (in the middle of an illumination cycle) from the moment of switching the light on to avoid the initial spikes in the photocurrent. Average values presented with standard deviation from three independent electrodes.*

Both surface-captured and dissolved labelled DNA were tested in the presence of 10 µM HQ (Table 3.3). Interestingly, the photocurrent dropped about twice in the case of type II chromophores linked DNA, captured at the electrode, but enhanced about 3-7 times for dissolved ones. This suppression can be explained by a comparatively slow overall kinetics of the transformation of HQ into BQ under the action of $^1O_2$ following a fast [2+4]-cycloaddition of $^1O_2$ with the formation of an endoperoxide.[187] In other words, HQ rapidly quenches $^1O_2$ forming the intermediate but slowly forms the final redox-active product

(BQ). In contrast, the direct reduction of $^1O_2$ at the electrode is expected to be fast. Thus, the use of HQ enhances the photocurrent only when $^1O_2$ is generated at some distance from the electrode so that $^1O_2$ cannot reach it due to the short lifetime (~3.5 μs in quencher-free $H_2O$). In the case of dissolved labelled DNAs, most of $^1O_2$ is generated in bulk and can result in a photocurrent only due to its reaction with HQ leading to BQ that produces photocurrent. Importantly, no noticeable photocurrent was observed in the presence of HQ for DNA labelled with the non-fluorescent PS MalG, fluorescent dye ATTO532, and ACMA. This confirms the essential role of $^1O_2$ in the scheme with the HQ/BQ redox cycle.

To further improve the sensitivity of the detection paradigm with HQ as a redox reporter, the captured DNA was immobilized on magnetic beads (2.8 μm in diameter) instead of attaching captured DNA directly to the electrode. DNA-ChlE6 (with the 659 nm red laser) and DNA-EryB (with the 532 nm green laser) which showed the highest photocurrents in dissolved form in the presence of HQ were chosen. DNA-MalG and ATTO532-DNA were chosen as the control in the respective region of light. A 406 nm blue laser was not considered for further study owing to its higher blank responses. The beads capturing the labelled DNA through hybridization were retained by a magnet below a working electrode. For this reason, planar gold-sputtered electrodes were used. The magnetic beads carry a much larger number of capture DNA probes than it would be present on the electrode surface (theoretical value ca. 150 pmol/cm$^2$ in case of magnetic beads compared to ca. 20 pmol/cm$^2$ in case of gold electrode surface[66, 121] but keep the DNA above the electrode, in the layer which is few μm thick. Because of the distance, the photocurrent in absence of HQ is lower for the case of magnetic beads compared to DNA directly immobilized on gold electrodes, which is in agreement with the diffusion distance of $^1O_2$ (ca. 0.2 μm) limited by its lifetime. Noteworthy, only gold-sputtered planar electrodes were applicable for the measurements since the regular screen-printed carbon electrodes showed high blank photocurrents (Figure 3.11). Further optimization studies with increased concentrations of HQ at different electrode surfaces are warranted for improving the sensitivity of a given sensing application which will be the focus of the next chapter.

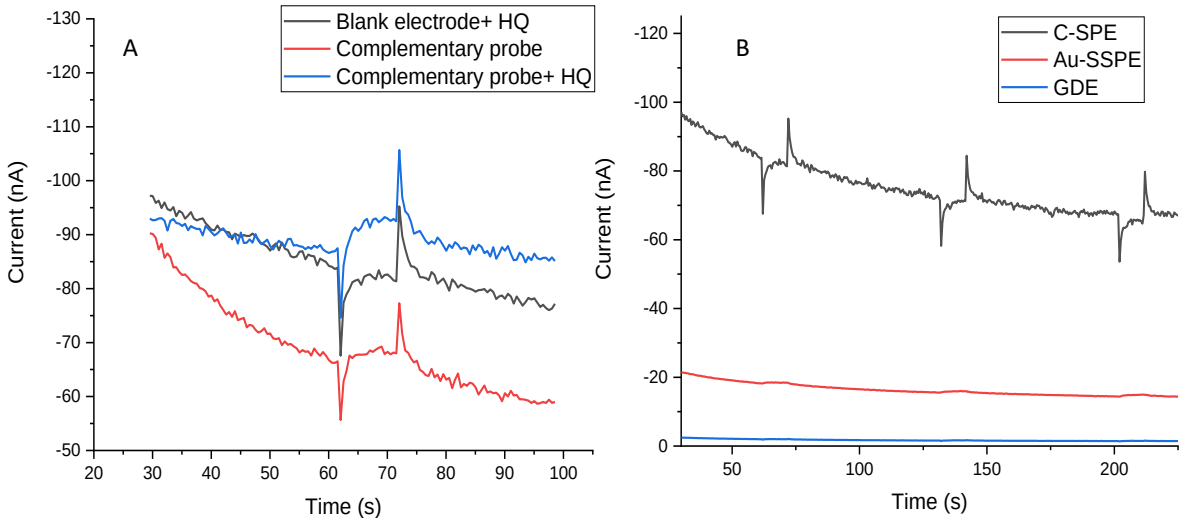


*Figure 3.11 Chronoamperograms presenting (A) photocurrent response of 50 nM labelled DNA captured on magnetic beads. Blank electrode denotes the response from the gold surface without any beads only containing 10 µM HQ in the buffer. (B) Blank responses from C- SPE, Au- SSPE, and GDE without any beads. Amperometry was performed at -0.15 V vs internal pseudo-Ag reference in PB pH7 using a red (659 nm) laser.*

In the absence of HQ, only a minor photocurrent marginally higher than the blank photocurrent was registered after incubation with 50 nM complementary DNA labelled with the dyes. However, in the presence of HQ, the photocurrent response increased by 28 and 20 times for DNA-ChlE6 and DNA-EryB respectively (Figure 3.12 C). There was also signal decay observed for consecutive illuminations similar to surface-captured labelled DNA over consecutive illuminations due to the cleavage of labelled DNA probes from magnetic beads. When compared to the four and seven folds increase for dissolved labelled DNA (Figure 3.12 B) and about twice the response drop for surface-captured DNA (Figure 3.12 A), thus suggesting that the usage of beads indeed enhances the analytical performance of the sensing strategy. The overall sensitivity of the sensing platform increased compared to gold disk electrodes by 56 times and the signal-to-blank ratio improved by three times for ChlE6 and eight times for EryB. Moreover, the use of magnetic beads in combination with the disposable electrodes facilitated the workflow and allowed to conduct of a large test to evaluate the concentration and analytic performances (Figure 3.13). As the result, the photocurrent increased proportionally with the concentration of the labelled DNA and presented a linear dynamic range of 250 pM - 25 nM and 50 pM - 10 nM, detection limits of 17 pM and 10 pM and sensitivity of 116 A/M/cm$^2$ and 213 A/M/cm$^2$ were calculated for DNA-ChlE6 and DNA-EryB respectively.

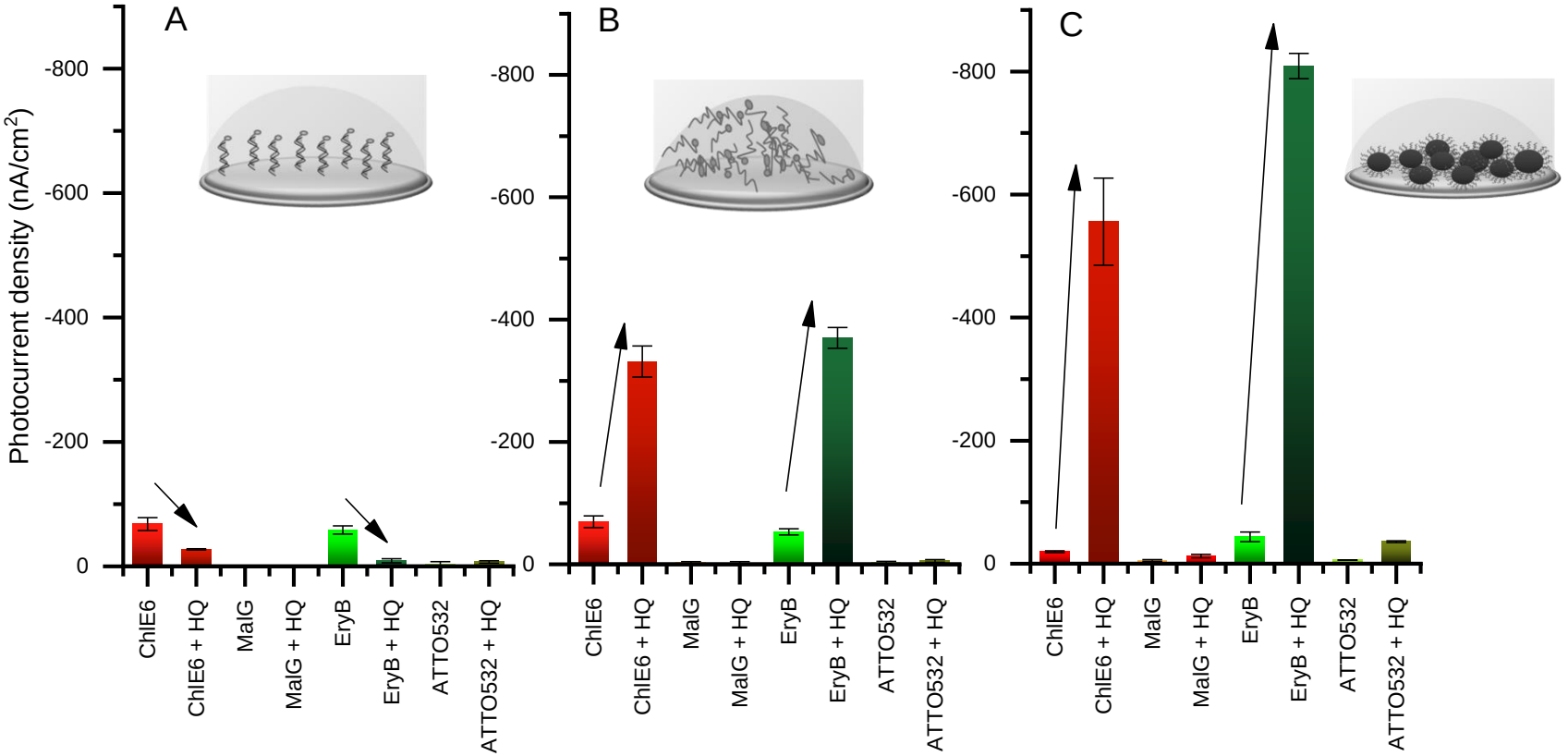


*Figure 3.12 Comparison of photocurrent responses (A) Surface-captured labelled DNA, (B) dissolved labelled DNA and (C) magnetic beads-captured labelled DNA, in the presence and absence of 10 µM HQ. Arrows indicate the increase/decrease of response with HQ. Error bars indicate the standard deviation from three independent electrodes.*

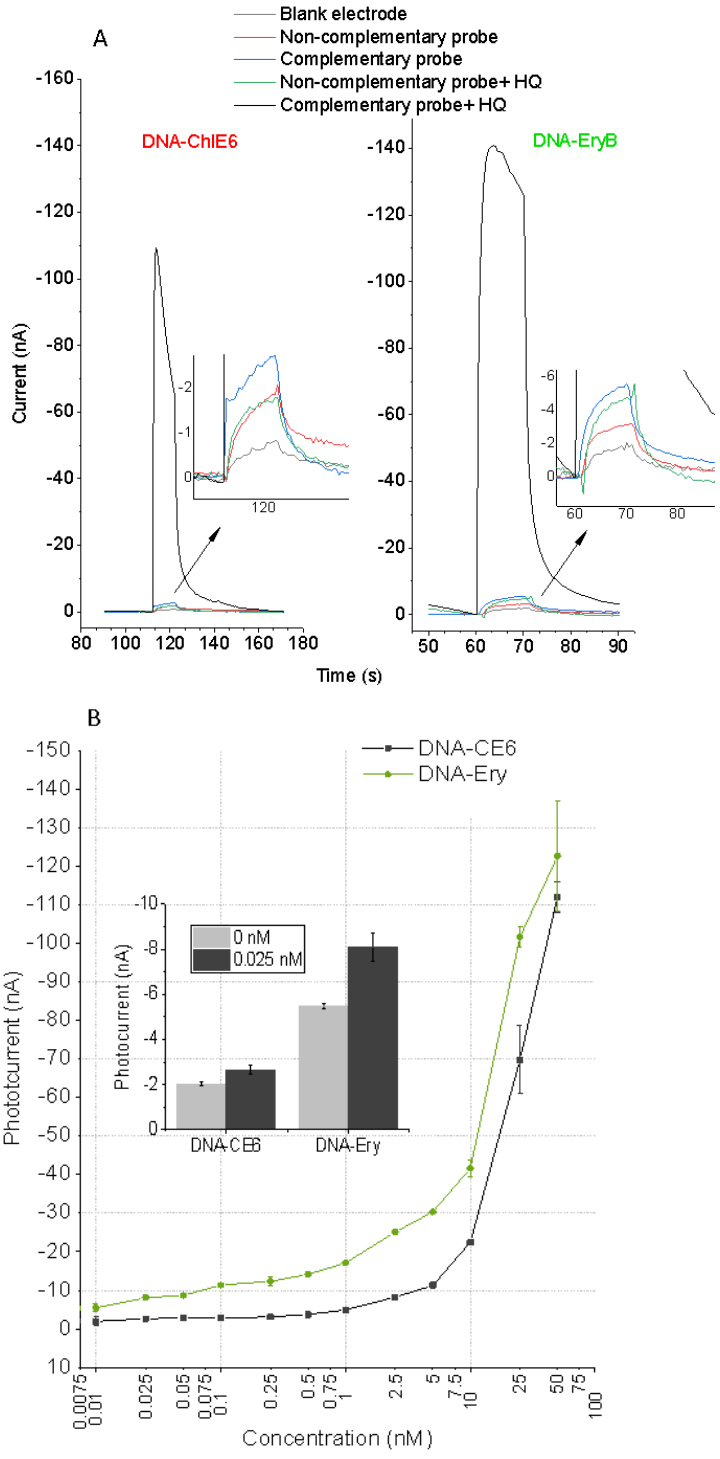


*Figure 3.13 (A) Chronoamperograms from magnetic beads-captured labelled DNA probes (50 nM) with chlorin e6 and erythrosine, after incubation with complementary and non-complementary capture probes attached to magnetic beads. (B) Chronoamperometric detection of different concentrations of DNA-ChlE6 and DNA-Ery using the magnetic beads-based photoelectrochemical platform. Error bars indicate the standard deviation from three independent electrodes.*

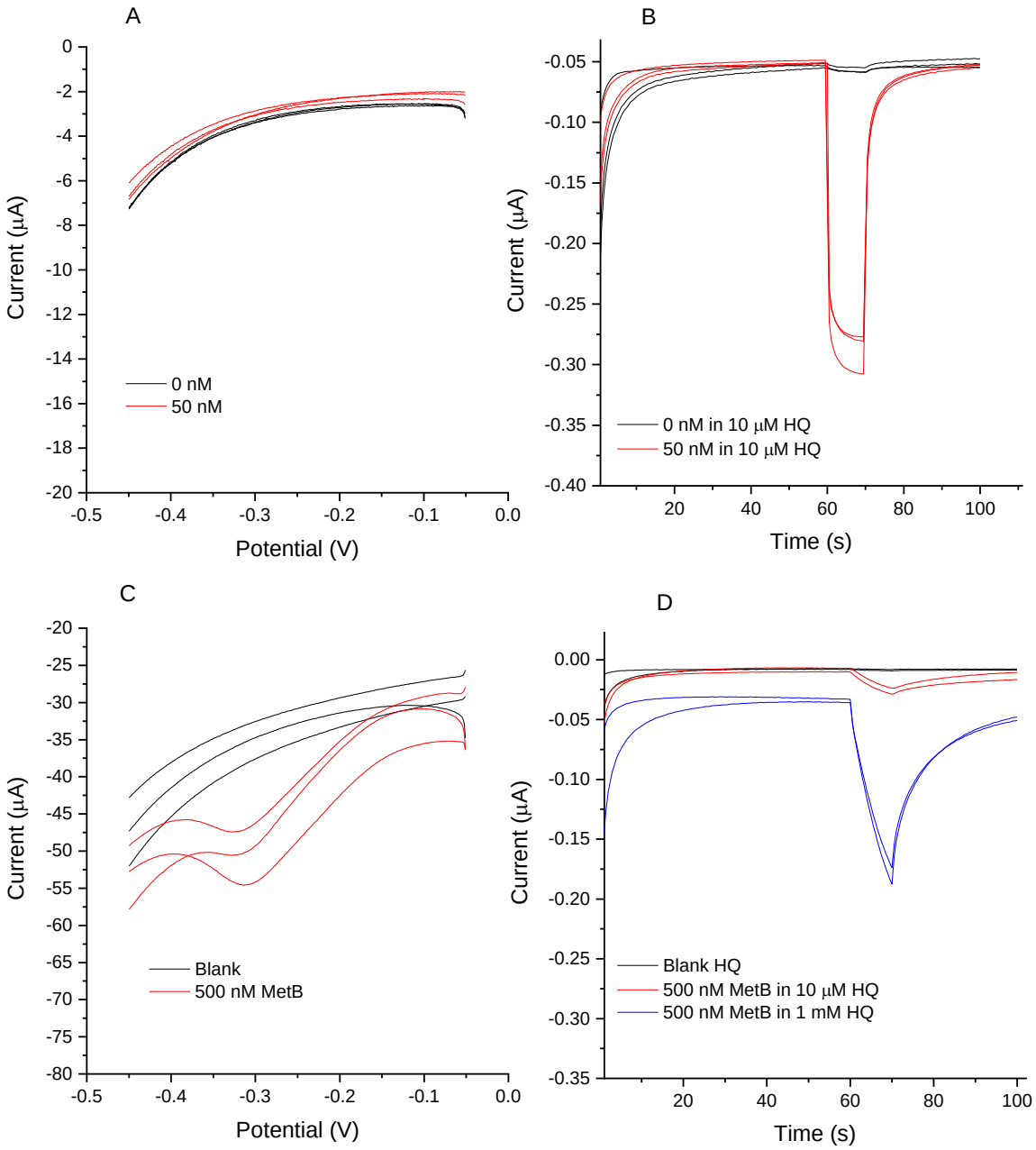


*Figure 3.14 (A) Square wave voltammetric (SWV) behaviour of magnetic beads after incubation in 50 nM target DNA labelled with MetB in comparison to the blank. SW amplitude = 75 mW, frequency 100 Hz, scan rate: 100 mV/s. Measuring buffer, 0.1 M KCl, 0.01 M $KH_2PO_4$ pH 7. (B) the photocurrent response of magnetic beads in the presence of 10 µM HQ after incubation in 50 nM target DNA labelled with MetB in comparison to the blank. Illumination with the 659 nm red diode laser, 30 mW. Measuring buffer, 0.1 M KCl, 0.01 M $KH_2PO_4$ pH 7. Potential applied = -0.15 V vs quasi-Ag reference (C) SWV response of 0.5 µM MetB demonstrates the expected peak position for MetB in the conditions of measurements with labelled DNA. (D) the photocurrent response of 0.5 µM MetB in the presence of 10 µM HQ, same conditions as in (B).*

Noteworthy, the performances of MB as an electrochemical tag (normally applied in a different detection scheme as a "signal-off" sensor also called E-DNA) are well documented in the literature and can be compared with our assay.[188-193] In the electrochemical scheme, a DNA probe with MB tag is attached to the surface and the formation of a duplex with a target DNA suppresses the voltammetric response of MB. The peak current in the voltammetric response of MB is around 200-500 nA and is generally consistent in the literature.[188-193] Our amperometric photocurrent on the same type of electrodes is only 3.5 nA (Figure 3.5 A), i.e. about 100-folds lower than the voltammetric peak current, but, with a good signal/noise ratio even for low absolute currents due to averaging of the signal over time. Furthermore, the use of magnetic beads and HQ as the redox reporter further amplifies the amplitude of our amperometric responses about 50x times (Figure 3.14). More importantly, the electrochemistry of MB-tagged DNA is extremely sensitive to the distance between the tag and the electrode. Indeed, MB shows no SWV peak when the labelled DNA molecules are captured by the magnetic beads and placed on the electrode (Figure 3.14 A) due to no actual contact between MB and the electrode. However, the photocurrent of (240 ±20) nA was measured in the same conditions in the presence of 10 uM HQ as the redox reporter to capture $^1O_2$ (Figure 3.14 B). This is advantageous compared to the use of MB as an electrochemical tag.

## 3.5 Conclusion

A novel photo-electrochemical sensing strategy based on the ability of a range of molecular imaging probes to produce $^1O_2$ was evaluated for the detection of DNA-DNA interaction. The $^1O_2$ production efficiency of these compounds in aqueous measuring solutions has been measured with UV/Visible spectroscopy. The detectability of these chromophores as photoelectroactive labels was assessed from their PEC response in free form, labelled to DNA dispersed in solution and at the surface of the electrode using RGB diode lasers. Labels undergoing type II photosensitization mechanism produced photocurrents in nano ampere (nA) and the ones with type I mechanism and fluorescence did not give any noticeable response. Out of all the labels, chlorin e6 proved to be an efficient chromophore for measurements with the red laser. While erythrosine presents a good choice for measurements with the green laser. The photocatalytic activity of the PSs labelled to DNA in the presence of a redox reporter hydroquinone has been evaluated in solution and attached to the surface of the electrode.

The practically attractive analytical performance of the $^1O_2$-based sensing strategy was achieved using a magnetic beads-based photo-electrochemical disposable platform. With an easy baseline current subtraction by switching the laser on and off at near-zero

potentials, this also offers a simple solution to effectively measure response only from the labelled DNA. These results can be transferred to a sandwich-type DNA recognition sensor where the target DNA/RNA bridges the labelled DNA (for detection) and the DNA-probe immobilized on the surface (to capture).

# Chapter 4

# Application of the sensing strategy for quantification of prostate cancer miRNAs

*Amperometric detection of miR-141*

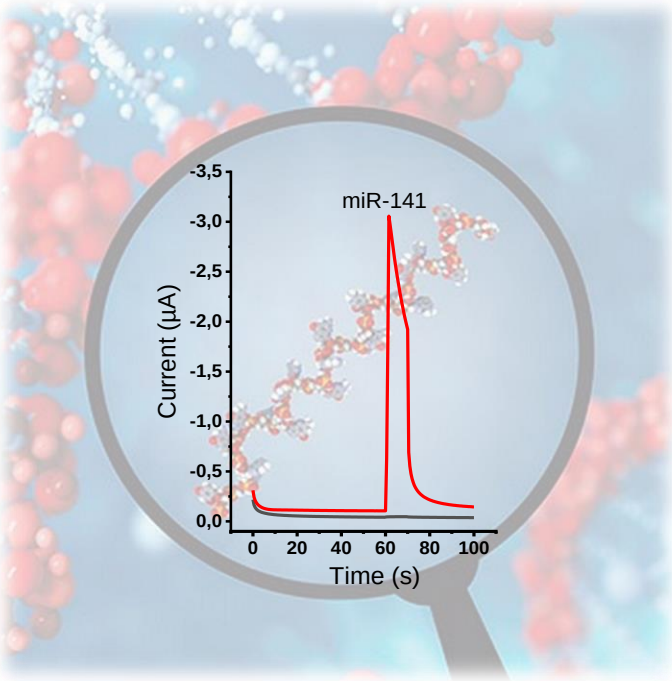


**Adapted from the following manuscript:**

*Thiruvottriyur Shanmugam S., Campos R., Trashin S., Daems E., Carneiro D., Fraga A., Ribeiro R., De Wael K. Quantification of prostate cancer miRNAs using a singlet oxygen-based photoelectrochemical strategy, manuscript in preparation.*

***Contribution:*** *I performed the experiments resulting in sections 4.4.1 – 4.4.4 and wrote the first draft of the manuscript.*

## 4.1 Abstract

Dysregulation of miRNA expression occurs in many cancers, making miRNAs useful in cancer diagnosis and therapeutic guidance. In the clinical context, the limited amount of miRNA in circulation often limits its quantification using current methods. Here, a PCR-free and sensitive $^1O_2$-based PEC detection and quantification of miR-145 and miR-141 in buffer and buffer diluted human plasma has been presented. Functionalized magnetic beads capture a specific target miRNA and a labelled DNA oligonucleotide probe in a sandwich-like format, concentrate the formed complex at the sensor surface and provide an interface for the photoinduced redox signal amplification. The detection oligonucleotide bears a molecular PS, i.e. chlorin e6, that produces $^1O_2$, thus oxidizing hydroquinone into benzoquinone followed by reduction of benzoquinone at the electrode surface creates the redox cycling loop. After optimization of the measurement and assay parameters, detection limits of 3.5 pM and 9.8 pM for miR-145 and miR-141, respectively, were obtained in 10-fold buffer-diluted human plasma without any other sample processing or pretreatment. Successful quantification of pM levels of both miRNAs in plasma samples from prostate cancer (PCa) patients confirms the applicability of this technology in a clinical setting and as a sensitive tool to aid clinical reasoning.

## 4.2 Introduction

The standard practice for cancer diagnostics is based on a combination of cross-sectional imaging and tissue biopsies. Imaging techniques elucidate the presence, location and size of a tumour, but lack information regarding tumour grading and molecular characterization.[194] Therefore, tissue biopsy is subjected to a histopathological analysis to confirm malignancy and determine the cancer type and subtype. Sometimes, this examination is followed by molecular testing to identify which biomarkers are present and guide personalized treatment plans since patients with certain biomarkers are eligible for specific targeted therapy. A tissue biopsy is, however, highly invasive and does not account for a tumour's heterogeneity.[195] The use of liquid biopsies opens the possibility to collect biofluids in a minimally invasive way and thus track biomarker levels throughout the disease course and during treatment. Monitoring biomarkers in biofluids allows for increased accuracy in treatment decisions and reactionary treatment strategies, leading to personalized medicine.[11, 196] This is particularly important when a change from drug-sensitive to drug-resistant disease occurs.

Liquid biopsies allow the detection of various cancer biomarkers, such as circulating tumour cells,[197] circulating tumour DNA[198] and non-coding microRNAs (miRNAs).[199] Particularly, aberrant amounts of circulating miRNAs have been increasingly shown to have a biological impact and are clinically associated with cancer.[200, 201] Moreover, miRNAs also play an important role in genetic pathways such as chemoresistance. Thus the high or low expression levels of circulating miRNAs originating from tumour cells are promising to predict the chemotherapeutic response of an individual.[137] A striking example is the dysregulation of certain miRNAs associated with prostate cancer aiding in diagnosis and prognosis. An enhanced plasmatic expression of miR-141[202, 203] and miR-145 is associated with prostate cancer progression and prognosis.[204-207]

Currently, the standard technique for detecting and quantifying miRNA is RT-qPCR and gene sequencing options.[208-212] While both techniques offer high sensitivity and reliable variant detection, RT-qPCR can only detect known sequences and quantify them. Whereas, with the gene sequencing techniques, one can detect both known and novel nucleic acid sequences, though need additional quantification via PCR and fluorimeters. The downsides of these techniques include the high cost, complex sample preparation, risks of contamination, long analysis time and low miniaturization potential which limits the use in POC testing. [208, 209, 211] Electrochemical and PEC platforms offer rapid and sensitive analysis of miRNAs directly in biological samples with low concentrations of biomarkers and demonstrated great potential for POC due to technological advances in microelectronics

and low-cost sensor transducers, i.e. disposable electrodes.[65, 66, 118, 147, 149, 150] Nevertheless, current approaches involve complex electrode fabrication with different semiconductors/nanomaterials, are labour-intensive and need enzymes for catalytic amplification to achieve the required sensitivity. To overcome such drawbacks, the use of a $^1O_2$-based PEC detection methodology is proposed. The use of PS generating $^1O_2$ offers an excellent signal-to-noise ratio, enabling the acquisition of a specific response separately from the baseline by switching the light on/off and reducing costs because enzymes and complex electrode functionalization are avoided.[213, 214] This offers a robust alternative for redox and enzymatic labels allowing us to develop a new type of sensitive and accurate electrochemical nucleic acid sensors.

Previously, the usability of various PSs for the PEC detection of DNA was tested.[215] Here, the validation of the concept by testing its applicability for the detection of miR-145-5p and miR-141-3p (will be termed miR-145 and miR-141 here on for simplicity) concerning PCa diagnosis[216, 217] is presented. The method relies on the hybridization of the target miRNA with two other shorter DNA probes in a sandwich-like format. The biotinylated DNA capture probe hybridizes with half of the target and binds to streptavidin-coated magnetic beads, whereas the labelled DNA detection probe hybridizes with the second half of the target and brings along a $^1O_2$-producing PS that is detectable by photoelectrochemistry (Figure 4.1). ChlE6 was selected as a $^1O_2$-producing label based on our previous studies[106, 218] and HQ was chosen as a redox reporter for chemical capturing of short-lived $^1O_2$ in micrometres-thick layers of magnetic beads, enhancing the signal. Here, for the first time, the $^1O_2$-based PEC approach is applied to detect miRNAs in plasma from PCa patients, thus providing data that can be considered for clinical diagnostics in addition to clinicopathological information.

Additionally, intending to (i) transfer the insights to more commonly available commercial electrode platforms, and (ii) improve sensitivity. PEC performance of twelve commercially available screen-printed electrodes, three gold-based and nine carbon-based have been compared to understand the impact of working electrode material on the PEC detection using a pure type II PS ChlE6, and a mixed type I and type II PS methylene blue (MetB) at the 5’ or 3’ end of the detection probe.

## 4.3 Materials and methods

### 4.3.1 Reagents

The buffer components (Tris, EDTA, NaCl, HCl, $KH_2PO_4$ and KCl) and Tween 20 were purchased from Sigma-Aldrich (Merck, Belgium). HQ was supplied by Acros Organics (Belgium). Streptavidin-coated magnetic beads (M280-Dynabeads) were purchased from Invitrogen (ThermoFischer Scientific, Belgium). Pooled male human plasma (K3 EDTA) was acquired from Bio-connect (The Netherlands). DNA oligonucleotides were used as capture probes with bionylated 5' end and as detection probes with ChlE6/ MetB/ MalG labels. These bind to the complementary target RNA oligonucleotides in a sandwich manner illustrated in Figure 4.1 A.

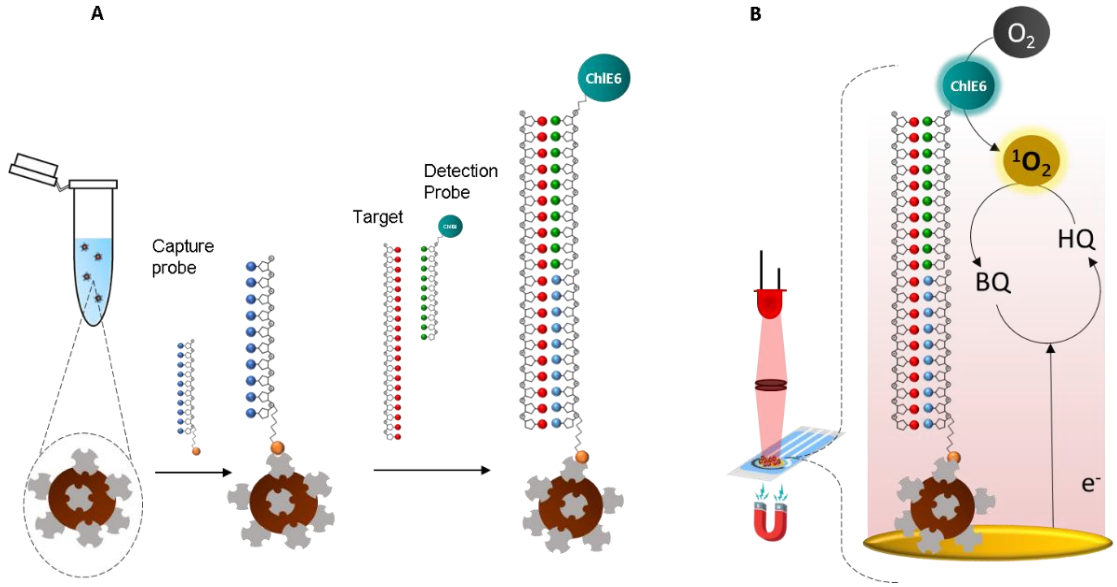


*Figure 4.1 Schematic representation of (A) the sandwich assay and (B) $^1O_2$-based PEC detection of miRNA.*

The DNA and RNA oligonucleotides were purchased from Eurogentec (Belgium), except for leuco malachite green (MalG) and MetB-labelled detection probes which were purchased from Metabion (Germany). MalG-labelled probes were used in the experiments as the type I control PS. MetB-labelled probes were used in the study on the impact of working electrode material on PEC detection. The sequences and modifications of the oligonucleotides are presented in Table 4.1. The main electrode, gold-sputtered planar electrode (AUTR10) was purchased from DropSens (The Netherlands). Eleven other different types of disposable electrodes were used to perform the PEC measurements to study the impact of working electrode material as listed in Table 4.2.

*Table 4.1 Sequences and respective modifications of the capture and detection oligonucleotides used to detect the targets (miR-145 and miR-141), and the sequence of the negative control.*

| | **Name** | **5' modification** | **Sequence (5' --> 3')** | **3' modification** |
|---|---|---|---|---|
| miR-145 | Detection (D145) | | GGA AAA CTG GAC | ChlE6 or MetB |
| | Detection (D145) | ChlE6 or MetB | GGA AAA CTG GAC | |
| | Capture (C145) | Biotin-TEG | AGG GAT TCC TG | |
| | Target (miR-145-5p) | | GUC CAG UUU UCC CAG GAA UCC CU | |
| miR-141 | Detection (D141) | | AGA CAG TGT TA | ChlE6 or MalG (control) |
| | Capture (C141) | Biotin-TEG | CCA TCT TTA CC | |
| | Target (miR-141-3p) | | UAA CAC UGU CUG GUA AAG AUG G | |
| | Negative control (miR-375-3p) | | UUU GUU CGU UCG CUC GCG UGA | |

*Table 4.2 List of the screen-printed electrodes used to study the impact of working electrode material on PEC detection. A complete description of the electrodes can be found on the website of producers.*

| **Supplier** | **Model** | **Abbreviations in this chapter** | **WE** | **CE** | **RE** | **Diameter of WE (mm)** |
|---|---|---|---|---|---|---|
| Dropsens | **AUTR10**[a] | **Au-OT** | **Gold** | **Carbon** | **Silver** | **4** |
| | PW-AU10 | Au-PW | Gold | Carbon | Silver | 4 |
| | C223AT | Au SPE | Gold | Gold | Silver | 1.6 |
| | DRP-110 | Gr SPE | Carbon | Carbon | Silver | 4 |
| | DRP-110SWCNT | SWCNT | SWCNT-COOH/Carbon | Carbon | Silver | 4 |
| | DRP-110CNT | MWCNT | MWCNT-COOH/Carbon | Carbon | Silver | 4 |
| | DRP-110GPHOX | G Ox | Graphene Oxide/Carbon | Carbon | Silver | 4 |
| | DRP-110PANI | PANi | PANi/Carbon | Carbon | Silver | 4 |
| | DRP-110MC | MPC | Mesoporous Carbon/Carbon | Carbon | Silver | 4 |
| | DRP-110CNF | CNF | Carbon Nanofiber/Carbon | Carbon | Silver | 4 |

| | | | | | | |
|---|---|---|---|---|---|---|
| | DRP-410 | Co-Ph | cobalt(II)phthalocyanine/carbon | Carbon | Silver | 4 |
| ItalSens | IS-C | IS-C | Carbon | Carbon | Silver | 3 |
| [a] *AUTR10 is the main electrode used for all other PEC detections in this study. The reference names of the electrodes mentioned are as mentioned in the manufacturer's catalogue.* | | | | | | |

### 4.3.2 Buffers and solutions

The 2X Tris EDTA (TE) buffer solution (pH 7.5, adjusted using HCl), containing 10 mM Tris, 1 mM EDTA (Titriplex III), and 2 M NaCl was prepared. This 2X TE-buffer was mixed with (i) Tween 20 to yield a 2x TE + 0.05 % Tween 20 (2XTE-$T_{20}$), or (ii) ultrapure water (UPW, 18.2 MΩ $cm^{-1}$ double deionized water, Sartorius Arium® Ultrapure Water Systems) and Tween 20 to yield a 1xTE + 0.05 % Tween 20 (1XTE-$T_{20}$) buffer, herein named hybridization buffer. The measuring buffer with/without HQ at different concentrations, consisted of 0.1 M KCl and 0.01 M $KH_2PO_4$ adjusted to pH 7 with KOH.

### 4.3.3 Sandwich hybridization assay

**Hybridization assay with magnetic beads**

Before the PEC analysis, the target miRNAs were captured and hybridized with capture and detection probes onto the magnetic beads via a sandwich hybridization assay. First, streptavidin-coated magnetic particles (10 µL, 10 mg/mL) were dispersed in an Eppendorf containing a 1 mL hybridization buffer (Figure 1 (A)). The solution was vortexed and the magnetic beads accumulated at the side of the Eppendorf were directed to the magnetic rack (∼1 min). The solution was removed and suspended in 500 µL of 2XTE-$T_{20}$ buffer, then 500 µL of 100 nM capture probe in UPW+0.05% Tween 20 were added to the beads leading to a final incubation solution containing 1 mL of capture probe at 50 nM in hybridization buffer. This step lowers the NaCl concentration in the 2X buffer from 2 M to 1 M ensuring optimal binding of the capture probes.[219] This concentration of capture probes was chosen to ensure saturation of all the beads with capture probes, given that the beads have a binding capacity of ∼200 pmol of single-strand oligonucleotides per 1 mg of beads according to the manufacturer's information sheet.[219] This solution was incubated for 15 min at room temperature using continuous rotation (10 rpm, rotary shaker). Following the incubation with capture probes, the beads were again accumulated using a magnetic rack, the solution was discarded and the functionalized beads were resuspended in a new hybridization buffer containing the PS labelled detection probe (24 nM, concentration corresponding to the highest concentration of target used in this study) and target miRNA

(at different concentrations between 24 nM and 1.5 pM). This solution was incubated for one hour at room temperature in a rotary shaker at 10 rpm. Following the incubation, the beads were washed three times with 1 mL hybridization buffer and re-suspended in 10 µL of the same buffer until the PEC detection was performed.

Standard curves were constructed with different concentrations (from 24 nM to 1.5 pM) of target miRNAs in buffer solution while keeping the concentration of detection and capture probes constant at 24 nM and 50 nM, respectively. The specificity of the sensing strategy was evaluated by measuring the photocurrents for different concentrations of target miRNAs in the presence of two other miRNAs (for example, detecting the target miR-145 in the presence of miR-141 and miR-375). Negative control tests were performed using a miRNA that is not complementary to capture and detection probes and in the absence of the target miRNA.

Optimization of parameters and standard curves with plasma (diluted 10-fold with hybridization buffer) was performed using pooled male human plasma (K3 EDTA). Eight plasma samples from PCa patients in the age group of 62-72 years were obtained from Centro Hospitalar do Porto, Portugal after the appropriate informed consent and approval from The Health Ethics Committee (CES) from Centro Hospitalar do Porto (Ref: 2017.154(131-DEFI/123-CES). Due to the limited quantity of the clinical samples, miR-145 was analyzed in all samples while miR-141 was analyzed in six of the samples.

**Chemisorption assay via gold-thiol linking**

A comparative analysis was made with another sandwich assay where the capture probe of miR-141 was chemisorbed on the surface of the gold working electrode, without any beads. Hereto, electrodes were incubated in a 1 µM thiolated capture DNA probe containing 0.2 µM mercaptohexanol (MH, purity >98.0%, TCI chemicals) in hybridization buffer (40 µL) overnight (~16 hours) and then in 1 mM MH for two hours, for backfilling and removing weakly bound DNA molecules. For the hybridization step, a 40 µL drop consisting of detection probe solution (24 nM) and the target miR-141 (20 nM) in hybridization buffer was placed on the electrode for one hour and copiously washed with hybridization buffer before PEC detection.

### 4.3.4 PEC detection

PEC measurements were carried out using a PalmSens4 potentiostat (PalmSens, The Netherlands) using PSTrace 5.9 software. PEC measurements for studying the impact of the

label's position and working electrode materials were performed using a potentiostat Autolab 302N running Nova 2.1 software. A light-emitting diode (LED) operated at 660 nm (Thorlabs, Inc.) was used and the diameter of the light beam was adjusted using a collimator to only illuminate the working electrode. The light power was adjusted to 30 mW using a light power meter (Thorlabs, Inc.). The measurements were performed with 60 s OFF, 10 s ON & 30 s OFF light-chopped conditions for uniformity, with the ON/OFF switch preprogrammed with PSTrace or Nova 2.1 and controlled by a relay trigger.

After performing the hybridization assay, the beads were resuspended in 10 µL of measuring buffer and transferred into the measuring drop (90 µL of measuring buffer placed on the electrode surface), where all the beads precipitated at the working electrode due to a neodymium magnet underneath it. Photocurrents in this setup were measured at reference voltage *vs.* the inbuilt reference electrodes at -0.07 V vs. SCE. Polynomial baseline correction was constructed through background current values (in dark) and subtracted from the chronoamperograms to obtain baseline-corrected photocurrent responses. For ease of visual comparison among the electrodes, all the chronoamperograms are plotted after baseline subtraction.

## 4.4 Results and discussion

### 4.4.1 Validation of the sensing strategy in buffer

The PEC response of the target miRNA (miR-141) hybridized with the capture and detection probes, in a sandwich-like format, was first evaluated. Figure 4.2 A shows the light-chopped chronoamperogram recorded after hybridizing 20 nM target (miR-141) with the probes, compared to the control experiment without the target. Upon illumination, the photocurrent responses in the presence of the target miRNA exceeded 50 times the response of the control. The decay of the photocurrent in time and with the number of illuminations is attributed to NA cleavages by the photogenerated ROS, which is well pronounced for the model DNA-duplexes directly attached to the gold electrode surface via Au-thiol linking.[106, 215] Nevertheless, when the light is switched on, the photocurrent appears near-instantly giving the maximal photocurrent in the first three seconds, while the signal decay shows more sluggish kinetics. Thus, the photocurrent at three seconds after the start of the first illumination will be used as a representative analytical response for the sensing strategy. Moreover, the role of the redox reporter became clear when comparing the PEC responses from the detection of 20 nM miR-141 using magnetic beads

in the absence and presence of 10 µM HQ. Without HQ, the photocurrent was only 5% of that in the presence of HQ (Figure 4.2 B, magnetic beads).

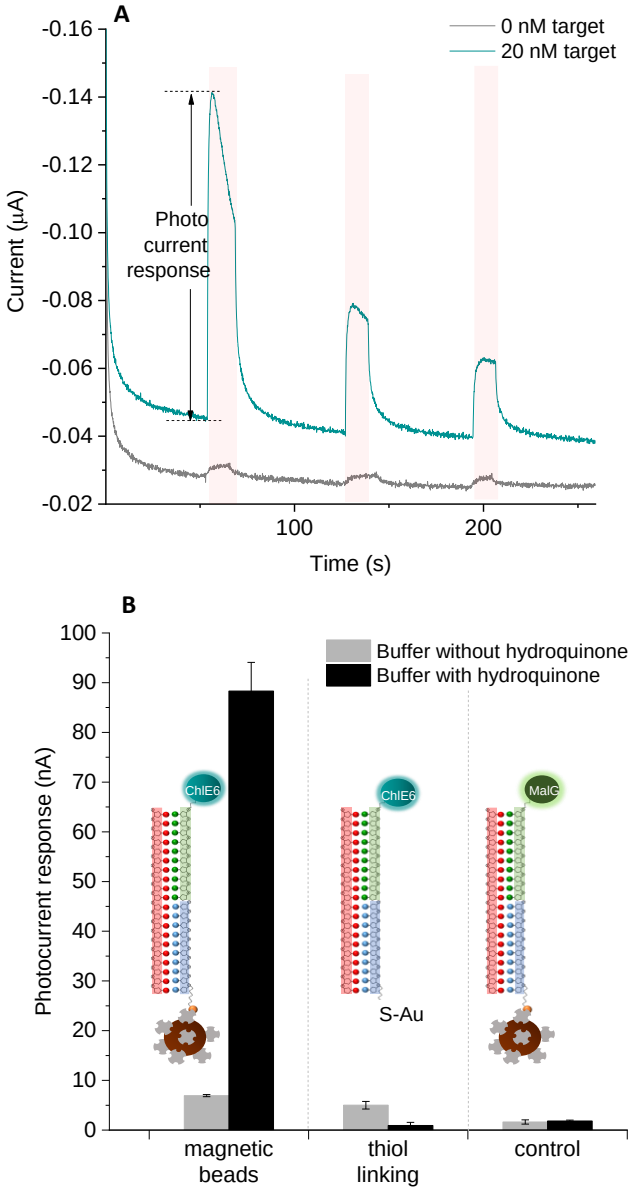


*Figure 4.2 (A) Chronoamperogram under light chopped conditions (light ON periods are shown as light red bars) for the magnetic beads with biotinylated capture probe and ChlE6-labelled detection probe hybridized with 20 nM miR-141 in the presence of 10 µM HQ; control obtained in the absence of miRNA (0 nM). (B) Comparison of PEC responses from the detection of 20 nM miR-141 in the absence and presence of 10 µM HQ: Chronoamperometric measurements were carried out at -0.15 V vs. quasi-internal Ag reference. Error bars represent the standard deviation (n = 3).*

This behaviour agrees with the mechanisms when a comparatively short-lived $^1O_2$ (lifetime ~3.5 µs in water)[220, 221] generates the photocurrent. Only 30% of the generated $^1O_2$ can

diffuse 100 nm and less than 0.1 % of $^1O_2$ can diffuse more than 200 nm in water.[220, 221] Thus, only $^1O_2$ that is generated close to the electrode surface can effectively contribute to the photocurrent in the absence of HQ, whereas most PS-labelled detection probes on the bead surface (2.8 μm in diameter) do not contribute unless HQ is added to the solution to form in the reaction with $^1O_2$ a stable product, BQ. Then, BQ diffuses over μm-long distances to get reduced at the electrode to form HQ, making the redox cycle complete (Figure 4.3 A). This way HQ enhances the PEC response when beads are used.

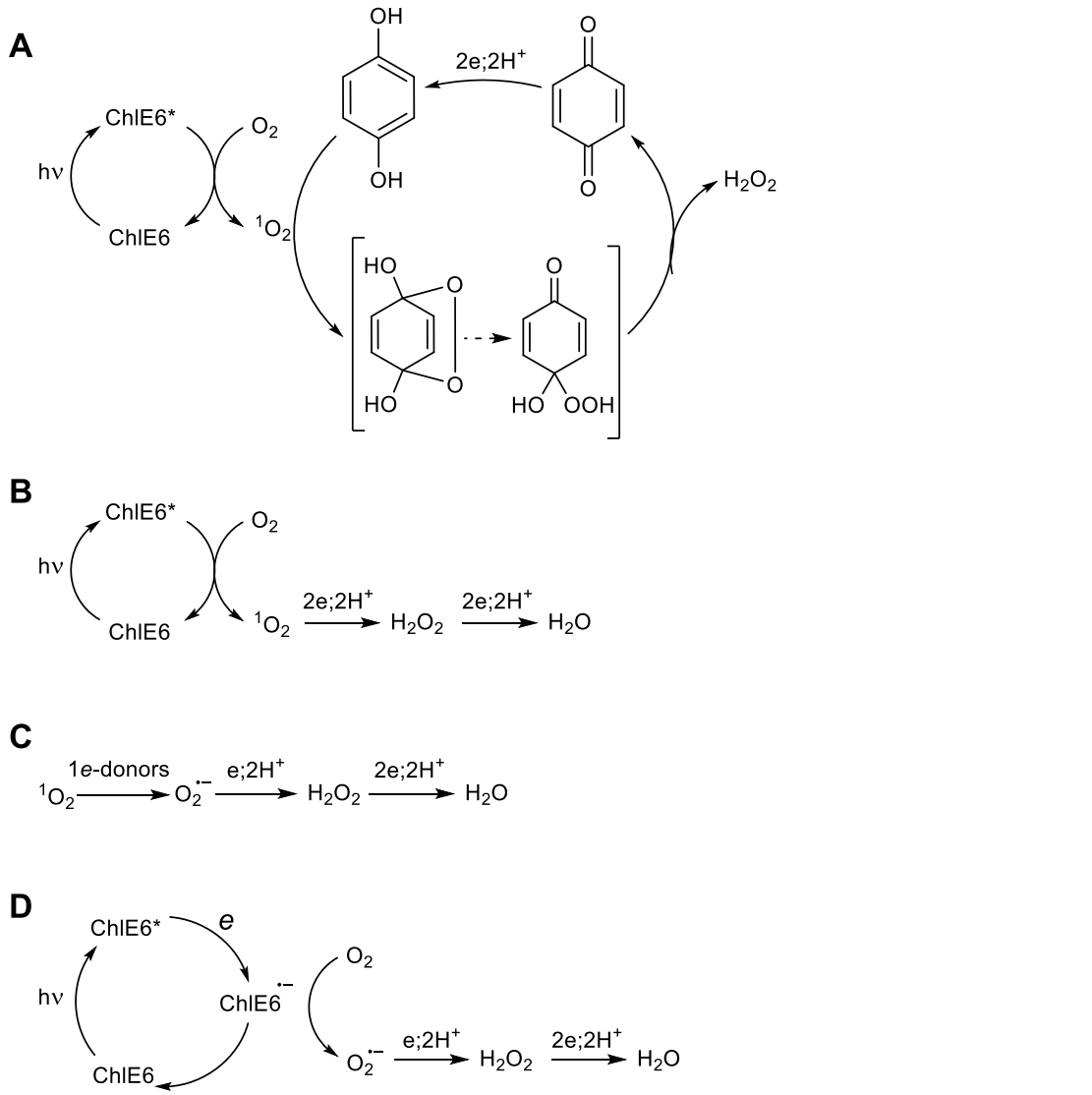


*Figure 4.3 PEC reaction pathways in the (A) presence and (B) absence of HQ, (C) and (D) side reactions leading to the formation of radicals at the surface of the electrode.*

The photocurrent in the absence of HQ (Figure 4.2 B, magnetic beads) was close to the photocurrent obtained for the same sandwich complex hybridized directly on the gold

electrode via thiol linking (Figure 4.2 B, thiol linking). Noteworthy, HQ does not enhance but suppresses the photocurrent when the detection probe in the sandwich is captured directly at the electrode (Figure 4.2 B, thiol linking). In these conditions, $^1O_2$ can contribute directly to PEC by getting reduced at the electrode surface, while HQ redirects the reaction path in a multistep process with a fast first $^1O_2$ cycloaddition step and comparatively slow step of the molecular reorganization of the endoperoxide into peroxide and BQ (Figure 4.3 B, C compared to A), which expectedly impedes the overall reaction rate. Moreover, photoexcited ChlE6* is prone to the formation of radicals such as superoxides $O_2^{\cdot-}$ and HQ-derived cation radical, which can further quench $^1O_2$ and the ChlE6 triplet state formation (Figure 4.3 D). Thus, HQ enhances photocurrent in the presence of magnetic beads but not for the probe directly attached to the gold electrodes. In other words, HQ helps to involve all the large surface area of magnetic beads in the generation of photocurrent, making the benefit of the magnetic beads more pronounced.

Thus, the introduction of magnetic beads resulted in (i) a large surface area available for capturing the target miRNA (e.g. the calculated geometric surface area (GSA) of 100 µg beads is ~ 1.48– 1.72 $cm^2$, [219] compared to the GSA of Au-OT is 0.13 $cm^2$), thus a large effective concentration of the capture probe; (ii) effective mass transfer to the capture probe since the beads are dispersed in the solution and can be stirred in there using rotation; (iii) effective washing from non-bound detection probe (seen from negligible photocurrents in the absence of target); (iv) rapid accumulation of the beads on the sensor surface by a magnet and (v) sensitive amperometric reading of the molecular label due to redox cycling of HQ/BQ without the need of direct electrical contact between the detection probe and the electrode.

Finally, an alternative chromophore, MalG, which does not generate $^1O_2$ [170] but intensively absorbs the light used ($\varepsilon_{MalG}$ is 22000 at 660 nm) did not produce any noticeable photocurrent in the absence or presence of HQ when used under the same conditions as for ChlE6 (Figure 4.2 B, $\varepsilon_{ChlE6}$ 12000 at 660 nm)[215] with magnetic beads. This important control experiment additionally demonstrates that the photocurrents in the absence and presence of HQ are specific to $^1O_2$-generating ChlE6 and not due to any theoretically possible photoactivity of the beads, e.g. caused by local heating of the beads due to light absorbance by beads themself or the chromophore.

### 4.4.2 Optimization of working parameters and analytical performance

After demonstrating the PEC detectability of miRNA using the sandwich assay with the magnetic beads, the influence of various working parameters on the assay performance

was investigated. First, the sensor's working potential as a major parameter affecting the sensitivity of the system was optimized (Figure 4.4).

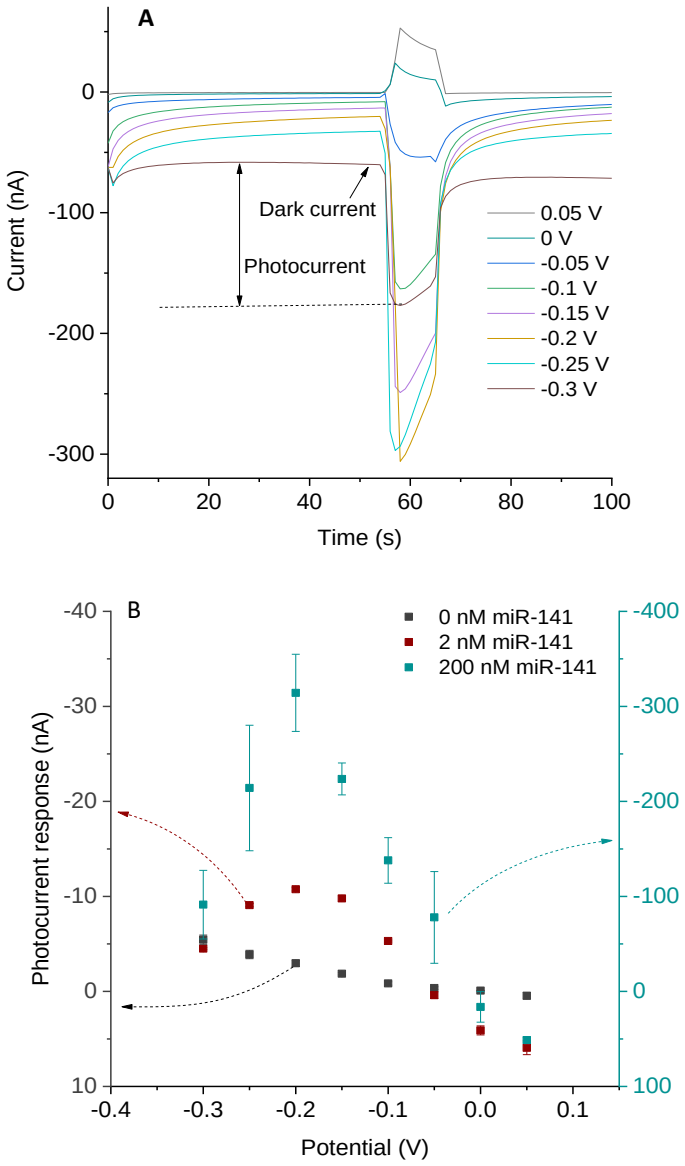


*Figure 4.4 Chronoamperograms (raw data) at different electrode potentials for electrodes with magnetic beads incubated in 200 nM miR-141. (B) Dependence of the photocurrent response on the applied electrode potentials for 0 nM, 2 and 200 nM miR-141. The measurements were conducted in the presence of 10 µM HQ; 100 µg beads were used per measurement. The y-scale from the left is for 0 nM and 2 nM and the y-scale from the right is for 200 nM. Error bars represent the standard deviation (n = 3).*

The photocurrent response to the target increases when going from +0.05 to -0.2 V but drops at more negative potentials likely due to intense oxygen reduction at the electrode, which is additionally observed as an increase in the dark background current (Figure 4.4 A). Furthermore, the background reduction of $O_2$ likely leads to depletion of available $O_2$ at the

near electrode space and increased formation of superoxide, a known quencher of $^1O_2$.[176] Hence, the potential of -0.2 V *vs.* quasi-Ag reference (corresponding to -0.07 V *vs.* SCE) resulted in the maximal response for both 20 nM and 200 nM target miRNA and low blanks and dark current (Figure 4.4 B), this potential was chosen as the optimal potential and was used in the following experiments.

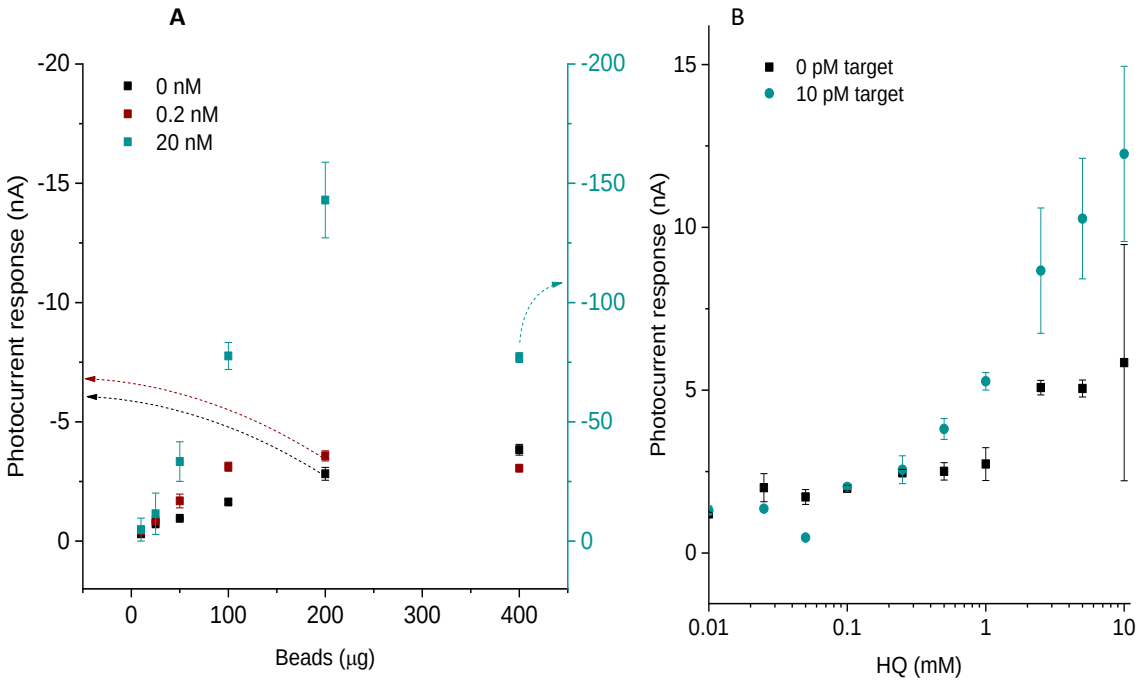


*Figure 4.5 (A) Effect of magnetic beads quantity used per analysis on the photocurrent response for 0 nM, 0.2 nM and 20 nM miR-141 target. Concentration of HQ used: 10 µM; potential: -0.2 V vs quasi-Ag reference. The y-scale from the left is for 0 nM and 0.2 nM and the y-scale from the right is for 20 nM. (B) Effect of HQ concentration used in the measuring buffer for detecting 0 and 10 pM miR141-target. Amount of beads per analysis: 100 µg; potential: -0.2 V vs quasi-Ag reference. Error bars represent the standard deviation (n = 3).*

Next, the optimal quantity of beads used per analysis was determined, in turn, transferred onto the electrode for a single measurement (Figure 4.5 A). The volume and concentrations of capture and detection probes were kept constant throughout (i.e. 50 µmols and 24 µmols respectively). An excessive amount of capture and detection probes was provided (the optimal amount recommended by the supplier is approximately 200 pmols per mg of beads) to saturate all the beads. The maximum response was achieved when using 200 µg of beads for 20 nM target. However, for a lower concentration (0.2 nM) of the target, there was only a 14% increase when using 200 µg instead of 100 µg when compared to the 46% increase for 20 nM target. The decrease in photocurrent response for beads more than 200 µg is likely due to the blocking of light penetration for underlying layers of beads by the first 2-3 layers of beads. That is, when the light is projected onto beads set in layers under the influence of magnetic attraction, the light can penetrate only through the first few layers of beads, before becoming substantially attenuated by scattering and/or absorption.

This can additionally impede the diffusion of HQ/BQ through the thick layer of beads. Moreover, the standard deviation among repetitions and the background increased to 200 µg compared to 100 µg. Thus, the use of 100 µg of beads was chosen.

Lastly, the effect of the HQ concentration used during the measurements was optimized to reach the maximum detectability in the low target concentration range without any amplification. The detectability of a very low concentration, 10 pM of miR-141 compared to the blank control was evaluated at concentrations of HQ ranging from 0.01 to 10 mM (Figure 4.5 B). The concentration of 1 mM HQ resulted in the best response in combination with low blanks (high signal-to-noise ratio) and demonstrated good reproducibility (SD = 5%) compared to higher HQ concentrations (SD = 22%). Thus, 1 mM HQ was chosen as the optimal redox reporter concentration for further studies. With these optimized parameters, control experiments were performed with only detection probe and target miR-141 (D/T), only capture probe and target miR-141 (C/T) and with only capture and detection probe (C/D) in the absence of target. This was compared with the signal when the target is present in the system along with the capture and detection probe (C/D/T) (Figure 4.6). In the absence of either capture, detection probe, or target, the sandwich duplex did not form, thus no noticeable signal was obtained.

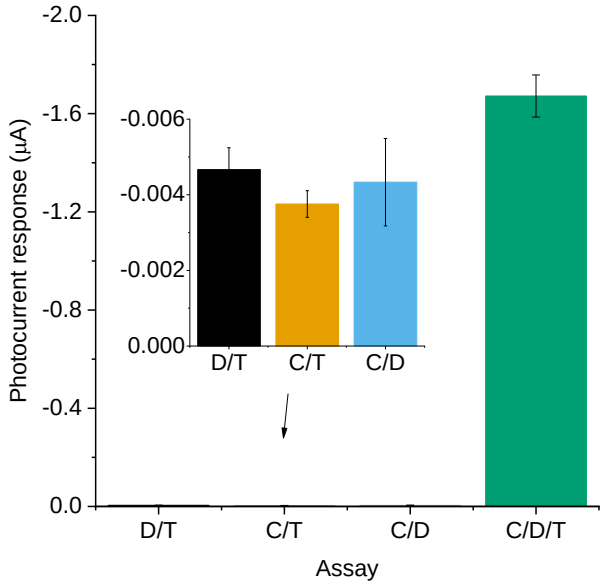


*Figure 4.6 Assay controls with inset showing the zoomed part of photocurrents from the blank controls. Concentration of target miRNA-141 is 20 nM. Amount of beads per analysis: 100 µg; potential: -0.2 V vs quasi-Ag reference; HQ concentration: 1 mM. D indicates the presence of detection probe; C indicates the presence of capture probe; T indicates the presence of the target. Error bars represent the standard deviation (n = 3).*

Following the optimization of the assay, the analytical performance of the sensing strategy has been evaluated in buffer solution. Figure 4.7 shows the calibration plots for miR-145 in the concentration range from 0.06 pM to 10 nM, including two controls. The first control tests specificity by measuring the different concentrations of miR-145 in a mixture with 24 nM of two other miRNAs (miR-141 and miR-375). The method demonstrates good specificity with a photocurrent response proportional to the concentration of miR-145 despite the presence of the other targets. In the second control (negative control), the concentration of a target not complementary to the capture and detection probes was varied in the same range and resulted in negligible photocurrents similar to blanks (0 pM target). The limit of detection was calculated to be 3.3 pM, calculated from the slope ($2.93 \times 10^{-4}$ µA/pM, LOD =3*S.$D_{blank}$/slope [222]) of the calibration curve in the range 0 pM – 38.4 pM. The lowest tested concentration that significantly differed from the blanks was 8 pM.

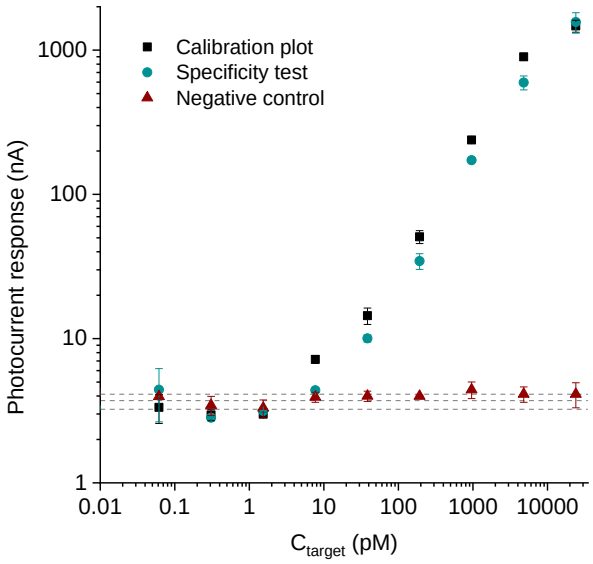


*Figure 4.7 PEC detection of miR-145 in hybridization buffer with optimized parameters. Specificity test depicts the behaviour of the calibration curve in the presence of two other miRNAs (miR-141 and miR-375) each in concentration of 24 nM. Dashed lines indicate the response for 0 pM miR145. Amount of beads per analysis: 100 µg; potential: -0.2 V vs quasi-Ag reference; concentration of HQ: 1 mM. Error bars represent the standard deviation (n = 2).*

### 4.4.3 Matrix effect

The ability of the system to detect miRNAs in clinically relevant sample matrices ensures future uptake of the sensing technology. Plasma and serum are often the matrices of interest for clinical applications. The photocurrent responses of 10 pM miR-141 spiked in serum and plasma (both 1:20 diluted in buffer) were compared to the response obtained in a buffer solution (Figure 4.8). The photocurrent response decreased by 24% in serum

and by 59% in plasma in agreement with the complexity of the matrices. The blank responses from serum (0 pM target) did not differ from the blank responses (0 pM target) obtained in pure buffer solution. These negligible responses from blanks indicate that there is no noticeable unspecific binding of PS-labelled detection probes or other sources of unspecific response due to serum components. Whereas the average photocurrent of blanks (0 pM target) in plasma was slightly higher (ca 10%) compared to responses obtained in buffer solution, which is within the standard deviation of the photocurrents in the buffer. This is likely due to more complexity of plasma's composition with components such as fibrinogen. However, there were no false positives due to the complexity of the serum or plasma matrices. The specific response decreased due to the matrix effect, which is expected due to the interference from proteins in serum and plasma, lowering the interaction between DNA probes and miRNA due to steric hindrance effects.[223] Nevertheless, 10 pM miR-141 in plasma could be detected suggesting further applicability of the assays in POC devices without the need for sample processing, such as nucleic acid extraction. Moreover, the dilution factor and hybridization time should be further optimized to minimize the matrix effect.

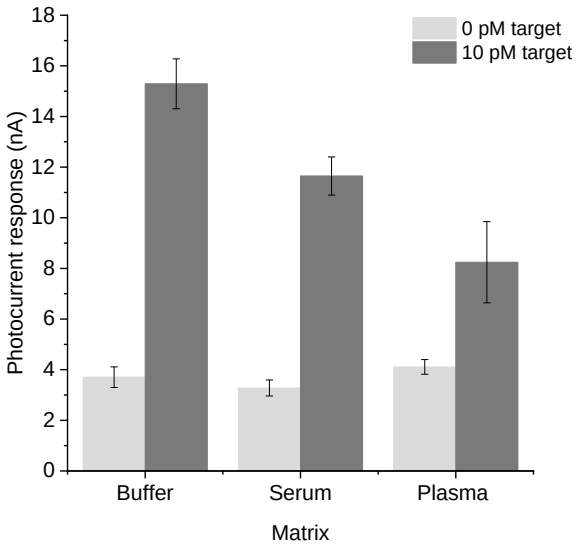


*Figure 4.8 PEC responses from miR-141 in different matrices. Serum and plasma were diluted 20-fold with buffer. Amount of beads per analysis: 100 µg; potential: -0.2 V vs quasi-Ag reference; concentration of HQ: 1 mM. Error bars represent the standard deviation (n = 3).*

### 4.4.4 Analysis of plasma samples from PCa patients

The applicability of the sensing strategy to evaluate clinical samples was demonstrated through the analysis of samples from PCa patients receiving treatment at Centro Hospitalar Universitário do Porto in Portugal. To ensure the lowest contribution of the matrix on the

photocurrent, the effects of the plasma dilution and the incubation time on the photocurrent response of the target were studied by spiking miRNA in commercially available pooled plasma from healthy men (Figure 4.9). The plasma was diluted 5, 10, 20 and 50-fold (indicated as plasma dilution factor, $d_f$) with hybridization buffer and then spiked with 2 nM miR-141 target (photocurrent response for target, **I**). Blank measurements without miRNA target were performed for all dilutions (photocurrent response in the absence of target, $\mathbf{I_0}$) which showed negligible photocurrent responses indicative of no unspecific binding of detection probes in the absence of target (Figure 4.9 A). The absolute photocurrent responses, I, of miRNA target spiked in diluted plasma decreased significantly with increasing plasma fraction as shown in Figure 4.9 B. This can be justified by response suppression due to the matrix effect.[223] However, to compare practical usability in real sample analysis the ratio of signal (**I**) and dilution ($d_f$) was plotted as shown in Figure 4.9 C. Diluting the plasma 10-fold yielded a good signal similar to 20-fold dilution but with lower noise (i.e. smaller error bar), yet, lower blanks ($\mathbf{I_0}$= 5 µA) compared to the 20-fold ($\mathbf{I_0}$= 6 µA). Thus, 10-fold plasma dilution was selected for further experiments with plasma.

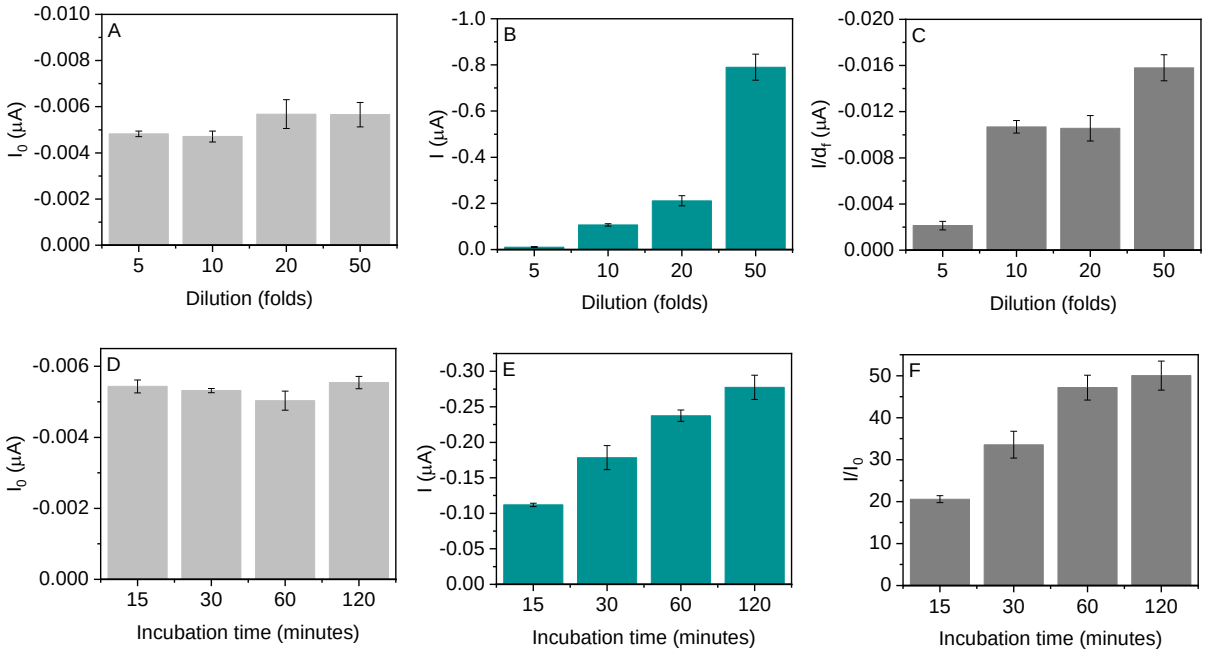


Figure 4.9 *Effect of plasma dilution for hybridization on the photocurrent response from 0 nM (A) and 2 nM (B) miR-141. (C) Normalization of the photocurrent responses from 2 nM miR-141 with dilution factor ($d_f$, :5, 10, 20, 50). Effect of incubation time for hybridization on the photocurrent response from 0 nM (D) and 2 nM (E) miR-141. (F) effect of incuabtion time on the signal to blank ratio. A 10-fold plasma dilution was used for studying the effect of incubation time. Error bars represent the standard deviation (n = 3).*

The effect of the incubation time in plasma on the photocurrent response was evaluated by varying incubation times between 15 minutes and two hours. Increasing photocurrents (**I**) with increasing incubation time was observed with negligible photocurrents in the absence of target ($\mathbf{I}_0$) (Figure 4.9 D, E). While 15 minutes of incubation was enough to capture the target miRNAs and give recognizable photocurrent, incubating for one hour doubled the response. Increasing the incubation time to two hours presented a similar $\mathbf{I}/\mathbf{I}_0$ ratio (Figure 4.9 F), thus one hour incubation time was opted for further investigations. Nevertheless, the results obtained with 15 minutes of incubation showed that when a quick diagnostic test is required aiming for POC analysis, the time of analysis might be shortened.

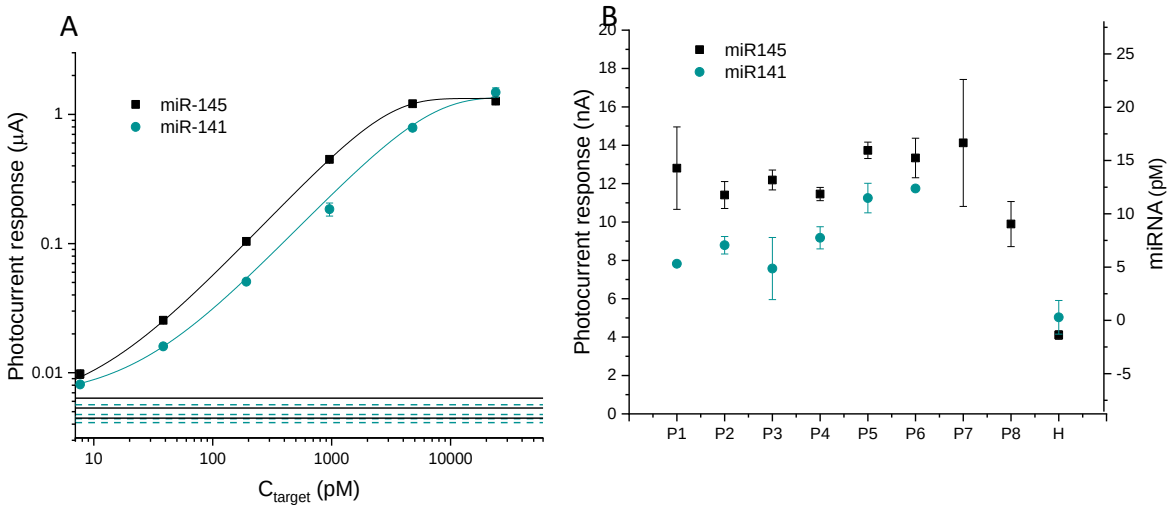


*Figure 4.10 (A) Standard curve constructed with healthy male pooled plasma spiked with different concentrations of miR-145 and miR-141. (B) photocurrent responses and calculated concentrations of miRNAs from prostate cancer patient samples (P1-P8). Pooled plasma from healthy men (H) was included as a control. Error bars represent the standard deviation (n = 2).*

To compare and estimate the levels of miR-145 and miR-141 in patient samples, standard curves with optimized parameters were constructed by spiking different concentrations (between 1.5 pM and 24 nM) of miRNAs in commercially available pooled plasma from healthy men, 10-fold diluted (Figure 4.10 A). A detection limit of 3.5 pM and 8.3 pM was achieved for miR-145 and miR-141, respectively (Table 4.3). Analysis was done for plasma samples derived from eight patients (P1-P8) with PCa with an age range between 64-72 years, presenting with clinicopathological characteristics depicted in Table 4.4. These plasma samples from PCa subjects have been centrifuged twice, to separate plasma from cells. Due to the differences in the patient sample volume, all the plasma samples (P1-P8) and pooled plasma from healthy men (H) were analysed for the most relevant miR-145[206] and seven samples (P1-P6 and H) were analysed for miR-141, all diluted 10-fold before the hybridization step (4.10 B). The concentration of the miRNAs in pooled plasma from healthy

men does not significantly exceed the background signal in pure buffer and is considered to be below the LOD in plasma.

As depicted in Figure 4.10 B, all the PCa patient samples exhibited different photocurrent responses in the range of 8 – 18 nA, all higher than the response from the pooled healthy male plasma which was 4.5 – 5.5 nA. Photocurrents from the PCa patient plasma samples were converted into miRNA concentrations using the slope of the calibration plot (Figure 4.10 B, Table 4.4). This yielded an increase in miR-141 and miR-145 compared to the healthy plasma samples. Results correlate well with the expected higher expression of miR-141 and miR-145 in prostate cancer patients, as reported in the literature. [204, 206, 224-228]

*Table 4.3 Limits of detection for miR-145 and miR-141 in 10-fold diluted plasma.*

| | **miR-145** | **miR-141** |
|---|---|---|
| *Slope (µA/pM)* | $5.30\times10^{-4}$ | $2.77\times10^{-4}$ |
| *$S.D._{blank}$ (µA)* | $6.20\times10^{-4}$ | $7.67\times10^{-4}$ |
| *LOD (pM) =3×$S.D._{blank}$/slope* | 3.5 | 8.3 |

Interestingly, the photocurrents and, thus, the concentration of miR-145 in patient samples were always higher and varied less compared to miR-141. Therefore, miR-145 seems to be a more appropriate diagnostic marker, although a larger study is needed to include blank control samples from individuals to better assess variability in miRNA levels in patients and control groups, or by following up with patients to ascertain whether they present disease progression.[207]

To the best of our knowledge, in the literature, the levels of these two miRNAs are either given as relative expressions or fold-change of miRNAs comparing plasma/serum samples and seldom in absolute numbers.[206, 224-229] These relative values or ratios are presented in terms of copy numbers per volume of plasma/serum or cycle threshold (Ct) numbers from PCR amplicons after normalization with reference genes. Shen et al. and Cheng et al. performed Taqman-based quantitative RT-PCR assays to measure target miRNAs, including miR-145 and miR-141, respectively.[206, 227] The data was presented as copy number/µL of the target in both cases (90– 150 copies/ µL of miR-145 in plasma samples from 82 different PCa patients[206] and 225- 89811 copies/ µL of miR-141 in serum samples from 21 PCa patients[227]). Paunescu et al., Zhang et al., Porzycki et al., and Nguyen et al. used RT-PCR assay to quantify miRNAs including miR-145 and/or miR-141 and differentially expressed microRNAs between cancer and control plasma samples in terms of fold change or relative expression of the Ct values.[224-226, 228] These miRNA detection protocols include total RNA extraction from the liquid biopsy specimen, miRNA isolation, cDNA conversion,

amplification and detection steps, thus, requiring careful data normalization to interpret relative changes in miRNA levels.[230] Very recently, Kshirsagar et al. presented a PCR-free (without the need for cDNA conversion) single-step quantification of miRNAs, including miR-141 in sera of PCa patients and healthy controls. Gold nanoparticles with fluorescent DNA probes were used to hybridize with miRNA and quantify them by measuring the fluorescence intensity. Comparing the detection signals with the standard calibration curve, the results were presented as relative expressions of miRNAs in 42 PCa patient vs 43 healthy donor serum samples.[229] These works do not give the concentrations of miRNAs as such, i.e. as pM concentrations in plasma, thus, not allowing us to compare our assay results with the literature values. However, the relative picture of our result demonstrating increased expression of miR-141 and miR-145 in PCa patients compared to healthy controls agrees with the literature. Importantly, our assay offers accurate and sensitive miRNA detection in untreated plasma without any pre-amplification steps, which is straightforward for interpretation and may provide better knowledge regarding variations and dysregulation in levels of circulating miRNAs, opening new opportunities for POC usage. In fact, our assay offers detection of miRNAs in the same manner as for regular biomarkers of protein origin, such as PSA. This can be of special interest when accurate detection is needed rather than detection of a certain mutation or appearance of a certain sequence, where sequencing and PCR-related techniques are of typical use.

*Table 4.4 Clinicopathological features of patient samples and concentrations of miRNAs calculated for non-diluted patient samples in this study with photoelectrochemistry.*

| | **Clinical data** | | | | | **Found levels of miRNA[a]** | |
|---|---|---|---|---|---|---|---|
| | **Age** | **Gleason score** | **ISUP** | **PSA (ng/mL)** | **Stage_pT (tumour)** | **miR-145 (pM)** | **miR-141 (pM)** |
| P1 | 69 | 4+3 | 3 | 1.3 | 3b | 145 ± 41 | 59 ± 4 |
| P2 | 71 | 4+3 | 3 | 66 | 3a | 118 ± 14 | 98 ± 18 |
| P3 | 72 | 3+3 | 1 | 7.4 | 3a | 133 ± 10 | 69 ± 36 |
| P4 | 71 | 3+4 | 2 | 8 | 2 | 119 ± 7 | 113 ± 23 |
| P5 | 62 | 4+4 | 4 | 13.1 | 2 | 163 ± 8 | 196 ± 31 |
| P6 | 68 | 3+4 | 2 | 23.2 | 3a | 155 ± 20 | 215 ± 3 |
| P7 | 72 | 4+3 | 3 | 7.3 | 3a | 171 ± 64 | - |
| P8 | 64 | 3+3 | 1 | 7.7 | 2 | 89 ± 23 | - |

*[a] values are presented after $d_f$ corrections for miRNA concentrations in 100% plasma. The measurements were conducted twice and the found levels are presented as average values ± standard deviation of 2 independant measurements.*

### 4.4.5 Approaches to further enhance the sensitivity: impact of label's position and different electrode materials on the PEC response

While our sensing strategy yielded good detection limits in the picomolar range, ways to improve the sensitivity and broaden the applicability of this strategy to more commonly used and cheaper commercial electrode surfaces were further investigated. Previous experiments were conducted using electrodes with gold-sputtered working electrode surfaces. The applicability of other working electrode materials has been tested in this section. Moreover, the influence of the label position at the detection DNA probe (attached to the 3' or 5' end, Figure 4.11) has been studied in the context of the hybridization efficiency, possible quenching of the $^1O_2$ quantum yield or the generated $^1O_2$ itself by the DNA and the surface of magnetic beads. The position of the reporter molecule in electrochemical assays affects not only the hybridization efficiency [231] but also the process of charge transfer.[231-233]

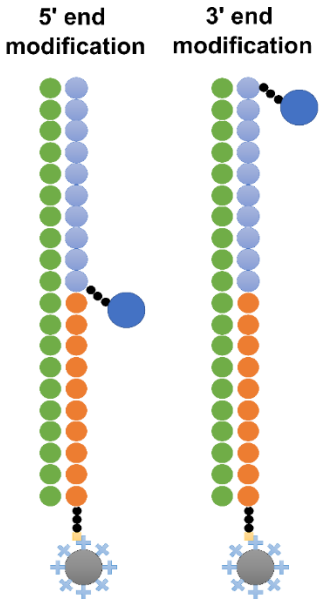


*Figure 4.11 Schematic representation of the sandwich duplexes formed after the hybridization assay with PS linked to the detection probes in two different positions.*

Gooding and co-workers showed that the hybridization process is more efficient when a MetB label is in the distal end of the DNA monolayer and lower when the label is placed internally in the DNA strand.[231] Regarding the effect on charge transfer, the same group has reported different results depending on the DNA surface density. For low DNA surface density, the charge transfer process is faster when the MetB label is close to the surface[231] but at higher DNA surface coverage the faradaic current generated is higher when the MetB label is at the distal end of the DNA film.[232] Using ferrocene (Fc) Kraatz and co-workers showed that the rate of electron transfer is about three times higher when the Fc label is

in the distal end than when it is in the proximal end of the DNA monolayer, with the authors attributing this result to the elastic bending and free rotational motions of the dsDNA.[234] The literature indicates that the label interacts with the DNA duplex and the underlying surface in a complex way. In the context of our work, such interaction may impact the lifetime of the photoexcited triplet state (due to quenching), resulting in side reactions of the photoexcited molecule and $^1O_2$, or physically quenching $^1O_2$. To study this effect, ChlE6 (undergoing type II photosensitization) and MetB (an electroactive molecule undergoing type II and type I photosensitization) were linked to either the 5' and 3' end of the detection probe (Figure 4.11). The working electrode material was also varied to establish its influence on the registered photocurrent. For this, 12 different types of screen-printed electrodes available commercially from DropSens were tested. The materials of the working electrode included three gold-based, nine carbon-based, also modified with CNT, graphene, glucose oxidase, polyaniline and other coatings.

Figure 4.12 shows the light-chopped chronoamperograms recorded after hybridization with 24 nM and 0 nM miR-145. The detection strand was labelled with ChlE6 and MetB on both the 5' and 3' end as indicated in the respective figures. Firstly, photocurrent responses of different amplitudes were observed for MetB and ChlE6 on different electrodes owing to different compositions of ink/metal printed on the electrodes. ChlE6 provided significantly higher (about 4x higher) responses compared to MetB, thus making ChlE6 more preferential than MetB for applications. Additionally, ChlE6 when labelled at 5' end (middle position in the duplex) yielded a higher response compared to the conventional 3' labelling (position at the edge of the duplex). This is possibly due to the quenching of the quantum yield of the PS's triplet state formation and $^1O_2$ by an exposed nucleobase at the edge of the DNA duplex, while nucleobases are sterically hindered inside the duplex in the middle of DNA. The increase of the response by 1.5x can be beneficial to proportionally improve the sensitivity of the sensor and decrease its LOD, although the difference is rather minor. The highest response was obtained for Au-PW with ChlE6 at the 5' end, while the lowest response was given by the enzymatic G-Ox electrode for both MetB and ChlE6, most likely because the enzyme passivated surface is blocking the photoinduced electron transfer at this near zero potential. This suggests the suitability of gold-based electrodes for the measurements, compared to other electrodes tested. However, carbon-based electrodes such as Gr SPE, SWCNT and MWCNT give a comparatively better response with ChlE6 at 5' and 3' end. The photocurrent profile for different electrodes was similar for both DNA sequences and both labels' positions. Some minor differences can be attributed to an impact on the hybridization kinetics and efficiency.

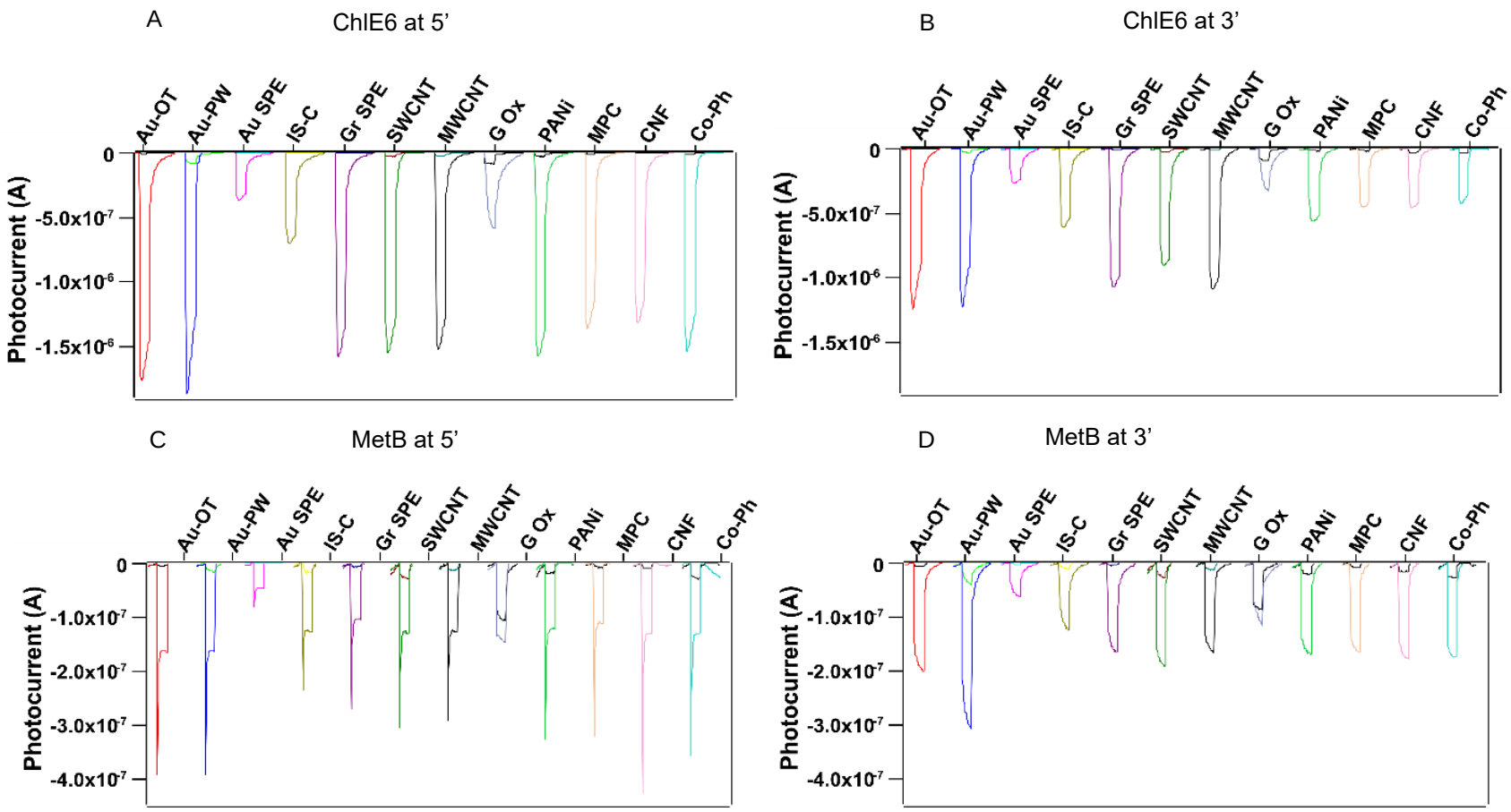


*Figure 4.12 Chronoamperograms resulting from the PEC detection of 24 nM and 0 nM miR-145 with the detection strand labelled with ChIE6 and MetB on the 5' end (A), (C) and on the 3' end (B), (D). Measurements were done in the presence of 1 mM HQ; Chronoamperometric measurements were carried out at -0.2 V vs. quasi-internal Ag reference. Amount of magnetic beads used: 100 µg.*

The photocurrent responses for MetB at the 5'end of the detection probe give spikes immediately after the light is on, followed by a steady-state photocurrent. These spikes are observed for all electrode materials except electrodes with glucose oxidase (G-Ox). The nature of these spikes is not fully clear and can be related to the electrode process due to photoinduced electron transfer (ET) from MetB to the electrode since MetB is prone to ET reactions as previously observed for labelled oligos placed directly on the gold electrodes (chapter 3). However, it is unclear why it is absent for the 3'-position in the case of magnetic beads. (Figure 4.12 C & D). Still, the spike current in sum with the steady-state current at the beginning of the illumination is about twice higher as the steady-state photocurrent a few seconds later, thus it can be useful for more sensitive detection of DNA. Interestingly, the steady photocurrents (not considering the spikes) are nearly the same when MetB is positioned at 3' and 5' ends. However, further detailed studies are needed to better understand the nature of the spikes and the reason for their occurrence when the MetB label is only present at 5' end and not at 3' end.

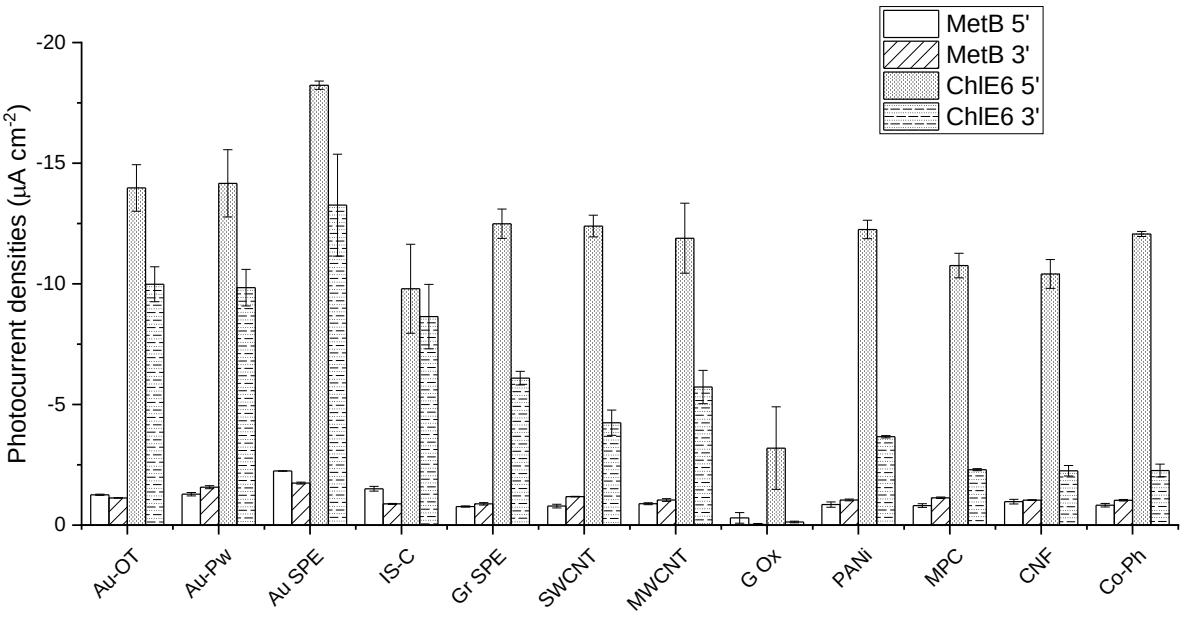


*Figure 4.13 Comparison of photocurrent densities from different electrodes. The values are obtained from photocurrents (Fig 4.12) normalized per geometrical surface area. Error bars represent the standard deviation (n = 2).*

Although photocurrent responses are important in characterizing the suitability of the electrode platforms for PEC measurements, comparing their photocurrent densities will give a broader picture of the working electrode materials as such, rather than the whole electrode platform. Figure 4.13 represents the photocurrent densities obtained from various electrode platforms from the geometrical surface area (GSA) of the working

electrode. While the photocurrent responses from Au-PW and Au-OT electrodes provide the highest sensitivity, which is five times higher than that of Au SPE (Figure 4.12), Au SPE surprisingly yields a higher photocurrent density (ChlE6 at 5' on Au SPE, Figure 4.13), followed by similar densities from gold-sputtered surfaces and carbon-based electrodes. This suggests that gold SPE with similar or larger GSA as the AU-OT (with GSA = 0.5 $cm^2$) can indeed be used for PEC detection in combination with magnetic beads and are attractive and effective alternatives to Au-OT electrodes as will be additionally discussed in chapter 6.

## 4.5 Conclusion

This chapter describes a PCR-free $^1O_2$-PEC method for detecting and quantifying miRNA in plasma samples. The method combines the usability of (i) magnetic beads to capture target miRNA from a complex matrix such as plasma and (ii) our original concept of employing $^1O_2$ in PEC sensing for robust and sensitive detection and quantification. It features a low-cost electrochemical setup equipped using a LED and without additional PCR or other amplification techniques for detecting low picomolar levels of miRNAs spiked in diluted plasma of healthy men. Elevated levels of miR-145 and miR-141 in plasma samples of PCa patients were successfully detected. Furthermore, steps to further lower the detection limits were taken. The sensitivity increased 1.5—2x after attaching the ChlE6 label at the 5'end instead of the conventional 3'-end, for gold and carbon-based electrodes. Thus, developing a multichannel system using commercially available 96-well electrochemical plates with working electrodes made of gold or carbon ink has become well justified. Given the versatility of the magnetic beads, this strategy can also be extended to other NA sequences, being relevant for liquid biopsy applications and demonstrating the general feasibility and clinical relevance of our detection method.

# Chapter 5
# Electrochemiluminescence and photoelectrochemistry for miRNA quantification

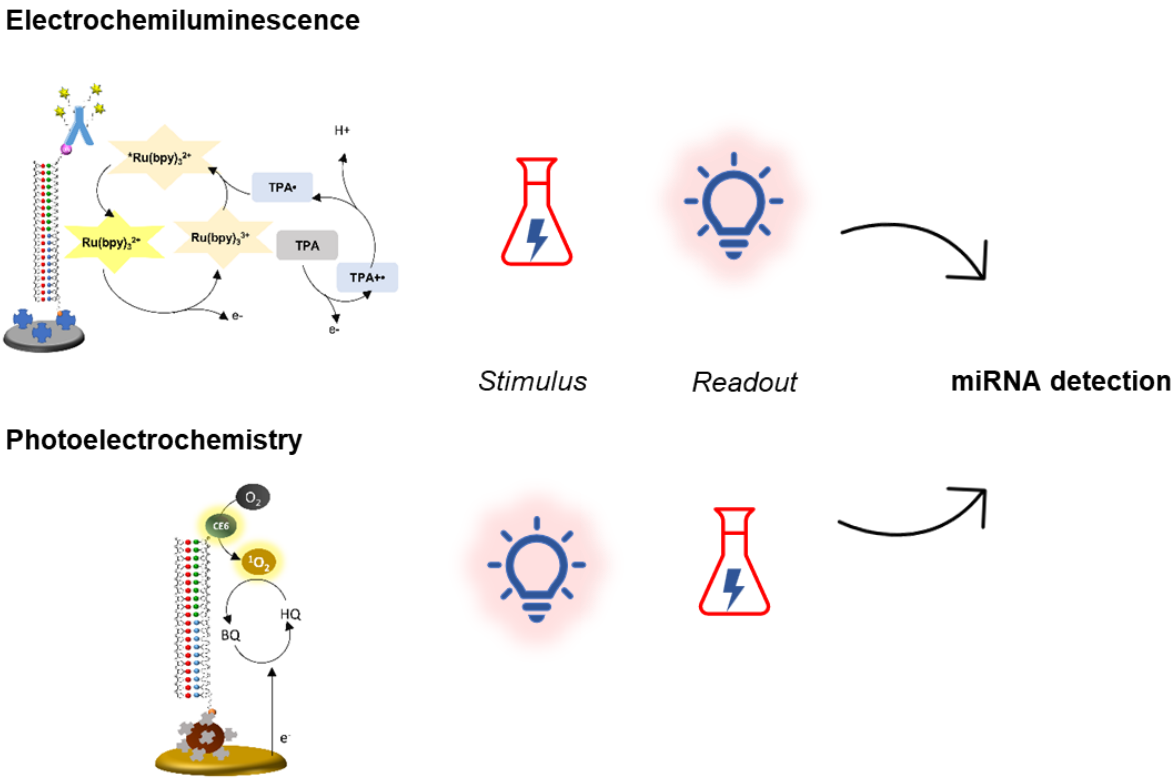


Detection of a circulating miRNA using two oligonucleotide-based assays

**Adapted from the following manuscript:**

*Campos R.‡, Thiruvottriyur Shanmugam S.‡, Daems E., Ribeiro R., De Wael K. Development of electrochemiluminescent and photoelectrochemical oligonucleotide-based assays for the quantification of prostate cancer associated miR-141-3p in Human Serum. Manuscript in preparation. ‡ Shared first authors.*

***Contribution:** I performed the photoelectrochemical experiments resulting in section 5.4.3 and wrote the first draft of the manuscript along with Campos R.*

## 5.1 Abstract

In this study, our $^1O_2$-based PEC assay has been compared with a principally inverse state-of-art oligonucleotide-based electrochemiluminescence (ECL) assay for the specific and sensitive detection of a circulating miRNA (miR-141) associated with prostate cancer. In both assays, the excitation and readout of the signal are independent: an electrochemical stimulation followed by an optical readout for ECL and the inverse for PEC assay. The 'sandwich' approach is incorporated, consisting of a biotinylated capture probe immobilized on streptavidin-functionalized surfaces and a detection probe labelled with digoxigenin or chlorin e6 for the ECL and PEC assay, respectively. Both assays allow the detection of miR-141 in the pM range in human serum, even in the presence of other miRNAs. The developed PEC assay, therefore, has the potential for cost-efficient universal oligonucleotide target detection via the redesign of capture and detection probes compared to its complementary ECL technique.

## 5.2 Introduction

Monitoring biomarkers in biofluids allows for increased accuracy in treatment decisions and reactionary treatment strategies, leading to personalized medicine. [11, 196] This is particularly important when a change from a drug-sensitive to a drug-resistant disease occurs. In prostate cancer, miR-141 is overexpressed and its levels can be correlated to the total PSA levels.[199, 235-237] The high chemical stability of these nucleic acids in body fluids makes them powerful biomarkers that are present at levels suitable for testing in biofluid samples from patients. To address the aforementioned drawbacks of current miRNA detection techniques (Chapter 1), research into electrochemiluminescence (ECL) and PEC detection of nucleic acids have been gaining momentum. Additionally, in the field of analytical chemistry, ECL has become a powerful transduction tool, broadly applied in environmental, bioanalytical and clinical diagnostic fields.[238] Moreover, it is important to compare our developed $^1O_2$-based PEC assay to the state-of-art ECL assay, now available in the clinical diagnostic market[239, 240] given their capability to detect nucleic acids without any need for additional amplification technique.

ECL, also electrogenerated chemiluminescence, is the emission of photons from a molecular species (luminophore) following an electron-transfer (ET) reaction in solution, triggered by electrochemical reactions.[241] When applying a potential, the luminophore, undergoes a high-energy ET reaction in the presence of a co-reactant, which can generate electronically excited states emitting light. Thus, ECL produces light from an electrochemical stimulus, as opposed to photoelectrochemistry, where an electrochemical signal (current) is produced upon illumination. It involves the production of reactive intermediates from stable precursors at the surface of an electrode. These intermediates then react under a variety of conditions to form excited states that emit light.[242]

ECL-based detection combines high sensitivity, low background, and fast response[243, 244] and advantageously avoids the interference of background light sources resulting in improved signal-to-noise ratios. The use of ECL for miRNA detection has gained interest in recent years with, in particular, ruthenium-based systems in the presence of a co-reactant such as tripropylamine (TPA) being a textbook example.[244, 245] However, there are other ways to improve the ECL signal, such as a two-stage isothermal strand-displacement polymerase reaction,[246] and the combination of ECL signal quenchers (namely carbon dots) with a duplex-specific nuclease.[247] However, such assays are expensive and complex, thereby limiting their applicability in POC testing.

Recent reports on the ECL detection of miRNAs associated with oncological diseases include those performed by the group of Chai and Yuan[248, 249] and the group of Zhou.[250] In their first work,[248] the group of Chai and Yuan designed dual miRNAs-fuelled DNA nanogears for detection of the miRNA with a single luminophore. In buffer, miR-155 was detected down to fM levels and detection of the miRNA was also possible in cancer cell lysates, although no quantification was performed in this sample matrix. In their second work,[249] the authors developed a DNA walking machine to detect miR-21 and miR-155 but the detection was only performed in the buffer. Even though the work developed by this group is very impressive, it lacks the analysis of clinical samples and that is key in the development of an assay to be used as POC testing. Zhou's group developed an ECL biosensing platform to detect miR-21 and the protein mucin 1 and they were able to detect both targets in human serum. The catalytic hairpin assembly process is initiated by the presence of miR-21, whose presence brings CdS:Mn quantum dots to the electrode surface, leading to an ECL response. The detection of mucin 1 is triggered by its aptamer, which allows Au nanoparticles to approach the CdS:Mn quantum dots leading to a decrease in the ECL signal. This is a very complex architecture, which limits its application in a real setting. The three works discussed above highlight the difficulty of working with clinical samples and confirm that, to date, no routine assay is available to detect miRNAs in serum or plasma from oncological patients. The ECL assay developed here is straightforward, not requiring complex strategies or detection mechanisms.

Amgen Research has reported the quantification of oligonucleotides in biological matrices using a commercially available ECL instrument.[251, 252] The use of a sandwich assay, together with locked nucleic acids (LNA) allowed oligonucleotide detection between 0.3 pM and 16.7 nM in serum. Despite the high cost of the assays and the need to home-label the reporting antibody, the promising results lead us to develop a DNA-based sandwich assay for the detection of miR-141 as a term of comparison to the PEC approach that has been developed in parallel.

$^1O_2$-based PEC sensing is an inviting approach for detecting oligonucleotides because of its sensitivity and technological advances in microelectronics. Additionally, the utilization of disposable electrodes provides a low-cost approach.[85, 253-255] The $^1O_2$-based PEC detection of oligonucleotide involving a series of light-responsive probes generating singlet oxygen ($^1O_2$) upon illumination was demonstrated in chapter 3. The sensitivity was improved by using hydroquinone (HQ) as a redox reporter for the chemical capturing of short-lived $^1O_2$, allowing amperometric detection of the target. [215, 256]

The aim of this work is to develop and carry out a comparative PEC and ECL assay for the detection and quantification of miR-141 in human serum. Due to the separation between excitation and readout signal, greater sensitivity can be achieved in both ECL and PEC techniques.[169, 243, 257] We have optimized the ECL assay parameters such as concentration of probes, amount of anti-DIG antibody used and optimal serum dilution during the hybridization step. The analytical performance with the optimized parameters has been evaluated for the detection of miR-141 in hybridization buffer and diluted serum. Hybridization assay and measurement parameters for PEC assay and detection have been extensively optimized in chapter 4 and have been employed here for evaluating the analytical performance of PEC detection of miR-141 in hybridization buffer and diluted serum. These assays possess the characteristics that POC assays should display, namely robustness, sensitivity and specificity while being able to quantify miRNAs in complex biological matrices.

## 5.3 Materials and Methods

### 5.3.1 Materials

Sodium phosphate monobasic, sodium phosphate dibasic, sodium chloride, magnesium chloride, Tween 20 and human serum were purchased from Sigma-Aldrich (Overijse, Belgium). DNA and miRNA sequences used in this work were purchased from Eurogentec (Liège, Belgium) and are shown in Table 5.1. Stock solutions of 100 µM were prepared by reconstitution in ultrapure water (UPW).

*Table .5.1 DNA and RNA sequences used to detect miR141 using ECL and PEC assay.*

| **Name** | **5' modification** | **Sequence (5' – 3')** | **3' modification** |
|---|---|---|---|
| Target (miR-141-3p) | - | UAA CAC UGU CUG GUA AAG AUG G | - |
| Capture | Biotin-TEG | CCA TCT TTA CC | - |
| Detection (ECL) | - | AGA CAG TGT TA | Digoxigenin |
| Detection (PEC) | | | Chlorin E6 |
| Negative Control (miR-375-3p) | - | UUU GUU CGU UCG GCU CGC GUG A | - |
| Negative Control (miR-145-5p) | - | GUC CAG UUU UCC CAG GAA UCC CU | - |

For the ECL assay, goat polyclonal anti-digoxygenin (anti-DIG) antibody (Abcam, Cat. Ab76907) was conjugated with multiple tris(2,2'-bipyridyl) ruthenium(II) ($Ru(bpy)_3^{2+}$) labels

using the MSD Gold Sulfo-Tag NHS-Ester conjugation kit (Meso Scale Diagnostics, R31AA-1). MSD GOLD 96-well Streptavidin QUICKPLEX Plate Pack (L55SA), MSD GOLD 96-well Small Spot Streptavidin SECTOR Plate (L45SA) and MSD GOLD Read Buffer (R92TG) were purchased from Meso Scale Discovery, USA.

For the PEC assay, streptavidin-coated magnetic beads (M280-Dynabeads, Invitrogen) were used for the sandwich hybridization assay. A 2XTE buffer solution (pH 7.5, adjusted using HCl), containing 10 mM Tris, 1 mM EDTA (Titriplex III), and 2 M NaCl was prepared. This 2X TE buffer was mixed with (i) Tween 20 to yield a 2x TE + 0.05 % Tween 20 (2XTE-$T_{20}$) buffer, (ii) ultra-pure water and Tween 20 to yield a 1X TE + 0.05% Tween 20 (1XTE-$T_{20}$) buffer (named the hybridization buffer from here on). Measuring buffer with 1 mM hydroquinone (HQ, Acros Organics, Belgium) was prepared using a background electrolyte consisting of 0.1 M KCl and 0.01 M $KH_2PO_4$ adjusted to pH 7.

### 5.3.2 ECL Assay preparation

Before the immobilization on the well plate, the three strands forming the sandwich were allowed to react for one hour at room temperature in hybridization buffer or diluted serum (2-fold, 5-fold, 10-fold, 20-fold, 50-fold diluted with hybridization buffer). Unless stated otherwise, the concentrations of the capture and detection probe were 24 nM and the concentration of the target varied from 24 nM to 1.5 pM (8 dilutions with a 5-fold ratio, including a non-target control). Upon reaction, 50 µL of the master mix was transferred to a well, that had previously been washed once with 150 µL of PBS-$T_{20}$ (1.8 mM $KH_2PO_4$ + 10 mM $Na_2HPO_4$ + 2.7 mM KCl and 137 mM NaCl with 0.05% Tween 20) and tap-dried, allowing to interact for one hour at room temperature at 550 rpm in a plate shaker. The plate was then washed three times with 150 µL PBS-$T_{20}$ and tap-dried before adding 25 µL of anti-DIG antibody solution. After one hour of reaction, the plate was washed again three times with 150 µL PBS-$T_{20}$ and tap-dried. Then 150 µL of MSD GOLD Read Buffer A was added and the plate was read immediately in the MSD Quick Plex SQ 120 controlled by the Methodical Mind reader software.

### 5.3.3 Sandwich hybridization with magnetic beads and PEC detection

Streptavidin-coated magnetic particles (10 µL, 10 mg $mL^{-1}$) were dispersed in an Eppendorf containing 1 mL of 1XTE-$T_{20}$ buffer. The solution was vortexed, and the magnetic beads accumulated at the side of the Eppendorf were directed to the magnetic rack (approximately 1 min). The solution was removed and suspended in 500 µL of 2XTE-$T_{20}$ buffer, to which 500 µL of 100 nM capture probe solution in UPW + 0.05% Tween 20, was added, leading to a final incubation containing 1 mL of capture probe at 50 nM in 1XTE-$T_{20}$.

This solution was incubated for 15 min at room temperature in a rotary shaker at 10 rpm. Followed by the accumulation of the beads using a magnetic rack with the solution being discarded and the beads resuspended in diluted serum (20-fold in 1XTE-$T_{20}$) containing 24 nM detection probe and different concentrations. The mixture was then incubated for 1 hour at room temperature, in the dark, in a rotary shaker at 10 rpm. Following the incubation, the beads were washed 3 times with 1 mL 1XTE-$T_{20}$ buffer and stored in 10 µL of the same buffer until measurements. To perform the PEC measurement, 90 µL of the measuring solution was placed on the electrode surface and another 10 µL of the same solution was used to extract the beads from the Eppendorf. This 10 µL magnetic bead slurry was then added to the solution on top of the electrode before starting the measurement. Amperometry at −0.2 V *vs.* quasi-internal Ag reference was performed with light 60 s OFF/10 s ON/30 s OFF. The PEC response was acquired by subtracting the initial current at light ON from the baseline current.

### 5.3.4 Specificity and selectivity

To assess the specificity and the selectivity of the probes, ECL and PEC measurements were performed in the presence of negative controls (another miRNA), instead of the desired target, and in a mixture containing the target and two other RNA strands, respectively. The standard curves, in both hybridization buffer and serum, obtained in these conditions, were compared to those obtained in the presence of the target only.

## 5.4 Results and discussion

In this chapter, the PEC response and ECL response of the duplex formed by the target miRNA (miR-141) hybridized with the capture and detection probe in a sandwich-like format (Figure 5.1 A and C) have been evaluated. In ECL, streptavidin-modified electrodes trap the sandwich duplex via the biotinylated capture probe. The detection probe is labelled with digoxygenin and will by recognized by the $Ru(bpy)_3^{2+}$-labelled anti-DIG antibody and is close to the electrode surface for the ECL reaction in presence of the co-reactant TPA (Figure 5.1 B). The oxidation of TPA generates the TPA radical cation ($TPA^{\bullet+}$) that undergoes deprotonation resulting in the formation of the TPA radical ($TPA^{\bullet}$). $TPA^{\bullet}$ is a strong reducing species that reacts with the electrogenerated $Ru(bpy)_3^{3+}$ to form the $Ru(bpy)_3^{2+}$ excited state which emits light.[38-40] This mechanism influences the ECL intensity and depends on the $Ru(bpy)_3^{2+}$ concentration which is directly proportional to the concentration of the anti-DIG antibody, and in-turn the target miRNA.

The PEC assay uses the same sandwich approach as the ECL assay, but in combination with streptavidin-modified micron-sized magnetic beads to improve the sensitivity of the assay by concentrating the sandwich hybrids on the electrode surface, while also providing enough room for the redox amplification.[35]

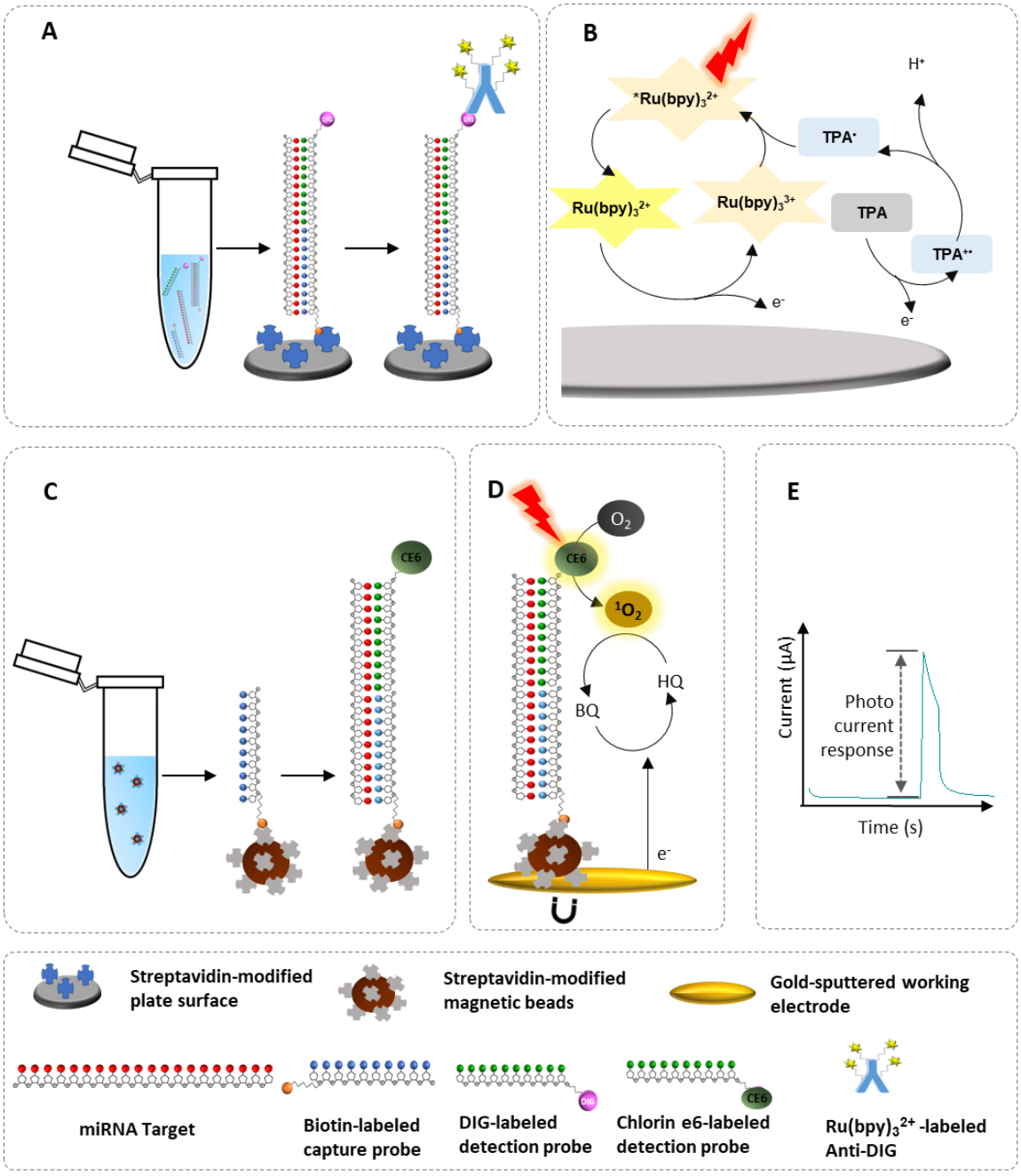


*Figure 5.1 Schematic representation of the (A) ECL assay, (B) ECL detection mechanism, (C) PEC assay, (D) PEC detection mechanism and (E) PEC measurement. The lower panel shows the various components of both assays.*

The biotinylated capture probe binds to the streptavidin on the beads and the sandwich is completed upon the reaction of the capture probe with the remaining free part of the target while the other part of the target is hybridized with the detection probe. The functionalized beads are simply deposited on disposable gold-sputtered electrodes, with a magnet below, as is schematically shown in Figures 5.1 C and D. The use of neodymium magnets below the electrode during the measurements ensures that the beads do not disperse in solution and are kept close to the surface of only the working electrode.

As mentioned in the materials and methods section, the PEC detection probe is labelled with chlorin e6, a type II PS (producing $^1O_2$). $^1O_2$ has a short lifetime in water (~3.5 µs in quencher-free $H_2O$[41]) and can diffuse only around 200 nm, while magnetic beads are around 2.8 µm in diameter. To circumvent the short lifetime of $^1O_2$ a stable redox reporter, hydroquinone (HQ) was used. During illumination and upon recognition of the target, HQ is oxidized by $^1O_2$, producing benzoquinone (BQ). Afterwards, BQ is reduced back to HQ at the electrode surface resulting in an amplified cathodic current through redox cycling resulting in photocurrent responses (Figure 5.1 D & E).

### 5.4.1 ECL assay- optimization of parameters

With an aim to develop an oligonucleotide-based ECL assay to detect miR-141, the concentration of capture and detection probes, the amount of anti-DIG antibody and the serum dilution were initially optimized. The ECL supplier indicates that the binding capability of the plate is 0.3 pmol/well, measured by titrating the plate with biotin-tagged immunoglobulin G (IgG), which corresponds to a concentration of biotinylated capture probe of 6 nM (the volume used in the well was 50 µL). Because the binding capability was determined for IgG, and not for oligonucleotides, higher concentrations of oligo (12 nM and 24 nM) were also tested. As can be seen in Figure 5.2, 24 nM allowed the detection of the target at higher concentrations without saturation of the signal, this concentration of capture and detection probes was chosen to perform all the following experiments. Next, the concentration of anti-DIG antibody was varied between 0.5 and 2 µg/mL (Figure 5.2 B). The concentration of antibody has no significant effect on the ECL counts. Consequently, the lowest concentration of anti-DIG antibody (0.5 µg/mL) was used during the remainder of the experiments.

To investigate the influence of the serum matrix on the hybridization of the sandwich assay, the hybridization with different concentrations of target (miR-141) was performed in various dilutions of serum (2-fold, 5-fold, 10-fold, 20-fold, 50-fold diluted with hybridization buffer). As can be seen in Figure 5.3, only at a 20-fold and 50-fold dilution it is possible to detect the target miRNA at the pM level. For the other dilutions with high concentrations of serum, matrix effects from high concentrations of serum prevented the generation of ECL signal. Though the measurements are performed in measuring buffer, during the hybridization step, most likely, proteins in the serum at higher concentrations foul the electrode surface and remain on the surface even after the washing steps, thus passivating the surface. The 20-fold dilution was opted since it gives similar results to the 50-fold dilution and means a lower dilution of the target. The same dilution has been used by Thayer *et al.* for the detection of siRNA in human excreta when using an instrument from Meso Scale Discovery.[25, 26]

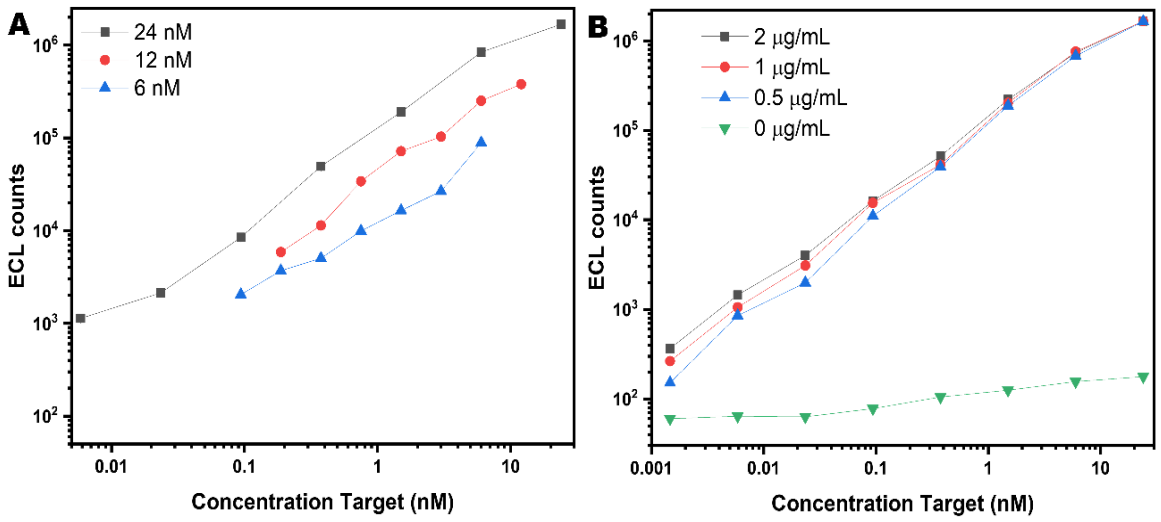


*Figure 5.2 Optimization of various parameters to be used in the ECL assay for the detection of miR-141. (A) concentration of probe and (B) amount of anti-DIG antibody. Mean data is shown with error bars representing standard deviation (n=2). Axes are in log scale.*

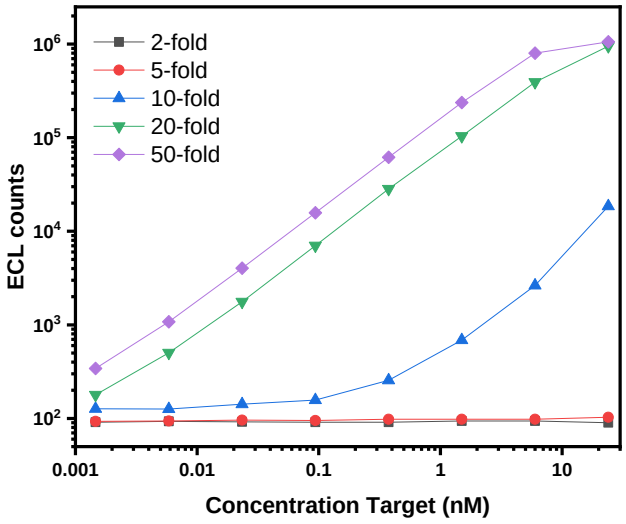


*Figure 5.3 Optimization of the serum dilution to be used in the ECL assay for the detection of miR-141. The serum was diluted in different folds with hybridization buffer. Mean data are shown with error bars representing standard deviation. Axes are in log scale.*

### 5.4.2 ECL assay- analytical performance in buffer and diluted serum

After optimization of the crucial parameters, the analytical performance of our ECL sandwich assay in hybridization buffer and in diluted serum (20-fold dilution) during the hybridization step was optimised (Figure 5.4). Apart from varying the concentration of the targets and building a (i) calibration plot, two controls such as (ii) negative control, by varying the concentration of the target not complementary to the capture and detection probes and (iii) specificity, by measuring the different concentrations of target in the

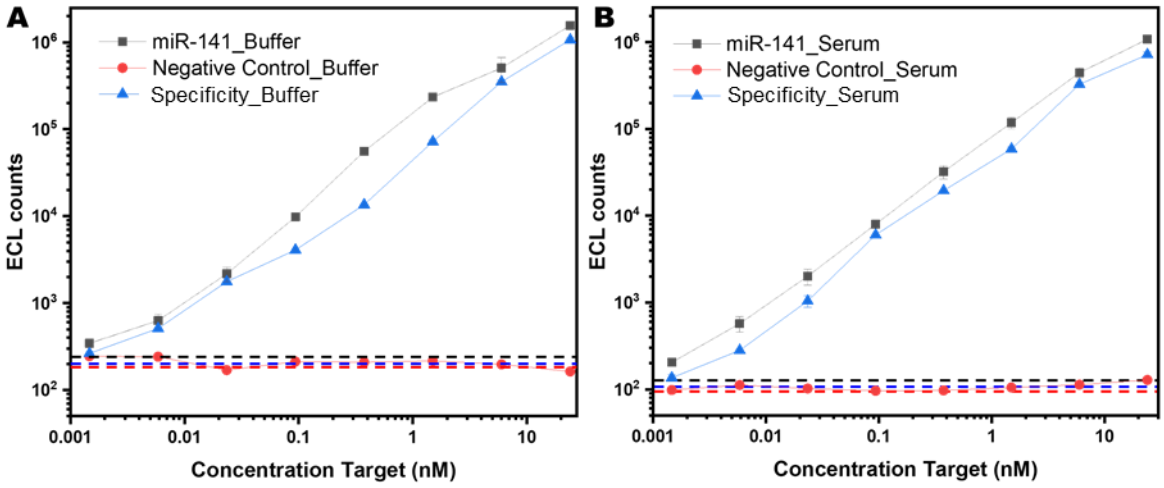


*Figure 5.4 ECL detection of miR-141 with the hybridization performed in (A) hybridization buffer and in (B) 1:20 human serum. Mean data is shown with error bars representing standard deviation. Axes are in log scale. The dashed lines correspond to the zero concentration of target of the respective condition.*

mixture with 24 nM of two other miRNAs were tested. For this purpose, three different target solutions were tested: (i) miR-141, (ii) miR-145 as a negative control, and (iii) miR-141 in the presence of 24 nM of two other miRNAs (miR-145 and miR-375). The concentration of miR-141 ranged from 1.5 pM to 24 nM in both buffer and diluted serum. In the first control (called negative control), the concentration of miR-145, which is not complementary to the capture and detection probes, was varied between 1.5 and 24 nM. The addition of this target did not result in an ECL response for buffer and diluted serum, clearly indicating that the probes are specific for miR-141. The second control test (termed specificity) shows that different concentrations of miR-141 can be detected in a mixture with two other miRNAs (miR-145 and miR-375), with the detection range not being affected. The ECL assay demonstrates good specificity with an ECL response proportional to the concentration of miR-141 and negligible ECL counts for the negative control. These observations are valid for the assays performed in buffer and in diluted serum, where it is shown linearity within the tested range with good differentiation in signal between the tested concentrations. Another interesting remark is that no noticeable matrix effect was seen between the hybridization in buffer and diluted serum with a detection range between 1.5 pM and 24 nM in diluted human serum. The detectability (lowest detected concentration 1.4 nM) decreased by only 1.6 times in serum in agreement with the complexity of the matrix. The limit of detection in buffer was calculated to be 0.12 pM and calculated from the slope (157787 ECL counts/nM, LOD =3*S.$D_{blank}$/slope) of the calibration curve in the range 0. 005 nM –1.5 nM and 8 pM was the lowest tested concentration that significantly differed from the blanks.

Thus, the analytical performance of our ECL assay with advantages from the specificity of a sandwich assay and the sensitivity of ECL detection was successfully demonstrated. The use of a 96-well plate for the detection allows high throughput and could easily be transferred to a POC setting.

### 5.4.3 PEC Assay

Following the successful demonstration of the analytical performance of the ECL strategy, further simplification and the development of a robust detection strategy that can be transferred to POC testing were investigated. To compare ECL with an inverse technique (in ECL the stimulus is electrochemical and the readout light, while in PEC it is the inverse), and to avoid the use of antibodies, a bio-inspired $^1O_2$-based PEC assay to detect miR-141 was developed. The optimal parameters to conduct the PEC assay were determined in chapter 4.

To evaluate the analytical performance of the PEC assay, calibration plots with (i) different target concentrations (i.e. miR-141), (ii) a negative control (i.e. miR-145), and (iii) varying miR-141 concentrations in a mixture with miR-145 and miR-375 (specificity test) were performed. Similarly to ECL, the hybridization was performed in both hybridization buffer and 20-fold diluted serum. As can be observed in Figure 5.5, both when the hybridization was performed in buffer or diluted serum, the assay shows good specificity with a PEC response proportional to the concentration in the presence of miR-141 but only negligible photocurrents when the target is a negative control. The specificity was assessed by performing experiments in solutions containing a variable amount of miR-141 (between 1.5 pM and 24 nM) while keeping the concentration of two other miRNAs (miR-145 and miR-375) at 24 nM. In the case of buffer, no statistically relevant difference is observed between the measurements performed with miR-141 alone or in the presence of the two other miRNAs (Figure 5.5 A).

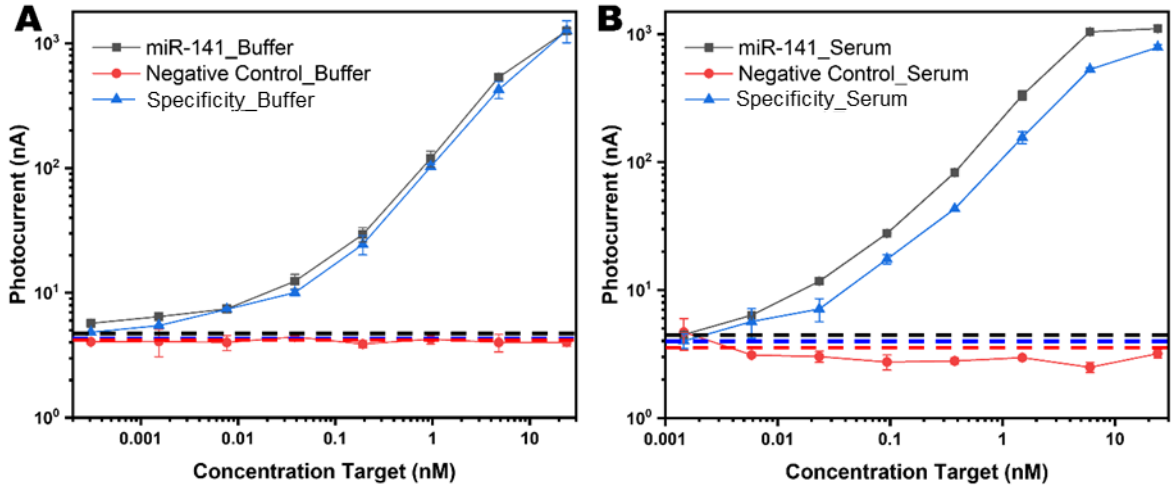


*Figure 5.5 Detection of miR-141 with the hybridization performed in (A) hybridization buffer and in (B) 1:20 human serum, using PEC assay. Mean data is shown with error bars representing standard deviation. Axes are in log scale. The dashed lines correspond to the zero concentration of target of the respective condition.*

The limit of detection was calculated to be 0.62 pM, calculated from the slope (117 nA/nM, LOD =3*S.$D_{blank}$/slope) of the calibration curve in the range 0 nM – 1 nM and 1.5 pM was the lowest tested concentration that significantly differed from the blanks. In 20-fold diluted serum, Figure 5.4.5 B, the assay can still detect and differentiate miR-141 down to 1.5 pM (when compared to the negative control), and only a small decrease in signal is observed (for example, only a 7% decrease in response for 1.5 pM). The limit of detection was calculated to be 3.6 pM, calculated from the slope (218 nA/nM, LOD =3*S.$D_{blank}$/slope) of the calibration curve in the range 0 nM – 1 nM. The small decrease in photocurrent during the selectivity tests in serum is, most likely, due to the interference of the serum matrix with the hybridization of the sandwich assay.[42]

## 5.5 Conclusion

In this work, two oligonucleotide-based assays for the quantification of miRNAs in human serum were successfully developed, i.e. an ECL assay and a PEC assay. The biomarker miR-141 could be detected by both approaches at pM levels in the human matrix. Both the ECL and PEC assays showed the ability to detect the target miR-141 at pM levels in human serum, even though the first is based on a commercially available instrument and the latter is still in a laboratory phase of development. Both assays owe their robustness to easy-to-use design, specificity of the sandwich format and sensitivity to signal amplification provided by the $Ru(bpy)_3^{3+}$-TPA system and HQ-BQ system, respectively. Combining these characteristics allowed the detection of miR-141 in human serum at clinically relevant levels by both approaches. Compared to ECL, the PEC assay presents three main advantages: (i) it is cheaper (there is no need to use antibodies), (ii) it is faster, the ECL assay takes about four hours while the PEC assay requires less than two hours and (iii) it is portable with the possibility to use small LEDs and pocket-size potentiostats.

The accomplishments of this work pave the way for the construction of a multiple analyte platform that could allow faster and simpler detection of many cancer-related miRNAs. It is worth noting that the exploratory PEC assay performed similarly to the developed ECL assay that was performed on a commercially available platform (the assay itself is innovative, but the platform is commercially available). While the ECL assay is advantageous in terms of not requiring a light source and the simultaneous acquisition of results from 96 samples, it does require complicated instrumentation. The PEC assay does need a light source for excitation, but it has less complicated instrumentation and can be further extended for multiplexed detection, which will be the focus of the next chapter. Furthermore, the developed assays have the potential for universal oligonucleotide detection by redesigning the capture and detection probes. They can also be applied to other matrices and, optimally, avoids pretreatment of the sample.

# Chapter 6
# Multiplexed photoelectrochemical detection of miRNAs


*LeDlisa96x illumination plate used for multiplexing in this chapter*

**Adapted from the following technical report:**

*Thiruvottriyur Shanmugam S., Campos R., Laurijssen D., Trashin S., Steckel J., Ribeiro R., De Wael K. Novel 96-well LED arrays for multiplexed photoelectrochemical detection of miRNAs.*

***Contribution:*** *I performed all the experiments (excluding the design and development of LED arrays, which was done by Laurijssen D.) and wrote the first draft of the manuscript.*

## 6.1 Abstract

After the application of the technology to detect miRNAs in patient samples, in this final leg of the thesis, the capability to offer a multiplexed detection of targets in samples has been explored. To the best of our knowledge, there is no well-plate LED setup for PEC detection that exists to function with 96-well electrochemical plate. A technical report describing how the concept was conceived, designed and developed with a set of preliminary results is presented in this chapter. First, a high-throughput detection with 96X multi-channel electrode systems and in-house designed and constructed 96XLED illumination sources have been developed. Such a system allows for performing multiple measurements at the same time, constructing calibration plots and quantifying unknown miRNA concentrations in patient samples at the same time. Screen-printed arrays of 96-well carbon electrode plates were used because of their fast, high-throughput and disposable features to fulfil the need of clinical demands. These 96 well illuminations can be controlled by a LED control subsystem. The application of this strategy was used to test plasma samples from PCa patients for detecting two miRNAs, miR-141 and miR-145. This demonstrated the possible future of the electrochemical ELISA-like immunoassay in clinical practices. Secondly, another type of multiplexing capability, with an aim to simultaneously detect different miRNAs at the same electrode surface was also explored.

## 6.2 Introduction

Multiplexing capability of any diagnostic platform promises a great potential to become a routine tool for quantitative analysis of multiple miRNAs simultaneously, providing important data for biomedical research and clinical early diagnosis. It is particularly essential to enhance the reliability in the diagnosis, staging and follow-up of diseases and personalized treatment. RT-qPCR, the gold standard technique for miRNA quantification and analysis, is the most frequently used approach because of its high-throughput feature. However, the need for different steps such as extraction of miRNA from biological matrices, reverse transcription, and purified primers calls for the development of multiplexed diagnostic tools with easy-to-implement features.

Multiplexed sensor platforms give results in a faster way compared to traditional single biosensors, reducing the sample size that is needed for consecutive single measurements. Currently, electrochemical multiplexing of biomolecules can be achieved in mainly three ways: (i) detection of different targets in different spots or wells,[258] (ii) detection of different targets using different labels such as enzymes, dyes, redox reporters[259] and (iii) regional separation of different detection sites (e.g. microfluidics with different functionalized electrodes).[260, 261] These approaches have drawbacks, mainly complexity due to device fabrication, assay preparation for the detection with different wells, and limitation in levels of multiplexing and probable cross-sensitivity due to diffusion between single detection sites in the microfluidics. However, these drawbacks are addressable, and the benefits outweigh these drawbacks. To the best of our knowledge, there is no work done on multiplexed PEC setup for detecting miRNA or any other biomolecules in the literature. Using the $^1O_2$-based PEC detection strategy for the multiplexed approach will solve certain drawbacks of multiplexed electrochemical setups such as the complexity of assays and stability of enzymes by using PS as a detection label. In this chapter, two PEC multiplex approaches are explored using: (i) screen printed arrays of electrodes for detecting different targets in different wells (section 6.3) and (ii) different labels for simultaneous detection of different miRNAs at the same electrode surface (section 6.4). It is important to note that both approaches offer a type of multiplexed detection that is principally different (high-throughput PEC multiplexing in different electrode wells vs. PEC multiplexing with different labels). A detailed description of both approaches will be presented in the following sections.

## 6.3 High throughput PEC multiplexing in different electrode wells

Screen-printed electrode arrays have been commercially available and are used in the electrochemical detection of nucleic acids, antigens and antibodies. [262-267] In most of these multiplexing systems, a multichannel system was used to implement electrochemical measurements along with a multichannel screen-printed array of eight or multiples of eight electrodes (8X or 16X or 96X electrodes) with either in-house made connectors or the ones from the suppliers. These electrode arrays, especially the 96X ones have become attractive tools for electrochemical analysis due to simultaneous detection, high-throughput, and disposable features[268-270] to fulfil the need of clinical demands like ELISA. Recently, Jirakova et al. developed a multiplexed immunosensor platform for miRNA detection in clinical samples using 8X electrodes array system.[271] They combined the use of magnetic beads coated with antibodies, a process called hybridization chain reaction (HCR) for adding more biotin-streptavidin conjugates along with horseradish peroxidase enzymatic detection strategy. Amplified signal response for sensitively detecting miR-21, let-7a and miR-31 (LOD of 0.66 pM) in patient samples was achieved. However, this system requires antibodies, enzymes, and very controlled steps for HCR.

Disposable 96X electrode well plates offer several advantages over performing individual 96 electrode measurements for nucleic acid/miRNA detection. The first and foremost advantage is the time that is saved in simultaneous analysis. These standardized 96X electrode well plates (microtiter plates with standard ANSI/SLAS footprint)[272] allow parallelization of experiments letting the analysts rapidly explore, optimize a large number of parameters and generate a complete data set. Simultaneous measurements using multi-channel potentiostats with 4, 8 or 12 independent potentiostats have been made possible using commercially available multi-potentiostats, since the channels can perform experiments independently of each other. Secondly, the use of small wells with built-in working, reference and counter electrodes reduces the working volume for electrochemical measurement. Though each well can accommodate ~300 µL of liquid, ~50 µL is enough to cover the electrodes and perform measurements, thus drastically reducing the sample volume from 0.5 – 1 mL to 50 µL. Another main advantage is to build a calibration plot with known concentrations and quantify the unknown concentrations in the patient sample at the same time, thus avoiding errors due to different sets of analysis. Also, multiplexing in different arrays for different targets is possible at the same time by only changing the nucleic acid probes complementary to the target of interest. However, to the best of our knowledge, there is no device that allows PEC detection by incorporating an illumination system controlled along with the electrochemical control.

With a high potential for multiplexed analysis and the opportunity for quantification with only nominal sample preparation steps, 96X electrode systems make it more appropriate than other approaches for our PEC POC testing. In this work, the advantages of (i) 96X electrode plate systems coupled with multi-potentiostats and (ii) $^1O_2$-based PEC strategy will be explored to create a high-throughput system for miRNA quantification. However, a question remains: how to develop an appropriate illumination system for the 96X well electrochemical plate? The solution was sorted out by designing an in-house LED array printed circuit board (PCB, named **LeDlisa96x**) with controls to trigger illumination at intervals during measurements. A detailed description of the design of the LeDlisa96x (section 6.3.2) with details on the design of LED row and column control subsystem and an overview of the digital subsystem is presented first. This is followed by the application of this innovative setup for the analysis of different miRNAs in patient samples is presented (section 6.3.3). It is important to mention that though all our previous PEC studies were successfully performed on sputtered gold working electrodes, this study was limited by the unavailability of such electrodes in 96X format. Therefore, 96X carbon working electrodes on PCB were opted, indeed missing out on the sensitivity usually offered by the sputtered gold surfaces. However, this study is a proof-of-concept to illustrate the possibility of multiplexing with the sensing technology.

### 6.4.1 Experimental methods

All the reagents and nucleic acid sequences mentioned in this chapter were purchased as stated in chapter 4 (section 4.3.1). The sandwich assay using magnetic beads is also according to the protocol mentioned in chapter 4 (section 4.3.3). Another set of eight plasma samples from PCa patients in the age group of 54-74 years was obtained from Centro Hospitalar do Porto, Portugal after the appropriate informed consent and approval from The Health Ethics Committee (CES) from the Centro Hospitalar do Porto (Ref: 2017.154(131-DEFI/123-CES). These patient samples are different from the set obtained for analysis in chapter 4.

The electrochemical array of 96X screen-printed carbon electrodes (96X110, has 96 three-electrode electrochemical cells with carbon working electrode), a specific connector (DRP-CONNECTOR96X), 96X magnetic support (DRP-MAGNET96X), and an automatic controller for the CONNECTOR96X (SYNCONN96X) was purchased from Metrohm DropSens (Oviedo, Spain). SYNCONN96X allows executing the assays sequentially without the need of employing manual rotating selectors. Multichannel potentiostat (MultiPalmSens4) was purchased from PalmSens (Netherlands) which was operated using Multitrace software from the same company. All the components for LeDlisa96X were purchased from the PCB manufacturer Eurocircuits.

### 6.4.2 The design of the LeDlisa96x

The design and development of LED illumination sources (LeDlisa96x) for the 96X electrochemical system were made in a collaboration with FTI-CoSys Lab, University of Antwerp and Flanders Make Strategic Research Centre, Lommel, Belgium. The design of the LeDlisa96x consisted of three subsystems: the LED array, the LED control subsystem and the digital subsystem.

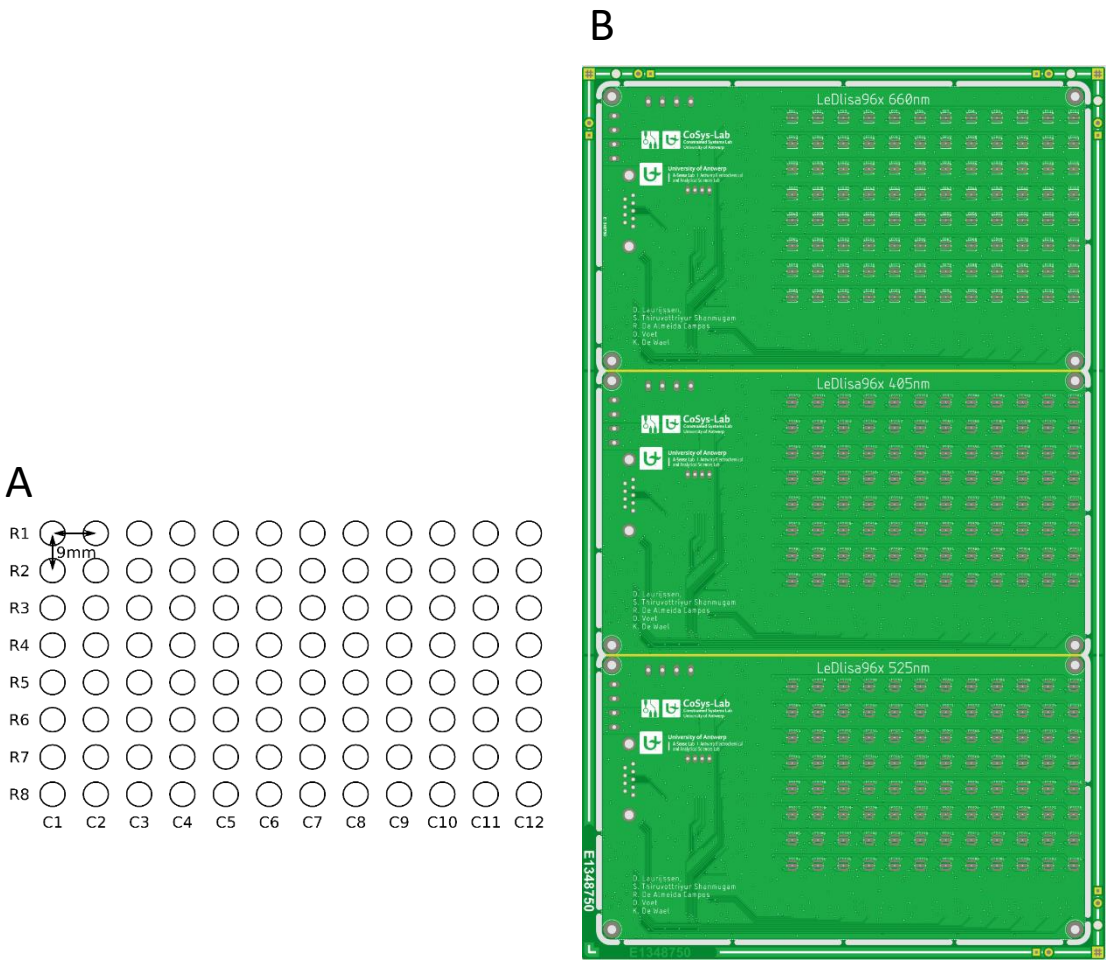


*Figure 6.1 LeDlisa96x well plate layout (A) and panel design of LeDlisa (B) for 660 nm (red), 405 nm (blue) and 525 nm (green) LEDs.*

The LED array is based on the 96x Elisa well plate layout, consisting of 12 columns (C1- C12) and 8 rows (R1- R8) equally spaced with a pitch of 9mm, thus providing compatibility with this industry-standard platform (Figure 6.1 A). For every element of this array, a high-power LED has been provided thus yielding 96 LEDs per PCB. Due to the nature of the envisioned experiments with different PSs, three different wavelengths of LEDs have been used (525 nm, 405 nm and 660 nm). While modularity of such a design would be

beneficial, in this prototyping stage it is not the most cost-effective solution due to manufacturing costs surmounting the raw material costs. Three identical-looking yet different boards could be panelized to reduce manufacturing costs (Figure 6.1 B).

The LED control subsystem (Figure 6.2 A) is based on a matrix of rows and columns that allows control of either each LED individually or on a per row/column basis. The logic (on or off) state of every row of LEDs is controlled by a double MOSFET configuration, where a high current P-MOSFET transistor is used in a high-side switch configuration to connect the +5V to the LED's anode through its series resistor in combination with a general-purpose

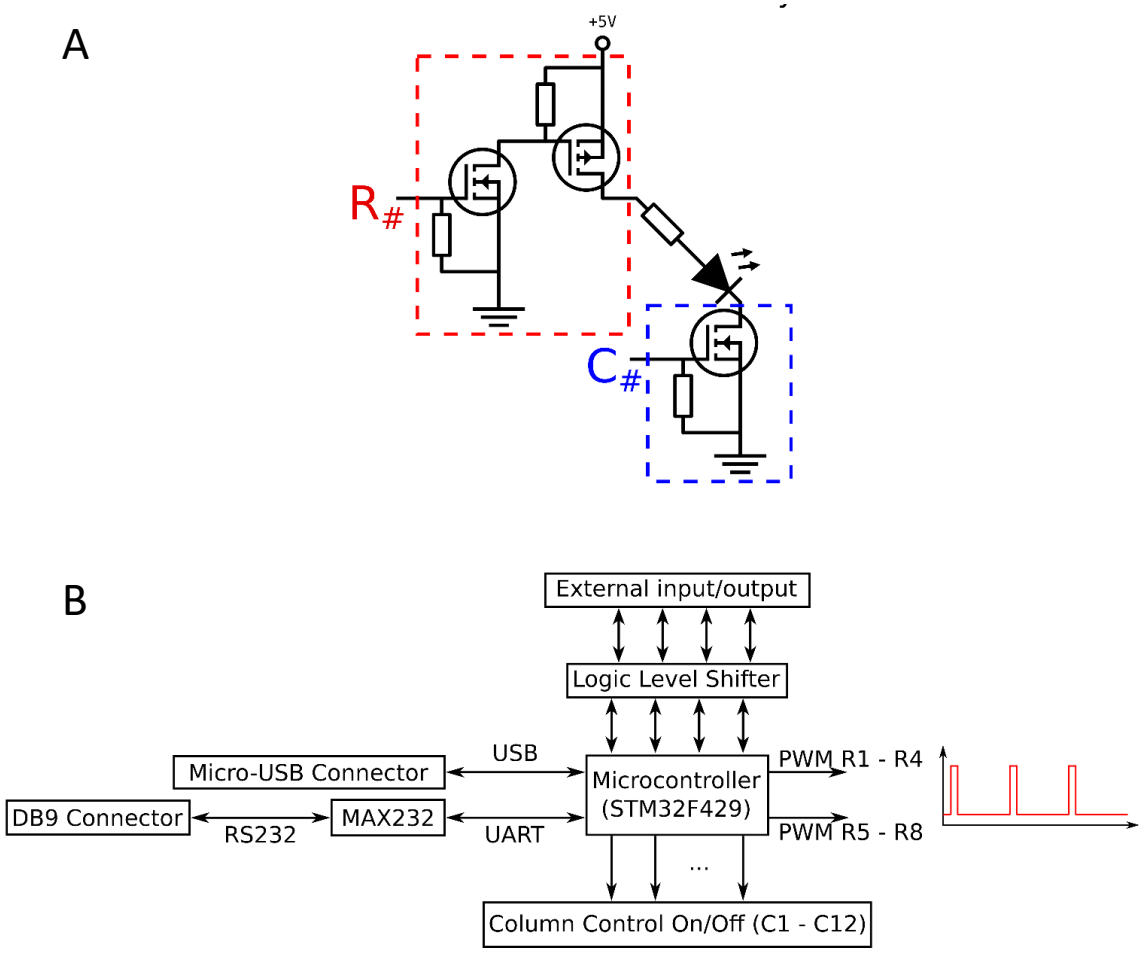


*Figure 6.2 (A) LED row and column control subsystem, (B) Overview of the digital subsystem.*

N-MOSFET transistor for compatibility reasons with the rest of the digital subsystem. The columns of the LED array are controlled by high-current N-MOSFET transistors with a threshold voltage compatible with the digital subsystem's output voltages and therefore do not need an additional transistor.

The maximum driving current, and hence its maximum brightness, for every LED, is determined by their accompanying series resistor. While no current regulation/limitation circuitry is introduced into this design, adjusting the LED brightness and luminescence was made possible by applying pulse width modulation (PWM) on the driving pins of the row control circuitry. This allows for strobing the light at high frequencies and thus dimming the luminescence of the LEDs while lowering the current consumption of the entire system and the heat generation. In this application, the PWM frequency was chosen to be 1 kHz where the duty cycle can be chosen individually for every row of the system.

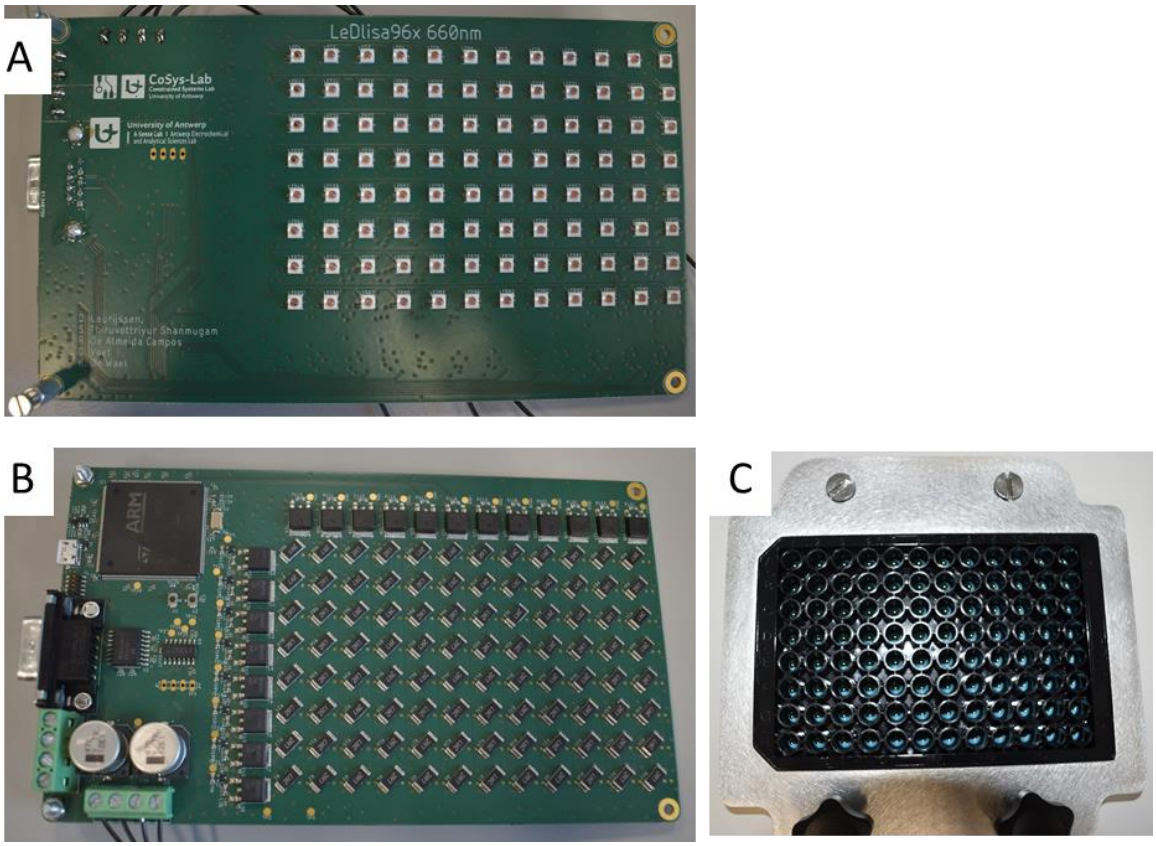


*Figure 6.3 Front (A) and back (B) view of LeDlisa96x with red LEDs to be used with the 96X screen-printed carbon electrodes (96X110, C).*

The digital subsystem is built around a microcontroller (Figure 6.2 B) from STMicroelectronics, in this case, an STM32F429B with a vast array of built-in peripherals with many general-purpose inputs and outputs (GPIO). The function of this digital subsystem is to (i) control the ON/OFF of LED array's rows and columns, (ii) to communicate with the computer via the Universal Serial Bus (USB) and (iii) to communicate with a Metrohm Dropsens multi-well potentiostat and control its measurement behaviour through a serial port (DB9 connector). It includes (i) peripherals to generate PWM signals to control rows and columns, (ii) an interface with logic level translator IC where the system

responds to external signals or vice versa where the system sends out signals to external devices, (iii) USB interface to communicate with the computer (for example, to be progammable to toggle LED column on/off, go to the next column, change the PWM duty cycle, etc..) and (iv) a UART pheripheral with a MAX232 interface driver connected to the DB9 connector and programmed to function simultaneously with the potentiostat. This makes the LeDlisa96x to exactly turn ON at the 60th second of the amperometry for 10 s in all the 8 wells starting from the 1st column (from C1, C2, C3....), after which it turns off for 30 s and then switches to the next column. However, more advanced communication protocols are still a work in progress.

The final product LeDlisa96x with all the subsystems is shown in Figure 6.3 and the entire multiplexing PEC prototype is shown in Figure 6.4.

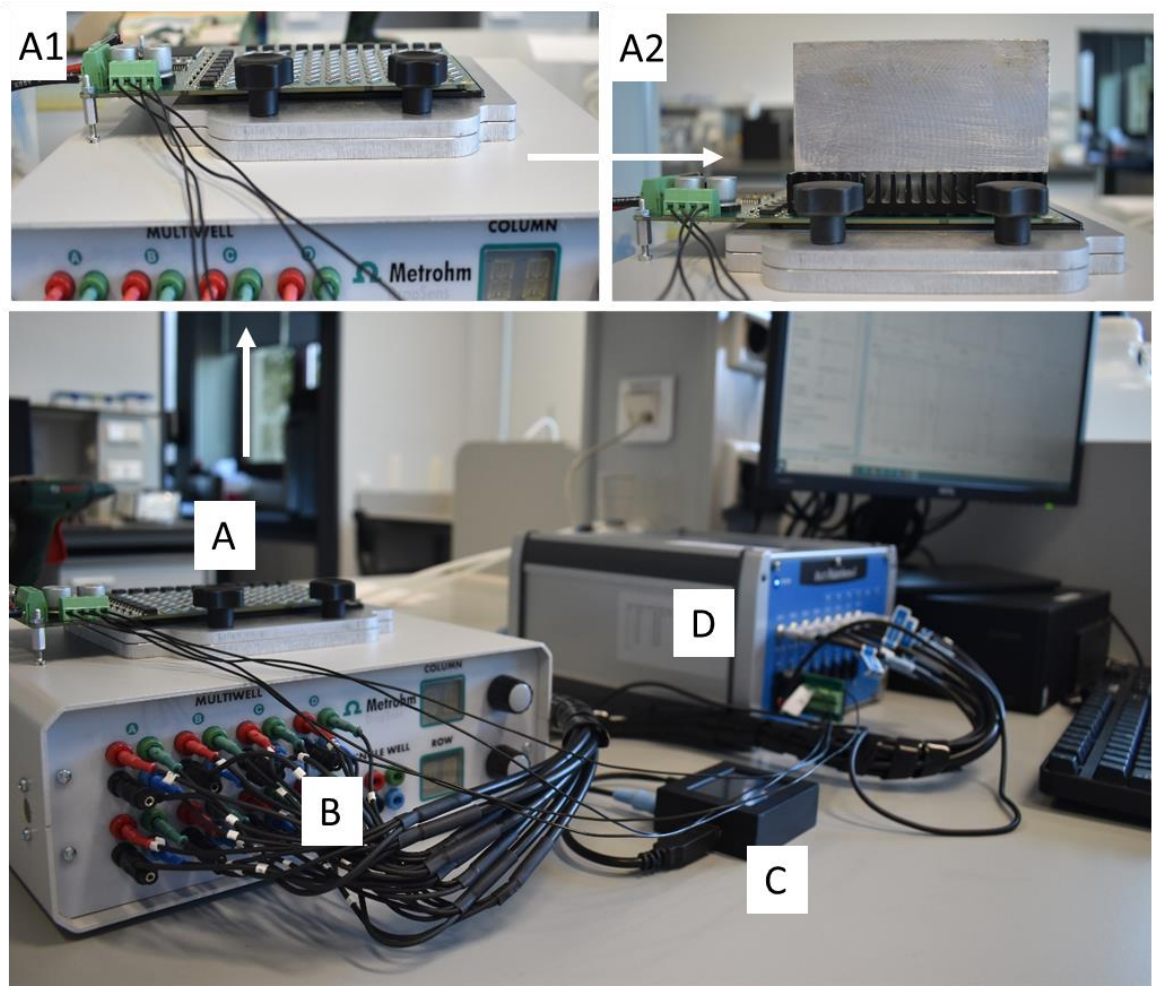


*Figure 6.4 High-throughput photoelectrochemical setup with in-house made LeDlisa96x (A), heat sink (A1) placed on the 96X electrochemical array and held in position with a dead weight (A2). This is connected with the specific connector (B) to the multipotentiostat with 8 channels (D).*

### 6.4.3 Preliminary investigations of the analytical performance of the multiplexed assay

As a first step, the PEC response from the well-known type II PS, ChlE6, in the presence of hydroquinone (HQ) using our setup was evaluated. This was done (i) to evaluate the proper functioning of the LeDlisa96x, (ii) to test the synchronized functioning of the script in the multitrace and LeDlisa96x and (iii) to ensure all the 96 LEDs give the same output. Tween 20 was added to facilitate proper washing of the electrodes in the wells after measurements and for accumulation of magnetic beads easily. Initially, the electrodes in the 96X wells were carefully rinsed with Milli-Q water and were dried with Argon or $N_2$. Though the minimal measuring solution volume that could be added to a well was 30 µL, 100 µL was added, a similar volume compared to our measurements in previous chapters. Then the electrochemical plate was carefully shifted to the connector, screws fastened and LeDlisa96x fixed on top of the plate gently. Heat sink and deadweight are added on top of LeDlisa96x after making sure the 96 LEDs are exactly affixed on top of each well.

The features of the PEC responses of ChlE6 in the presence of HQ were discussed in chapter 3 (section 3.4.3). The measured PEC responses of 5 µM ChlE6 (C1-C6) (48 wells) and blanks (C7-C12) (48 wells) with 1 mM HQ in phosphate buffer pH 7 and 0.05% tween 20 with a 96X well-plate are evaluated here. Figure 6.5 presents the screenshot of the multi-trace software window showing the simultaneous amperometric responses from measuring the first column (C1). In this way, all the 12 columns are measured consecutively in a short period of ~15 minutes for the entire 96 wells compared to ~three hours when done individually like AUTR10 disposable electrodes used in previous chapters. Photocurrents of -2.0 ± 0.4 µA and -0.030 ± 0.005 µA were obtained for 5 µM and 0 µM ChlE6 and both showed considerably lower relative standard deviation of 18 % and 17 % respectively. This shows good reproducibility capacity between different wells, ensuring proper contact between illumination source, electrodes and connectors.

After making sure proper functioning of the setup, the PEC responses of the duplex formed by the target miRNAs (miR-141, miR-145) hybridized with capture and detection probes in a sandwich-like format were evaluated using only 2 columns of the 96x wells (Table 6.1).

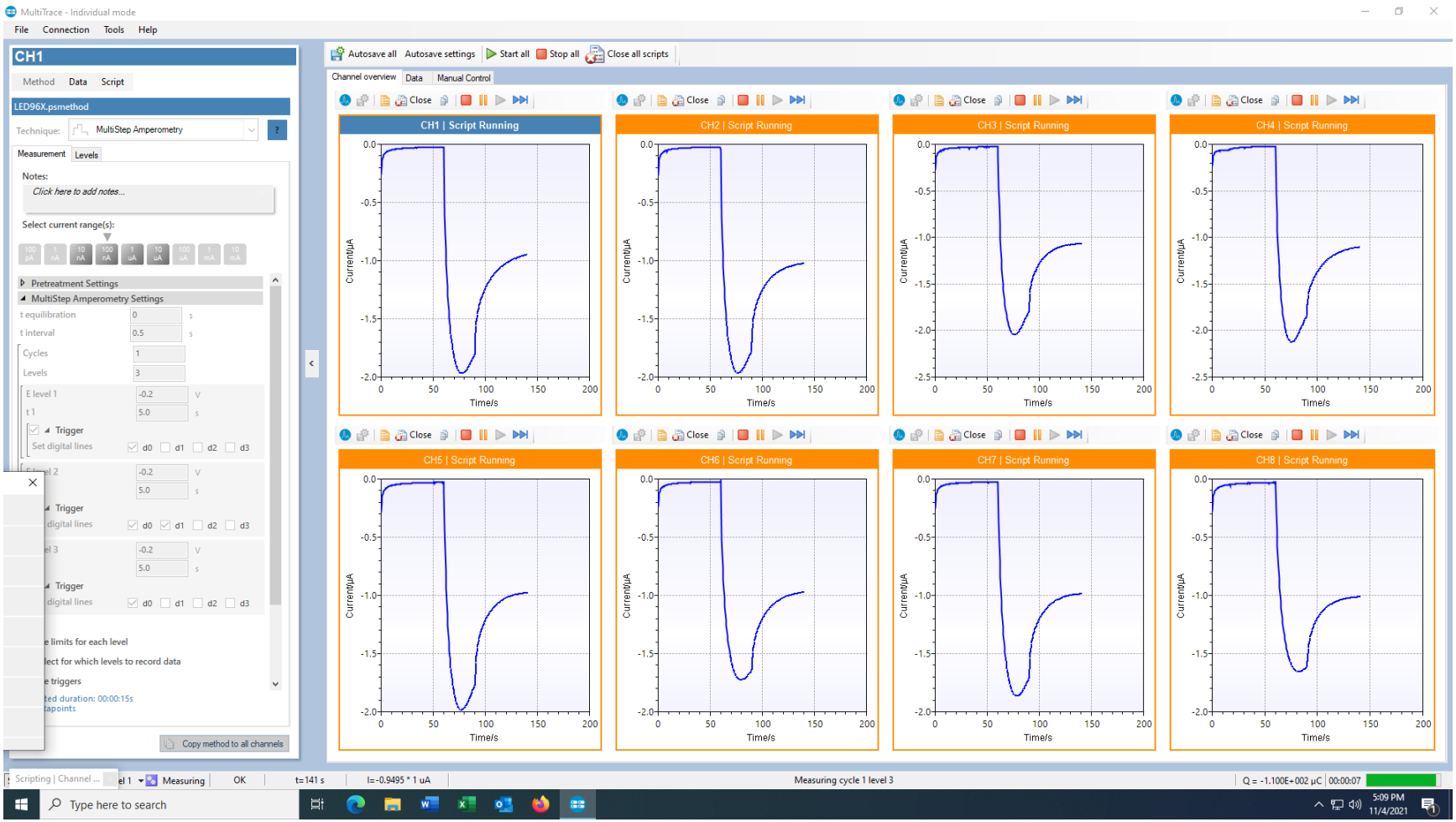


*Figure 6.5 Screen shot showing the instrumental read-out generated from simultaneous measurements of 8 different wells in a column containing 5 µM ChlE6 in presence of 1mM HQ.*

*Table 6.1 Experimental plans for 96X electrochemical plate for evaluation of 0 nM and 24 nM miR-141 and miR-145.*

| PEC detection of miR-145 (C1) and miR-141 (C2)*, nM | | | | | | | | | | | | |
|---|---|---|---|---|---|---|---|---|---|---|---|---|
| | **C1** | **C2** | **C3** | **C4** | **C5** | **C6** | **C7** | **C8** | **C9** | **C10** | **C11** | **C12** |
| **R1** | 0 | 0 | | | | | | | | | | |
| **R2** | 0 | 0 | | | | | | | | | | |
| **R3** | 0 | 0 | | | | | | | | | | |
| **R4** | 0 | 0 | | | | | | | | | | |
| **R5** | 24 | 24 | | | | | | | | | | |
| **R6** | 24 | 24 | | | | | | | | | | |
| **R7** | 24 | 24 | | | | | | | | | | |
| **R8** | 24 | 24 | | | | | | | | | | |

**In this set of experiments, only columns C1 and C2 were used. The rest of the columns were not measured and were used for optimization purposes for trigger and LeDlisa96x controls.*

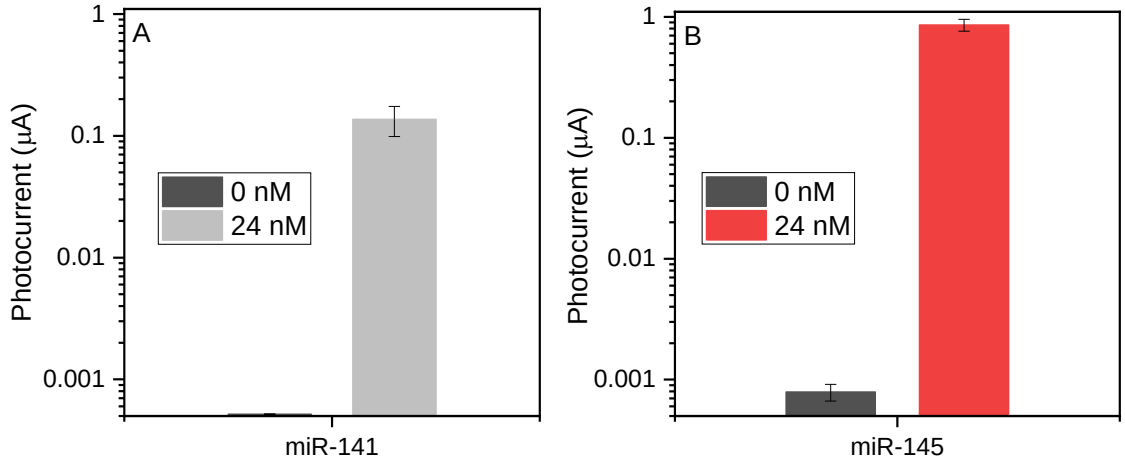


*Figure 6.6 (A) and (B) Comparison of PEC responses from the detection of 0 nM, 24 nM miR-141 and miR-145 in the presence of 1 mM HQ. Error bars represent the standard deviation (n = 4).*

Since this was the preliminary evaluation, the entire hybridization assay was performed in vials and then transferred the beads carefully to the well and 96X magnetic support DRP-MAGNET96X was used under the 96X electrochemical plate to assemble magnetic beads on the working electrodes. Figure 6.6 A and B present the photocurrent responses after hybridization with 24 nM miRNAs, in comparison to the blank control obtained without miRNAs. While the photocurrent responses of 24 nM miR-141 and 145 are 260 times and 1000 times higher than that of the blank control.

To evaluate the setup's suitability for high-throughput analysis, these two micro RNAs were quantified in samples from PCa patients receiving treatment at Centro Hospitalar Universitário do Porto. This was done by performing simultaneously (i) calibration plots of

spiked different concentrations in healthy pooled plasma and (ii) unknown concentrations in eight plasma samples from PCa patients (according to the plan in Table 6.2).

*Table 6.2 Experimental plans for 96X electrochemical plate for high throughput multiplexing of the patient samples.*

| | **miR-141 (pM)** | | | **miR-145 (pM)** | | | **miR-141** | | | **miR-145** | | |
|---|---|---|---|---|---|---|---|---|---|---|---|---|
| | **C1** | **C2** | **C3** | **C4** | **C5** | **C6** | **C7** | **C8** | **C9** | **C10** | **C11** | **C12** |
| **R1** | 0 | 0 | 0 | 0 | 0 | 0 | P9 | P9 | P9 | P9 | P9 | P9 |
| **R2** | 8 | 8 | 8 | 8 | 8 | 8 | P10 | P10 | P10 | P10 | P10 | P10 |
| **R3** | 16 | 16 | 16 | 16 | 16 | 16 | P11 | P11 | P11 | P11 | P11 | P11 |
| **R4** | 31 | 31 | 31 | 31 | 31 | 31 | P12 | P12 | P12 | P12 | P12 | P12 |
| **R5** | 63 | 63 | 63 | 63 | 63 | 63 | P13 | P13 | P13 | P13 | P13 | P13 |
| **R6** | 125 | 125 | 125 | 125 | 125 | 125 | P14 | P14 | P14 | P14 | P14 | P14 |
| **R7** | 250 | 250 | 250 | 250 | 250 | 250 | P15 | P15 | P15 | P15 | P15 | P15 |
| **R8** | 500 | 500 | 500 | 500 | 500 | 500 | P16 | P16 | P16 | P16 | P16 | P16 |

*Columns C1- C3 and C4- C6 were used for standard curves for miR-141 and miR-145 spiked healthy male pooled plasma (H) respectively. Columns C7- C9 and C10- C12 were used for testing unknown concentrations of miR-141 and miR-145 respectively in patient samples.*

Standard curves with optimized parameters (from chapter 4 section 4.4.2) were constructed by spiking different concentrations between 1.5 pM and 500 pM of miRNAs in commercially available pooled plasma from healthy men (H), 10-fold diluted (Figure 6.7 A and B). This low pM range concentrations were considered as per the range identified from findings in chapter 4 section 4.4.4 regarding the miRNAs quantified in patient samples. Concentrations as low as 15 pM were distinguishable when compared to blanks, even while using uneven working electrode surfaces like carbon compared to sputtered gold used in the previous chapters with 3.5 pM as the lowest distinguishable concentration. However, this work is the pilot investigation of the design and the setup of the PEC throughput system and hence the use of a common and “cheapest” 96X carbon electrochemical well plate. Further research is needed to develop a custom-made 96 electrochemical well with sputtered working electrodes on PCB boards, which is the plan for the future. Also, all the experiments were done in triplets here. However, if the assay is further optimized in terms of the number of beads to be used and on performing the entire assay in the wells (i.e. hybridization, washing steps, and measuring steps all in the 96X well plates), the

experiments can be performed in duplicates, thus accommodating more samples/miRNAs in a single set.

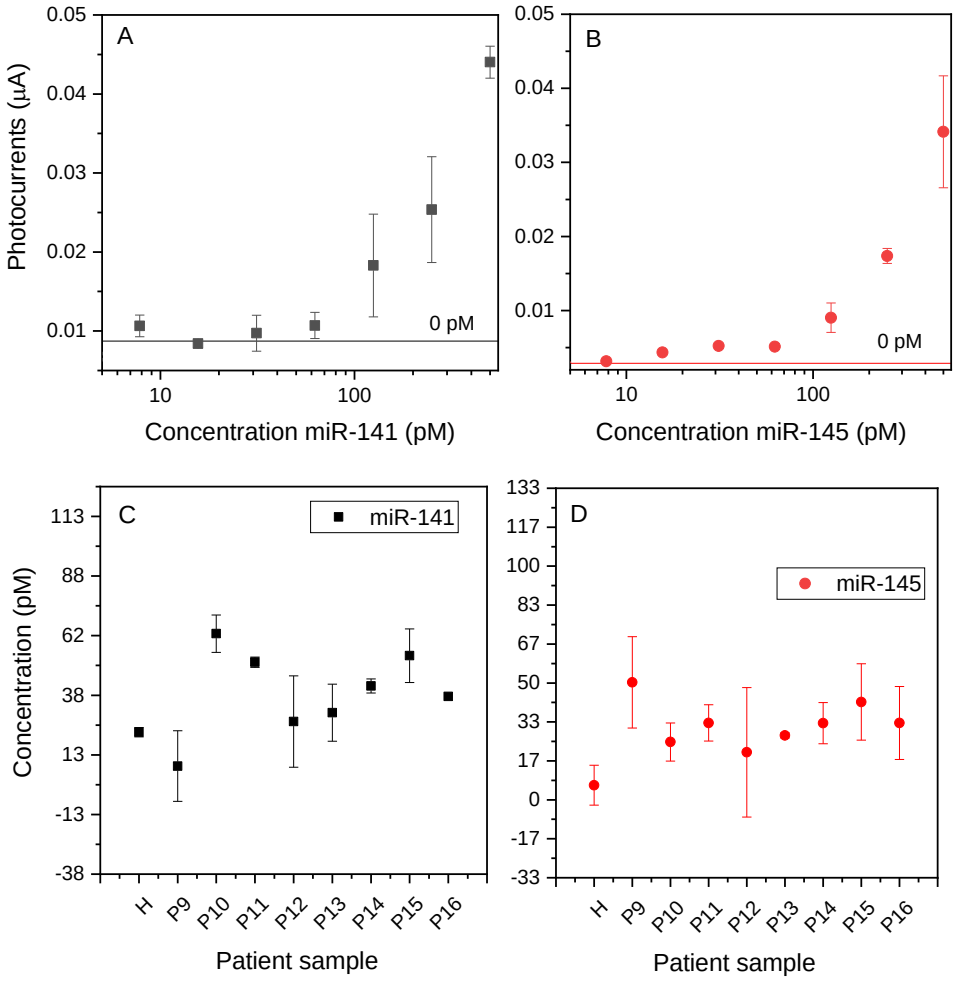


*Figure 6.7 (A) and (B) Standard curves constructed from 10-fold diluted healthy male pooled plasma, spiked with different concentrations of miR-141 and miR-145. The horizontal reference lines indicate the average blank values in each case without any miRNA. (C) and (D) calculated concentrations of miRNAs from 10-fold diluted PCa patient samples (P9- P16) and healthy male pooled plasma (indicated by 'H'). Error bars represent the standard deviation (n = 3).*

Trendlines were linearly fitted to the standard curves with equations y = 8.05E-05x + 5.00E-03 and y = 6.34E-05x + 2.00E-03 for miR-141 and 145 respectively (Figure 6.7 A & B) with $R^2$ > 99% for both trendlines. This was used to calculate the unknown concentrations for the patient's plasma samples. Analysis was done for plasma samples derived from 8 patients (P9-P16) with PCa presenting with clinicopathological characteristics depicted in Table 6.3. These plasma samples from PCa subjects have been centrifuged twice, to separate plasma from cells and are different from the sample set (P1-P8) used in chapter 4. As depicted in Figure 6.7 C & D, all the PCa patient samples exhibited different levels of

miRNA expression higher than the pooled healthy male plasma except for patient P1 who seem to present lower miR-141 concentration compared to the healthy plasma (H) while presenting higher miR-145 levels. However, the average miRNA concentrations in PCa patient plasma samples yielded an increase in miR concentrations compared to the healthy male pooled plasma. This is similar to the increased levels of miR-141 and miR-145 in P1-P8 samples compared to the control H sample in section 4.4.4, chapter 4. Though completely different sets of patient plasma samples and healthy pooled plasma samples were used in chapter 4 and this chapter, the ability to detect the trend in the increase of miRNA expression in PCa patient samples compared to healthy men agrees with the literature. [204, 206, 224-228] Thus, without the need for additional PCR or other amplification techniques, miRNA levels were measured successfully, and quantitatively in patient samples in a short span of 15 minutes compared to lengthy conventional measurements. This indeed is the starting point for several optimization steps aimed at robust estimation and quantification of miRNAs and these preliminary investigations open a whole new gateway for high-throughput miRNA detection that can be regularly used in lab-scale investigations or clinical scale day-to-day diagnostics.

*Table 6.3 Clinicopathological features of PCa patient samples.*

| | **Clinical data** | | | | **Calculated levels of miRNA** | |
|---|---|---|---|---|---|---|
| | **Age** | **Gleason score** | **PSA (ng/mL)** | **Stage_pT (tumour)** | **miR-145 (pM)** | **miR-141 (pM)** |
| P9 | 54 | 4+4 | 10.6 | 2 | 78 ± 16 | 503 ± 117 |
| P10 | 57 | 3+4 | 5.3 | 2 | 633 ± 39 | 247 ± 35 |
| P11 | 60 | 4+5 | 19.4 | 3b | 514 ± 10 | 329 ± 38 |
| P12 | 64 | 3+4 | 6.94 | 2 | 265 ± 57 | 203 ± 105 |
| P13 | 70 | 4+3 | 8.62 | 2 | 302 ± 39 | 276 ± 5 |
| P14 | 71 | 4+5 | 13.76 | 3a | 414 ± 12 | 328 ± 44 |
| P15 | 71 | 3+4 | 7.5 | 3a | 541 ± 52 | 419 ± 91 |
| P16 | 54 | 4+3 | 9.04 | 3a | 370 ± 44 | 329 ± 78 |

## 6.4 PEC multiplexing with different labels

This section of the multiplexing chapter explores the possibility of multiplexed detection of different targets using different labels. This simultaneous detection closely associated with the final readout of different electrochemical signals is made possible by the appropriate choice of labels exhibiting well-resolved signals unique to the label. Organic molecules/dyes are the most common redox species, that can be used as electroactive labels for the

simultaneous detection of different analytes. [273-275] With the benefits of easy accessibility and unique electrochemical signal peaks, metal ions like silver ions, lead(II) ions copper(II)ions, and other metal nanoparticles are also considered as good multiplexing labels. [276, 277] Here, the focus will be on using the type II PS that was discussed in previous chapters for multiplexing.

The suitability of four type II PS, namely MetB, ChlE6, EosY, and EryB for the simultaneous detection of multiple sequences (multiplexing) was tested using disposable gold-sputtered electrodes. While the fundamental optical and PEC properties of these PS were previously studied in chapter 3 using diode lasers and gold disk electrodes, the actual application calls for easily available commercial LEDs. However, here with an aim for multiplexing, their optical behaviour at the LEDs' wavelengths (660 nm, 520 nm and 405 nm) and PEC responses using magnetic beads, disposable sputtered gold electrodes and under LED illumination will be explored. As a proof of concept, two complementary oligonucleotides; one with the type II PS as the label (detection probe) and the other with biotin (capture probe) bound to magnetic beads was tested. This double-stranded duplex model was used in the following experiments for evaluating the PS multiplexing capabilities, this means being able to detect multiple photocurrent responses by using different light sources that have a specific wavelength emittance. If there was a photocurrent response for one or more LEDs, this could be linked directly to the presence of PS and, thus, the sequence of interest. The results from this fundamental study using duplex models will be transferred to the preferred sandwich model using magnetic beads for the multiplexed detection of target RNA sequences in the future.

### 6.4.1 Experimental methods

The methods used here are elaborated previously in chapter 3. Hence a brief description will be presented here for ease of understanding.

#### 6.4.1.1 Reagents

MetB (Merck KGaA, Germany), EryB (purity ≥ 95%, Merck Schuchardt OHG), EosY (purity ~99%, Sigma Aldrich), and ChlE6 (purity ≥ 98%, Cayman chemical company). The measuring buffer contains 100 mM KCl and 10 mM $KH_2PO_4$ at pH 7. To measure the absorbance of the PS, 100 µM stock solutions were made. MetB and ChlE6 dissolve respectively in water and DMSO, the stock solutions of EryB and EosY are prepared in absolute ethanol (purity ~ 99%, Fisher Scientific, Belgium).
To determine the photocurrent responses of the PSs, measuring buffers with HQ (Acros Organics International, Belgium) as the redox reporter was prepared. Streptavidin-coated

magnetic beads (M280-Dynabeads, Invitrogen) were used for multiplexing. A 2X TE buffer solution (pH 7.5), containing 10 mM Tris, 1 mM EDTA (Titriplex III), and 2 M NaCl was prepared. The pH of the buffer was adjusted using HCl. This 2X TE-buffer was mixed with (i) 0.05% Tween 20 to yield a 2XTE-$T_{20}$ buffer, (ii) ultra-pure water (UPW) and Tween 20 0.05% to yield a 1xTE-$T_{20}$ buffer, herein hybridization buffer.

Capture and detection probes necessary for the formation of a duplex structure (will be called 2 oligo duplex or simply duplex in this chapter) on the magnetic beads are given in Table 6.4. Capture and detection probes modified with EryB, EosY, and ChlE6, were obtained from Eurogentec. The probe with a linked MetB label was supplied by Metabion.

*Table 6.4 Capture and detection probe sequences used in this work for forming 2-oligo duplex for PEC multiplexing.*

| | **Name** | **5' modification** | **Sequence (5' --> 3')** | **3' modification** |
|---|---|---|---|---|
| 2-oligo duplex | Capture probe (C21) | Biotin-TEG | TAG CTT ATC AGA CTG ATG TTG A | |
| | Detection probe (D21) | | TCA ACA TCA GTC TGA TAA | ChlE6 or MetB or EosY or EryB |

#### 6.4.1.2 Absorbance measurements - UV-Vis Spectroscopy

All the PS have their absorbance spectra and AvaSpec-2048 L from Avantes equipped with an AvaLight-DH-S-BAL light source was used to record the UV–Vis spectra, to measure this specific absorbance for each of the four type II PS. Every stock solution was diluted with a measuring buffer to form a 2 µM, 5 µM and 10 µM dilution in the measuring buffer. The measuring buffer served as a blank. An Implen NanoPhotometer N60 (Implen GmbH, Germany) was used to measure the UV–Vis spectra of labelled DNA. The absorbances were converted to extinction coefficients to obtain an average value from three measurements.

#### 6.4.1.3 Hybridization assay

Streptavidin-coated magnetic particles (10 µL, 10 mg/mL) were dispersed in an Eppendorf containing 1 mL hybridization buffer. The solution was vortexed and the magnetic beads accumulated at the side of the Eppendorf were directed to the magnetic rack (∼1 min). The solution was removed and suspended in 500 µL of 2XTE-$T_{20}$ buffer, then 500 µL of 100 nM capture probe in UPW+0.05%Tween 20, were added to the beads leading to a final incubation solution containing 1 mL of capture probe at 50 nM in hybridization buffer. This solution was incubated for 15 min at room temperature using continuous rotation (10 rpm, rotary shaker). Following the incubation, the beads were accumulated again using a magnetic rack, the solution was discarded and the functionalized beads were resuspended

in hybridization buffer containing labelled detection probes (24 nM), and incubated for 1 hour at room temperature in a rotary shaker at 10 rpm. Following the incubation, the beads were washed 3 times with 1 mL hybridization buffer and stored in 10 µL of the same buffer until the PEC detection was performed.

#### 6.4.1.4 PEC detection

PEC measurements were performed using a potentiostat Autolab 302N running Nova 2.1 software. Light-emitting diode (LED) operated at 660 nm, 520 nm and 405 nm (Thorlabs, Inc.) were used and the diameter of the light beam was adjusted using a collimator to only illuminate the working electrode. The light power was adjusted to 30 mW using a light power meter (Thorlabs, Inc.). The measurements were performed with 60 s OFF, 10 s ON & 30 s OFF light-chopped conditions, with ON/OFF switch preprogrammed with PSTrace or Nova 2.1 and controlled by a relay trigger. Photocurrents in this setup were measured using AUTR10 at -0.2 V *vs.* quasi Ag reference electrode. The detailed procedure has been explained previously in chapter 4 section 4.3.4.

### 6.4.2 Results and discussions

For a PS to be suitable for $^1O_2$-based PEC multiplexing, three conditions need to be fulfilled. Firstly, they need to have a high absorbance at one wavelength (wavelength of the LED used) and almost none at another. This ensures that, when two PSs are combined in a multiplexing assay, the PSs generate a photocurrent at their respective wavelengths. Secondly, in response to illumination, the PS need to have an excited triplet state that exists for at least 1 µs and a $^1O_2$ quantum yield that is high enough ($\Phi_\Delta > 0.5$). Thirdly, the concentration of HQ needs to be high enough for the redox reaction between $^1O_2$ and HQ to occur. This is typically double the concentration of the PS present in the environment, but the optimal concentration of HQ was estimated to be 1mM, for magnetic beads-based assays. While the second and third points have been addressed in chapter 3, it is important to check their optical properties and PEC response with and without coupling to beads at different LED's wavelengths.

### 6.4.2.1 Absorbance spectra of PSs

To have an idea of which PS would have the highest photocurrent response under which LED, their corresponding absorbance spectra were analyzed. Figure 6.8 A presents the dark spectra of the LEDs used in this study, peaks of which are 408.7 nm (blue LED), 518.5 nm (green LED) and 657.8 nm (red LED). The spectra show broad peaks which slightly shifted maxima when compared with the spectra of the RGB diode lasers used before with 405, 520 and 660 nm maxima with narrow peaks. Thus, it is indeed important to evaluate the optical and PEC responses of the chromophores specific to these wavelengths. Figure 6.8 B and C represent the extinction coefficients (ε) of the chromophores in the free form or linked to detection probes at these wavelengths of the LEDs. The slight changes in the ε of the free chromophores compared to that linked to DNA detection probe have been already explained before in chapter 3 section 3.4.2 as a possibility due to changes in the microenvironment or shifts in pKa of dyes linked to DNA.

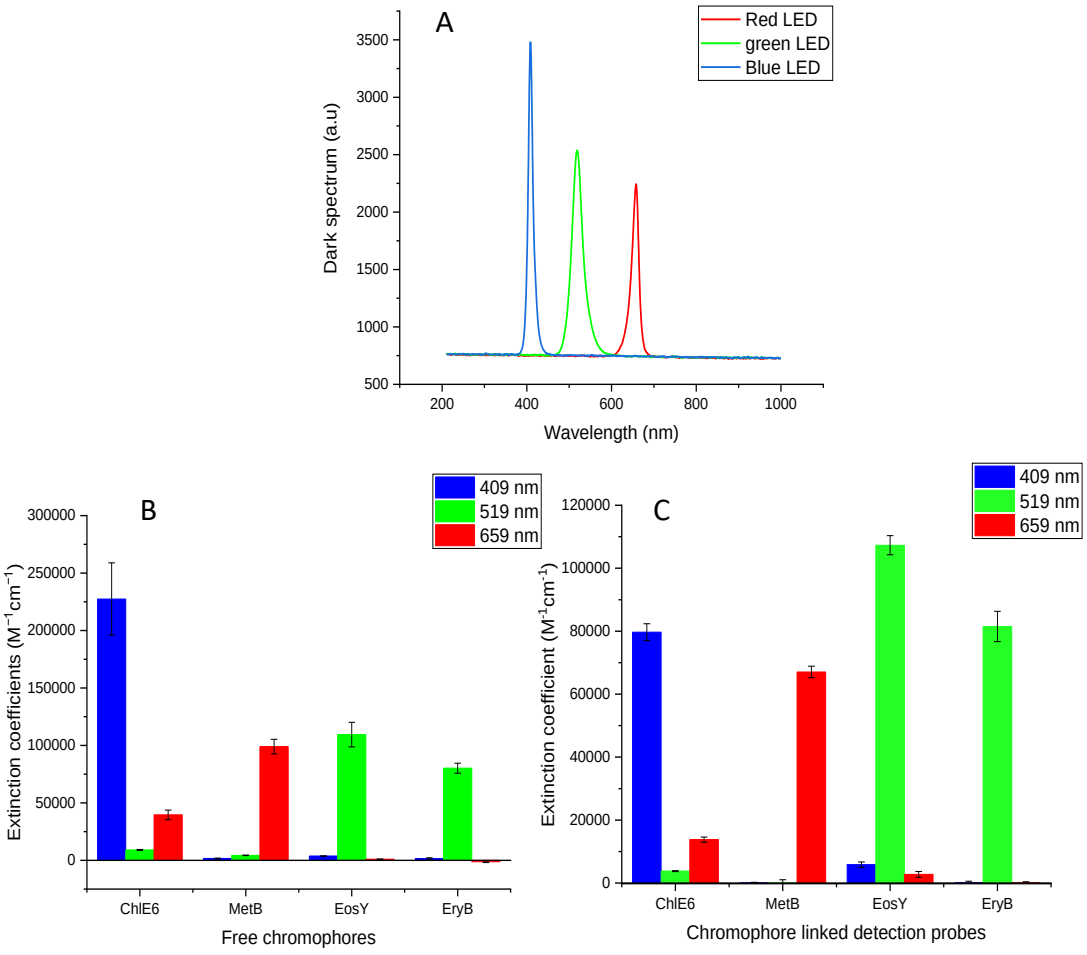


*Figure 6.8 (A) UV-Vis spectra of three LEDs: 405 nm (blue), 520 nm (green) and 660 nm (red) irradiating the phosphate buffer used in this study. (B) & (C) Extinction coefficients of free chromophores and chromophores labelled detection probes. Error bars represent the standard deviation (n = 3).*

MetB is suitable for PEC measurements using the red LED, since it has a high extinction coefficient at this wavelength. It is 100 times more than the extinction coefficients for the other two LEDs for MetB. This is expected since the absorbance maximum of MetB lies at 655 nm. EryB and EosY are both suitable candidates for PEC measurements using the green LED, since their absorbance maxima are close to 519 nm, i.e. 517 nm for EosY and 524 nm for EryB. Both Eos Y and EryB also have extinction coefficients for the green LED, which is 100 times higher than the extinction coefficients for the red and blue LEDs. Moreover, the absorbance maxima of MetB correspond to the absorbance minima of EosY and EryB, and vice versa. This is the first indication that it might be possible to use both PS in one solution to detect two sequences at once. ChlE6, on the other hand, is not a suitable candidate for multiplexing, because it has a non-negligible extinction coefficient for every LED used.

#### 6.4.2.2 PEC properties of the free chromophores and chromophores linked to DNA

To illustrate the possibility to perform a multiplex assay, PEC properties of the free chromophores and chromophores linked to DNA were studied. Results (Figure 6.9 A and B) demonstrate that there is an increase in photocurrent response every time a chromophore is illuminated at an LED wavelength where it shows a high absorbance (e.g. MetB under a red LED).

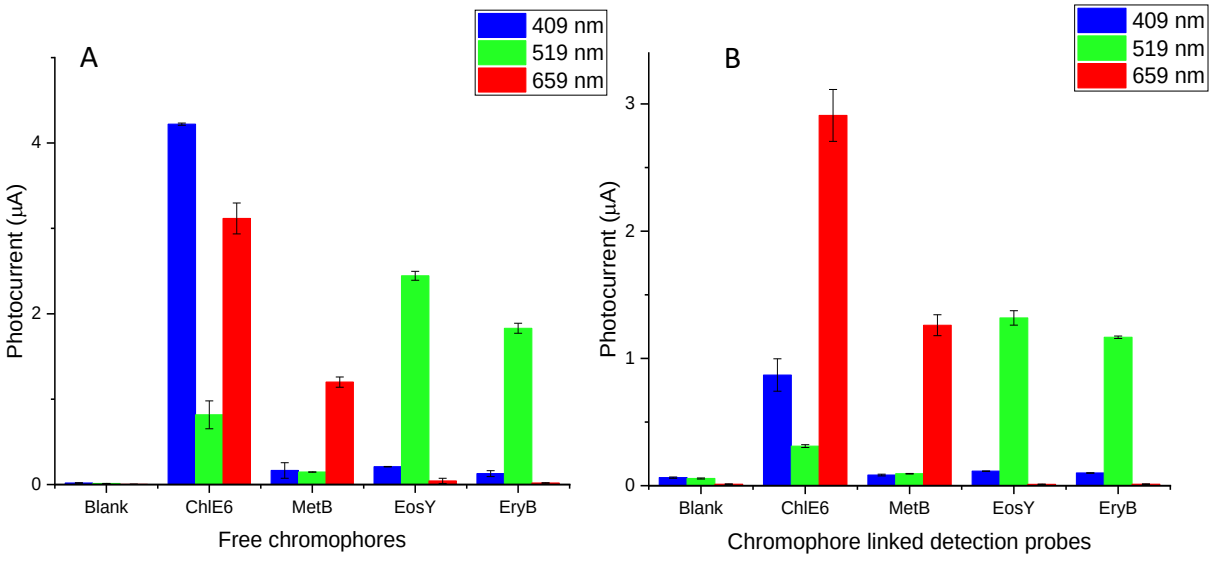


*Figure 6.9 Photocurrents from 5 µM free chromophores (A) and 5 µM chromophore labelled detection probes (B) under blue, red and green light illumination. Error bars represent the standard deviation (n = 3).*

The blank measurement, where no PS was added to the buffer, generates a low (current < 100 nA) photocurrent response for every LED, as expected. ChlE6 has a high response for the red LED and the highest response for the blue LED out of all chromophores and a non-

negligible response for the green LED. While, when linked to the detection probe, ChlE6 presented a maximum response for red LED, followed by noticeable responses in blue and green LEDs. As explained earlier, this behaviour is explained by a shift in positions of the absorbance maxima in linked chromophores compared to the free chromophores and changes in the microenvironment or shifts in pKa of dyes linked to DNA. Both free MetB and detection probe linked MetB presented a noticeable photocurrent response for the red LED only with negligible responses for green and blue LED similar to the blanks. EosY and EryB, both free and linked to detection probes have high (with EosY having the highest) photocurrent responses when the green LED is used with negligible responses in red and blue LEDs. However, for a multiplexing assay, the photocurrent response of a given PS ideally should give a high response for a certain wavelength and a negligible/no response in another. This makes EryB and EosY unsuitable to be used together in a multiplexing assay with green light since they both generate a high response at the same wavelength. Therefore, it would not be possible to detect two different sequences using these PS. ChlE6 is also unsuitable, because it generates a photocurrent for all LED wavelengths, even at 520 nm, where it does not have a high absorbance possibly due to high $^1O_2$ quantum yield (0.77) and noticeable absorbance at 519 nm ($\varepsilon$ = 9066 $M^{-1}$ $cm^{-1}$). For this reason, it can't be combined with any of this PS. Current research is ongoing to explore much more PS to extend the multiplexing functionalities.

## 6.5 Conclusion

**This chapter demonstrated the opportunity of PEC multiplexing for miRNAs using two principally different concepts: (**i) a high-throughput system for detection of different targets in different electrode wells and (ii) detection of different targets at the same electrode.

Integrating the sensitive and selective $^1O_2$-based PEC detection of DNA and the versatility of the 96X microtitre electrode well plates, a high-throughput platform for detecting miRNA was introduced. An illumination system "LeDelisa96x", replacing bulky LED lights that were used in the previous chapters, was developed. LeDelisa96x was controlled by simple scripts using the software of the potentiostat. Various advantages were achieved such as (i) the reduced analysis time from three hours to just 15 min for 96 independent measurements; (ii) accurate quantification of targets by obtaining a calibration curve in the same run, *i.e.* using the same measuring plate. The developed setup detected low picomolar levels of miRNAs spiked in diluted plasma of healthy men and could detect elevated levels of miR-145 and miR-141 in samples of PCa patients. The 96X electrochemical well-plate provides a multiplexing opportunity by just changing the

oligonucleotide sequences for detection and capture probe complementary to the target in different wells. These attractive features along with the sensitivity provided by the $^1O_2$-based PEC detection paves way for its future as a practical alternative to RT-qPCR and as a point-of-care device for cancer diagnostics.

The developed second strategy successfully demonstrated the multiplexing capability of the system using different labels. Due to the low absorbance of MetB in the green LED and the negligible absorbance of EosY in the red LED, it is possible to use both PS for simultaneous detection of two targets when the detection probes are labelled by different labels. Following the useful insights on multiplexing from this fundamental study, multiplexed detection of two miRNA's relevant to PCa can be achieved using a sandwich assay. EosY labelled detection probe partially complementary to miR-145 and MetB labelled detection probe partially complementary to miR-141 can be used to detect miR-145 and miR-141 from liquid biopsies simultaneously. Apart from the possibility of incorporating the 96X well plates along with an RGB illumination source per well providing dual multiplexing, user-friendly portable detection devices can be designed for commercial purposes to provide data at a low cost.

# Chapter 7
# Conclusions and outlook

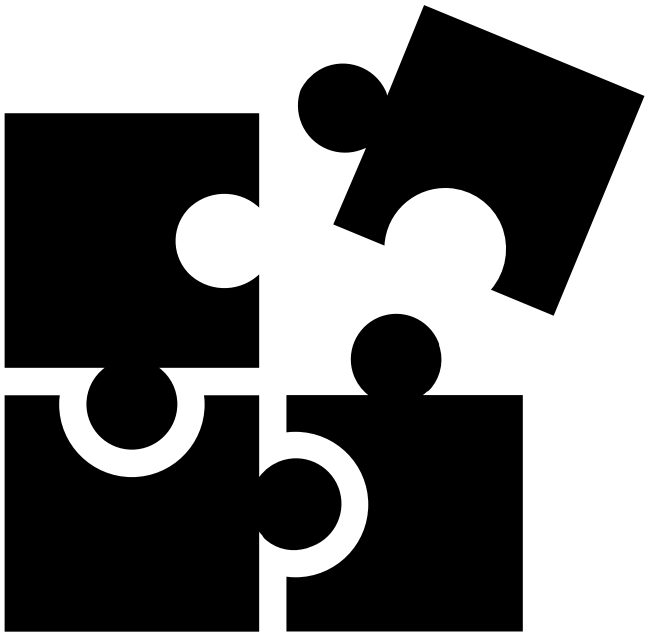

## 7.1 Conclusions

This Ph.D. research introduces a robust and easy-to-use sensing platform for short nucleic acid biomarkers like miRNAs. With a core objective of improving the early diagnosis of cancer, an innovative $^1O_2$-based PEC sensing strategy for the detection and quantification of cancer-related miRNAs in serum and plasma was used. A key feature of the developed PEC sensors is the use of molecular photosensitizing labels analogous to fluorescent labels but acting as photocatalysts, which are analogous to enzymes. Thus, the new system overcomes drawbacks of enzymatic sensors such as poor stability of enzymes and uses an electrochemical read-out that is superior to a fluorescence read-out.

Gold-sputtered microelectrodes were suggested as a platform for constructing electrochemical DNA sensors and tested using enzymatic signal amplification. For this, appropriate methods for cleaning and modifying the sputtered gold surface were developed. The LOD of sensors in optimized conditions were around 0.14 nM, which is unsatisfactory for miRNA detection in PCR-free conditions using 10× or more diluted serum and plasma samples. Nevertheless, the system is straightforward to use and based on commercially available low-cost disposable electrodes.

To boost the sensitivity, new fundamental concepts using type II PSs as molecular labels like fluorescent dyes were explored in detail. The PEC detectability of the tested dyes correlated well with the ability to produce $^1O_2$ and absorbance spectrum of the PSs. Although the direct photocurrent of labels was low in absolute values, it was well distinguished from the background due to the efficient separation of baseline currents (measured in dark before illumination) and photocurrents (measured during illumination). Moreover, additional enhancement of the photocurrent was achieved by using hydroquinone as a redox reporter for short-lived $^1O_2$ and DNA-probe modified magnetic beads as fast and efficient capture reagent. With a LOD of 10 pM, the system was ready to be further tested in spiked plasma and real samples.

Next, the applicability of this technology to detect two selected miRNAs in clinical samples of PCa-diagnosed patients was evaluated. A PCR-free quantitative method for the detection of miR-145 and miR-141 was developed and tested in 1:10 diluted patient plasma samples. After optimization of measurement and assay parameters, detection limits of 3.5 pM and 9.8 pM for miR-145 and miR-141 were successfully obtained in diluted human plasma without any further sample processing or pretreatment. In all patients, a significantly elevated level of miRNA-145 and miRNA-141 was found in agreement with the literature.

It is crucial to compare the performance of the developed technology with a state-of-the-art technique. For that purpose, the electrochemiluminescence (ECL) technique was compared with our PEC technique, owing to its similarity in being a labelled technique but also entirely inverse in principle to each other. With a combination of the triad of magnetic beads, type II PS as the label and a redox reporter, the PEC strategy performed equally well in comparison to ECL with complex antigen-antibodies labelling, co-reagents, and long incubation time (less than 4 hours for ECL and less than 2 hours for PEC, excluding sample pretreatment time) aiming for a sensitivity boost. This motivated taking the PEC strategy into a multiple analyte platform that could allow faster and simpler detection of many cancer-related miRNAs.

Lastly, two important multiplexing approaches to detect different target miRNAs are presented. The developed high-throughput approach with "LeDelisa96x" and 96X microtiter electrode-well plates detected different targets in different electrode wells. This provides multiplexing prospects by changing the oligonucleotide sequences for detection and capture probes complementary to the target in different wells. Secondly, the detection of different targets at the same electrode surface was presented with room for more creativity. At this stage, multiplexing using different $^1O_2$-producing PSs still must be optimized. In principle, more than two PSs can be used for multiplexing assays if they generate a substantial photocurrent only at their excitation wavelengths. Therefore, in the future, different detection probes can be designed to hybridize with various kinds of target DNA, each of them bounded to different PSs.

The developed PEC assays for miRNAs have the possibility for other nucleic acid sequence detection, simply by redesigning the capture and detection probes. The prospect of detecting miRNAs or other nucleic acids, associated with other disorders like cardiovascular diseases, fetal monitoring, and disease screening widens the applicability of these oligonucleotide-based PEC assays, which will support medical staff in decision-making, with the potential for personalized medicine. However, the length of the target sequences that can be detected by our technique has not been evaluated, yet, and the threshold *must* be further estimated. Furthermore, the versatility of using magnetic beads allows the detection/quantification not only in human serum or plasma but for other bio-matrices like urine, stool, and mucus samples without any elaborate pretreatment of the samples sans dilution. In addition to the strengths of the developed technology, it also offers (i) short time to result (1 hour, considering the shortest hybridization time) compared to a RT-qPCR, ddPCR (1 day), IdyIIa™ (4 hours), (ii) cost effective (cost of the device < €15,000) compared to the current established techniques (€35,000- €100,000) and (iii) measurement without the need for enzymatic reagents. However, there are challenges to be addressed, such as,

their suitability for POC systems. Further optimization and validation is needed to decrease the time to result from one hour to 10-15 minutes including hybridization and measurement steps. Since magnetic bead technology involves complementary hybridization, there is no need for additional centrifugation steps (which might result in loss of nucleic acids), other than the one used for seperating plasma from blood. This centrifugation step can also be avoided by using magnetic beads to both extract and undergo hybridization steps, thus offering an alternative approach for scaled-up automation for large numbers of samples.

## 7.2 Future perspectives

***Fundamental research direction***

The labelling of detection probes with type II PSs was always limited by their commercial availability, with little room for customization since most of the commercially available labels are fluorescent dyes used for optical detection. Much more efficient type II PSs are available in the literature and can be synthetically customized as $^1O_2$ labels for DNA detection probes in future. Hence a collaboration with an organic chemistry group to synthesize oligonucleotide detection probes labelled with type II PS will lead to a new opportunity. Especially, synthesizing PS with higher $^1O_2$ quantum yields and/or $\lambda_{max}$ only at a specific wavelength will aid in the field of multiplexed PEC detection and improve the already high sensitivity. Also, by using magnetic beads, signal amplification will be brought about by concentrating the analyte close to the electrode surface and will offer an interface for the HQ/BQ redox cycling. However, studying the effect of distance (e.g. 5 nm, 50 nm, 500 nm, 5 µm and 50 µm) of the label from the electrode surface in the presence of the redox reporter will give a clear picture of the mechanism. While this is out of scope for the current work with nucleic acids, since there will be problems with assembling the labelled DNA with a length > 50 nm due to steric hindrance, labelled polymeric modifications with labels at different distances from the electrode can be patterned and offer a solution to elude the mechanism.

***Application-oriented research direction***

Two application-oriented research directions are (i) improving sensitivity by introducing different signal amplification concepts and (ii) building a robust multiplexing system. Firstly, in the current work, a single detection probe with a single label for the PEC detection was used. However, the detection limit is still in the picomolar range. Improvement in the sensitivity once the position of the label from 3’ to 5’ end of the detection probe was

observed. To further lower the detection to the sub-femtomolar range, multiple type II PSs using (a) a detection probe with one label at the 3’ end, one at the 5’ end and one in the middle (b) hybridization chain reaction (HCR) was introduced, where the target triggers a surge of successive hybridizations building hundreds of repetitive units of the single sandwich used in the current work. Secondly, multiplexed detection of two or more miRNAs in the same vial will be performed and further incorporated in the 96x well with dual-LED per well offering more options for multiplexing.

The technology is currently used for the detection of circulating tumour DNA (ctDNA) with mutations representative of the cancerous tumour using optimal hybridization temperature. Though mutations are difficult to detect in a hybridization-based detection technique, it is made possible by using high-resolution melting (HRM) analysis. HRM is an apt PCR-based technique to validate the hybridization between the target with capture and detection probe, improving specificity. By using HRM analysis, the melting temperature of the double-stranded DNA duplex formed between capture, detection probes and the target sequence could be estimated. This, along with its hybridization temperature (simulated using online tools), allows effective hybridization only with mutated ctDNA and not the wild-type ctDNA, thus detecting specifically the mutated target.

Significant growth has been achieved since electrochemistry was considered for the detection of miRNA. However, there are some challenges left to address, before utilizing this sensitive technology for liquid biopsy application in clinically relevant setting. This technology is only a prototype and has been evaluated under laboratory conditions. The application of the sensing technology was limited to a minimum number of patient samples that was not sufficient for proper validation. Parameters such as data from large data set (>100), stability, shelf life, optimal functionality in diverse sample matrices (barely treated or diluted) are challenges to be addressed before we can develop this into a marketable POC testing product.

This thesis has presented an elegant and efficient platform and signal amplification technology to make a straightforward sensor. With all those innovative plans in the line, the aim would be to bring the technology to the market by making it a user-friendly and robust analytical or point-of-care screening device. Following the popular amperometric sensor for diabetes management, there has been a huge gap for inexpensive, simple but efficient commercial electrochemical sensors. With the recent global pandemic, the urge for developing rapid tests with more accuracy has been realized. Maybe in future, one can expect biomedical diagnostics not at the clinics but with easy-to-use devices at homes/in offices, creating a need for integrated bioelectronic devices. For this purpose, the future of

our PEC sensor will rely on manufacturing techniques for integrated systems, for example; LED integrated and miniaturized screen printed/vapour deposited chips producing inexpensive and miniaturized next-generation biosensors.

# Bibiliography


1. Sundarbose, K.; Kartha, R. V.; Subramanian, S., MicroRNAs as Biomarkers in Cancer. *Diagnostics* **2013,** *3* (1), 84-104.
2. Mithraprabhu, S.; Chen, M.; Savvidou, I.; Reale, A.; Spencer, A., Liquid biopsy: an evolving paradigm for the biological characterisation of plasma cell disorders. *Leukemia* **2021,** *35* (10), 2771-2783.
3. Zampetaki, A.; Mayr, M., Analytical challenges and technical limitations in assessing circulating miRNAs. *Thromb Haemost* **2012,** *108* (4), 592-8.
4. El Aamri, M.; Yammouri, G.; Mohammadi, H.; Amine, A.; Korri-Youssoufi, H., Electrochemical Biosensors for Detection of MicroRNA as a Cancer Biomarker: Pros and Cons. *Biosensors* **2020,** *10* (11), 186.
5. Group, F.-N. B. W., In *BEST (Biomarkers, EndpointS, and other Tools) Resource*, Silver Spring (MD): Food and Drug Administration (US): 2016.
6. Laterza, O. F.; Hendrickson, R. C.; Wagner, J. A., Molecular Biomarkers. *Drug information journal : DIJ / Drug Information Association* **2007,** *41* (5), 573-585.
7. Berk, M., The Classification of Biomarkers. *JAMA Psychiatry* **2015,** *72* (10), 1056-1057.
8. Robertson, E. G.; Baxter, G., Tumour seeding following percutaneous needle biopsy: The real story! *Clinical Radiology* **2011,** *66* (11), 1007-1014.
9. Heitzer, E.; Haque, I. S.; Roberts, C. E. S.; Speicher, M. R., Current and future perspectives of liquid biopsies in genomics-driven oncology. *Nat Rev Genet* **2019,** *20* (2), 71-88.
10. Ji, C.; Guo, X., The clinical potential of circulating microRNAs in obesity. *Nature Reviews Endocrinology* **2019,** *15* (12), 731-743.
11. Schwarzenbach, H.; Hoon, D. S. B.; Pantel, K., Cell-free nucleic acids as biomarkers in cancer patients. *Nature Reviews Cancer* **2011,** *11* (6), 426-437.
12. Biró, O.; Hajas, O.; Nagy-Baló, E.; Soltész, B.; Csanádi, Z.; Nagy, B., Relationship between cardiovascular diseases and circulating cell-free nucleic acids in human plasma. *Biomarkers in Medicine* **2018,** *12* (8), 891-905.
13. Chen, A.; Li, J.; Wang, L.; Huang, Q.; Zhu, J.; Wen, S.; Lyu, J.; Wu, W., Comparison of paired cerebrospinal fluid and serum cell-free mitochondrial and nuclear DNA with copy number and fragment length. *Journal of Clinical Laboratory Analysis* **2020,** *34* (6), e23238.
14. Pinzani, P.; Salvianti, F.; Zaccara, S.; Massi, D.; De Giorgi, V.; Pazzagli, M.; Orlando, C., Circulating cell-free DNA in plasma of melanoma patients: Qualitative and quantitative considerations. *Clinica Chimica Acta* **2011,** *412* (23), 2141-2145.
15. Mouliere, F.; Robert, B.; Arnau Peyrotte, E.; Del Rio, M.; Ychou, M.; Molina, F.; Gongora, C.; Thierry, A. R., High Fragmentation Characterizes Tumour-Derived Circulating DNA. *PLOS ONE* **2011,** *6* (9), e23418.

16. Li, F.; Wei, F.; Huang, W. L.; Lin, C. C.; Li, L.; Shen, M. M.; Yan, Q.; Liao, W.; Chia, D.; Tu, M.; Tang, J. H.; Feng, Z.; Kim, Y.; Su, W. C.; Wong, D. T. W., Ultra-Short Circulating Tumor DNA (usctDNA) in Plasma and Saliva of Non-Small Cell Lung Cancer (NSCLC) Patients. *Cancers (Basel)* **2020,** *12* (8).

17. Shi, J.; Zhang, R.; Li, J.; Zhang, R., Size profile of cell-free DNA: A beacon guiding the practice and innovation of clinical testing. *Theranostics* **2020,** *10* (11), 4737-4748.

18. Wei, Z.; Batagov, A. O.; Schinelli, S.; Wang, J.; Wang, Y.; El Fatimy, R.; Rabinovsky, R.; Balaj, L.; Chen, C. C.; Hochberg, F.; Carter, B.; Breakefield, X. O.; Krichevsky, A. M., Coding and noncoding landscape of extracellular RNA released by human glioma stem cells. *Nature Communications* **2017,** *8* (1), 1145.

19. Krol, J.; Loedige, I.; Filipowicz, W., The widespread regulation of microRNA biogenesis, function and decay. *Nature Reviews Genetics* **2010,** *11* (9), 597-610.

20. Kurihara, Y.; Watanabe, Y., Arabidopsis micro-RNA biogenesis through Dicer-like 1 protein functions. *Proceedings of the National Academy of Sciences of the United States of America* **2004,** *101* (34), 12753-12758.

21. Elbashir, S. M.; Harborth, J.; Lendeckel, W.; Yalcin, A.; Weber, K.; Tuschl, T., Duplexes of 21-nucleotide RNAs mediate RNA interference in cultured mammalian cells. *Nature* **2001,** *411* (6836), 494-498.

22. Zhu, L.; Ge, J.; Li, T.; Shen, Y.; Guo, J., tRNA-derived fragments and tRNA halves: The new players in cancers. *Cancer Letters* **2019,** *452*, 31-37.

23. Guglas, K.; Kołodziejczak, I.; Kolenda, T.; Kopczyńska, M.; Teresiak, A.; Sobocińska, J.; Bliźniak, R.; Lamperska, K., YRNAs and YRNA-Derived Fragments as New Players in Cancer Research and Their Potential Role in Diagnostics. *International Journal of Molecular Sciences* **2020,** *21* (16), 5682.

24. Iwasaki, Y. W.; Siomi, M. C.; Siomi, H., PIWI-Interacting RNA: Its Biogenesis and Functions. *Annual Review of Biochemistry* **2015,** *84* (1), 405-433.

25. Bratkovič, T.; Rogelj, B., Biology and applications of small nucleolar RNAs. *Cellular and Molecular Life Sciences* **2011,** *68* (23), 3843-3851.

26. Derrien, T.; Johnson, R.; Bussotti, G.; Tanzer, A.; Djebali, S.; Tilgner, H.; Guernec, G.; Martin, D.; Merkel, A.; Knowles, D. G.; Lagarde, J.; Veeravalli, L.; Ruan, X.; Ruan, Y.; Lassmann, T.; Carninci, P.; Brown, J. B.; Lipovich, L.; Gonzalez, J. M.; Thomas, M.; Davis, C. A.; Shiekhattar, R.; Gingeras, T. R.; Hubbard, T. J.; Notredame, C.; Harrow, J.; Guigó, R., The GENCODE v7 catalog of human long noncoding RNAs: analysis of their gene structure, evolution, and expression. *Genome Res* **2012,** *22* (9), 1775-89.

27. Szabo, L.; Salzman, J., Detecting circular RNAs: bioinformatic and experimental challenges. *Nature Reviews Genetics* **2016,** *17* (11), 679-692.

28. Han Li, C.; Chen, Y., Small and Long Non-Coding RNAs: Novel Targets in Perspective Cancer Therapy. *Curr Genomics* **2015,** *16* (5), 319-26.

29. Institute, N. C. FDA Approves Blood Tests That Can Help Guide Cancer Treatment. https://www.cancer.gov/news-events/cancer-currents-blog/2020/fda-guardant-360-foundation-one-cancer-liquid-biopsy.

30. Administration, U. S. F. a. D. Nucleic Acid Based Tests. https://www.fda.gov/medical-devices/in-vitro-diagnostics/nucleic-acid-based-tests#human.

31. Sung, H.; Ferlay, J.; Siegel, R. L.; Laversanne, M.; Soerjomataram, I.; Jemal, A.; Bray, F., Global Cancer Statistics 2020: GLOBOCAN Estimates of Incidence and Mortality Worldwide for 36 Cancers in 185 Countries. *CA Cancer J Clin* **2021,** *71* (3), 209-249.

32. Belgium fact sheet. https://gco.iarc.fr/today/data/factsheets/populations/56-belgium-fact-sheets.pdf.

33. Healthybelgium https://www.healthybelgium.be/en/medical-practice-variations/men.

34. Atan, A.; Güzel, Ö., How should prostate specific antigen be interpreted? *Turk J Urol* **2013,** *39* (3), 188-93.

35. Van Poppel, H.; Hogenhout, R.; Albers, P.; van den Bergh, R. C. N.; Barentsz, J. O.; Roobol, M. J., Early Detection of Prostate Cancer in 2020 and Beyond: Facts and Recommendations for the European Union and the European Commission. *European Urology* **2021,** *79* (3), 327-329.

36. Leslie, M. K. D. S. W. Prostate Specific Antigen. https://www.ncbi.nlm.nih.gov/books/NBK557495/.

37. Albertsen, P. C., Prostate cancer screening with prostate-specific antigen: Where are we going? *Cancer* **2018,** *124* (3), 453-455.

38. Tokudome, S.; Ando, R.; Koda, Y., Discoveries and application of prostate-specific antigen, and some proposals to optimize prostate cancer screening. *Cancer Manag Res* **2016,** *8*, 45-47.

39. Bussemakers, M. J.; van Bokhoven, A.; Verhaegh, G. W.; Smit, F. P.; Karthaus, H. F.; Schalken, J. A.; Debruyne, F. M.; Ru, N.; Isaacs, W. B., DD3: a new prostate-specific gene, highly overexpressed in prostate cancer. *Cancer Res* **1999,** *59* (23), 5975-5979.

40. CRI https://www.cri.be/nl/pca3.

41. Haese, A.; de la Taille, A.; van Poppel, H.; Marberger, M.; Stenzl, A.; Mulders, P. F. A.; Huland, H.; Abbou, C.-C.; Remzi, M.; Tinzl, M.; Feyerabend, S.; Stillebroer, A. B.; van Gils, M. P. M. Q.; Schalken, J. A., Clinical Utility of the PCA3 Urine Assay in European Men Scheduled for Repeat Biopsy. *European Urology* **2008,** *54* (5), 1081-1088.

42. van Gils, M. P. M. Q.; Hessels, D.; van Hooij, O.; Jannink, S. A.; Peelen, W. P.; Hanssen, S. L. J.; Witjes, J. A.; Cornel, E. B.; Karthaus, H. F. M.; Smits, G. A. H. J.; Dijkman, G. A.; Mulders, P. F. A.; Schalken, J. A., The Time-Resolved Fluorescence-Based PCA3 Test on Urinary Sediments after Digital Rectal Examination; a Dutch Multicenter Validation of the Diagnostic Performance. *Clinical Cancer Research* **2007,** *13* (3), 939-943.

43. O'Brien, J.; Hayder, H.; Zayed, Y.; Peng, C., Overview of MicroRNA Biogenesis, Mechanisms of Actions, and Circulation. *Front Endocrinol (Lausanne)* **2018,** *9*, 402.

44. Mitchell, P. S.; Parkin, R. K.; Kroh, E. M.; Fritz, B. R.; Wyman, S. K.; Pogosova-Agadjanyan, E. L.; Peterson, A.; Noteboom, J.; O'Briant, K. C.; Allen, A.; Lin, D. W.; Urban, N.; Drescher, C. W.; Knudsen, B. S.; Stirewalt, D. L.; Gentleman, R.; Vessella,

R. L.; Nelson, P. S.; Martin, D. B.; Tewari, M., Circulating microRNAs as stable blood-based markers for cancer detection. *Proceedings of the National Academy of Sciences* **2008,** *105* (30), 10513-10518.

45. Xiong, D. D.; Lv, J.; Wei, K. L.; Feng, Z. B.; Chen, J. T.; Liu, K. C.; Chen, G.; Luo, D. Z., A nine-miRNA signature as a potential diagnostic marker for breast carcinoma: An integrated study of 1,110 cases. *Oncol Rep* **2017,** *37* (6), 3297-3304.

46. Condrat, C. E.; Thompson, D. C.; Barbu, M. G.; Bugnar, O. L.; Boboc, A.; Cretoiu, D.; Suciu, N.; Cretoiu, S. M.; Voinea, S. C., miRNAs as Biomarkers in Disease: Latest Findings Regarding Their Role in Diagnosis and Prognosis. *Cells* **2020,** *9* (2), 276.

47. Kozomara, A.; Birgaoanu, M.; Griffiths-Jones, S., miRBase: from microRNA sequences to function. *Nucleic Acids Research* **2018,** *47* (D1), D155-D162.

48. Mestdagh, P.; Hartmann, N.; Baeriswyl, L.; Andreasen, D.; Bernard, N.; Chen, C.; Cheo, D.; D'Andrade, P.; DeMayo, M.; Dennis, L.; Derveaux, S.; Feng, Y.; Fulmer-Smentek, S.; Gerstmayer, B.; Gouffon, J.; Grimley, C.; Lader, E.; Lee, K. Y.; Luo, S.; Mouritzen, P.; Narayanan, A.; Patel, S.; Peiffer, S.; Rüberg, S.; Schroth, G.; Schuster, D.; Shaffer, J. M.; Shelton, E. J.; Silveria, S.; Ulmanella, U.; Veeramachaneni, V.; Staedtler, F.; Peters, T.; Guettouche, T.; Wong, L.; Vandesompele, J., Evaluation of quantitative miRNA expression platforms in the microRNA quality control (miRQC) study. *Nature Methods* **2014,** *11* (8), 809-815.

49. Dave, V. P.; Ngo, T. A.; Pernestig, A.-K.; Tilevik, D.; Kant, K.; Nguyen, T.; Wolff, A.; Bang, D. D., MicroRNA amplification and detection technologies: opportunities and challenges for point of care diagnostics. *Laboratory Investigation* **2019,** *99* (4), 452-469.

50. Chen, C.; Tan, R.; Wong, L.; Fekete, R.; Halsey, J., Quantitation of MicroRNAs by Real-Time RT-qPCR. In *PCR Protocols*, Park, D. J., Ed. Humana Press: Totowa, NJ, 2011; pp 113-134.

51. Androvic, P.; Valihrach, L.; Elling, J.; Sjoback, R.; Kubista, M., Two-tailed RT-qPCR: a novel method for highly accurate miRNA quantification. *Nucleic Acids Research* **2017,** *45* (15), 144-144.

52. Kramer, M. F., Stem-loop RT-qPCR for miRNAs. *Curr Protoc Mol Biol* **2011,** *Chapter 15*, Unit 15.10.

53. Chen, C.; Ridzon, D. A.; Broomer, A. J.; Zhou, Z.; Lee, D. H.; Nguyen, J. T.; Barbisin, M.; Xu, N. L.; Mahuvakar, V. R.; Andersen, M. R.; Lao, K. Q.; Livak, K. J.; Guegler, K. J., Real-time quantification of microRNAs by stem–loop RT–PCR. *Nucleic Acids Research* **2005,** *33* (20), e179-e179.

54. Mestdagh, P.; Feys, T.; Bernard, N.; Guenther, S.; Chen, C.; Speleman, F.; Vandesompele, J., High-throughput stem-loop RT-qPCR miRNA expression profiling using minute amounts of input RNA. *Nucleic Acids Research* **2008,** *36* (21), e143-e143.

55. Veedu, R. N.; Vester, B.; Wengel, J., Enzymatic Incorporation of LNA Nucleotides into DNA Strands. *ChemBioChem* **2007,** *8* (5), 490-492.

56. Cirillo, P. D. R.; Margiotti, K.; Mesoraca, A.; Giorlandino, C., Quantification of circulating microRNAs by droplet digital PCR for cancer detection. *BMC Res Notes* **2020,** *13* (1), 351.

57. Dong, L.; Meng, Y.; Sui, Z.; Wang, J.; Wu, L.; Fu, B., Comparison of four digital PCR platforms for accurate quantification of DNA copy number of a certified plasmid DNA reference material. *Scientific Reports* **2015,** *5* (1), 13174.

58. Motameny, S.; Wolters, S.; Nürnberg, P.; Schumacher, B., Next Generation Sequencing of miRNAs - Strategies, Resources and Methods. *Genes (Basel)* **2010,** *1* (1), 70-84.

59. Dang, T.; Lavagi-Craddock, I.; Bodaghi, S.; Vidalakis, G., Next-Generation Sequencing Identification and Characterization of MicroRNAs in Dwarfed Citrus Trees Infected With Citrus Dwarfing Viroid in High-Density Plantings. *Front Microbiol* **2021,** *12*, 646273-646273.

60. Li, W.; Ruan, K., MicroRNA detection by microarray. *Anal Bioanal Chem* **2009,** *394* (4), 1117-24.

61. Dong, H.; Lei, J.; Ding, L.; Wen, Y.; Ju, H.; Zhang, X., MicroRNA: Function, Detection, and Bioanalysis. *Chemical Reviews* **2013,** *113* (8), 6207-6233.

62. Zou, L.; Li, R.; Zhang, M.; Luo, Y.; Zhou, N.; Wang, J.; Ling, L., A colorimetric sensing platform based upon recognizing hybridization chain reaction products with oligonucleotide modified gold nanoparticles through triplex formation. *Nanoscale* **2017,** *9* (5), 1986-1992.

63. He, C.; Chen, S.; Zhao, J.; Tian, J.; Zhao, S., Ultrasensitive detection of microRNA-21 based on electrophoresis assisted cascade chemiluminescence signal amplification for the identification of cancer cells. *Talanta* **2020,** *209*, 120505.

64. Kim, W. H.; Lee, J. U.; Song, S.; Kim, S.; Choi, Y. J.; Sim, S. J., A label-free, ultra-highly sensitive and multiplexed SERS nanoplasmonic biosensor for miRNA detection using a head-flocked gold nanopillar. *Analyst* **2019,** *144* (5), 1768-1776.

65. Gillespie, P.; Ladame, S.; O'Hare, D., Molecular methods in electrochemical microRNA detection. *ANALYST* **2019,** *144* (1), 114-129.

66. Thiruvottriyur Shanmugam, S.; Trashin, S.; De Wael, K., Gold-sputtered microelectrodes with built-in gold reference and counter electrodes for electrochemical DNA detection. *Analyst* **2020,** *145* (23), 7646-7653.

67. Labuda, J.; Brett, A. M. O.; Evtugyn, G.; Fojta, M.; Mascini, M.; Ozsoz, M.; Palchetti, I.; Paleček, E.; Wang, J., Electrochemical nucleic acid-based biosensors: Concepts, terms, and methodology (IUPAC Technical Report). *Pure and Applied Chemistry* **2010,** *82* (5), 1161-1187.

68. Wang, T.; Viennois, E.; Merlin, D.; Wang, G., Microelectrode miRNA Sensors Enabled by Enzymeless Electrochemical Signal Amplification. *Analytical Chemistry* **2015,** *87* (16), 8173-8180.

69. Gao, Z.; Yang, Z., Detection of microRNAs using electrocatalytic nanoparticle tags. *Anal Chem* **2006,** *78* (5), 1470-7.

70. Campuzano, S.; Torrente-Rodríguez, R. M.; López-Hernández, E.; Conzuelo, F.; Granados, R.; Sánchez-Puelles, J. M.; Pingarrón, J. M., Magnetobiosensors based on viral protein p19 for microRNA determination in cancer cells and tissues. *Angew Chem Int Ed Engl* **2014,** *53* (24), 6168-71.

71. Torrente-Rodríguez, R. M.; Ruiz-Valdepeñas Montiel, V.; Campuzano, S.; Farchado-Dinia, M.; Barderas, R.; San Segundo-Acosta, P.; Montoya, J. J.; Pingarron, J. M.,

Fast Electrochemical miRNAs Determination in Cancer Cells and Tumor Tissues with Antibody-Functionalized Magnetic Microcarriers. *ACS Sensors* **2016,** *1* (7), 896-903.

72. Wang, J.; Hui, N., Electrochemical functionalization of polypyrrole nanowires for the development of ultrasensitive biosensors for detecting microRNA. *Sensors and Actuators B: Chemical* **2019,** *281*, 478-485.

73. Moccia, M.; Caratelli, V.; Cinti, S.; Pede, B.; Avitabile, C.; Saviano, M.; Imbriani, A. L.; Moscone, D.; Arduini, F., Paper-based electrochemical peptide nucleic acid (PNA) biosensor for detection of miRNA-492: a pancreatic ductal adenocarcinoma biomarker. *Biosensors and Bioelectronics* **2020,** *165*, 112371.

74. Wang, M.; Shen, B.; Yuan, R.; Cheng, W.; Xu, H.; Ding, S., An electrochemical biosensor for highly sensitive determination of microRNA based on enzymatic and molecular beacon mediated strand displacement amplification. *Journal of Electroanalytical Chemistry* **2015,** *756*, 147-152.

75. Xia, N.; Zhang, Y.; Wei, X.; Huang, Y.; Liu, L., An electrochemical microRNAs biosensor with the signal amplification of alkaline phosphatase and electrochemical–chemical–chemical redox cycling. *Analytica Chimica Acta* **2015,** *878*, 95-101.

76. Fang, C. S.; Kim, K.-s.; Yu, B.; Jon, S.; Kim, M.-S.; Yang, H., Ultrasensitive Electrochemical Detection of miRNA-21 Using a Zinc Finger Protein Specific to DNA–RNA Hybrids. *Analytical Chemistry* **2017,** *89* (3), 2024-2031.

77. Wang, H.; Jian, Y.; Kong, Q.; Liu, H.; Lan, F.; Liang, L.; Ge, S.; Yu, J., Ultrasensitive electrochemical paper-based biosensor for microRNA via strand displacement reaction and metal-organic frameworks. *Sensors and Actuators B: Chemical* **2018,** *257*, 561-569.

78. Zhang, K.; Dong, H.; Dai, W.; Meng, X.; Lu, H.; Wu, T.; Zhang, X., Fabricating Pt/Sn–In2O3 Nanoflower with Advanced Oxygen Reduction Reaction Performance for High-Sensitivity MicroRNA Electrochemical Detection. *Analytical Chemistry* **2017,** *89* (1), 648-655.

79. Li, X.; Peng, G.; Cui, F.; Qiu, Q.; Chen, X.; Huang, H., Double determination of long noncoding RNAs from lung cancer via multi-amplified electrochemical genosensor at sub-femtomole level. *Biosensors and Bioelectronics* **2018,** *113*, 116-123.

80. Fu, P.; Xing, S.; Xu, M.; Zhao, Y.; Zhao, C., Peptide nucleic acid-based electrochemical biosensor for simultaneous detection of multiple microRNAs from cancer cells with catalytic hairpin assembly amplification. *Sensors and Actuators B: Chemical* **2020,** *305*, 127545.

81. Smith, D. A.; Newbury, L. J.; Drago, G.; Bowen, T.; Redman, J. E., Electrochemical detection of urinary microRNAs via sulfonamide-bound antisense hybridisation. *Sensors and Actuators B: Chemical* **2017,** *253*, 335-341.

82. Yaman, Y. T.; Vural, O. A.; Bolat, G.; Abaci, S., One-pot synthesized gold nanoparticle-peptide nanotube modified disposable sensor for impedimetric recognition of miRNA 410. *Sensors and Actuators B: Chemical* **2020,** *320*, 128343.

83. Kannan, P.; Maiyalagan, T.; Lin, B.; Lei, W.; Jie, C.; Guo, L.; Jiang, Z.; Mao, S.; Subramanian, P., Nickel-phosphate pompon flowers nanostructured network enables the sensitive detection of microRNA. *Talanta* **2020,** *209*, 120511.

84. El Aamri, M.; Yammouri, G.; Mohammadi, H.; Amine, A.; Korri-Youssoufi, H., Electrochemical Biosensors for Detection of MicroRNA as a Cancer Biomarker: Pros and Cons. *Biosensors-Basel* **2020,** *10* (11), 46.

85. Sfragano, P. S.; Pillozzi, S.; Palchetti, I., Electrochemical and PEC platforms for miRNA and other epigenetic markers of cancer diseases: Recent updates. *ELECTROCHEMISTRY COMMUNICATIONS* **2021,** *124*.

86. Tabata, M.; Miyahara, Y., Liquid biopsy in combination with solid-state electrochemical sensors and nucleic acid amplification. *JOURNAL OF MATERIALS CHEMISTRY B* **2019,** *7* (43), 6655-6669.

87. Low, S. S.; Ji, D. Z.; Chai, W. S.; Liu, J. J.; Khoo, K. S.; Salmanpour, S.; Karimi, F.; Deepanraj, B.; Show, P. L., Recent Progress in Nanomaterials Modified Electrochemical Biosensors for the Detection of MicroRNA. *MICROMACHINES* **2021,** *12* (11).

88. Zhao, W.-W.; Xu, J.-J.; Chen, H.-Y., Photoelectrochemical bioanalysis: the state of the art. *Chemical Society Reviews* **2015,** *44* (3), 729-741.

89. Voccia, D.; Palchetti, I., Photoelectrochemical Biosensors for Nucleic Acid Detection. *J Nanosci Nanotechnol* **2015,** *15* (5), 3320-32.

90. Li, F.; Zhou, Y.; Yin, H.; Ai, S., Recent advances on signal amplification strategies in photoelectrochemical sensing of microRNAs. *Biosensors and Bioelectronics* **2020,** *166*, 112476.

91. Zhang, X., The Application of DNA Amplification Strategies in the Field of Photoelectrochemical Biosensor. In *Nucleic Acid Amplification Strategies for Biosensing, Bioimaging and Biomedicine*, Zhang, S.; Bi, S.; Song, X., Eds. Springer Singapore: Singapore, 2019; pp 153-171.

92. Sui, C.; Wang, T.; Zhou, Y.; Yin, H.; Meng, X.; Zhang, S.; Waterhouse, G. I. N.; Xu, Q.; Zhuge, Y.; Ai, S., Photoelectrochemical biosensor for hydroxymethylated DNA detection and T4-β-glucosyltransferase activity assay based on WS2 nanosheets and carbon dots. *Biosensors and Bioelectronics* **2019,** *127*, 38-44.

93. Ma, X. Y.; Ma, Y. H.; Ejeromedoghene, O.; Kandawa-Schulz, M.; Song, W.; Wang, Y. H., Photoelectrochemical detection of microRNAs based on target-triggered self-assembly of energy band position-matched CdS QDs and C3N4 nanosheets. *Microchimica Acta* **2022,** *189* (2).

94. Niu, X.; Zhao, Y.; Wang, F.; Wu, J.; Qu, F.; Tan, W., Ultrasensitive Photoelectrochemical Biosensor Based on Novel Z-Scheme Heterojunctions of Zn-Defective CdS/ZnS for MicroRNA Assay. *Analytical Chemistry* **2021,** *93* (51), 17134-17140.

95. Zhao, Y. C.; Xiang, J. Z.; Cheng, H.; Liu, X. J.; Li, F., Flexible photoelectrochemical biosensor for ultrasensitive microRNA detection based on concatenated multiplex signal amplification. *Biosensors & Bioelectronics* **2021,** *194*.

96. Li, M.-J.; An, S.-Y.; Wu, Y., Photoelectrochemical monitoring of miRNA based on Au NPs@g-C3N4 coupled with exonuclease-involved target cycle amplification. *Analytica Chimica Acta* **2021,** *1187*, 339156.

97. Xiao, J.; Deng, K.; Liu, Z.; Li, C.; Wang, J.; Yi, Q.; Huang, H.; Zhou, H., A photocathode based on BiOI-Bi/CNTs for microRNA detection coupling with target recycling strand displacement amplification. *Sensors and Actuators B: Chemical* **2021,** *348*, 130691.

98. Zhu, M.; Chai, Y.; Yuan, R.; Zu, B.; Yuan, Y., Dual catalytic hairpin assembly and enzyme cascade catalysis amplification based sensitive dual-mode biosensor with significantly enhanced opposite signal readout. *Sensors and Actuators B: Chemical* **2021,** *348*, 130676.

99. Liu, T.; Gu, M.; Dong, Y.; Wang, G.-L., Methylene blue embedded duplex DNA as an efficient signal stimulator of petal-like BiVO4 for ultrasensitive photoelectrochemical bioassay. *Analytica Chimica Acta* **2021,** *1182*, 338945.

100. Niu, X. K.; Lu, C. T.; Su, D.; Wang, F.; Tan, W. H.; Qu, F. L., Construction of a Polarity-Switchable Photoelectrochemical Biosensor for Ultrasensitive Detection of miRNA-141. *Analytical Chemistry* **2021,** *93* (40), 13727-13733.

101. Yang, R. Y.; Jiang, G. H.; Liu, H. M.; He, L. L.; Yu, F.; Liu, L. E.; Qu, L. B.; Wu, Y. J., A dual-model "on-super off" photoelectrochemical/ratiometric electrochemical biosensor for ultrasensitive and accurate detection of microRNA-224. *Biosensors & Bioelectronics* **2021,** *188*.

102. Hao, M.; Miao, P.; Wang, Y.; Wang, W.; Ge, S.; Yu, X.; Hu, X.-X.; Ding, B.; Zhang, J.; Yan, M., Near-Infrared Light-Initiated Photoelectrochemical Biosensor Based on Upconversion Nanorods for Immobilization-Free miRNA Detection with Double Signal Amplification. *Analytical Chemistry* **2021,** *93* (32), 11251-11258.

103. Li, Z.; Yang, H.; Hu, M.; Zhang, L.; Ge, S.; Cui, K.; Yu, J., Cathode Photoelectrochemical Paper Device for microRNA Detection Based on Cascaded Photoactive Structures and Hemin/Pt Nanoparticle-Decorated DNA Dendrimers. *ACS Applied Materials & Interfaces* **2020,** *12* (15), 17177-17184.

104. Song, X.; Hou, T.; Lu, F.; Wang, Y.; Liu, J.; Li, F., Homogeneous photoelectrochemical biosensing via synergy of G-quadruplex/hemin catalysed reactions and the inner filter effect. *Chemical Communications* **2020,** *56* (12), 1811-1814.

105. Zang, Y.; Fan, J.; Zhang, H.; Xu, Q.; Jiang, J.; Xue, H., Dual-functional β-CD@CdS nanorod/WS2 nanosheet heterostructures coupled with strand displacement reaction-mediated photocurrent quenching for an ultrasensitive MicroRNA-21 assay. *Electrochimica Acta* **2020,** *334*, 135581.

106. Trashin, S.; Rahemi, V.; Ramji, K.; Neven, L.; Gorun, S. M.; De Wael, K., Singlet oxygen-based electrosensing by molecular photosensitizers. *Nature Communications* **2017,** *8* (1).

107. Weissleder, R.; Mahmood, U., Molecular Imaging. *Radiology* **2001,** *219* (2), 316-333.

108. Aveline, B. M., Chapter 2 Primary processes in photosensitization mechanisms. In *Comprehensive Series in Photosciences*, Calzavara-Pinton, P.; Szeimies, R.-M.; Ortel, B., Eds. Elsevier: 2001; Vol. 2, pp 17-37.

109. Blair, E. O.; Corrigan, D. K., A review of microfabricated electrochemical biosensors for DNA detection. *Biosens Bioelectron* **2019,** *134*, 57-67.

110. Xu, D.; Huang, K.; Liu, Z.; Liu, Y.; Ma, L., Microfabricated Disposable DNA Sensors Based on Enzymatic Amplification Electrochemical Detection. *Electroanalysis* **2001,** *13* (10), 882-887.

111. Carter, Z. A.; Kataky, R., A G-quadruplex aptamer based impedimetric sensor for free lysine and arginine. *Sensors and Actuators B: Chemical* **2017,** *243*, 904-909.

112. Santos-Cancel, M.; Lazenby, R. A.; White, R. J., Rapid Two-Millisecond Interrogation of Electrochemical, Aptamer-Based Sensor Response Using Intermittent Pulse Amperometry. *ACS Sens* **2018,** *3* (6), 1203-1209.

113. Toldrà, A.; Furones, M. D.; O'Sullivan, C. K.; Campàs, M., Detection of isothermally amplified ostreid herpesvirus 1 DNA in Pacific oyster (Crassostrea gigas) using a miniaturised electrochemical biosensor. *Talanta* **2020,** *207*, 120308.

114. Allen J. Bard, G. I., Fritz Scholz, *Electrochemical Dictionary*. Springer Berlin, Heidelberg: 2012.

115. Carvalhal, R. F.; Sanches Freire, R.; Kubota, L. T., Polycrystalline Gold Electrodes: A Comparative Study of Pretreatment Procedures Used for Cleaning and Thiol Self-Assembly Monolayer Formation. *Electroanalysis* **2005,** *17* (14), 1251-1259.

116. Frankenthal, R. P.; Thompson, D. E., The Anodic Behavior of Gold in Sulfuric Acid Solutions: Effect of Chloride and Electrode Potential. *Journal of The Electrochemical Society* **1976,** *123* (6), 799-804.

117. Fischer, L. M.; Tenje, M.; Heiskanen, A. R.; Masuda, N.; Castillo, J.; Bentien, A.; Émneus, J.; Jakobsen, M. H.; Boisen, A., Gold cleaning methods for electrochemical detection applications. *Microelectronic Engineering* **2009,** *86* (4-6), 1282-1285.

118. Rashid, J. I. A.; Yusof, N. A., The strategies of DNA immobilization and hybridization detection mechanism in the construction of electrochemical DNA sensor: A review. *Sensing and Bio-Sensing Research* **2017,** *16*, 19-31.

119. Pagliarini, V.; Neagu, D.; Scognamiglio, V.; Pascale, S.; Scordo, G.; Volpe, G.; Delibato, E.; Pucci, E.; Notargiacomo, A.; Pea, M.; Moscone, D.; Arduini, F., Treated Gold Screen-Printed Electrode as Disposable Platform for Label-Free Immunosensing of Salmonella Typhimurium. *Electrocatalysis* **2018,** *10* (4), 288-294.

120. Lao, R.; Song, S.; Wu, H.; Wang, L.; Zhang, Z.; He, L.; Fan, C., Electrochemical Interrogation of DNA Monolayers on Gold Surfaces. *Analytical Chemistry* **2005,** *77* (19), 6475-6480.

121. Steel, A. B.; Levicky, R. L.; Herne, T. M.; Tarlov, M. J., Immobilization of nucleic acids at solid surfaces: effect of oligonucleotide length on layer assembly. *Biophys J* **2000,** *79* (2), 975-981.

122. Steel, A. B.; Herne, T. M.; Tarlov, M. J., Electrochemical Quantitation of DNA Immobilized on Gold. *Analytical Chemistry* **1998,** *70* (22), 4670-4677.

123. Yu, Z. L.; Yang, C. W.; Triffaux, E.; Doneux, T.; Turner, R. F.; Bizzotto, D., Measuring and Remediating Nonspecific Modifications of Gold Surfaces Using a Coupled in Situ Electrochemical Fluorescence Microscopic Methodology. *Anal Chem* **2017,** *89* (1), 886-894.

124. Jambrec, D.; Conzuelo, F.; Zhao, B.; Schuhmann, W., Potential-pulse assisted thiol chemisorption minimizes non-specific adsorptions in DNA assays. *Electrochimica Acta* **2018,** *276*, 233-239.

125. Jambrec, D.; Kayran, Y. U.; Schuhmann, W., Controlling DNA/Surface Interactions for Potential Pulse-Assisted Preparation of Multi-Probe DNA Microarrays. *Electroanalysis* **2019**.

126. Rant, U.; Arinaga, K.; Scherer, S.; Pringsheim, E.; Fujita, S.; Yokoyama, N.; Tornow, M.; Abstreiter, G., Switchable DNA interfaces for the highly sensitive detection of

label-free DNA targets. *Proceedings of the National Academy of Sciences* **2007,** *104* (44), 17364-17369.

127. Rant, U.; Arinaga, K.; Fujita, S.; Yokoyama, N.; Abstreiter, G.; Tornow, M., Dynamic Electrical Switching of DNA Layers on a Metal Surface. *Nano Letters* **2004,** *4* (12), 2441-2445.

128. Leung, K. K.; Yu, H.-Z.; Bizzotto, D., Electrodepositing DNA Self-Assembled Monolayers on Au: Detailing the Influence of Electrical Potential Perturbation and Surface Crystallography. *ACS Sensors* **2019,** *4* (2), 513-520.

129. Xu, X.; Makaraviciute, A.; Pettersson, J.; Zhang, S.-L.; Nyholm, L.; Zhang, Z., Revisiting the factors influencing gold electrodes prepared using cyclic voltammetry. *Sensors and Actuators B: Chemical* **2019,** *283*, 146-153.

130. Gębala, M.; Stoica, L.; Guschin, D.; Stratmann, L.; Hartwich, G.; Schuhmann, W., A biotinylated intercalator for selective post-labeling of double-stranded DNA as a basis for high-sensitive DNA assays. *Electrochemistry Communications* **2010,** *12* (5), 684-688.

131. Ma, S.; Hu, Y.; Zhang, Q.; Guo, Z.; Wang, S.; Shen, Q.; Liu, C.; Liu, Z., Adenine/Au complex-dependent versatile electrochemical platform for ultrasensitive DNA-related enzyme activity assay. *Sensors and Actuators B: Chemical* **2018,** *273*, 760-770.

132. Hoare, J. P., A Cyclic Voltammetric Study of the Gold-Oxygen System. *Journal of The Electrochemical Society* **1984,** *131* (8).

133. Burke, L. D.; Nugent, P. F., The electrochemistry of gold: I the redox behaviour of the metal in aqueous media. *Gold Bulletin* **1997,** *30* (2), 43-53.

134. Makaraviciute, A.; Xu, X.; Nyholm, L.; Zhang, Z., Systematic Approach to the Development of Microfabricated Biosensors: Relationship between Gold Surface Pretreatment and Thiolated Molecule Binding. *ACS Appl Mater Interfaces* **2017,** *9* (31), 26610-26621.

135. Xiao, Y.; Lai, R. Y.; Plaxco, K. W., Preparation of electrode-immobilized, redox-modified oligonucleotides for electrochemical DNA and aptamer-based sensing. *Nature Protocols* **2007,** *2*, 2875.

136. Łukaszewski, M., Electrochemical Methods of Real Surface Area Determination of Noble Metal Electrodes – an Overview. *International Journal of Electrochemical Science* **2016**, 4442-4469.

137. Tavallaie, R.; De Almeida, S. R.; Gooding, J. J., Toward biosensors for the detection of circulating microRNA as a cancer biomarker: an overview of the challenges and successes. *Wiley Interdiscip Rev Nanomed Nanobiotechnol* **2015,** *7* (4), 580-92.

138. Conway, B. E.; Angerstein-Kozlowska, H.; Sharp, W. B. A.; Criddle, E. E., Ultrapurification of water for electrochemical and surface chemical work by catalytic pyrodistillation. *Analytical Chemistry* **1973,** *45* (8), 1331-1336.

139. Ricci, F.; Lai, R. Y.; Heeger, A. J.; Plaxco, K. W.; Sumner, J. J., Effect of molecular crowding on the response of an electrochemical DNA sensor. *Langmuir* **2007,** *23* (12), 6827-34.

140. Jambrec, D.; Gebala, M.; La Mantia, F.; Schuhmann, W., Potential-Assisted DNA Immobilization as a Prerequisite for Fast and Controlled Formation of DNA Monolayers. *Angew Chem Int Ed Engl* **2015,** *54* (50), 15064-8.

141. Srisombat, L.; Jamison, A. C.; Lee, T. R., Stability: A key issue for self-assembled monolayers on gold as thin-film coatings and nanoparticle protectants. *Colloids and Surfaces A: Physicochemical and Engineering Aspects* **2011,** *390* (1), 1-19.

142. Niemz, A.; Ferguson, T. M.; Boyle, D. S., Point-of-care nucleic acid testing for infectious diseases. *Trends in Biotechnology* **2011,** *29* (5), 240-250.

143. Li, Y.; Sthal, C.; Bai, J.; Liu, X.; Anderson, G.; Fang, Y., Development of a real-time RT-qPCR assay for the detection of porcine respirovirus 1. *Journal of Virological Methods* **2021,** *289*, 114040.

144. Rahat, B.; Ali, T.; Sapehia, D.; Mahajan, A.; Kaur, J., Circulating Cell-Free Nucleic Acids as Epigenetic Biomarkers in Precision Medicine. *Frontiers in Genetics* **2020,** *11* (844).

145. Bronkhorst, A. J.; Ungerer, V.; Holdenrieder, S., Early detection of cancer using circulating tumor DNA: biological, physiological and analytical considerations. *Critical Reviews in Clinical Laboratory Sciences* **2020,** *57* (4), 253-269.

146. Bhargava, A.; Kumar Khare, N.; Bunkar, N.; Chaudhury, K.; Chand Pandey, K.; K. Jain, S.; K. Mishra, P., Cell-Free Circulating Epigenomic Signatures: Non-Invasive Biomarker for Cardiovascular and Other Age-Related Chronic Diseases. *Current Pharmaceutical Design* **2017,** *23* (8), 1175-1187.

147. Sfragano, P. S.; Pillozzi, S.; Palchetti, I., Electrochemical and PEC platforms for miRNA and other epigenetic markers of cancer diseases: Recent updates. *Electrochemistry Communications* **2021,** *124*, 106929.

148. Kim, H.-s.; Abbas, N.; Shin, S., A rapid diagnosis of SARS-CoV-2 using DNA hydrogel formation on microfluidic pores. *Biosensors and Bioelectronics* **2021,** *177*, 113005.

149. Ferapontova, E. E., DNA Electrochemistry and Electrochemical Sensors for Nucleic Acids. *Annu Rev Anal Chem (Palo Alto Calif)* **2018,** *11* (1), 197-218.

150. Santhanam, M.; Algov, I.; Alfonta, L., DNA/RNA Electrochemical Biosensing Devices a Future Replacement of PCR Methods for a Fast Epidemic Containment. *Sensors* **2020,** *20* (16), 4648.

151. García-González, R.; Costa-García, A.; Fernández-Abedul, M. T., Methylene blue covalently attached to single stranded DNA as electroactive label for potential bioassays. *Sens Actuators B Chem* **2014,** *191*, 784-790.

152. Kokkinos, C., Electrochemical DNA Biosensors Based on Labeling with Nanoparticles. *Nanomaterials* **2019,** *9* (10), 1361.

153. Wang, Q.; Zhang, H.; Shen, X.; Wang, F.; Mao, C., A Flexible DNA Biosensor for Breast Cancer Marker BRCA1 Detection. *ChemistrySelect* **2020,** *5* (48), 15259-15263.

154. Liu, Z.-J.; Yang, L.-Y.; Wei, Q.-X.; Ye, C.-L.; Xu, X.-W.; Zhong, G.-X.; Zheng, Y.-J.; Chen, J.-Y.; Lin, X.-H.; Liu, A.-L., A novel ligase chain reaction-based electrochemical biosensing strategy for highly sensitive point mutation detection from human whole blood. *Talanta* **2020,** *216*, 120966.

155. Demchenko, A. P., Photobleaching of organic fluorophores: quantitative characterization, mechanisms, protection. *Methods Appl Fluoresc* **2020,** *8* (2), 022001.

156. Malatesta, M.; Giagnacovo, M.; Costanzo, M.; Conti, B.; Genta, I.; Dorati, R.; Galimberti, V.; Biggiogera, M.; Zancanaro, C., Diaminobenzidine photoconversion is a

suitable tool for tracking the intracellular location of fluorescently labelled nanoparticles at transmission electron microscopy. *Eur J Histochem* **2012,** *56* (2), e20-e20.

157. Horaková-Brazdilova, P.; Fojtova, M.; Vytras, K.; Fojta, M., Enzyme-Linked Electrochemical Detection of PCR-Amplified Nucleotide Sequences Using Disposable Screen-Printed Sensors. Applications in Gene Expression Monitoring. *Sensors (Basel)* **2008,** *8* (1), 193-210.

158. Zhao, W. W.; Xu, J. J.; Chen, H. Y., Photoelectrochemical DNA biosensors. *Chem Rev* **2014,** *114* (15), 7421-41.

159. Victorious, A.; Saha, S.; Pandey, R.; Soleymani, L., Enhancing the Sensitivity of Photoelectrochemical DNA Biosensing Using Plasmonic DNA Barcodes and Differential Signal Readout. *Angewandte Chemie International Edition* **2021,** *60* (13), 7316-7322.

160. Liu, X. P.; Chen, J. S.; Mao, C. J.; Niu, H. L.; Song, J. M.; Jin, B. K., Enhanced photoelectrochemical DNA sensor based on TiO2/Au hybrid structure. *Biosens Bioelectron* **2018,** *116*, 23-29.

161. Tokudome, H.; Yamada, Y.; Sonezaki, S.; Ishikawa, H.; Bekki, M.; Kanehira, K.; Miyauchi, M., Photoelectrochemical deoxyribonucleic acid sensing on a nanostructured TiO2 electrode. *Applied Physics Letters* **2005,** *87* (21).

162. Wang, M.; Yin, H.; Shen, N.; Xu, Z.; Sun, B.; Ai, S., Signal-on photoelectrochemical biosensor for microRNA detection based on Bi2S3 nanorods and enzymatic amplification. *Biosens Bioelectron* **2014,** *53*, 232-7.

163. Haag, W. R.; Hoigne´, J. r.; Gassman, E.; Braun, A. M., Singlet oxygen in surface waters — Part I: Furfuryl alcohol as a trapping agent. *Chemosphere* **1984,** *13* (5), 631-640.

164. Kochevar, I. E.; Redmond, R. W., [2] Photosensitized production of singlet oxygen. In *Methods in Enzymology*, Academic Press: 2000; Vol. 319, pp 20-28.

165. Appiani, E.; Ossola, R.; Latch, D. E.; Erickson, P. R.; McNeill, K., Aqueous singlet oxygen reaction kinetics of furfuryl alcohol: effect of temperature, pH, and salt content. *Environ Sci Process Impacts* **2017,** *19* (4), 507-516.

166. Núñez Montoya, S. C.; Comini, L. R.; Sarmiento, M.; Becerra, C.; Albesa, I.; Argüello, G. A.; Cabrera, J. L., Natural anthraquinones probed as Type I and Type II photosensitizers: singlet oxygen and superoxide anion production. *Journal of Photochemistry and Photobiology B: Biology* **2005,** *78* (1), 77-83.

167. Abe, H.; Ikebuchi, K.; Wagner, S. J.; Kuwabara, M.; Kamo, N.; Sekiguchi, S., Potential involvement of both type I and type II mechanisms in M13 virus inactivation by methylene blue photosensitization. *Photochem Photobiol* **1997,** *66* (2), 204-8.

168. Gandin, E.; Lion, Y.; Van de Vorst, A., QUANTUM YIELD OF SINGLET OXYGEN PRODUCTION BY XANTHENE DERIVATIVES. *Photochemistry and Photobiology* **1983,** *37* (3), 271-278.

169. Zhao, W.-W.; Xu, J.-J.; Chen, H.-Y., Photoelectrochemical DNA Biosensors. *Chemical Reviews* **2014,** *114* (15), 7421-7441.

170. Wojtovich, A. P.; Foster, T. H., Optogenetic control of ROS production. *Redox Biol* **2014,** *2*, 368-376.

171. Sjöback, R.; Nygren, J.; Kubista, M., Characterization of fluorescein–oligonucleotide conjugates and measurement of local electrostatic potential. *Biopolymers* **1998,** *46* (7), 445-453.

172. Spikes, J. D.; Bommer, J. C., Photosensitizing properties of mono-l-aspartyl chlorin e6 (NPe6): A candidate sensitizer for the photodynamic therapy of tumors. *Journal of Photochemistry and Photobiology B: Biology* **1993,** *17* (2), 135-143.

173. Fernandez, J. M.; Bilgin, M. D.; Grossweiner, L. I., Singlet oxygen generation by photodynamic agents. *Journal of Photochemistry and Photobiology B: Biology* **1997,** *37* (1), 131-140.

174. Shahinyan, G. A.; Amirbekyan, A. Y.; Markarian, S. A., Photophysical properties of methylene blue in water and in aqueous solutions of dimethylsulfoxide. *Spectrochimica Acta Part A: Molecular and Biomolecular Spectroscopy* **2019,** *217*, 170-175.

175. Ghanadzadeh, A.; Zeini, A.; Kashef, A.; Moghadam, M., Concentration effect on the absorption spectra of oxazine1 and methylene blue in aqueous and alcoholic solutions. *Journal of Molecular Liquids* **2008,** *138* (1), 100-106.

176. Guiraud, H. J.; Foote, C. S., Chemistry of superoxide ion. III. Quenching of singlet oxygen. *Journal of the American Chemical Society* **1976,** *98* (7), 1984-1986.

177. Ray, S. K.; Dhakal, D.; Lee, S. W., Insight Into Malachite Green Degradation, Mechanism and Pathways by Morphology-Tuned α-NiMoO(4) Photocatalyst. *Photochem Photobiol* **2018,** *94* (3), 552-563.

178. Redmond, R. W.; Gamlin, J. N., A compilation of singlet oxygen yields from biologically relevant molecules. *Photochem Photobiol* **1999,** *70* (4), 391-475.

179. Lutkus, L. V.; Rickenbach, S. S.; McCormick, T. M., Singlet oxygen quantum yields determined by oxygen consumption. *Journal of Photochemistry and Photobiology A: Chemistry* **2019,** *378*, 131-135.

180. Pellosi, D. S.; Batistela, V. R.; Souza, V. R. d.; Scarminio, I. S.; Caetano, W.; Hioka, N., Evaluation of the photodynamic activity of Xanthene Dyes on Artemia salina described by chemometric approaches. *Anais da Academia Brasileira de Ciências* **2013,** *85*, 1267-1274.

181. Glembockyte, V.; Lin, J.; Cosa, G., Improving the Photostability of Red- and Green-Emissive Single-Molecule Fluorophores via Ni2+ Mediated Excited Triplet-State Quenching. *The Journal of Physical Chemistry B* **2016,** *120* (46), 11923-11929.

182. Motten, A. G.; Martínez, L. J.; Holt, N.; Sik, R. H.; Reszka, K.; Chignell, C. F.; Tonnesen, H. H.; Roberts, J. E., Photophysical studies on antimalarial drugs. *Photochem Photobiol* **1999,** *69* (3), 282-7.

183. Valencia U, C.; Lemp, E.; L. Zanocco, A., QUANTUM YIELDS OF SINGLET MOLECULAR OXYGEN, O2(1Dg), PRODUCED BY ANTIMALARIC DRUGS IN ORGANIC SOLVENTS. *Journal of the Chilean Chemical Society* **2003,** *48*, 17-21.

184. Scurlock, R. D.; Ogilby, P. R., Production of singlet oxygen (1Δg O2) by 9,10-dicyanoanthracene and acridine: quantum yields in acetonitrile. *Journal of Photochemistry and Photobiology A: Chemistry* **1993,** *72* (1), 1-7.

185. Guo, Y.; He, D.; Xie, A.; Qu, W.; Tang, Y.; Zhou, L.; Zhu, R., The Electrochemical Oxidation of Hydroquinone and Catechol through a Novel Poly-geminal

Dicationic Ionic Liquid (PGDIL)–TiO2 Composite Film Electrode. *Polymers* **2019,** *11* (11), 1907.

186. Ferapontova, E. E.; Domínguez, E., Direct Electrochemical Oxidation of DNA on Polycrystalline Gold Electrodes. *Electroanalysis* **2003,** *15* (7), 629-634.

187. Lam, W. W. Y.; Lee, M. F. W.; Lau, T.-C., Kinetics and Mechanism of the Oxidation of Hydroquinones by a trans-Dioxoruthenium(VI) Complex. *Inorganic Chemistry* **2006,** *45* (1), 315-321.

188. Shen, Z.; Nakayama, S.; Semancik, S.; Sintim, H. O., Signal-on electrochemical Y or junction probe detection of nucleic acid. *Chemical Communications* **2012,** *48* (61), 7580-7582.

189. Kang, D.; Zuo, X.; Yang, R.; Xia, F.; Plaxco, K. W.; White, R. J., Comparing the Properties of Electrochemical-Based DNA Sensors Employing Different Redox Tags. *Analytical Chemistry* **2009,** *81* (21), 9109-9113.

190. Kang, D.; White, R. J.; Xia, F.; Zuo, X.; Vallée-Bélisle, A.; Plaxco, K. W., DNA biomolecular-electronic encoder and decoder devices constructed by multiplex biosensors. *NPG Asia Materials* **2012,** *4* (1), e1-e1.

191. Xiao, Y.; Qu, X.; Plaxco, K. W.; Heeger, A. J., Label-Free Electrochemical Detection of DNA in Blood Serum via Target-Induced Resolution of an Electrode-Bound DNA Pseudoknot. *Journal of the American Chemical Society* **2007,** *129* (39), 11896-11897.

192. Rowe, A. A.; Bonham, A. J.; White, R. J.; Zimmer, M. P.; Yadgar, R. J.; Hobza, T. M.; Honea, J. W.; Ben-Yaacov, I.; Plaxco, K. W., CheapStat: An Open-Source, "Do-It-Yourself" Potentiostat for Analytical and Educational Applications. *PLOS ONE* **2011,** *6* (9), e23783.

193. Kara, P.; Kerman, K.; Ozkan, D.; Meric, B.; Erdem, A.; Nielsen, P. E.; Ozsoz, M., Label-Free and Label Based Electrochemical Detection of Hybridization by Using Methylene Blue and Peptide Nucleic Acid Probes at Chitosan Modified Carbon Paste Electrodes. *Electroanalysis* **2002,** *14* (24), 1685-1690.

194. Desroches, J.; Jermyn, M.; Pinto, M.; Picot, F.; Tremblay, M. A.; Obaid, S.; Marple, E.; Urmey, K.; Trudel, D.; Soulez, G.; Guiot, M. C.; Wilson, B. C.; Petrecca, K.; Leblond, F., A new method using Raman spectroscopy for in vivo targeted brain cancer tissue biopsy. *Scientific Reports* **2018,** *8*, 1792.

195. Sokolenko, A. P.; Imyanitov, E. N., Molecular Diagnostics in Clinical Oncology. *Front Mol Biosci* **2018,** *5*, 76.

196. Nieva, J. J.; Kuhn, P., Fluid biopsy for solid tumors: A patients companion for lifelong characterization of their disease. *Future Oncology* **2012,** *8* (8), 989-998.

197. Akpe, V.; Kim, T. H.; Brown, C. L.; Cock, I. E., Circulating tumour cells: a broad perspective. *Journal of The Royal Society Interface* **2020,** *17* (168), 20200065.

198. Maia, M. C.; Salgia, M.; Pal, S. K., Harnessing cell-free DNA: plasma circulating tumour DNA for liquid biopsy in genitourinary cancers. *Nature Reviews Urology* **2020,** *17* (5), 271-291.

199. Jafri, M. A.; Al-Qahtani, M. H.; Shay, J. W., Role of miRNAs in human cancer metastasis: Implications for therapeutic intervention. *Seminars in Cancer Biology* **2017,** *44*, 117-131.

200. Fabris, L.; Ceder, Y.; Chinnaiyan, A. M.; Jenster, G. W.; Sorensen, K. D.; Tomlins, S.; Visakorpi, T.; Calin, G. A., The Potential of MicroRNAs as Prostate Cancer Biomarkers. *European Urology* **2016,** *70* (2), 312-322.

201. Vanacore, D.; Boccellino, M.; Rossetti, S.; Cavaliere, C.; D'Aniello, C.; Di Franco, R.; Romano, F. J.; Montanari, M.; La Mantia, E.; Piscitelli, R.; Nocerino, F.; Cappuccio, F.; Grimaldi, G.; Izzo, A.; Castaldo, L.; Pepe, M. F.; Malzone, M. G.; Iovane, G.; Ametrano, G.; Stiuso, P.; Quagliuolo, L.; Barberio, D.; Perdonà, S.; Muto, P.; Montella, M.; Maiolino, P.; Veneziani, B. M.; Botti, G.; Caraglia, M.; Facchini, G., Micrornas in prostate cancer: An overview. *Oncotarget* **2017,** *8* (30), 50240-50251.

202. Brase, J. C.; Johannes, M.; Schlomm, T.; Fälth, M.; Haese, A.; Steuber, T.; Beissbarth, T.; Kuner, R.; Sültmann, H., Circulating miRNAs are correlated with tumor progression in prostate cancer. *International Journal of Cancer* **2011,** *128* (3), 608-616.

203. Sita-Lumsden, A.; Fletcher, C. E.; Dart, D. A.; Brooke, G. N.; Waxman, J.; Bevan, C. L., Circulating nucleic acids as biomarkers of prostate cancer. *Biomarkers in medicine* **2013,** *7* (6), 867-877.

204. Xu, Y.; Qin, S.; An, T.; Tang, Y.; Huang, Y.; Zheng, L., MiR-145 detection in urinary extracellular vesicles increase diagnostic efficiency of prostate cancer based on hydrostatic filtration dialysis method. *The Prostate* **2017,** *77* (10), 1167-1175.

205. Mugoni, V.; Ciani, Y.; Nardella, C.; Demichelis, F., Circulating RNAs in prostate cancer patients. *Cancer Letters* **2022,** *524*, 57-69.

206. Shen, J.; Hruby, G. W.; McKiernan, J. M.; Gurvich, I.; Lipsky, M. J.; Benson, M. C.; Santella, R. M., Dysregulation of circulating microRNAs and prediction of aggressive prostate cancer. *The Prostate* **2012,** *72* (13), 1469-1477.

207. Rana, S.; Valbuena, G. N.; Curry, E.; Bevan, C. L.; Keun, H. C., MicroRNAs as biomarkers for prostate cancer prognosis: a systematic review and a systematic reanalysis of public data. *British Journal of Cancer* **2022,** *126* (3), 502-513.

208. Chen, C.; Tan, R.; Wong, L.; Fekete, R.; Halsey, J., Quantitation of microRNAs by real-time RT-qPCR. *Methods Mol Biol* **2011,** *687*, 113-34.

209. Moldovan, L.; Batte, K. E.; Trgovcich, J.; Wisler, J.; Marsh, C. B.; Piper, M., Methodological challenges in utilizing miRNAs as circulating biomarkers. *J Cell Mol Med* **2014,** *18* (3), 371-390.

210. Chen, C.; Ridzon, D. A.; Broomer, A. J.; Zhou, Z.; Lee, D. H.; Nguyen, J. T.; Barbisin, M.; Xu, N. L.; Mahuvakar, V. R.; Andersen, M. R.; Lao, K. Q.; Livak, K. J.; Guegler, K. J., Real-time quantification of microRNAs by stem-loop RT-PCR. *Nucleic acids research* **2005,** *33* (20), e179-e179.

211. Miotto, E.; Saccenti, E.; Lupini, L.; Callegari, E.; Negrini, M.; Ferracin, M., Quantification of circulating miRNAs by droplet digital PCR: comparison of EvaGreen- and TaqMan-based chemistries. *Cancer Epidemiol Biomarkers Prev* **2014,** *23* (12), 2638-42.

212. Hu, Y.; Lan, W.; Miller, D., Next-Generation Sequencing for MicroRNA Expression Profile. *Methods Mol Biol* **2017,** *1617*, 169-177.

213. Trashin, S.; Rahemi, V.; Ramji, K.; Neven, L.; Gorun, S. M.; De Wael, K., Singlet oxygen-based electrosensing by molecular photosensitizers. *Nature Communications* **2017,** *8* (1), 16108.

214. Trashin, S.; Morales-Yánez, F.; Thiruvottriyur Shanmugam, S.; Paredis, L.; Carrión, E. N.; Sariego, I.; Muyldermans, S.; Polman, K.; Gorun, S. M.; De Wael, K., Nanobody-Based Immunosensor Detection Enhanced by Photocatalytic-Electrochemical Redox Cycling. *Analytical Chemistry* **2021,** *93* (40), 13606-13614.

215. Shanmugam, S. T.; Trashin, S.; De Wael, K., Singlet oxygen-based photoelectrochemical detection of DNA. *Biosensors and Bioelectronics* **2022,** *195*, 113652.

216. Zaman, M. S.; Chen, Y.; Deng, G.; Shahryari, V.; Suh, S. O.; Saini, S.; Majid, S.; Liu, J.; Khatri, G.; Tanaka, Y.; Dahiya, R., The functional significance of microRNA-145 in prostate cancer. *British Journal of Cancer* **2010,** *103* (2), 256-264.

217. Richardsen, E.; Andersen, S.; Melbø-Jørgensen, C.; Rakaee, M.; Ness, N.; Al-Saad, S.; Nordby, Y.; Pedersen, M. I.; Dønnem, T.; Bremnes, R. M.; Busund, L.-T., MicroRNA 141 is associated to outcome and aggressive tumor characteristics in prostate cancer. *Scientific Reports* **2019,** *9* (1), 386.

218. Khan, S. U.; Trashin, S. A.; Korostei, Y. S.; Dubinina, T. V.; Tomilova, L. G.; Verbruggen, S. W.; De Wael, K., Photoelectrochemistry for Measuring the Photocatalytic Activity of Soluble Photosensitizers. *ChemPhotoChem* **2020,** *4* (4), 300-306.

219. Invitrogen Dynabeads™ M-280 Streptavidin. https://www.thermofisher.com/order/catalog/product/11205D.

220. Wilkinson, F.; Helman, W. P.; Ross, A. B., Rate Constants for the Decay and Reactions of the Lowest Electronically Excited Singlet State of Molecular Oxygen in Solution. An Expanded and Revised Compilation. *Journal of Physical and Chemical Reference Data* **1995,** *24* (2), 663-677.

221. Latch, D. E.; McNeill, K., Microheterogeneity of Singlet Oxygen Distributions in Irradiated Humic Acid Solutions. *Science* **2006,** *311* (5768), 1743-1747.

222. Borman, P.; Elder, D., Q2(R1) Validation of Analytical Procedures. In *ICH Quality Guidelines*, 2017; pp 127-166.

223. Mahshid, S. S.; Camiré, S.; Ricci, F.; Vallée-Bélisle, A., A Highly Selective Electrochemical DNA-Based Sensor That Employs Steric Hindrance Effects to Detect Proteins Directly in Whole Blood. *Journal of the American Chemical Society* **2015,** *137* (50), 15596-15599.

224. Paunescu, I. A.; Bardan, R.; Marcu, A.; Nitusca, D.; Dema, A.; Negru, S.; Balacescu, O.; Balacescu, L.; Cumpanas, A.; Sirbu, I. O.; Petrut, B.; Seclaman, E.; Marian, C., Biomarker Potential of Plasma MicroRNA-150-5p in Prostate Cancer. *Medicina (Kaunas)* **2019,** *55* (9), 564.

225. Zhang, H.-L.; Qin, X.-J.; Cao, D.-L.; Zhu, Y.; Yao, X.-D.; Zhang, S.-L.; Dai, B.; Ye, D.-W., An elevated serum miR-141 level in patients with bone-metastatic prostate cancer is correlated with more bone lesions. *Asian J Androl* **2013,** *15* (2), 231-235.

226. Porzycki, P.; Ciszkowicz, E.; Semik, M.; Tyrka, M., Combination of three miRNA (miR-141, miR-21, and miR-375) as potential diagnostic tool for prostate cancer recognition. *International Urology and Nephrology* **2018,** *50* (9), 1619-1626.

227. Cheng, H. H.; Mitchell, P. S.; Kroh, E. M.; Dowell, A. E.; Chéry, L.; Siddiqui, J.; Nelson, P. S.; Vessella, R. L.; Knudsen, B. S.; Chinnaiyan, A. M.; Pienta, K. J.; Morrissey, C.; Tewari, M., Circulating microRNA Profiling Identifies a Subset of Metastatic Prostate

Cancer Patients with Evidence of Cancer-Associated Hypoxia. *PLOS ONE* **2013,** *8* (7), e69239.

228. Nguyen, H. C. N.; Xie, W.; Yang, M.; Hsieh, C.-L.; Drouin, S.; Lee, G.-S. M.; Kantoff, P. W., Expression differences of circulating microRNAs in metastatic castration resistant prostate cancer and low-risk, localized prostate cancer. *The Prostate* **2013,** *73* (4), 346-354.

229. Kshirsagar, P.; Seshacharyulu, P.; Muniyan, S.; Rachagani, S.; Smith, L. M.; Thompson, C.; Shah, A.; Mallya, K.; Kumar, S.; Jain, M.; Batra, S. K., DNA-gold nanoprobe-based integrated biosensing technology for non-invasive liquid biopsy of serum miRNA: A new frontier in prostate cancer diagnosis. *Nanomedicine: Nanotechnology, Biology and Medicine* **2022,** *43*, 102566.

230. Gevaert, A. B.; Witvrouwen, I.; Vrints, C. J.; Heidbuchel, H.; Van Craenenbroeck, E. M.; Van Laere, S. J.; Van Craenenbroeck, A. H., MicroRNA profiling in plasma samples using qPCR arrays: Recommendations for correct analysis and interpretation. *PLOS ONE* **2018,** *13* (2), e0193173.

231. Silva, S. M.; Hoque, S.; Gonçales, V. R.; Gooding, J. J., The Impact of the Position of the Redox Label on Charge Transfer and Hybridization Efficiency at DNA Interfaces. *Electroanalysis* **2018,** *30* (7), 1529-1535.

232. Silva, S. M.; Tavallaie, R.; Gonçales, V. R.; Utama, R. H.; Kashi, M. B.; Hibbert, D. B.; Tilley, R. D.; Gooding, J. J., Dual Signaling DNA Electrochemistry: An Approach To Understand DNA Interfaces. *Langmuir* **2018,** *34* (4), 1249-1255.

233. Dauphin-Ducharme, P.; Arroyo-Currás, N.; Adhikari, R.; Somerson, J.; Ortega, G.; Makarov, D. E.; Plaxco, K. W., Chain Dynamics Limit Electron Transfer from Electrode-Bound, Single-Stranded Oligonucleotides. *The Journal of Physical Chemistry C* **2018,** *122* (37), 21441-21448.

234. Song, H.; Diakowski, P. M.; Hudson, R. H. E.; Kraatz, H.-B., Effect of Ferrocene Position on Charge Transfer in ds-DNA Films. *Journal of Inorganic and Organometallic Polymers and Materials 2011 22:1* **2011,** *22* (1), 178-182.

235. Jin, W.; Fei, X.; Wang, X.; Chen, F.; Song, Y., Circulating miRNAs as Biomarkers for Prostate Cancer Diagnosis in Subjects with Benign Prostatic Hyperplasia. *Journal of Immunology Research* **2020,** *2020*, ID 5873056.

236. Porzycki, P.; Ciszkowicz, E.; Semik, M.; Tyrka, M., Combination of three miRNA (miR-141, miR-21, and miR-375) as potential diagnostic tool for prostate cancer recognition. *International Urology and Nephrology 2018 50:9* **2018,** *50* (9), 1619-1626.

237. Zedan, A. H.; Osther, P. J. S.; Assenholt, J.; Madsen, J. S.; Hansen, T. F., Circulating miR-141 and miR-375 are associated with treatment outcome in metastatic castration resistant prostate cancer. *Scientific Reports 2020 10:1* **2020,** *10* (1), 1-9.

238. Muzyka, K., Current trends in the development of the electrochemiluminescent immunosensors. *Biosensors and Bioelectronics* **2014,** *54*, 393-407.

239. Meso Scale Discovery. https://www.mesoscale.com/en/technical_resources/our_technology/ecl.

240. Roche's technology. http://roche-html5.coservice.ch/app/webroot/book/en/ecl-unique-immunoassay-technology.html.

241. Fiorani, A.; Valenti, G.; Iurlo, M.; Marcaccio, M.; Paolucci, F., Electrogenerated chemiluminescence: A molecular electrochemistry point of view. *Current Opinion in Electrochemistry* **2018,** *8*, 31-38.

242. Richter, M. M., Electrochemiluminescence (ECL). *Chemical Reviews* **2004,** *104* (6), 3003-3036.

243. Forster, R. J.; Bertoncello, P.; Keyes, T. E., Electrogenerated Chemiluminescence. *Annual Review of Analytical Chemistry* **2009,** *2* (1), 359-385.

244. Miao, W., Electrogenerated Chemiluminescence and Its Biorelated Applications. *Chemical Reviews* **2008,** *108* (7), 2506-2553.

245. Noffsinger, J. B.; Danielson, N. D., Generation of Chemiluminescence upon Reaction of Aliphatic Amines with Tris(2,2'-bipyridine)ruthenium(III). *Analytical Chemistry* **1987,** *59* (6), 865-868.

246. Wang, M.; Zhou, Y.; Yin, H.; Jiang, W.; Wang, H.; Ai, S., Signal-on electrochemiluminescence biosensor for microRNA-319a detection based on two-stage isothermal strand-displacement polymerase reaction. *Biosensors and Bioelectronics* **2018,** *107*, 34-39.

247. Yang, J.; Xia, Q.; Guo, L.; Luo, F.; Dong, Y.; Qiu, B.; Lin, Z., A highly sensitive signal-on biosensor for microRNA 142-3p based on the quenching of Ru(bpy)32+-TPA electrochemiluminescence by carbon dots and duplex specific nuclease-assisted target recycling amplification. *Chemical Communications* **2020,** *56* (49), 6692-6695.

248. Zhang, P.; Lin, Z.; Zhuo, Y.; Yuan, R.; Chai, Y., Dual microrna-fueled DNA nanogears: A case of regenerated strategy for multiple electrochemiluminescence detection of microrna with single luminophore. *Analytical Chemistry* **2017,** *89* (2), 1338-1345.

249. Peng, L.; Zhang, P.; Chai, Y.; Yuan, R., Bi-directional DNA Walking Machine and Its Application in an Enzyme-Free Electrochemiluminescence Biosensor for Sensitive Detection of MicroRNAs. *Analytical Chemistry* **2017,** *89* (9), 5036-5042.

250. Li, J.; Liu, J.; Bi, Y.; Sun, M.; Bai, J.; Zhou, M., Ultrasensitive electrochemiluminescence biosensing platform for miRNA-21 and MUC1 detection based on dual catalytic hairpin assembly. *Analytica Chimica Acta* **2020,** *1105*, 87-94.

251. Thayer, M. B.; Lade, J. M.; Doherty, D.; Xie, F.; Basiri, B.; Barnaby, O. S.; Bala, N. S.; Rock, B. M., Application of Locked Nucleic Acid Oligonucleotides for siRNA Preclinical Bioanalytics. *Scientific Reports* **2019,** *9* (3566), 1-9.

252. Thayer, M. B.; Humphreys, S. C.; Chung, K. S.; Lade, J. M.; Cook, K. D.; Rock, B. M., POE Immunoassay: Plate-based oligonucleotide electro-chemiluminescent immunoassay for the quantification of nucleic acids in biological matrices. *Scientific Reports* **2020,** *10* (1), 10425.

253. Ferapontova, E. E., DNA Electrochemistry and Electrochemical Sensors for Nucleic Acids. *Annual Review of Analytical Chemistry* **2018,** *11* (1), 197-218.

254. Shanmugam, S. T.; Trashin, S.; Wael, D. K., Gold-sputtered microelectrodes with built-in gold reference and counter electrodes for electrochemical DNA detection. *Analyst* **2020,** *145* (23), 7646-7653.

255. Gillespie, P.; Channon, R. B.; Meng, X.; Islam, M. N.; Ladame, S.; O'Hare, D., Nucleic acid sensing via electrochemical oligonucleotide-templated reactions. *Biosensors and Bioelectronics* **2021,** *176*, 112891.

256. Trashin, S.; Rahemi, V.; Ramji, K.; Neven, L.; Gorun, S. M.; De Wael, K., Singlet oxygen-based electrosensing by molecular photosensitizers. *Nature Communications* **2017,** *8* (1), 1-10.

257. Chen, M.; Ning, Z.; Chen, K.; Zhang, Y.; Shen, Y., Recent Advances of Electrochemiluminescent System in Bioassay. *Journal of Analysis and Testing* **2020,** *4* (2), 57-75.

258. Povedano, E.; Gamella, M.; Torrente-Rodríguez, R. M.; Ruiz-Valdepeñas Montiel, V.; Montero-Calle, A.; Solís-Fernández, G.; Navarro-Villoslada, F.; Pedrero, M.; Peláez-García, A.; Mendiola, M.; Hardisson, D.; Feliú, J.; Barderas, R.; Pingarrón, J. M.; Campuzano, S., Multiplexed magnetic beads-assisted amperometric bioplatforms for global detection of methylations in nucleic acids. *Analytica Chimica Acta* **2021,** *1182*, 338946.

259. Grabowska, I.; Hepel, M.; Kurzątkowska-Adaszyńska, K., Advances in Design Strategies of Multiplex Electrochemical Aptasensors. *Sensors* **2022,** *22* (1), 161.

260. Dincer, C.; Bruch, R.; Kling, A.; Dittrich, P. S.; Urban, G. A., Multiplexed Point-of-Care Testing – xPOCT. *Trends in Biotechnology* **2017,** *35* (8), 728-742.

261. Ghindilis, A. L.; Smith, M. W.; Schwarzkopf, K. R.; Roth, K. M.; Peyvan, K.; Munro, S. B.; Lodes, M. J.; Stöver, A. G.; Bernards, K.; Dill, K.; McShea, A., CombiMatrix oligonucleotide arrays: Genotyping and gene expression assays employing electrochemical detection. *Biosensors and Bioelectronics* **2007,** *22* (9), 1853-1860.

262. Erdem, A.; Congur, G.; Eksin, E., Multi channel screen printed array of electrodes for enzyme-linked voltammetric detection of MicroRNAs. *Sensors and Actuators B: Chemical* **2013,** *188*, 1089-1095.

263. Centi, S.; Stoica, A. I.; Laschi, S.; Mascini, M., Development of an Electrochemical Immunoassay Based on the Use of an Eight-Electrodes Screen-Printed Array Coupled with Magnetic Beads for the Detection of Antimicrobial Sulfonamides in Honey. *Electroanalysis* **2010,** *22* (16), 1881-1888.

264. Lee, J.-K.; Gu, Y.; Park, M.; Jose, J.; Pyun, J.-C., Electrochemical ELISA Based on E. Coli with Autodisplayed Z-Domains. *Procedia Engineering* **2011,** *25*, 944-947.

265. Delibato, E.; Volpe, G.; Romanazzo, D.; De Medici, D.; Toti, L.; Moscone, D.; Palleschi, G., Development and Application of an Electrochemical Plate Coupled with Immunomagnetic Beads (ELIME) Array for Salmonella enterica Detection in Meat Samples. *Journal of Agricultural and Food Chemistry* **2009,** *57* (16), 7200-7204.

266. Neves, M. M. P. S.; González-García, M. B.; Hernández-Santos, D.; Fanjul-Bolado, P., Screen-Printed Electrochemical 96-Well Plate: a High-Throughput Platform for Multiple Analytical Applications. *Electroanalysis* **2014,** *26* (12), 2764-2772.

267. Nguema Edzang, R. W.; Duong, T. H.; Briand, J. F.; Lejars, M.; Raimundo, J. M.; Bressy, C.; Brisset, H., Bacterial anti-adhesion activity based on the electrochemical properties of polymethacrylates bearing ferrocenyl pendant groups. *Biofouling* **2018,** *34* (9), 1055-1063.

268. Piermarini, S.; Micheli, L.; Ammida, N. H.; Palleschi, G.; Moscone, D., Electrochemical immunosensor array using a 96-well screen-printed microplate for aflatoxin B1 detection. *Biosens Bioelectron* **2007,** *22* (7), 1434-40.

269. Neagu, D.; Perrino, S.; Micheli, L.; Palleschi, G.; Moscone, D., Aflatoxin M1 determination and stability study in milk samples using a screen-printed 96-well electrochemical microplate. *International Dairy Journal* **2009,** *19* (12), 753-758.

270. Brisset, H.; Briand, J.-F.; Barry-Martinet, R.; Duong, T. H.; Frère, P.; Gohier, F.; Leriche, P.; Bressy, C., 96X Screen-Printed Gold Electrode Platform to Evaluate Electroactive Polymers as Marine Antifouling Coatings. *Analytical Chemistry* **2018,** *90* (8), 4978-4981.

271. Jirakova, L.; Hrstka, R.; Campuzano, S.; Pingarrón, J. M.; Bartosik, M., Multiplexed Immunosensing Platform Coupled to Hybridization Chain Reaction for Electrochemical Determination of MicroRNAs in Clinical Samples. *Electroanalysis* **2019,** *31* (2), 293-302.

272. Hu, Z.; Liu, W.; Hong, B.; Hao, B., Metrological standardizing for future microfluidic-based point-of-care diagnostic products. *Sensors & Transducers* **2014,** *173* (6), 250.

273. Kong, F. Y.; Xu, B. Y.; Du, Y.; Xu, J. J.; Chen, H. Y., A branched electrode based electrochemical platform: towards new label-free and reagentless simultaneous detection of two biomarkers. *Chem Commun (Camb)* **2013,** *49* (11), 1052-4.

274. Alizadeh, N.; Salimi, A.; Hallaj, R., Magnetoimmunosensor for simultaneous electrochemical detection of carcinoembryonic antigen and α-fetoprotein using multifunctionalized Au nanotags. *Journal of Electroanalytical Chemistry* **2018,** *811*, 8-15.

275. Zhu, Q.; Chai, Y.; Yuan, R.; Zhuo, Y., Simultaneous detection of four biomarkers with one sensing surface based on redox probe tagging strategy. *Analytica Chimica Acta* **2013,** *800*, 22-28.

276. Wang, H.; Ma, Z., Simultaneous detection of multiple tumor markers by label-free electrochemical immunoassay using chip-like glass carbon electrodes. *Sensors and Actuators B: Chemical* **2018,** *256*, 402-407.

277. Rong, Q.; Feng, F.; Ma, Z., Metal ions doped chitosan–poly(acrylic acid) nanospheres: Synthesis and their application in simultaneously electrochemical detection of four markers of pancreatic cancer. *Biosensors and Bioelectronics* **2016,** *75*, 148-154.

# List of abbreviations

| | |
|---|---|
| $^1O_2$ | Singlet oxygen |
| ALP | Alkaline Phosphatase |
| anti-DIG | Anti-digoxygenin |
| BQ | Benzoquinone |
| ChlE6 | Chlorin e6 |
| CV | Cyclic voltammetry |
| DNA | De-oxy ribonucleic acid |
| EC | Electrochemistry |
| ECL | Electrochemiluminescence |
| ELISA | Enzyme-linked immunosorbent assay |
| EosY | Eosin Y |
| EryB | Erythrosin B |
| FFA | Furfuryl alcohol |
| GDE | Gold disk electrode |
| HQ | Hydroquinone |
| LED | Light emitting diode |
| LeDlisa96x | In-house LED array printed circuit board |
| MB | Mercaptobutanol |
| MetB | Methylene blue |
| MH | Mercaptohexanol |
| miRNA, miR | Micro RNA |
| MOSFET | Metal–oxide–semiconductor field-effect transistor |
| MU | Mercaptoundecanol |
| NA | Nucleic acid |

| | |
|---|---|
| NGS | Next generation sequencing |
| PEC | Photoelectrochemical |
| PNA | Peptide nucleic acid |
| POC | Point-of-care |
| PS | Photosensitizer |
| PSA | Prostate-specific antigen |
| RNA | Ribo nucleic acid |
| ROS | Reactive oxygen species |
| RT-qPCR | Reverse transcription-quantitative polymerase chain reaction |
| Ru(bpy) | Ruthenium II bipyridine |
| RuHex | Ruthenium (III) hexamine chloride |
| SAM | Self-assembled monolayers |
| SCE | Saturated calomel electrode |
| SEM | Scanning electrode microscope |
| SO-based PEC | Singlet oxygen-based photoelectrochemical |
| SPE | Screen printed electrode |
| ssDNA | Single stranded DNA |
| TCEP | Tris (2-carboxyethyl) phosphine |
| TPA | Tri-n-propylamine |

# List of Tables

# List of Figures

# Academic curriculum vitae

*Published articles*

**S. Thiruvottriyur Shanmugam.**, S. Trashin, K. De Wael, Singlet oxygen-based photoelectrochemical detection of DNA, Biosensors and Bioelectronics 195 (2022) 113652.

**S. Thiruvottriyur Shanmugam,** R. Van Echelpoel, G. Boeye, J. Eliaerts, M. Samanipour, H. Y. V. Ching, A. Florea, S. Van Doorslaer, F. Van Durme, N. Samyn, M. Parrilla, K. De Wael, Towards Developing a Screening Strategy for Ecstasy: Revealing the Electrochemical Profile, ChemElectroChem 8 (2021) 4826.

S. Trashin, F. Morales-Yánez, **S. Thiruvottriyur Shanmugam**, L. Paredis, E.N. Carrión, I. Sariego, S. Muyldermans, K. Polman, S.M. Gorun, K. De Wael, Nanobody-Based Immunosensor Detection Enhanced by Photocatalytic-Electrochemical Redox Cycling, Analytical Chemistry 93(40) (2021) 13606–13614.

J. Schram*, **S. Thiruvottriyur Shanmugam***, N. Sleegers, A. Florea, N. Samyn, A.L. van Nuijs, K. De Wael, Local conversion of redox inactive molecules into redox active ones: A formaldehyde based strategy for the electrochemical detection of illicit drugs containing primary and secondary amines, Electrochimica Acta 367 (2021) 137515.

**S. Thiruvottriyur Shanmugam**, S. Trashin, K. De Wael, Gold-sputtered microelectrodes with built-in gold reference and counter electrodes for electrochemical DNA detection, Analyst 145(23) (2020) 7646-7653.

G. Moro, H. Barich, K. Driesen, N.F. Montiel, L. Neven, C.D. Mendonça, **S. Thiruvottriyur Shanmugam**, E. Daems, K. De Wael, Unlocking the full power of electrochemical fingerprinting for on-site sensing applications, Analytical and Bioanalytical Chemistry 412(24) (2020) 1-14.

L. Neven*, **S. Thiruvottriyur Shanmugam***, V. Rahemi, S. Trashin, N. Sleegers, E.N. Carrión, S.M. Gorun, K. De Wael, Optimized photoelectrochemical detection of essential drugs bearing phenolic groups, Analytical Chemistry 91(15) (2019) 9962-9969.

S. Sathiyamoorthy, G. Girijakumari, P. Kannan, K. Venugopal, **S. Thiruvottriyur Shanmugam** , P. Veluswamy, K. De Wael, H. Ikeda, Tailoring the functional properties of polyurethane

foam with dispersions of carbon nanofiber for power generator applications, Applied Surface Science 449 (2018) 507-513.

## *Manuscripts in preparation for submission*

R. Campos*, **S. Thiruvottriyur Shanmugam***, E. Daems, R. Ribeiro, K. De Wael. Development of electrochemiluminescent and photoelectrochemical oligonucleotide-based assays for the quantification of prostate cancer associated miR-141-3p in Human Serum. Manuscript in preparation.

**S. Thiruvottriyur Shanmugam.,** Campos R., Trashin S., Daems E., Carneiro D., Fraga A., Ribeiro R., De Wael K. Quantification of prostate cancer miRNAs using a singlet oxygen-based photoelectrochemical strategy. Manuscript in preparation.

***** Shared first authors

## *Patent applications*

Electrochemical measurement of primary or secondary amines.
Inventors: K. De Wael, **S. Thiruvottriyur Shanmugam**
Published- Ref. No. WO 2021/038111, March 2021.

Photoelectrochemical particle assay.
Inventors: K. De Wael, **S. Thiruvottriyur Shanmugam**
Filed- Ref No. EP21182783.7, June 2021.

## *Book chapter*

S. C. Kollarahithlu, S. Sathiyamoorthy, **S. Thiruvottriyur Shanmugam**, K. De Wael, J. Das, P. Veluswamy, Foodborne Outbreaks: Sources and Mode of Transmission of Foodborne Pathogenic Microorganisms, Global Food Safety, Microbial Interventions and Molecular Advancements, Apple Academic Press, in production, Pub Date: June 2022.

## *Conference contributions*

Singlet oxygen-based photoelectrochemical DNA sensors, 72nd Annual ISE Meeting, 30 August 2021, online, oral presentation.

Gold thin-film based photo-electrochemical planar DNA sensors, 9th International Workshop on Surface Modification for Chemical and Biochemical Sensing, SMCBS 2019, November 8 – 12 2019, Zelechów, Poland, poster presentation.

Gold thin-film based photoelectrochemical planar DNA sensors, 2nd European biosensor symposium, EBS2019, February 18 - 21 2019, Firenze, Italy, poster presentation.

Wireless electrochemical sensor for on-site detection of ecstasy, ChemCYS 2018, Chemistry Conference for Young Scientists, February 21-23, 2018, Blankenberge, Belgium, oral presentation.